ISTANBUL TECHNICAL UNIVERSITY ★ INSTITUTE OF SCIENCE AND TECHNOLOGY

KINETIC AND THERMODYNAMIC ANALYSIS OF GENETICALLY ENGINEERED INORGANIC BINDING PEPTIDES FOR BIONANOTECHNOLOGY

PhD. Thesis by
Urartu Özgür Şafak ŞEKER

Department : Advanced Technologies

Programme : Molecular Biology-Genetics and Biotechnology

Thesis Supervisors: Prof. Dr. Candan TAMERLER
Prof. Dr. Mehmet SARIKAYA

SEPTEMBER 2009

İSTANBUL TECHNICAL UNIVERSITY ★ INSTITUTE OF SCIENCE AND TECHNOLOGY

KINETIC AND THERMODYNAMIC ANALYSIS OF GENETICALLY ENGINEERED INORGANIC BINDING PEPTIDES FOR BIONANOTECHNOLOGY

PhD. Thesis by
Urartu Özgür Şafak ŞEKER
(521032203)

Date of submission : 27 May 2009
Date of defence examination : 23 September 2009

Supervisor (Chairman) : Prof. Dr. Candan TAMERLER (ITU)
Co-Supervisor : Prof. Dr. Mehmet SARIKAYA (UW)
Members of the Examining Committee : Prof. Dr. Pemra DORUKER (BU)
Prof. Dr. Mustafa ÜRGEN (ITU)
Assoc. Prof. Dr. Cenk SELÇUKİ (EU)
Assoc. Prof. Dr. Z. Petek ÇAKAR (ITU)
Assist. Prof. Dr. Fatma Neşe KÖK (ITU)

SEPTEMBER 2009

İSTANBUL TEKNİK ÜNİVERSİTESİ ★ FEN BİLİMLERİ ENSTİTÜSÜ

BİYONANOTEKNOLOJİ UYGULAMALARI İÇİN GENETİK MÜHENDİSLİĞİ İLE OLUŞTURULAN ANORGANİKLERE ÖZGÜL PEPTİDLERİN KİNETİK VE TERMODİNAMİK ANALİZLERİ

DOKTORA TEZİ

Urartu Özgür Şafak ŞEKER
(521032203)

Tezin Enstitüye Verildiği Tarih : 27 Mayıs 2009
Tezin Savunulduğu Tarih : 23 Eylül 2009

Tez Danışmanı : Prof. Dr. Candan TAMERLER (İTÜ)
Tez Eş Danışmanı : Prof. Dr. Mehmet SARIKAYA (UW)
Diğer Jüri Üyeleri : Prof. Dr. Mustafa ÜRGEN (İTÜ)
Prof. Dr. Pemra DORUKER (BÜ)
Doç. Dr. Cenk SELÇUKİ (EÜ)
Doç. Dr. Zeynep Petek ÇAKAR (İTÜ)
Yard. Doç. Dr. Fatma Neşe KÖK (İTÜ)

EYLÜL 2009

FOREWORD

First and foremost, I would like to thank to my supervisors Prof. Dr. Candan Tamerler and Prof. Dr. Mehmet Sarikaya for their invaluable advises, guiding and mentorship. I am grateful to both being so generous for sharing their time, knowledge and ideas. I was so lucky to spend this last five years with them, that will be an unforgettable research and life experience for me so that it may last throughout my life time.

I am so thankful to my research partner Brandon Wilson, being open to discuss anything about research and being such a good friend in all the times. I want to thank Chris So for his willingness to help at any time. Dr Hanson Fong is the other person, who spent a lot of time on my SPR substrates, I am thankful to him. I am grateful to Dr Ersin Emre Oren for teaching oyme the initial steps of molecular modeling and sharing the molecular models of the GEPIs.

Prof. Dr John S. Evans and his research group from New York University supported us with their structural studies on GEPIs, I am thankful to them.

I want to express my gratitude to Prof. Dr. Hilmi Volkan Demir for being supportive, open minded and positive during our studies at Bilkent University. I like to thank to Gulis Zengin for her research partnership and friendship and all the members of the Devices and Sensors Research Group lead by Prof Demir at Bilkent.

I am grateful to my dear friends Volkan Demir, Tutku Aykanat, İbrahim Gülseren and Deniz Şahin for their continuous moral support. Also I am grateful to Deniz and Volkan, for sharing their homes during my homeless times. Acknowledgments section would be incomplete if I would not mention about Senem Donatan and Beril Akinci, I am thankful to Senem Donatan and Beril Akinci for their friendship, and sharing so many thing together, I am happy to have them. Thanks to Turgay Kacar and Mustafa Gungormus for their friendship in Seattle. Many thanks go to all the members of the Biomimetics Research group in ITU, for their moral and technical support.

Everything will be less enjoyable and harder without the presence of Ceyda, I felt so confident and strong with her. A huge “thanks” is for her patience and her love over these years.

Last but not the least; I am deeply grateful to my family, my father Casim Şeker, my mother Güldane Şeker and brother Volkan. There are no words exist to express my gratitude to my parents, they supported me and they believed in me whatever I did, which makes me feel so strong over these thirty years.

This study is supported by Turkish State Planning Organization, and Genetically Engineered Materials Science and Engineering Center and NSF-MRSEC, TUBITAK-NSF Joint Project (TBAG-107T250).

Istanbul, June 2009 Urartu Ozgur Safak Seker

TABLE OF CONTENTS

Page

ABBREVIATIONS

AFM : Atomic Force Microscopy
SPR : Surface Plasmon Resonance
QCM-D : Quartz Crystal Microbalance Dissipation Monitoring
SAM : Self Assembled Monolayers
GEPI : Genetically Engineered Inorganic Binding Peptides
Qdots : ZnS/CdSe Core-Shell Semiconductor Nanoparticles
SEM : Scanning Electron Microscopy
TEM : Transmission Electron Microscopy
1-GBP : Open linear gold binding Peptide
31-GBP : Open linear three repeat gold binding Peptide
1-QBP : Open linear silica binding Peptide
31-QBP : Open linear three repeat silica binding Peptide
1-PtBP : Open linear platinum binding Peptide
31-PtBP : Open linear three repeat platinum binding Peptide
c-PtBP : Closed loop cyclic platinum binding peptide
***dn*QBP** : In silico designed, second generation silica binding peptide
AP : Alkaline phosphatase
SAAP : Streptavidin – alkalinephosphotase fusion
bioGEPI : biotinylated peptide
PNPP : para-Nitrophenylphosphate

LIST OF TABLES

Page

LIST OF FIGURES

Page

KINETIC AND THERMODYNAMIC ANALYSIS OF GENETICALLY ENGINEERED INORGANIC BINDING PEPTIDES FOR BIONANOTECHNOLOGY

SUMMARY

Molecular recognition properties of genetically engineered inorganic binding peptides (GEPI), were investigated with respect to their binding kinetics and thermodynamics. Phage display or cell surface display selected GEPIs for different materials were characterized. In the molecular characterization of GEPIs, adsorption kinetics and thermodynamics of GEPIs were realized in conjugation with secondary structural analysis of the peptides. To characterize binding kinetics and thermodynamics of GEPIs, we employed surface plasmon resonance sensor, and quartz crystal microbalance. Both the affinity and materials selectivity of gold, platinum and silica binding peptides were tested. The effect of conformational constraints and multiple repeats on the affinity and material selectivity of GEPIs was investigated. As a case study the structure-affinity relationship in gold binding peptides was analyzed, using a thermodynamic approach. Following the molecular characterization of GEPIs, proof of demonstration studies was carried out, in which GEPIs were utilized as molecular linkers and material synthesizer. In this perspective, we utilized GEPIs as molecular linkers, for the immobilization of alkaline phosphatase on gold, platinum and silica; for the targeted assembly of semiconductor nanoparticles on LED device; as molecular erector for the real time monitoring of fibrillation in Huntington's disease; and finally as synthesizer in the morphology controlled synthesis of silica.

In the scope of the thesis, GEPIs have been exploited to create new generation of biomimetic molecular linkers. The effectiveness of GEPIs on material surfaces were tested using surface sensitive tools. Various practical bio-nanotechnological examples in the usage of GEPIs as molecular linkers were demonstrated as representative towards their wide range applications to overcome the challenges at the nano- bio- interface.

BİYONANOTEKNOLOJİ UYGULAMALARI İÇİN GENETİK MÜHENDİSLİĞİ İLE OLUŞTURULAN ANORGANİKLERE ÖZGÜL PEPTİDLERİN KİNETİK VE TERMODİNAMİK ANALİZLERİ

ÖZET

Bu çalışma kapsamında genetik mühendisliği kullanılarak oluşturulmuş anorganiklere özgül bağlanan peptidlerin (GEPI) kinetik ve termodinamik araçlarla moleküler tanıma özellikleri incelenmiştir. Faj gösterim ya da hücre yüzey gösterim teknikleri kullanılarak seçilen GEPI moleküllerinin karakterizasyonu yapılmıştır. GEPI'lerin moleküler karakterizasyonu adsorpsiyon kinetikleri ve termodinamikleri, ikincil yapı çalışmaları ile bir bütünlük içerisinde gerçekleştirilmiştir.GEPI'lerin bağlanma kinetik ve termodinamik analizleri yüzey plazmon rezonans spektrometresi ve kuvartz kristal mikroterazi kullanılarak gerçekleştirilmiştir. Altın yüzeyine, silika yüzeyine ve platin yüzeyine özgül olarak bağlanan peptidlerin sadece afiniteleri değil aynı zamanda malzeme seçicilikleri de incelenmiştir. Bir durum çalışması olarak altına özgül olarak bağlanan peptitd yapı-aktivite ilişkisi de, termodinamik bir bakış açısı kullanılarak gerçekleştirilmiştir. GEPI'lerin moleküler karakterizasyonunu takiben GEPI'lerin moleküler bağlayıcı ve malzeme sentezleyicisi olarak kullanımlarını ispat amacıyla kanıtlama çalışmaları yapılmıştır. Bu bağlamda, GEPI'leri moleküler bağlayıcı olarak, alkali fosfataz enziminin altın, silika ve platin yüzeylerine immobilizasyonu, yarı iletken nanotaneciklerin LED aygıtlarının yüzeylerine tutuklanması çalışmalarında; moleküler tutucu olarak, Huntington hastalık etmen proteininin fibrilasyonunun gerçek zamanlı olarak incelenmesi amacıyla, ve son olarak da morfoloji kontrollü silika sentezi için malzeme yapıcı olarak kullanımları gösterilmiştir.

Bu tez kapsamında GEPI molekülleri yeni nesil moleküler bağlayıcılar olarak kullanılmışlardır. GEPI'lerin moleküler bağlanma afinite ve özgüllükleri yüzey hassas metodlar incelenmiştir. GEPI'lerin birçok değişik biyo-nano teknolojik örneklerde moleküler bağlayıcı olarak kullanımları, nano- biyo- arakesitindeki zorlukları aşabilmek için uygun moleküler araçlar olduğunu ortaya koyacak şekilde sunulmuştur.

1. INTRODUCTION

Surface functionalization is a method to introduce functional groups to a surface of interest. These functional groups can be chemical, or biochemical molecules. Using this method, one can create functional materials and functional surfaces from bulk material substrates. Surface functionalization is an important phenomenon in technological implications. It has been used widely in electronic, chemical, biochemical and biomedical applications. The surface functional chemical molecules are the indispensable parts in fabrication of new electronic devices (Kilian et al., 2009, Demir et al., 2007). One can change the hydrophobicity and hydrophobicity properties of a surface by introducing polymers on a surface of interest, one can design implant surfaces which are resistant for cell and protein adhesion in biomedical application (Ratner and Bryant, 2004).

Traditionally, many different chemical molecules have been utilized towards creating functional surfaces. However, thiols have been used as the predominant elements of surface functionalization. They have been widely used as molecular linkers to immobilize molecules and other entities on a surface of interest. The advantages of the thiols are their wide range of availability and their ease of synthesis and functionalization for a certain purpose. For example, one can attach carboxyl, amine or a benzene groups at the end of a thiol molecule using a chemical reaction (Rajagopalan et al., 2009, Sainsbury et al., 2007, Goren et al., 2006). However, in a multi-material system, thiols are not good enough for immobilization on desired material part. The need for specificity and material selectivity of the linker molecules is gained importance in parallel with the increase in the number of studies in the area of nano and micro-technologies. Applicability of multimaterial systems brings enormous opportunities in these technological areas. The available linkers like thiol, silane groups and other organic molecules do not provide any specificity and selectivity. In technological applications multi material surfaces for implants, electronics systems have been extensively used. Silane and thiol based molecules are forming self assembled monolayers (SAM) on solid surface. The SAMs of thiol and

silane based molecules are formed through a covalent bonding. A thiol based molecule can form SAMs on many different metallic surfaces. This spontaneous process does not have any selectivity for a multimaterial system (Love et al., 2005). For the assembly of certain molecules to the desired surface in a multimaterial system, chemically available linkers lack specificity. In order to create micro and nanostructures composed of to the point assembled molecules we need specific recognition capability, in other words we need multimaterial specificity for the linker molecules, which can distinguish between two surfaces (Sarikaya et al., 2004, Sano et al., 2007). To build a controlled and targeted assembly with the molecular linkers for multimaterial specificity, molecules with high selectivity and specificity must be used. Using peptidic aptamers one can easily anchor biomolecules and other entities on solid inorganic surfaces with specific activity (Tamerler and Sarikaya, 2007, Tamerler et al., 2006a, Park et al., 2007). In biological systems molecular recognition is used in many different processes. Protein and peptides are the key molecules which are functioning through molecular recognition in their biochemical roles (Hayashi et al., 2006, Sarikaya et al, 2003, Tamerler et al, 2006a).

Nature is building hard tissues such as bones, teeth and shells, by using inorganic and organic materials together. Natural hard tissue with the man made technological ones, one can easily differentiate the uniqueness of the natural hard tissues. The growth of these hard tissues are mainly controlled and directed by proteins and peptides (Sarikaya, 1999, Sarikaya, 2003). Most of the time, natural hard tissues are synthesized at room temperatures and at neutral pH values. However traditional manufacturing methods mainly involve high temperature and high pressure processes (Sarikaya, 1999). Proteins take important role in the formation of the biological hard tissues. Proteins are mainly functioning through binding to the minerals and so they are controlling the growth of the mineral crystals or they function as framework proteins, in this case they serve as scaffold for minerals to deposit (Sarikaya, 1999; Sarikaya et al 2003; and Long et al, 1998; Weiner, 1978).

One can use the specificity and selectivity of the proteins towards minerals and natural inorganic surfaces in biological systems, and can tailor novel proteins that can be used for a controlled adhesion on a targeted inorganic surface *in vitro*. Their role in the formation of the biological hard tissues has been also demonstrated at some content. However, a tedious and labor intensive way is to extract these proteins

from the source tissues of the mineral forming organisms (Cariolou et al., 1988, Berman et al., 1988, Sarikaya, 1999). Another approach, by exploiting the tools of computational biology and genetic engineering, it is also theoretically possible to design a peptide or protein with inorganic binding capacity. However there are some constraints for the calculation of the inorganic surface – biomolecule interaction. The force field parameters for the calculation of this type interaction need to be optimized (Evans et al., 2008). Additionally, the specificity of a peptide needs to be defined mathematically. The energy landscape of a peptide on many different materials needs to be calculated, but these approaches need a very long computational time. Another point is the effect of the structured water at the peptide-inorganic interface and to include the effect of the explicit water effect will dramatically increase the computational cost (Schrevandijk et al., 2007, Kuhlman et al, 2003). Again looking back into the natural hard tissues and the biomineralization mechanisms, there is a remarkable mechanism working behind the formation of the optimal molecular and cellular structures which is the evolution of molecules and organisms to carry out a certain function.

In last decade a high number of studies were carried out to tailor proteins, particularly enzymes were designed to carry out some unnatural processes. The process is called irrational design of the proteins using the tools of genetic engineering and protein engineering. Later, these approaches were incorporated with forced evolution of the designed molecules under desired step pressures to select and evolve the best adapted proteins (Moore and Arnold, 1996; Bloom et al., 2006). This approach was simplified for selecting antibodies and ligand molecules by creating libraries by insertion of the random polypeptide sequences in the coat protein of the bacteriophage (Smith, 1985) or cell surface protein of bacteria (Wittrup, 2001). These combinatorial libraries have a diverse population of random peptide sequences ($\sim 10^9$). In these libraries peptides were either displayed in constrained or linear forms (Schwartz, 2007).

Sarikaya, made the first attempt and build the strategy towards utilizing proteins to synthesize materials by mimicking Mother Nature, his envision with Aksay extended the horizon of biomimetics towards creating functional materials by using biomolecules (Sarikaya and Aksay, 1993).

Within the search for biomolecules with desired inorganic binding capability, combinatorial peptide libraries were exploited. The first attempt was made by a molecular biologist, *Stanley Brown*, who created his own cell surface display library and screened for the binding affinity of the iron oxide (Brown, 1992). He identified first man made inorganic binding peptides, which are not naturally occurring. This is followed by the selecting of the gold and chromium binding peptides (Brown, 1997); however these peptides were displayed as fusion protein, inserted into the alkaline phosphatase. Sarikaya envisioned this area to create new generation of biomimetic linker molecules, and with his group he build the strategy of the field to cover the issues about using the inorganic binding peptides as template molecules for synthesis of nano-materials, and utilizing them as molecular linkers (Sarikaya et al., 2003, Brown et al., 2000). Sarikaya group does not only utilize these molecules as molecular linker and molecular templates; they also pioneered the research towards understanding the molecular binding mechanism of the genetically engineered peptides (Braun et al., 2001). In last decade a number of different inorganic binding peptides were selected towards many other different materials such as Pt, Pd, Silica, ZnO_2, Cu_2O. All of these peptides were named "Genetically Engineered Inorganic Binding Peptides", which is abbreviated as GEPI.

In this study, the kinetics and thermodynamics of binding of GEPIs and GEPI fused proteins have been explored. All of the peptides were synthesized singly to investigate their binding kinetics and to assess quantitatively the specific affinity of each to its material of selection. The peptides were also post-selection engineered to contain multiple copies of the same original sequences to quantify the effects of repeating units. SPR spectroscopy, normally using gold surfaces, was modified to contain a thin film (a few nm thick) of the material of interest (silica or hydroxyapatite, platinum) on gold to allow the quantitative study of the adsorption kinetics of specific solid-binding peptides. Additionally, quartz crystal microbalance is utilized to monitor the binding of GEPIs and GEPI fused proteins. The SPR experiments, carried out at different concentrations, on all three materials substrates, resulted in Langmuir behavior that allowed the determination of the kinetic parameters, including adsorption, desorption, and equilibrium binding constants for each of the solids as well as free energy of adsorption and for a special case for gold binding peptides the binding enthalpy and entropy was determined. Furthermore, we

also tested multiple repeats of the peptide sequences, specifically three repeats, to see if there is a general trend of increased binding with increased number of binding domains. The effect of the structure on the binding affinity of these peptides was also investigated. Circular dichroism data both for the native state of the peptides in buffers and in a structure enhancer solution triflourethanol was used to explain the secondary structure of these peptides.

The interaction of the GEPIs with solid surfaces was not only monitored kinetically also a detailed study on the thermodynamics of the binding interaction of GEPIs with the solid surface was achieved towards understanding the binding mechanism of the GEPIs on gold surface. Not only was the affinity investigated, towards understanding the binding interaction of GEPIs, but also the materials selectivity of GEPIs towards a variety of solid surfaces was tested thoroughly for a better understanding and a better classification.

Finally, it was found that the binding of the peptides was strong enough to suggest that these inorganic binding peptides could potentially be used as specific molecular linkers to bind molecular entities to specific solid substrates due to their surface recognition characteristics. The knowledge generated on the binding interactions of the peptides, was further utilized to demonstrate the practical applicability of peptides as molecular linkers at bio-nano interfaces. Here GEPIs for protein immobilization as well as for targeted nanoparticle immobilization and materials synthesis was tested.

,

2. BACKGROUND

2.1 Surface Functionalization

Surface functionalization is modifying substrate materials for a certain purpose using chemical and biochemical molecules. These materials can be any given material which will be further utilized in biomedical, chemical, electronic and optic applications. In literature, different chemical functional groups were used for surface functionalization (Hoffman et al., 2009, Wrighton, 1986, Debs et al., 2009, Doud et al., 2005). Metal and semiconductors and metal oxide surfaces can easily adsorb different organic molecules. This adsorption process is a thermodynamically favorable phenomenon as the adsorbates lower the free energy between the metal (metal oxide) and the ambient environments, such as aqueous environment in the case of biomedical applications (Love et al., 2005). Surfaces coated (through adsorption) with certain chemical groups, these certain groups can alter the physicochemical properties of the surface of interest. These additional functional groups can change the wettability (Lee et al., 2001), conductivity (French et al., 2008), corrosion resistance (Jennings et al., 2006) and biomolecular and cell adhesion properties of a given surface (Ratner and Bryant, 2004). However, the key issue is to be able to control these processes, and to prevent the random adsorption of the chemically functional groups. Otherwise surface coated with the adsorption of the adventitious groups can cause the formation of surfaces with uncontrolled –poor functionality. So to prevent this, there is a need for some linker molecules to functionalize a given surface with desired physicochemical properties. This will allow us to create functional surfaces with controlled functionality, so that we can utilize them to immobilize biological and chemical entities for technological and scientific applications.

2.1.1 Molecular linkers

Molecular linkers are used to immobilize biological or chemical molecules on a given material for surface functionalization. Many chemical molecules can be used

as molecular linkers, in the literature for the immobilization of the proteins chemically synthesized linker molecules have been used. Silane and thiol based molecular linkers are the most widely used linker molecules to create long range of linker array to create functional surfaces for immobilization of biological elements such as protein, peptides and enzymes, also immobilization of the nanostructured materials for creating optically active surfaces such as metallic nanoparticle immobilization, core/shell nanoparticles immobilization. Thiols (R-SH, R denotes the rest of the molecule) are known for their binding ability with the gold surface, as the silane (SiH_4) based molecules are ready to make the covalent bonding with the SiO_2 surfaces. Silane and thiol based molecules are known to form hierarchical structures from pre-designed building blocks, typically involving multiple energy scales and multiple degrees of freedom (Bourgeat et al., 2002, Reynolds et al., 2009, Das et al., 2009, Love et al., 2005). These structures are called as the self assembled layers, and the process they involve during the formation of the arrays of structures in a autonomous manner is called as the self assembly process.

2.2 Self Assembly and Self Assembled Monolayers

Self assembled monolayers can be defined as the structures which are formed by means of spontaneous association of the molecules under equilibrium conditions. Self assembled molecules are structurally well defined and they are joined together by means of non covalent bonds. Molecular self assembly is unique in the biological systems, so self assembly underlies the formation of the very complex biological systems and structures. Self assembly processes involve many different event in the nature scaling form the organization of the cellular components to the planetary systems (weather systems) (Whitesides, 1991; Hartgerink, 2001).

Self assembled structures are containing information as coded in their individual units; this information can be charge, polarizability, magnetic dipole, mass etc. These characteristics mainly dictated by the type of the interaction. The self design is the key component in the formation of the self assembly in the naturally occurring systems, which are formed spontaneously. However, in the technological designs a detailed design of the self organizing components is crucial for the formation of the desired patterns (Whitesides and Grzybowski, 2002).

Self assembly can be summarized in two different classes. (1) the static self assembly, here the systems are not dissipating energy, and these systems are at global or local equilibrium. Molecular crystals, folded proteins can be given as examples. Here formation of the self assembled structures need energy, once the systems is formed it is stable, as an example the formation of a peptide nanofiber can be given mentioned in Figure (2) (Aizenberg et al., 1999; Blaaderen et al., 1997, Hartgerink et al., 2001). In dynamics self assembly, the interactions and patterns which cause the formation of the self assembled layers, are only formed if the systems is dissipating energy. The patterns formed by the competition between reaction and diffusion in oscillating chemical reactions can be given as simple examples, as the biological cells can be given as more complex examples to this phenomenon (Whitesides and Grzybowski, 2002).

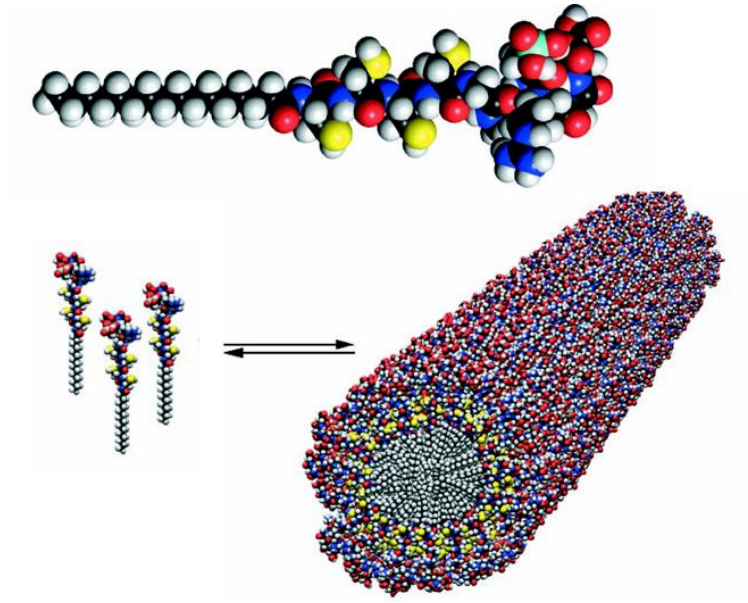

Figure 2.1: Molecular model of a peptide amphiphile, it shows the overall conical shape of the molecule going from the narrow hydrophobic tail to the crowded peptide region. Color scheme: C, black; H, white; O, red; N, blue; P,cyan; S, yellow. Schematic showing the self-assembly of PA molecules into a cylindrical micelle (Hartgerink et al., 2001).

Self assembly is a unique process which allows the formation of the excellent biological systems. Starting form the process of the central dogma, the main theory in molecular biology, self assembly takes place almost in every single molecular and cellular interaction and event in biological systems.

Self assembled monolayers are organic assemblies which are spontaneously formed upon adsorption onto the surface of the solids. After the adsorption of these organic

constituents on the solid surfaces they are forming regular arrays on the surfaces. The SAM forming organic molecules are adsorbed on the solid surface either from gas phase or liquid phase. During their organization on the solid surface possibly they organize into crystalline (or semi crystalline) structures (Love et al., 2005).

The molecules that form the SAMs have either a chemical functionality or they have a head group which shows a certain affinity towards the substrate. In many cases it is also possible that the head groups enable the displacement of the adventitious part of the SAM forming molecule on the surface. This happens in the cases where the head groups have a higher affinity towards the surface (Nuzzo et al.,1983; Biebuyck et al., 1984; Laibinis et al., 1991; Dubois et al., 1992). As we think about that there are a number of different materials, which are used in chemical and technological applications; there is a need to have a number of different SAMs forming molecules with different binding functionality. Today there are many different SAMs are being synthesized with different head groups that are binding on the surface of metals, metal-oxides and semiconductors. The group of SAMs which were studied in details is alkanethiols on gold, silver, copper, palladium, platinum and mercury (Carvalho et al., 2002 ; Li et al., 2003). The high affinity of alkanethiols towards the surfaces of noble and coinage metals makes it possible to generate well defined, densely packed organic surfaces, which provides functional and highly alterable chemical functionalities at the exposed interface. A schematic representation of the formation of the SAMs of thiols is shown in Figure 2.2 (Porter et al., 1987, Love et al., 2003; Muskal et al., 1996).

2.2.1 Adsorption kinetics and thermodynamics of SAMs: Structure

The characterization of the thiols on the surface has been important for their practical utilization and there are many different ways for the characterization of the SAMs in the literature. Raman spectroscopy (Bryant and Pemberton, 1991), X-ray photoelectron spectroscopy (Bain and Whitesides, 1989), X-ray diffraction (Samant and Brown, 1991), surface plasmon resonance spectroscopy, optical ellipsometry (Roy and Fendler, 2004) and scanning probe microscopy (Jackson et al., 2004) are some of the techniques given in the literature. The studies are mainly based on the kinetic and thermodynamics of adsorption of the thiols, as well as the formation

mechanism of the SAMs on gold surface it is the standard surface studied for the formation of the SAMs.

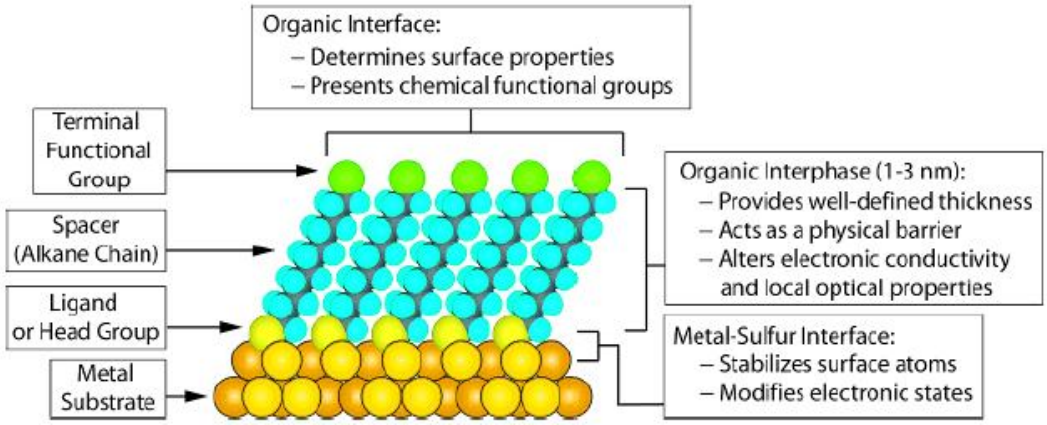

Figure 2.2: Schematic diagram of an ideal single-crystalline SAM of alkanethiolates. The SAM was formed on a gold surface with a (111) texture. The chemistry and structure of the SAM is explained on the Figure (Love et al., 2003).

The use of gold surface can be summarized in two main parts: (1) gold surface is a perfect surface to form a densely packed very well organized SAMs, because of the strong covalent bonding between gold and thiols (2) the interaction between gold and thiol molecules is well characterized. Gold is chosen as a standard surface for practical applications due to the ease of fabrication with different surface textures. The monitoring of the SAMs formation on gold surface is also easy by using spectroscopic, microscopic and analytical methods (Love et al., 2005). Other then gold, silver is the second common material which was studied for the SAMs formation. However, silver get oxidized very quickly, it is toxic for cells, and it is not the material of choice in most cases. But the SAMs formed on silver is more simple and clear compared to the one formed on gold. Copper is another material of interest for its usage in technological applications, but it is also susceptible to oxidation more than silver (Dowling et al., 2003). In fact there are different available techniques for the characterization of the thiol adsorption on a surface of interest, but the real time techniques are versatile and available to detect using different physicochemical conditions. Surface plasmon resonance spectroscopy and quartz crystal microbalance are the most popular tools for the real time characterization of the adsorption of the thiol and silane based molecules.

2.2.1.1 Surface plasmon resonance spectroscopy

The Surface Plasmon Resonance Spectroscopy consists of usually three layers the sample layer, the metal layer (usually gold or silver) and a layer for the light-coupling device such as prism. The mechanism in a prism coupler based SPR system is simple. The incident light hits the interface between the metal layer and prism, and it is totally reflected. The surface plasmon wave is generated; at the point where the resonance condition is satisfied (at this point the light hits the prism-metal layer interface at resonance angle). Surface plasmon wave is connected to the charge-density change at the surface. Charge-density oscillation is highly sensitive to the changes that occur at the sensing layer. If this oscillation is excited, there will be a decrease in the intensity of reflected light. This decrease can be recorded as minima in the reflection spectrum (Homola et. al., 2001).

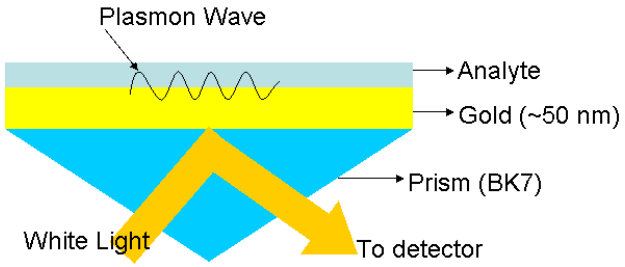

Figure 2.3: A schematic of a prism coupler based SPR setup. The configuration used in this setup is a Kreschtmann configuration.

If any biomolecule is adsorbed on to the sample-metal layer interface, the refractive index will change. The change will cause an alternation in the resonance conditions of the surface plasmon resonance wave. These variations at the resonance conditions will directly effect the position of the minima on the reflection spectrum. The amount of wavelength shift recorded in the minima of the reflection spectrum can be observed in the sensogram. The sensogram is a graphical interpretation of the event (increases and decreases in the dip position) as a function of the time (Sambles et al., 1991, Lukosz, 1991). This can be regarded as a monitor to follow up changes due to the adsorption. SPR has become very popular in last decade as a real time molecular interaction monitoring tool. During looking the biomolecular interactions one of the interacting entities was immobilized on the surface of the sensor chip (Homola et al., 2005). The SPR sensor chip is mainly a ~50 nm gold coated glass. To immobilize a protein or peptide on gold surface, the surface is either functionalized using a chemical linker such as thiol molecules, or commercially available surfaces, can be

utilized. To modify the surface using a thiol molecule, SPR gold sensor chip is dipped in a solution in that a –COOH or –NH_2terminated thiol molecule (dodecathiol, ethandithiol) dissolved (Solanki et al., 2007, Kawaguchi et al., 2007).

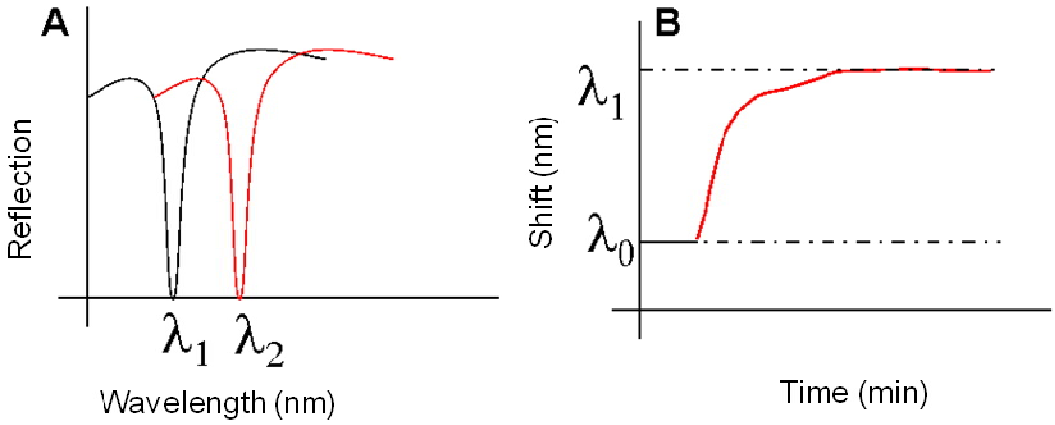

Figure 2.4: (A) Reflection spectrum of SPR. The black curve represents the initial resonance conditions as the red curve represents the resonance condition after a biomolecules adsorbed on sample-metal layer interface. (B) SPR sensogram representing the change in the dip position of the SPR as a function of time.

Following the overnight incubation and washing excess amount of the thiol from the surface, the –COOH groups decorated via thiols linkage needs to be activated using EDC (1-Ethyl-3-[3-dimethylaminopropyl] carbodiimide hydrochloride)/NHS (*N*-hydroxysulfosuccinimide). After the activation of the surface –COOH using NHS/EDC the antibody or protein in interest can be immobilized. After the immobilization of the protein/antibody on the surface, the other interacting entity will be flown over the prepared sensor surface. SPR has been widely used to probe protein-protein, protein-small molecule, protein-carbohydrate, protein-DNA interactions. As mentioned earlier mainly gold surface was used as the sensing layer of the SPR sensor chip. Silver is also another possible surface that can be exploited. However silver oxidizes very fast, which makes it a bad choice. Theoretically it would be possible to excite plasmon of a lot of other materials like, copper, aluminum. However, operational difficulties such as inadequate transmission of the used light through the film, acts a barrier to use SPR for wide range of applications using different metals (Jung et al., 1998, Kovalenko et al., 2001).

It should be mentioned that all the above given cases are true for Kreschtman`s configuration. Other surface plasmon resonance configuration Otto configuration is suitable to use other metals. However this configuration is not suitable to use to

monitor biomolecular interactions, because the analyte has to be placed within the air gap, which has to be less than 2 μm in order to achieve a successful detection. Therefore Otto configuration is mainly used to determine material properties such as dielectric constants (Abdulhalim, 2009).

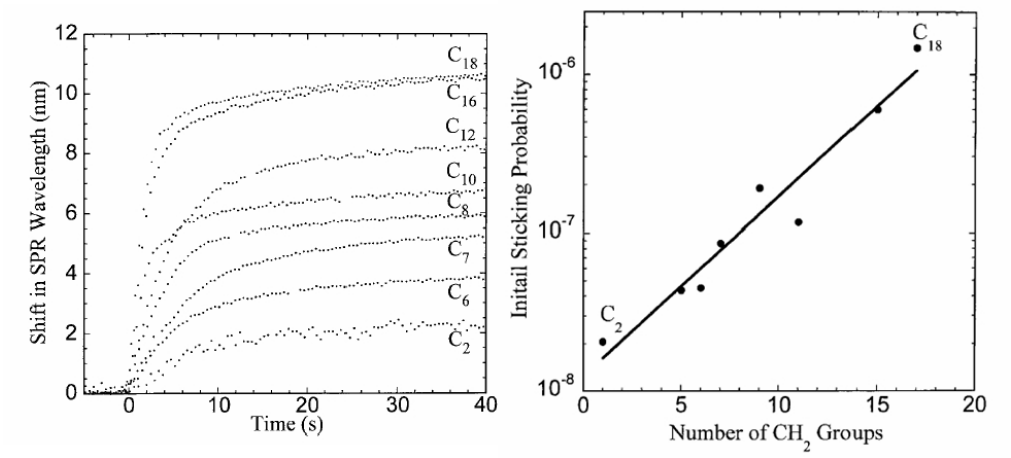

Figure 2.5: A) SPR responses of the adsorption of several alkanethiols from ethanol on Au surface at ambient conditions. B) Initial sticking probability as a function of chain length (Jung et al., 1998).

Surface plasmon resonance spectroscopy was utilized for characterization of the adsorption of the thiol based molecules. Quantification of the adsorption of te alkethiol molecules with varying chain length has been investigated using SPR. The amount of the adsorbed thin film of thiols has been quantified using a calibration approach of the SPR refractive index change. This approach does not only yield in the thickness of the adsorbed film per area, it also resulted in the fractional coverage and surface concentration of the adsorbed material. These approaches have been further utilized in a more detailed characterization of the self assembled monolayers using SPR (Jung et al., 1998). The sticking probability is another measure toward characterization of the adsorption properties of alkanethiols on surfaces. The sticking probability represents the rate of adsorption per molecular collision with the surface; basically it reflects the difficulty for a molecule to be adsorbed onto the surface by overcoming the adsorption energy barrier. This technique is also used to measure the effect of the chain length on the adsorption of alkanethiols on gold surface. Sticking probabilities of alkanethiols as a function of chain length implied a stabilization upon increasing the sticking probability from 10^{-8} to 10^{-6} with alkyl chain length. So this is also expressed stabilization of transition state by 0.65 kJ/mol per CH_2. Also a first

order Langmuir kinetics was followed, up to coverage of $4x10^{14}$ molecules/cm^2 (Jung and Campbell, 2000).

2.2.1.2 Quartz crystal microbalance

Quartz crystal microbalance is a mass sensitive method. In simplest case when the quartz resonator is covered with a rigid layer, the resonator functions as a purely gravimetric probe giving the mass of the deposited layer on the quartz resonator. In another case when the resonator is brought in contact with a viscous solution then the QCM behaves like a probe to detect the liquid properties such as density and viscosity. However, it is increasingly recognized that most of the systems of interest studied by QCM do not confirm to either of the cases above and the properties of many systems is somewhere in between these two extreme cases i.e. they are so called viscoelastic and their properties are a complex combination of elastic and viscous contributions from the material(s) of interest (Cernosek et al., 1998; Bandey et al., 1999). The conventional usage of the oscillator QCM is well established in many areas such as analytical chemistry, biochemistry and biotechnological applications. To have a complete knowledge on the mechanical properties (visco-elastic properties) of the adsorbed layers on QCM crystals many attempts were made. Impedance analysis is one of the successfully applied methodologies. This approach uses a model which simulates the behavior of a quartz crystal simultaneously loaded by a surface mass and a contacting Newtonian liquid (Cernosek et al., 1998; Bandey et al., 1999).

The oscillator method only measures the series frequency; the impedance analysis characterizes the quartz crystal and enables the measurement of several overtones. This provide a multidimensional information to describe complete behavior of the quartz crystal and its adlayers.

The crystals used in the QCM-D systems are available for the analysis of the interaction of the molecules with different kind of surfaces. The available crystals are gold, platinum, silica. The schematic representation of the crystal is represented in Figure 2.6.

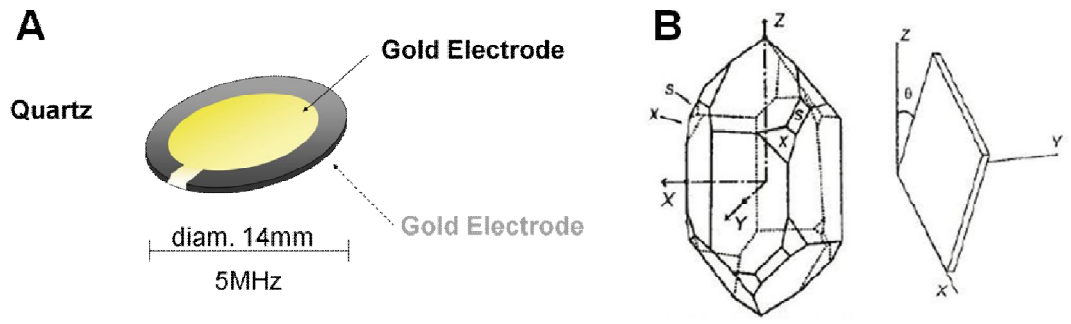

Figure 2.6: (A) Schematic illustration of a quartz crystal with its electrodes. (B) Crystallographic representation of quartz and the specific cut representing the AT-cut (Wang and Mittleman, 2004).

The binding kinetics of alkanethiol molecules on microcrystalline gold surface was first studied using a Quartz Crystal Microbalance (QCM). The adsorption of SAMs seems that the binding behavior of these molecules follows the Langmuir adsorption behavior. However, this behavior was only observed for a limited range of the concentration. Deviations inherent to the adsorption were noted during desorption (Kim et al., 1998, Pan et al., 1996). The equilibrium was demonstrated in the alkanethiol-gold system, the equilibrium was reached between the free gold sites and alkanethiol moieties. The adsorption free energies ΔG_{ads}= -5.5±0.4 kcal mol^{-1} for $n(C1_8H_{37}SH)$ and -4.4±0.2 kcal mol^{-1} for $n(C_8H_{17}SH)$ on the gold surface was calculated. The equilibrium state of the SAM formation is reached around one minute. The equilibrium state, during SAM formation proceeds at the edges of the formed SAM layer as well as the defect sites of the formed monolayer (Karpovich and Blanchard, 1994).

Because the adsorption mechanism of the alkanethiol from solution onto gold is an important issue the thermodynamics of the adsorption was studied to quantify the enthalpic and entropic force balance. In an adsorption study to with QCM, the entropy of adsorption (ΔS_{ads}) was found to be - 48 ±1 cal/(mol K). This entropy value is comparatively larger than that of liquid – solid phase transition; one can expect that entropy value for the adsorption of the alkanethiol on gold surface is regardless the chain length of the alkanethiol. Thus this larger change in entropy can assigned to the formation of the highly organized, two-dimensional crystalline array of thiol head groups on gold starting from the randomly distributed alkanethiol molecules in solution. Considering the thiol length independence of ΔS_{ads}, the enthalpy of adsorption (ΔH_{ads}) was calculated as - 19 kcal/mol (Schessler et al., 1996).

2.2.1.3 Kinetic models for the adsorption of SAMs

In adsorption studies kinetic models were used to determine the binding rate constants of thiol molecules to a give surface. Both in QCM and SPR studies Langmuir adsorption models were used to compute the association (k_a), dissociation constants (k_d) as well as the equilibrium adsorption constants (K_{eq}). Adsorption isotherms from the experimental data were fit using a simple Langmuir or a modified (i.e., bi-exponential) Langmuir adsorption model. The single isotherm is described by Equation (1) as:

$$\frac{d\theta}{dt} = k_a(1-\theta)C - k_d\theta \qquad \textbf{(2.1)}$$

Here, θ is the fraction of the available sites that are covered, k_a, and k_d are the association- and dissociation-rate constants, respectively, and C is the concentration of the thiol molecules adsorbed on gold surface (molar units). This model equation describes the increase in the surface coverage of a given molecule on a defined surface as a function of time and concentration (Karpovich, 1996). This equation explains adsorption of one molecule at one site type model. Towards the model a number of array of adsorption sites are defined on a surface, as the model interacts with the surface, the sites on the surface is filled by one by. The model assumes no intermolecular interaction as well as no heterogeneous surface. Also not any kind of mass transfer limitations and diffusion of the adsorbed molecule were considered. In most of the studies the Langmuir equation is modified, by considering surface topography and binding topology of the molecules adsorbed on a defined surface (Tamerler et al, 2005).

2.2.1.4 Thermodynamic models for the adsorption of SAMs

Thermodynamic analysis of the adsorption of chemical and biological molecules was carried out to explain the binding mechanism of a molecule to a given surface. Thermodynamic analysis of a binding event gives the opportunity to have an idea about the mode of binding. Van't Hoff equilibrium binding analysis of the equilibrium binding constants yield in the calculation of the thermodynamic constants, such as enthalpy, entropy and binding free energies. The surface based thermodynamics analysis uses the kinetic data to determine the thermodynamic constants. The equilibrium binding constant (K_{eq}) or equilibrium dissociation

constant (K_D) are used for computing the binding free energies using the following equation:

$$\Delta G = -RT \ln(K_{Eq}) \quad \textbf{(2.2)}$$

and, since

$$\Delta G = \Delta H - T\Delta S \quad \textbf{(2.3)}$$

by substituting the equation 2 into the equation 3. The Van't Hoff relationship can be defined as: ,

$$\ln(K_D) = (\frac{\Delta H}{RT}) - \frac{\Delta S}{R} \quad \textbf{(2.4)}$$

and from a plot K_D versus 1/T one can perform the calculations of ΔH and ΔS (Myzska et al., 2002, Dan et al., 2002).

2.2.2 SAMs in nano- and biotechnological applications

SAMs have found a large area in application, starting from surface modification of the thin films and nanostructures for building model surfaces to study biological interactions. Nanoparticles are important tools for the nanotechnological and biotechnological applications. They are colloidal systems; their shape is controlled by their size. Nanoparticles are unique structures with their optical and reactive properties with their large surface area. In nanoparticles with a size of ~2 nm most of the atoms are interfacial. This means that most of the atoms are exposed to the surroundings. This makes nanoparticles very reactive. The electronic states of the interfacial atoms of nanoparticles influence their chemical, electronic and optical properties (Love et al., 2005).

During the interaction of the SAMs with nanoparticles, chemistry is the main driving force and this process is independent from the size of the nanoparticles. SAMs can function by blocking the reactive surfaces of the nanoparticles (Templeton, 2000). They present new functional chemical groups on the surface of nanoparticles. To structure tailored and controlled surfaces on nanoparticles, functional groups on SAMs are important. Tailored organic surfaces of nanoparticles are important and useful for the application of the nanotechnology in many different branches of technology; one good example can be the immunoassays (Love et al., 2005).

Surfactant molecules play a crucial role in the synthesizing of the nanoparticles. They lower the interfacial energy by inhibiting the reactivity of the surfaces of the formed nanoparticles, during the nucleation of the nanoparticles. This fact was utilized to control the size and corresponding shape of the nanoparticles to be formed (Peng et al., 2000; Manna et al., 2000). Due to this chemical reactivity, thiols can be considered a different subclass of surfactants. By adjusting the nucleation rate and growth rate of the nanoparticles thiols can control the size and shape of the nanoparticles (Lee et al., 2002; Lee et al., 2003). Each of thiols can bind to a certain facet of the crystals and so they retard the growth of the nanoparticles at the plane by lowering the free energy at that plane. Using different thiols preferring different planes of crystals to bind, one can easily produce nanoparticles with various different sizes and shapes. As well as the type of the thiol molecule used, the concentration of the thiol molecules play an important role on the final shape and size of the nanoparticles, which can be followed in the Figure 2.7 (Hostetler et al., 1999; Murayama et al., 2004).

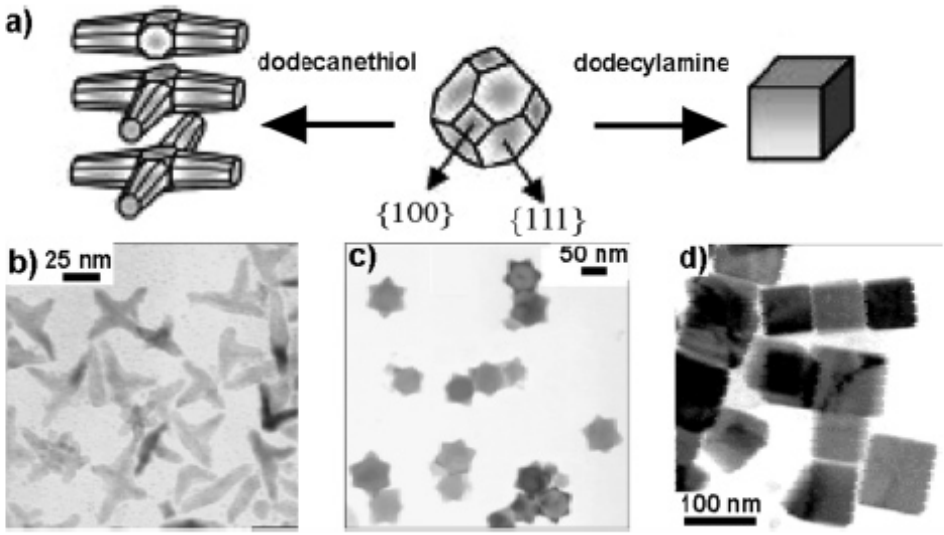

Figure 2.7: (a) The effect of the different types of the thiols on the shape of the PbS nanocrystals. TEM images of the nanoparticles formed: (b) rod based PbS multipods catalyzed by dodecanethiol, (c) star shaped nanocrystals pf PbS again in the presence of the dodecanethiol and (d) cubical nanoparticles formed in the presence of dodecylamine (Lee at al., 2002).

SAMs can also be used to functionalize the surfaces of the nanoparticles in different ways, the main strategies can be; (1) synthesizing the nanoparticles using thiol, (2) exchanging the existing ligand thiol molecules with another functional end group or modifying the thiol with an interfacial reaction. The last one is especially important

when a certain molecule is conjugated to the nanoparticles. One need to activate the thiol groups by a chemical reaction and later another chemical reaction should be employed to be able to synthesize nanoparticles with a desired surface modification (Marubayashi et al., 2003, Shon et al., 2001).

SAMs has been utilized in other applications for both activation and modification of the nano structures to enhance the properties of the overall structure. Nanorods are interesting structures for the physical properties that they offer. In literature there are many applications for the application of the nanorods, and these applications are mainly depend on the orthogonal functionalization of different sections with different SAMs. As an example for the bar-coded structures of Ni segments on Au nanorod can be given. In these structures his tagged peptides and protein can be delivered in a targeted manner on Ni segments via the -COOH groups decorated on native oxide of Ni (Salem et al., 2004).

Arrays of nanostructures (hexagonal and triangular shapes) can be produced by masking a solid support using polystyrene and silica beads. After deposition on top of these beads and later removing the beads by a mechanical effect, an array of immobilized nanoparticles in triangular shapes was formed. Van Duyne and his coworkers have already showed how to control and modify the size and shape of these nano structures on the solid surfaces, the AFM image and a representative adsorption curve of such an array is given in figure 2.8 (Haynes et al., 1999). This nano features found to have interesting optical properties. Adding SAMs on this nano features creates a shift in localized surface plasmon of the triangular structure. After the assembly of SAMs on the surface, a further activation of the SAMs enables one to be able to immobilize different biological entities on a biosensor surface (Jensen et al., 1999; Jensen et al., 2000; Malinsky et al., 2001).

Another interesting application of the SAMs is sythesis of the core-shell (silica/gold) nanoparticles for killing the tumor cells in the body. In this approach Hallas and her coworkers first immobilized nanoparticles from gold colloids on a silica nanoparticles surface through electrostatic interactions, later the additional gold nanoparticles enables the growth of the silica nanoparticles through fusion, and these nanoparticles were later coated with a PEG-SAM layer to prevent the body to exhaust them from the circulation from the body (Westcott et al., 1998; Averitt et al., 1999).

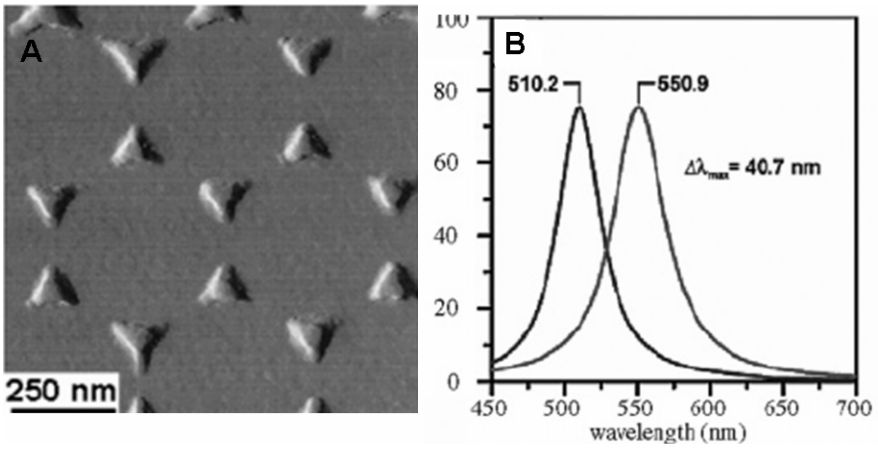

Figure 2.8: A) Tapping AFM image of silver nanoparticles formed on silica surface by nanosphere lithography. B) UV-Vis spectra of an individual silver nanoparticle after and before modification with SAM, on the array of nanoparticles seen on A. (Haynes et al., 1999)

After the delivery of core-shell nanoparticles in the body, near infrared light is used for local heating of these nanoparticles and thus killing the tumor cells (Jackson et al., 2001; Hirsch et al., 2003).

2.2.3 Biological applications of SAMs

SAMs were used in many different applications in biology. First they were used as model surfaces to mimic the biological membrane. The biological membrane is known to be a naturally occurring nanostructure with complex and dynamic behaviors. Cell membranes composed of supramolecular assemblies of proteins, glycoproteins and large oligosaccharides bound or embedded in lipid bilayers or protein coat. There are many cell membrane bounded structures which are functioning towards the fundamental processes of the cell. Therefore, to study the dynamic system like a cell membrane it is crucial to create self assembled structures. At this point SAMs offer a wide range of compatibly properties to mimic the functionality and structure of the cell membranes (Xiong et al, 2001, Xiong et al., 2002). SAMs are formed through self assembly; they are compatible with many analytical techniques (SPR, QCM, FTIR and AFM). Another advantage they are not affected by the mass transfer limitation compared to that of thick gel structures. But the main disadvantage of the usage of the SAMs is their static nature; one should remember that cell membrane is not that static (Mrksich et al., 1995; Marx, 2003).

Nonfouling surfaces are another area where SAMs are mostly used. These surfaces are characterized with their resistance to non specific adsorption of especially proteins. The alkanethiol groups are forming very densely packed structures on the gold surface and the individual molecules of thiols are known to get the same molecular conformation. In the case of the non fouling surface, ethylene glycol end group adapts to a helical conformation. These structures cause repelling the water molecules because of their high degree of hydrophobicity (Mrksich et al., 1997; Kingshott et al., 1999).

As another application of SAMs they are used in forming arrays of biomolecules. They were used as molecular linkers for this purpose. These kinds of assemblies are important, especially to explore the basic biology of ligand –receptor interaction, enzymatic activities and screening libraries of potential drugs. Some of the commonly immobilized biomolecules are DNA, proteins, carbohydrates and antibodies (Riepl et al., 2002; Culha et al., 2003). Beside the immobilization of the proteins and biomolecules, SAMs can also be utilized for the immobilization of the cells after a chemical modification with certain molecules cells can interact with them.

2.3 Inorganic Binding Peptides and Proteins

Self assembled monolayers of different kinds of chemical materials have been visited in previous sections. Although they promise wide range applicability, there are some fundamental challenges that these linker molecules cannot achieve. The major challenge is the large scale fabrication of nano and micro structures in a controlled and specific fashion. This challenge can be succeeded by taking the advantage of molecular biomimetics.

In the field of molecular biomimetics, formation of novel hybrid materials can be realized by incorporating proteins and peptides into material systems. And by using the molecular recognition capabilities of the proteins one can resolve the problems during the assembly of the nano and micro structured materials (Sarikaya et al., 2003, Tamerler, 2009). Molecular biomimetics offer three solutions, for the problem to control the fabrication of large scale nano and micro structure in an ordered fashion, the first one is the inorganic binding peptides and proteins are selected and designed at the molecular level through genetic engineering, secondly utilization of

these peptides and proteins as molecular linkers to assemble proteins, nano entities and polymers on molecular targets and lastly biological molecules self are assembled and co-assembled into the ordered, hierarchical structures. This approaches promise us to create functional, ordered structures with a bottom up approaches like the ones exists in the nature (Sarikaya et al., 2003, Sarikaya et al., 2004, Tamerler , 2009).

2.3.1 Inorganic binding proteins and peptides

In nature hard tissues such as bones, teeth and shells are formed by using inorganic and organic materials together. This process has been carried out for million years. Natural hard tissues are known to be tough and strong enough to overcome mechanical pressures. Comparing the natural hard tissue with the man made technological ones, one can easily differentiate the uniqueness of the natural hard tissues. The growth of these hard tissues are mainly controlled and directed by soft materials. Basically these soft materials are biomolecules such proteins, carbohydrates and lipids. Looking into the construction process of the natural hard tissues the excellence of the production of the natural hard tissues can be well understood. However, traditional manufacturing methods generally involve high temperature and high pressure processes (Sarikaya et al 2003). Proteins are also functioning in the formation of the biological hard tissues. Proteins performing their activities through binding to the minerals and so they are controlling the growth of the mineral crystals or they function as framework proteins, in this case they serve as scaffold for minerals to deposit (Sarikaya, 1999;; and Long et al, 1998; Weiner, 1978).

2.3.1.1 Inspiration from nature: inorganic binding proteins

In living organism there are many different compartments which are composed of different biomaterials, which are formed by active inorganic binding proteins. There are many different samples for this hard tissues formed by this natural inorganic binding proteins. The shells of marine organisms, teeth and bones of the mammalian organisms and even magnetic nanoparticles in magnetotactic bacteria are formed by these inorganic binding proteins. There have been a number of different attempts made to characterize and extract the inorganic binding proteins from natural sources. In some case these proteins have been utilized in "*in vitro*" applications. Silicatein is

a protein extracted from the silica spicules of sponge, following the characterization of the protein, this protease like protein was found to synthesize silica in the presence of tetraethoxysilane (Shimizu et al, 1999, Cha et al., 1999). Another characterized silica forming groups of peptides are silaffins which found to play a critical role in the formation of the nano structured biosilica in diatoms. In silaffin group natSIL-1 and natSIL2 are capable of silica formation from silicilic acid, but these two need to be phosphorylated for silica formation activity (Poulsen et al., 2003). Calcite and calcium carbonate polymorphs are found in the composition of the marine organism. A calcite forming protein group from *Haliotis rufescens* was extracted from the shell of the organism, and a biomineralization assay was carried out using the extracted protein, it was observed that the protein cascade was able to biomineralize calcite form the precursor materials (Walters et al., 1997). Another interesting protein cascade was found in magnetotactic bacterium, this organism has nanosized magnetite particles, which are used by the organism for magnetotaxis. A protein cascade called magnetosome defined to be responsible for the formation of the magnetic nanoparticles with controlled morphology. The mechanism and genetic pathway of the formation of the magnetite crystals in the magnetosome of this bacterium was investigated. Today the genetic circuit and the proteins involved in the magnetite formation in magnetotactic bacteria was defined (Matsunaga et al., 2003, Schuler, 2008). Beside extraction of magnetite binding protein from the organism itself, also recombinant fusion proteins with magnetotactic protein Mm6 were constructed to mineralize magnetite from ferrous oxide (Amemiya et al., 2007). One can extract different inorganic binding proteins from the samples; however there are many disadvantages of this approach. In biomineralization of assembly processes, most of the time there is a group of protein cascade in a matrix, working in a cooperative action. Consequently, it can be labor intensive and time consuming to identify and characterize each of these proteins. To achieve these combinatorial biology and chemistry approaches have been employed to design and select inorganic binding peptides. These are called as the **G**enetically **E**ngineered **I**norganic binding **P**eptides (GEPI) (Sarikaya et al., 2003).

2.3.1.2 Combinatorial selection of GEPIs

In order to utilize biomolecules as molecular building block in material research many attempts have been made. Molecular biomimetic is one of the recent ones, the

idea is use the information from nature and molecular evolution to create man made molecules that can recognize inorganic surfaces. In living organisms' proteins, peptides, carbohydrates play a basic role in the formation of the biominerals. The production and assembly of these biological molecules is controlled by the genetic networks of the organisms. Through molecular recognition biological macromolecules serve as key molecules for the formation of the biological hard tissues. Biological macromolecules are able to produce large scale microstructures and nanostructures. In technological applications, towards functionalization of the materials surfaces and production of the large scale nano structured materials we can mimic the nature at molecular scale by employing proteins and peptides (Sarikaya et al., 2003, Sarikaya et al., 2004).

To create man made peptides, combinatorial approaches have been employed. Cell surface display (Wittrup, 2001) and phage display technologies (Smith, 1985) were employed for the selection of the GEPIs. These combinatorial libraries gave us the opportunity to select the high affinity peptides from a large population by a fast evolution approach. This can be described as mimicking nature to select and screen peptides with a designed functionality (Sarikaya et al 2003; Sarikaya 2004).

Cell surface display and phage display are the most common approaches that have been utilized in selection and screening of the peptides with the affinity towards a material. In both cases the approaches are same; a chimeric protein that consists of a target peptide genetically fused into the structure of a protein that naturally occurs on the surface of the bacteriophage or cellular organism is used for screening. In phage display the chimeric protein is the pIII coat protein of a M13 phage. This is the most commonly used commercially available system. In cell surface display the flagellin is used to display the desired sequence of the peptide, or another membrane protein can achieve this, in the first isolated inorganic binding peptide, maltoporin (which is a protein takes place in the transport of maltose in to the cytoplasm) was used as the chimeric protein to insert the peptide of interest to create a library of the peptide population for further screening and selection (Brown, 1992; Sarikaya et al., 2004; Tamerler et al., 2006; Tamerler and Sarikaya, 2007).

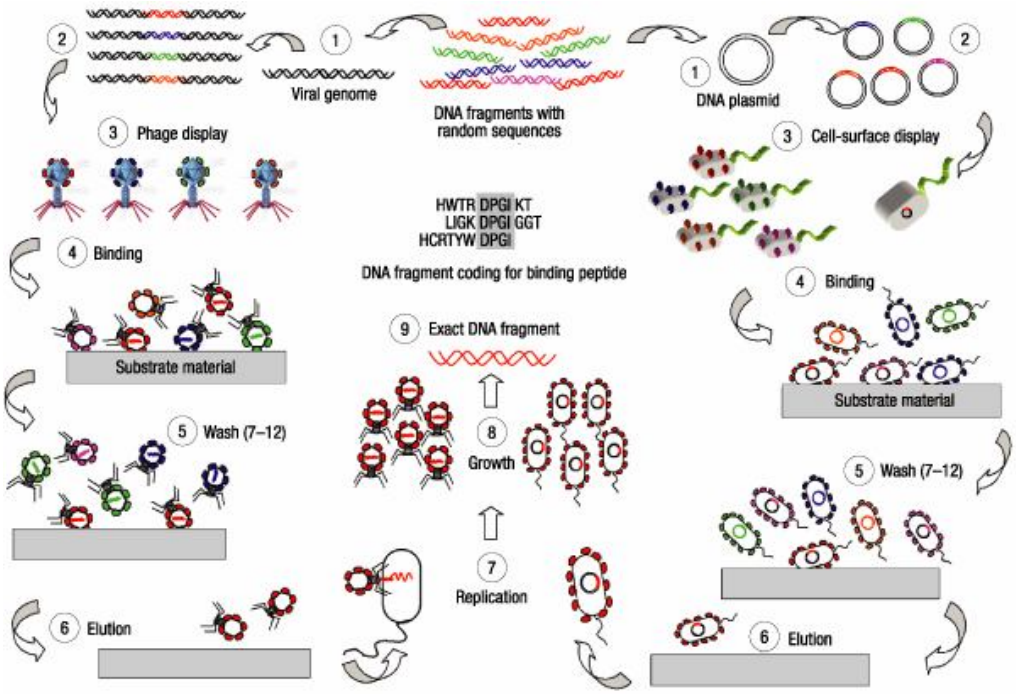

Figure 2.9: General protocol for the selection of the inorganic binding peptides using cell surface and phage display technologies (Sarikaya et al., 2003).

Peptide libraries have been used in selection of the many different ligand molecules towards certain biomolecules. Peptide libraries have been also used for the selection of the peptides with the affinity towards certain desired solid surfaces (Brown, 1997). In selection process, first, the peptide libraries are brought in contact with the material of interest, following an incubation period, nonbinders are removed by washing. Later, the specifically bound cells or phage particles are removed by harsh washing and this cycle takes place for 4-5 times as shown in Figure 2.9. The peptide encoding organisms were removed from the surface and the genetic material from the organism was extracted. After the isolation of the genetic material, DNA is sequenced and following the sequencing of the chimeric protein, the peptide which enhanced the binding of the phage particle or the cell is subject to further characterization (Sarikaya et al., 2003; Schwartz and Baneyx, 2007).

Starting from the selection of the cell mutants which are specifically adhering on the material of iron oxide surface, many different materials were used in last decade to select peptides which are specifically bound on inorganic surfaces (Brown, 1992). Especially technologically important materials were utilized in this approach. Because these peptides offer a number of capabilities like self assembly and specificity, a high attention was paid from different branches of science. The

inorganic binding peptide were selected are: (1) metal binders, Au binding peptides (Brown, 1997; Slocik et al., 2005), Ag binding peptides (Naik et al., 2002), Pt binding peptides, Pd binding peptides (Sarikaya, 2003), Germanium binding peptides (Dickerson et al., 2004); (2) metal-oxide binders, SiO_2 peptides (Chen, 2006; Naik et al., 2002), Cu_2O binding peptides, ZnO binding peptides (Thai et al., 2004; Umetsu et al., 2005), TiO_2 binding peptides (Chen, 2006), Al_2O_3 binding peptide (Sarikaya et al, 2003), Ti peptides (Sano et al., 2005); (3) semi conductor binders, GaN, GaAs, ZnS, CdS binding peptides (Whaley et al., 2000, Lee et al., 2002; Flynn et al., 2003) (4) mineral binders; mica binding peptides (Donatan et al., 2008); calcite (Sarikaya et al., 2004) and hydroxyapatite binding peptides (Gungormus et al., 2008), and (5) zeolites (Nygaard et al., 2002) and carbonnanotubes (Wang et al., 2003).

The first isolated peptide is the iron oxide binding peptides, the iron oxide adhering cell were harvested and following the harvesting , enrichment protocols were applied to isolate the peptides responsible for adhesion on iron oxide were defined. Genetic analysis revealed from the shuffling experiments that RRTVKHHVN is the sequence for the recognition of the Fe_2O_3, as in the following adsorption experiments cells containing this sequence did not show an significant adhesion on other materials (Brown, 1992).

The selection of this peptide started a new era for the screening and selection of the inorganic binding peptides. Actually Fe_2O_3 is not a good material to start with, as the surface of this material is not well defined, it is not pure. So the second peptide selection was made for gold which is biologically inert and has a great importance in material science and other applications such as in microchip fabrication. The gold binding peptides were displayed as a fusion partner in the structure of the alkaline phosphatase, in other words it is not selected separately on the cell surface. This gold binding peptide carrying chimeric peptides were screened for their binding affinity directly on gold powder and gold film surfaces, later the most widely used inorganic peptide gold binding peptide (GBP) was isolated. The amino acid sequence of the gold binding peptide was given as MHGKTQATSGTIQS. Chimeric proteins of AP were not only constructed containing one repeat of the GBP, also different repeating units of GBP were inserted from one up to nine repeats. It was remarkable that increasing number of repeats caused a better adhesion on gold surface (Brown, 1997).

Following the Fe_2O_3BP and GBP, the following peptide was selected for the binding to GaAS from a commercial phage display library, and this was the first phage display selected peptide in the literature. The selection of these peptide were carried out using following GaAs(100),GaAs(111)B, InP(100) and Si(100) substrates, GaAs(111)B, InP(100) and Si(100). These substrates were used for a systematic evaluation of the peptide-substrate interactions. After the selection of these peptides, they were characterized using X-ray photoemission spectroscopy (XPS) and transmission Electron Microcopy analysis. These were the demonstration how the phage particles selectively bound on the surface GaAs compared to that of the gold or other compounds including GaAs, such as AlGaAs, AlAs (Whaley et al., 2000).

After this breakthrough in the selection and screening of the inorganic binding peptides many other peptides were selected. Excluding some of the preliminary work most of the selected peptides were not well characterized for their binding affinity in a quantitative manner. Most of the characterizations were carried out while the peptides were being displayed on the body of the phage particles.

2.3.1.2 Theoretical Design of GEPIs

GEPIs selected form combinatorial libraries are called the first generation of the GEPIs, however using the bioinformatics tool new generation of peptides, called *in silico* designed peptides were produced by means of computational tools (Oren et al., 2007). In this approach the function structure relationship of the GEPIs were utilized. This binding similarity in GEPIs is dictated by the primary structure of a given inorganic binding peptide. In computational biology, the alignment of protein is a key tool to find out the evolutionary relation between the proteins. This approach has been used to find out functional sites in enzymes, or it is used to find out the evolutionary conserved motif in various different proteins. In this approach different sequences were aligned using an optimization procedure to find out the most possible relative arrangement of the sequences (Needleman and Wunsch, 1970; Smith and Waterman, 1981). During the alignment of the protein sequences similarity matrices were used, which are formed to find homology and evolutionary similarities between the proteins. During the design of these matrices, the inputs form the natural evolution was used. However, in peptide design there is a need for new matrices for combinatorially selected inorganic binding peptides. The developed matrices were

used to produce in silico designed inorganic binding peptides with predictable functionality (Oren et al., 2007). This approach need some input data from experimentally selected peptide, once the inputs about the inorganic binding peptides are given, the matrices are able to create new *de novo* designed GEPIs

2.3.2 Characterization of genetically engineered polypeptides

One of the challenges in the characterization of the peptides is that most of the available methods are not suitable for probing the peptide-protein and solid surface interactions. Besides, most of them do not offer an analysis for a wide range of applications by utilizing many different materials. For this purpose the binding affinity of the peptides were carried out using different methods. These are qualitative and quantitative approaches. Qualitative methods are surface plasmon resonance, quartz crystal microbalance and atomic force microscopy, qualitative methods are fluorescence microscopy, cell culture counting. And classification of the peptides was carried out both for the peptides on host and synthesized peptides.

2.3.2.1 Characterization of the peptides on hosts

Inorganic binding peptides are screened and selected from the combinatorial libraries namely phage display and cell surface display as mentioned earlier. Selected peptides are classified for their binding strength towards their target material. The peptides on their host were classified using QCM-D, fluorescence microscopy and cell culture counting methods.

The binding classification of the Ti binding peptide -on its host phage- which is known to bind on Ti surface, a hexapeptide was first analyzed with a QCM-D sensor. The phage particles expressing the Ti binding peptides were caused to bind on the Ti coated sensor surface (Sano et al., 2003).

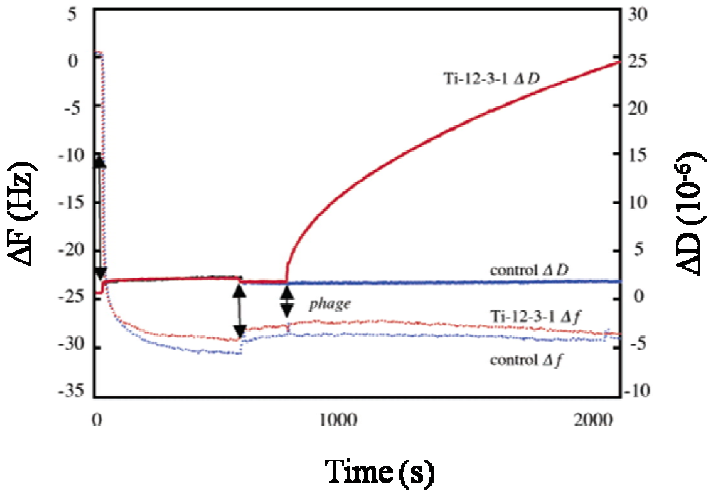

Figure 2.10: Comparison of a Ti binding and non-binding peptide using a quartz crystal microbalance in real time monitoring The change in the frequency and dissipation proves the strong binding affinity of the Ti binding peptide.

The effect of any amino acids in the peptide sequence was also tested by creating point mutations on host phage; here the effect of the arginine aminoacids on binding affinity was demonstrated. Beside this, a hypothetical binding mechanism was also suggested by just following the binding of Ti binding peptide encoding phage particles. In another similar study for monitoring the binding activity of the TiO_2 and SiO_2 binding peptide containing phage clones were investigated for their binding affinity as a function of pH and phage particles number. In this approach the authors have suggested that the number of the phage particles controls the orientation of the phage particles on sensor surface. This was directly controlled by the surface coverage of the phage particles at any time on the surface. So, the strong binders suspected to have a higher surface coverage compared to that of moderate or weak binders. This fact was also investigated by the change in the dissipated energy on the surface. Strong binding phage particles were vertically oriented (due to the higher surface coverage) and would have denser phage film as the weak binder formed looser film. By monitoring the effect of film density on the dissipated energy via QCM-D, the peptides were classified for their binding affinity (Chen et al., 2006).

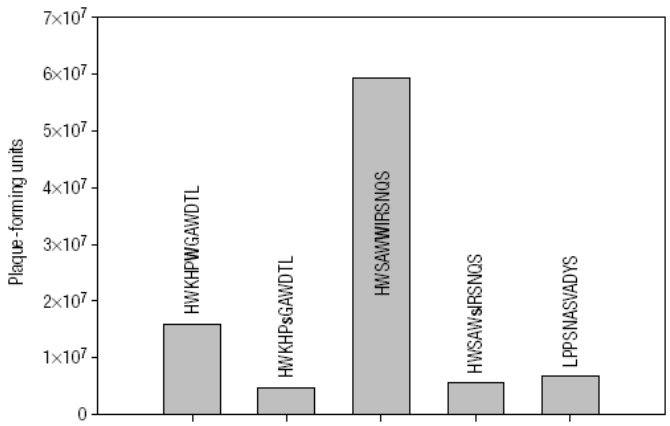

Figure 2.11: The comparison of the binding affinity of the carbon nanotube binding peptides upon the number of the bound phage plaques (Chen et al., 2006).

As an alternative but less accurate and shorter analysis technique, plaque counting assay was also carried out to determine the number of the binding phage clones containing the selected Ti binding peptide sequences. Ti particles in powder form were brought in contact with phage particles and later the unbound phages were pooled and the plaque forming colonies were counted and extending this procedure to all of the clones a comparison of the binding affinity for all of the clones was explored. Peptides with affinity to carbon nano tubes classified again using the phage plaque counting method. Each of the peptide's affinity was represented with theirs corresponding phage plaque numbers on agar plates. The comparison of the carbon nanotube binding peptides for their binding affinity on carbon nanotubes was given in 2.11 (Wang et al., 2003; Sano et al., 2005).

Another semi quantitative method to determine the binding affinity of the peptides in a qualitative manner as they were still on phage bodies is using fluorescence immunoassays. In this approach the phage first bound to the target material and following the washing steps the bound phages were labeled using a fluorescence dye labeled M13 phage antibody. By calculating the surface coverage of the phage particles a classification of the peptide is achieved in the case of Pt binding peptides and HABP peptides and AuBP (gold binding peptides) the fluorescence images are given in Figure 2.9 (Sarikaya et al., 2003; Gungormus et al., 2007, Hnilova et al., 2008).

2.3.2.2 Characterization of the synthesized peptides and peptide fused constructs

After characterization of the peptides using QCM-D, plaque counting or fluorescence microcopy, depending on the classification of the peptides they were synthesized either by using a chemical synthesis method or a biological synthesis method.

In the study of Ti binders, peptide sequence with the highest affinity towards Ti (TBP1- RKLPDAPGMHTW) was synthesized. This peptide was tested for its binding affinity by adsorption measurements of the unbound peptide on Ti particles in solution. A cross test was carried out on SiO_2 particles was carried out. The K_D values were calculated as 13.2±4 μM and 11.1±2.8 μM on Ti and silica respectively (Sano et al., 2005). In order to mimic the phage body the same peptide was inserted into ferritin molecules and the adsorption experiment was carried out using this cage shaped protein containing Ti binding peptide in its N terminus. The experiments were carried out using a QCM-D system, which uses a Ti coated crystal as substrate; the K_D values calculated for this time are smaller then that of peptide itself on Ti powder particles which were 3.82 μM and 4.44 μM for Ti and SiO_2 respectively. However, it is obvious in this case that the surface is not fully saturated, which can be an indication of that the when the Ti binding peptide is inserted into a designer protein the affinity of the peptide does not change (Sano et al., 2005).

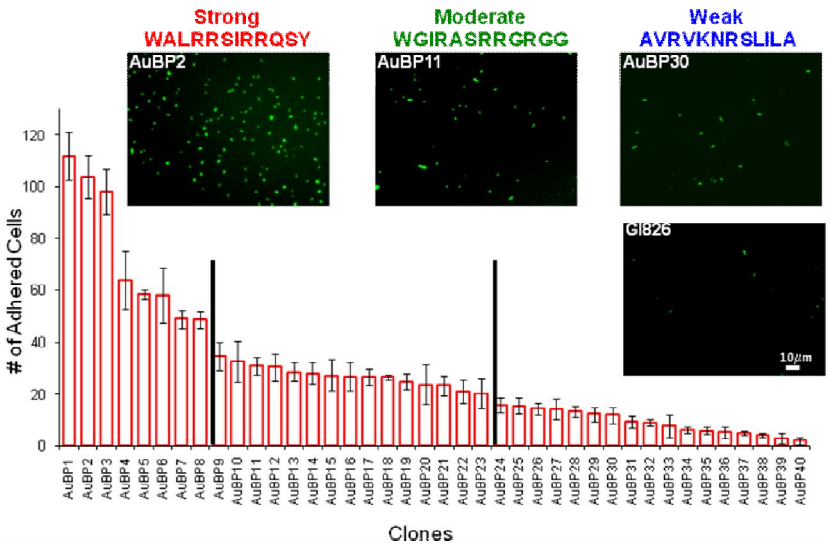

Figure 2.12: Binding classification of gold binding peptides selected from cell surface display library. The classification of the peptides was carried out upon the number of the adhered cell (Hnilova et al, unpublished data).

Affinity of Gold binding peptide was also determined using surface plasmon resonance spectroscopy (SPR) and QCM (Tamerler et al., 2006). The adsorption of the peptide was carried out not only using the original sequence of the gold binding peptide; instead the three repeat of the original sequence was used to determine the binding affinity of the gold binding peptide. The adsorption profiles of the gold binding peptide reveal that this peptide shows a two step adsorption. The K_D values calculated for GBP is 89 nM and 39 nM from QCM and SPR measurements respectively (Tamerler et al., 2006). This deviation may caused because of the different surface areas of the SPR and QCM sensor systems, which was also observed previously in the adsorption of the TBP inserted ferritin molecule (Sano et al., 2006).

2.3.2.3 Structural characterization of GEPIs

As a well known fact, proteins have primary, secondary and tertiary structures. The primary structure of the protein dictates the secondary and as well as the tertiary structures. And the protein folding is known to be the formation of the tertiary structure of the protein. Besides the hydrogen bonding, disulphide bonds are formed via the cysteines present in the primary structure of the protein. However inorganic binding peptides are 7-50 amino acids long. Most of them do not contain any cysteine residues, so these peptides do not have a tertiary structure. Protein folding is most important problem for the protein-protein interactions and molecular recognition (Voet and Voet, 2001).

To solve the binding mechanism problem some attempts was made and these studies can be classified in two main subtitles (1) the experimental approaches towards determination of the structural features of the inorganic binding peptides, (2) using the molecular modeling approaches.

Researchers have investigated the effect of Au^+ ions on the structural stability of the gold binding peptide. Gold binding peptide was tested in two different forms in this study. The original sequence and the three repeat forms of the original sequence of GBP were further characterized for the changes in their secondary structure in the presence of the Au^+ ions in solution. However GBP was not found to template gold nanoparticles from the Au^+ and thus no obvious changes was recorded in the secondary structure of the peptide. Both one and three repeats of the GBP were found

to be in labile and unstable form in solution. A further characterization of GBP using NMR was accomplished, -KTQATS- sequence and the -QAT- motif in particular, was found to be the Au^{+} interacting sites (Kulp et al, 2004).

In the naturally occurring protein from mollusk shell, the peptides responsible for the formation of the calcite was established to control the crystal growth by presence of unfolded polypeptide conformation, electrostatic surface pockets, and interactive sequence clustering (Collino and Evans, 2007).

In the carbon nanohorn binding peptides, like the gold binding peptide it was explored that the carbon nanohorn binding peptides were labile and possesses an inherent conformational instability (Kulp et al., 2005).

Besides these experimental studies conformational analysis of the inorganic binding peptides by means of computational methods were also explored by different researchers on different peptides. The first attempt was made by Shulten *et al.*, in their research they tried to model the possible orientation of the gold binding peptide on gold surface. The energy of the GBP was minimized and later the minimized geometry was manually positioned on a gold surface. During the positioning of the GBP on gold surface, as much as possible number of hydroxyl groups was positioned on the GBP face were aligned top plane of the Au atoms. Later a preconditioned water box added to the system and the overlapping water molecules were removed manually. The NAMD2 program was used and the force field was selected as the CHARMM26. The results of the prediction resulted in a periodic structure of the hydroxyls on the surface of the anti parallel sheet that is responsible for the binding on the gold surface. A similarity was also found between these systems and naturally occurring $CaCO_3$ binding peptide, as well as the antifreeze proteins with tandem repeats onto ice crystals (Braun et al., 2002).

Another study to understand the binding mechanism of the GEPIs to metallic surfaces, was carried out using platinum binding GEPIs. To understand the binding mechanism of the platinum binding peptide and to differentiate the affinities of these peptides, peptides from three different classifications, strong SD152 (PTSTGQA) and SD60 (QSVTSTK); moderate binders, SD128 (LGPSGPK); and weak binders, SD1 (APPLGQA) and SD6 (LNDGHNY) were further investigated. These peptides were first energy minimized using a modeling program called HyperChem, then

energy minimized structures were brought in contact with the platinum surface. The conformation search module was employed for the most relaxed structure of the peptide on the surface of the platinum. CHARMM22 force field was used during the calculation of the energies. It was concluded; even the strong binders on the platinum surface did not show a significant consensus. Each of the peptides displayed significant differences in their conformation on the platinum surfaces. Oxygen and hydrogen in hydroxyl groups may be suspected for the strong binding of the peptides, however there cannot be a conclusion driven from the weak binders. All these studies were carried out in vacuum conditions. Surprisingly the peptides showed a similar architecture on the platinum surface they look like to be adsorbed between the grooves of the platinum atoms. This structure was called as the molecular polypod, which can be seen in the following Figure 2.13 (Oren et al., 2005).

A Molecular dynamic simulations were accomplished towards understanding the effect of the -TST- region displayed mostly in the strong platinum binding peptides. This time Molecular dynamic simulations were carried out in the presence of the water molecules, and platinum surface. However any rearrangements in the platinum surface were not considered upon the interaction with the platinum binding peptide. It was found that --TST- region makes more intermolecular hydrogen bonds with the surrounding water molecules

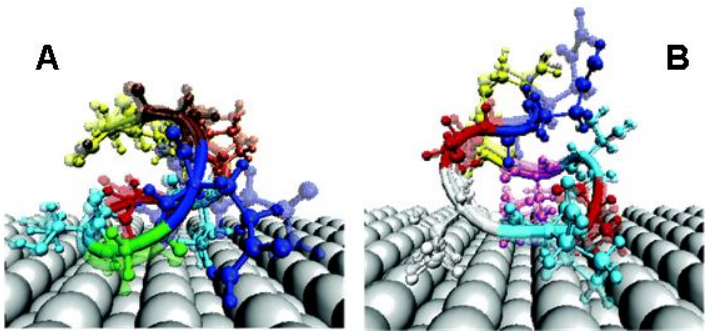

Figure 2.13: The conformations o a two strong Platinum binding peptides, (A) SD 152 and (B) SD 60 on platinum surfaces (Oren et al., 2005).

As some of the data suggest that -TST- region is not only important part during the binding, it was also observed that in the presence of the platinum surface -TST- region moves in a flexible manner. Flexibility seems to be an important factor. One of the remarkable finding can be summarized is entropy loss due to the reduce flexibility may play an important role in the binding and stability of these peptides.

The superimposed snapshots from different time points during the simulation was given in Figure 2.14 (Kantarci et al., 2005).

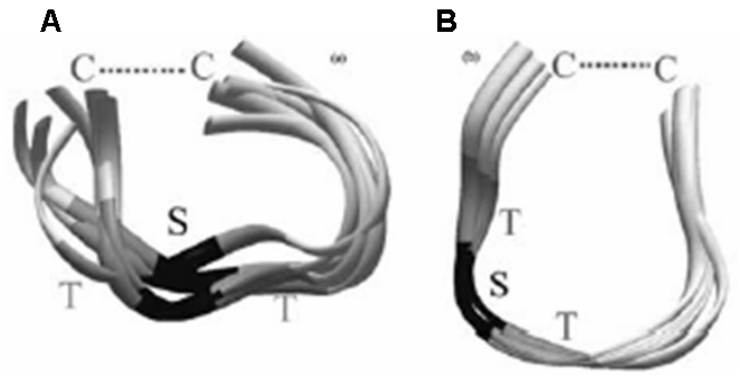

Figure 2.14: Monte Carlo simulations of SD152 in the absence (A) and presence (B) of the platinum surface (Kantarci et al., 2005).

SWCNTs (single wall carbon nanotubes) are in interest from technological viewpoint. *Walsh et al*, studied the binding mechanism of SWCNT binding GEPI, they used a implicit salvation method by employing the AMOEBAPRO force field. The main advantage using this force field is that it was approved for the electron density theory calculations. Results of this study suggested that the hydrophobic residues of the peptide tend to interact with the surface of the CNT. Computational study validated the experimental results, by means of classification of the peptides. Another observation was that the affinity of strong binders is coupled totally with the conformational flexibility of the peptide. A snapshot from the simulation was given in below Figure 2.15 (Tomasio and Walsh, 2007).

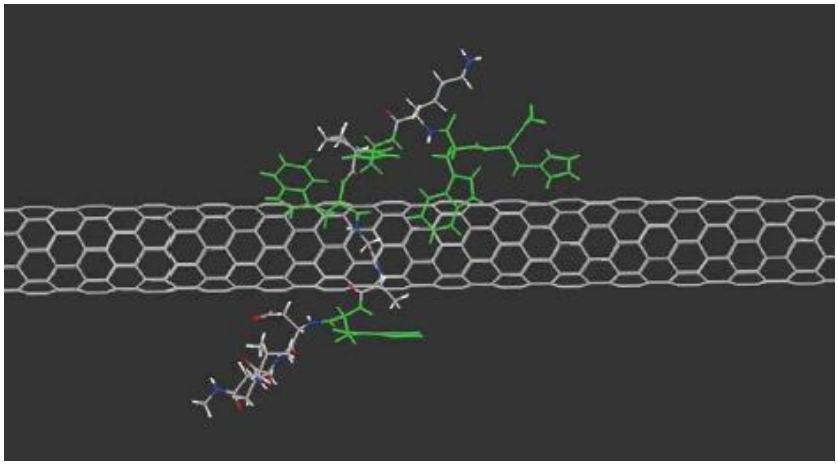

Figure 2.15: A snapshot from the simulation of the interaction of CNB peptide and carbon nanotube, the green labeled residues is tryptophan and histidine (Tomasio and Walsh, 2007).

2.3.2.4 Nanotechnological and biotechnological application of the genetically engineered peptides

In last decade inorganic binding peptides were screened and selected for various different materials. The rough characterization of these peptides was carried out using quick and dirty experimental methods. Despite the lack of detailed analysis and understanding of the binding-adsorption mechanism of the inorganic binding peptides some of the applications worked well. However, to be able to control the assembly of GEPIs, we should be able to control the affinity, specificity and conformational behavior of GEPIs. In the context of affinity, specificity, structural features of the GEPIs, we tried to find out hypothetical explanations for the interaction of GEPIs with inorganic surfaces. We have also explored some of the new nanobio- and biotechnological applications of GEPIs.

So far inorganic binding peptides were utilized in various different applications. Nanoparticle synthesis and to control the morphology of the biominerals from the salt solutions of the metal and precursors of the minerals, metal oxides were succeed and so called functions of the inorganic binding peptides.

Beside the nanoparticle synthesis the main utilization of the inorganic binding peptides is as self assembled monolayers for the directed assembly of the nanoparticles and proteins.

As an interesting and proof of principle approach, to build a self assembled layers of quantum dot nano emitters. A phage display library was first screened towards identification of ZnS and CdS binding peptides. Following the identification of these peptides, the precursors of the ZnS were mixed with the ZnS binding phage particles. The ZnS (ZnCl2 and NaS) later CdS ($CdCl_2$) precursors were added in the solution. The assembly of the CdS/ZnS on phage particles with affinity towards both ZnS and CdS was achieved. CdS binding phage particle catalyzed formation and assembly of quantum dot (CdS/ZnS) was achieved in a systematic manner with a purely biological approach. This approach can be scale up for the formation of the phage particle based quantum dot nanowires with advanced and desired functionality (Mao et al., 2003).

In most of the cases, GEPIs are supposed to be used as synthesized peptide not its form displayed on phage particle. So, the peptides can be used either as only

synthesized sequences or they can be inserted in the structure of a functional protein (e.g enzymes). The fusion protein consists of the GEPI and a functional protein is called as designer protein.

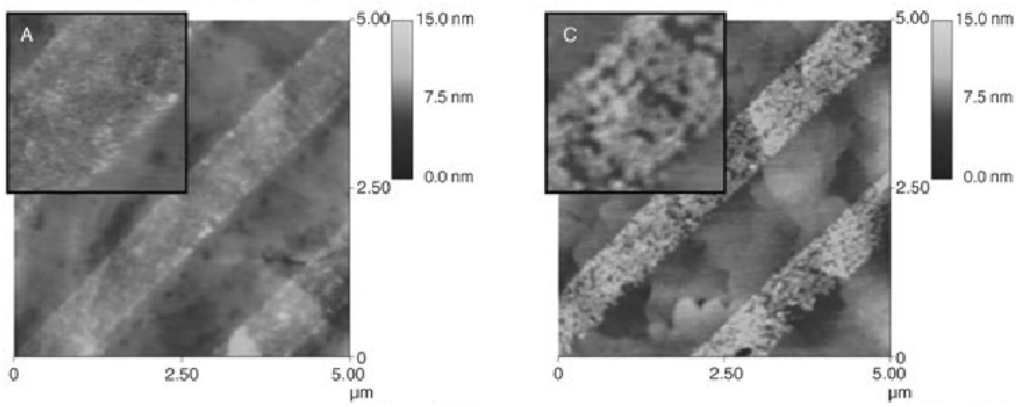

Figure 2.16: (A) The assembly of the gold nanoparticles on MMPA conjugated GBP on gold surface. Nanoparticle film is dense. (B) The assembly of the gold nanoparticles on GBP on gold surface. The nanoparticle film is looser and compared to the A (Zin et al., 2005).

Gold binding peptide is shown to bind to the gold surface; *Zin et al* used them to assemble gold nanoparticles to create ordered arrays of nanoparticles. However, the main concern was after the assembly of the GBP on a gold surface, can it still conserve its gold binding activity? To see this effect two different setups were made, (1) gold binding peptide was directly assembled on gold surface via micro contact printing, (2) first the assembly of a thiol molecule MMPA was carried out through micro contact printing and later the GBP was stacked to the MMPA thorough its N terminus via a Schiff base reaction. Later the gold nanoparticles were assembled on this chemically conjugated GBP on gold surface. The comparison of the first and second approaches revealed that the direct binding of GBP on gold decreases it capability to capture gold nanoparticles, as the chemical conjugation enhances the ability of GBP to capture gold nanoparticles, the nanoparticle films formed are shown on Figure 2.16 (Zin et al, 2005).

In a complimentary study, GBP was utilized for directed assembly on a multi-material patterned surface. The idea is to exploit not only the affinity also the specificity of the GBP. Right after the assembly of the biotinylated GBP (bioGBP) streptavidin coated Q-dots (SAQD) were immobilized via the biotin streptavidin linkage. After removing the non specifically interacting molecules gold surface was

detectable under fluorescence, the assembly is given in Figure 2.17 (Tamerler et al., 2006).

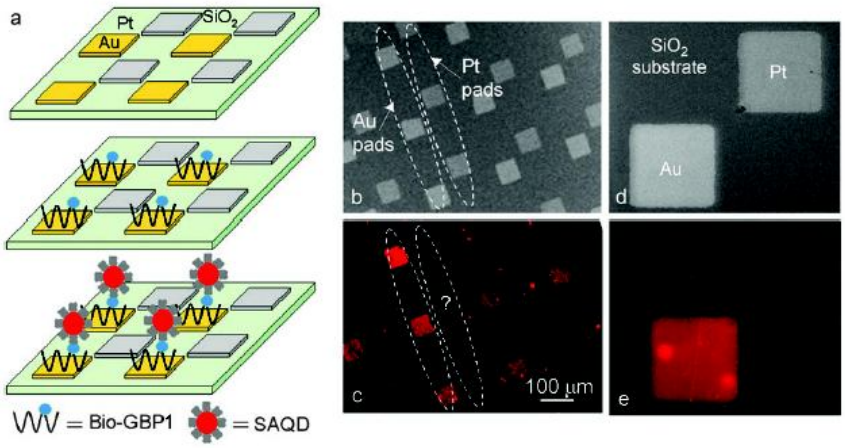

Figure 2.17: (a) Schematic of the assembly of the bioGBP on gold surface. (b) Bright field image of the patterned surface (c) Florescence image of the assembled Qdots on bioGBP decorate surface. (d) Bright field image of Pt/SiO_2/Au patterned surface (e) Florescence image of the assembled Qdots on gold surface not on silica or platinum (Tamerler et al., 2006a).

As we summarized above GBP was exploited in many different applications because of the wide range applications of the gold in nano- and bio- technological research areas. Utilizing GBP as a part in construction of a biosensor was carried out by fusing GBP in the permissive sites of the Green fluorescent protein (GFP). GFP-GBP designer protein was constructed and the activity of these proteins was monitored by its binding activity on gold surface, by its activity to form gold nanoparticles from Au^{+} solution and lastly it was used for *i*SPR (imaging SPR) and the thickness of the adsorbed protein layer of GFP-GBP was monitored (Park et al., 2006).

To control the emission of the Q dots depending on their distance from the surface of gold, GBP binding peptide was utilized as linker molecule. GBP was not only utilized as a molecular erector, it had been shown to be a good molecular linker, to immobilize nanoparticles (Zin et al., 2006).

Ti binding peptide was made another breakthrough towards using the GEPIs in nanotechnological applications. Ti binding peptide is called as a bi-functional peptide, as it was shown to control mineralization of the silica and it binds to Ti. Ti binding peptide was inserted in ferritin molecule and ferritin-TBP designer protein was constructed. Ferritin is engineered from its N terminus as it was demonstrated

that TBP does not loose its Ti binding activity after insertion into N terminus of the ferritin cage protein. Ferritin has a hollow structure; this hole can be filled up with Fe, Co and CdS nanoparticles. The inside of the ferritin molecule is known to be positively charged and the charge density allows non specific loading of nanoparticles inside the ferritin. So, to utilize this property of the ferritin-TBP, a Ti substrate was first decorated with TBP1 and later tetramethyl ortosilicate (TMOS) was added on top of the TBP, and TBP catalyzed the silification of the TMOS on Ti binding peptide decorated surface. Later the Fe nanoparticles filled with ferritin was assembled. The second layer, third and fourth layers was also formed by the silification activity of TBP by using TMOS.

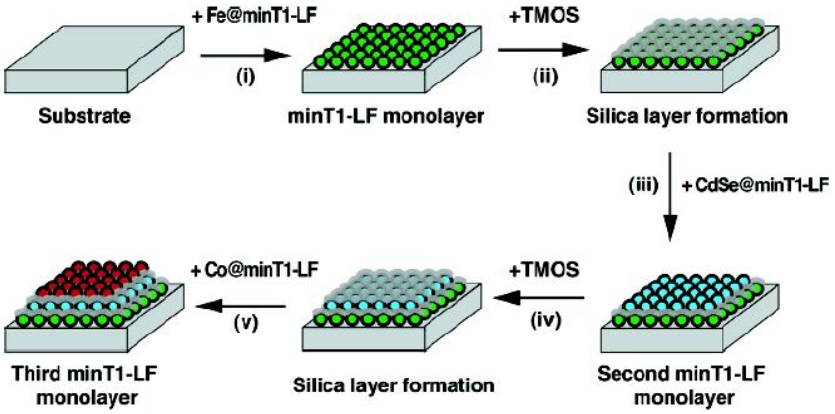

Figure 2.18: (i) Adsorption of the Ti binding peptide on Ti surface. (ii) addition of the TMOS and silica layer formation (iii) assembly of the CdSe filled, Ti binding peptide inserted ferritin on silica surface (iv) addition of TMOS and formation of the second silica layer (v) assembly of the CdSe filled, Ti binding peptide inserted ferritin on silica surface (Sano et al., 2006).

After silification each layer was decorated with Co filled ferritin particles and CdS loaded ferritin molecules. The schematic representation of the formation of Ti binding peptide enhanced layer by layer assembly is given below in Figure 2.18 (Sano et al., 2006). This was a perfect demonstration of the heterogeneous multilayer nanostructures, which can lead for the formation of the future batteries and memory elements and biosensors. After carrying out this study the challenge was to create the same assembly on a patterned surface.

Another idea for biotechnological application is to use the GEPIs as purification ad immobilization tags, for this purpose mainly some of the publicly available peptides were used. As a case study a phage display selected sapphire binding peptide was

genetically fused in the structure of the maltose binding peptide. Peptide mediated self assembly of the maltose binding peptide was demonstrated. The sapphire binding peptide fused into maltose binding protein was utilized for the construction of a biosensor for future applications (Krauland et. al, 2007).

To identify and detect the amount of a dioxin precursor, 2, 4-dichlorophenol, which is widely processed during the production on many industrial products such as dyes and polymers, a GEPI enhanced biosensor was developed. The biosensor systems utilized GBP to modify the gold sensor surface. After the modification of the gold sensor surface with GBP, adsorption of immobilized amount of 2, 4-dichlorophenol antibody on SPR gold surface was dramatically increased. It was observed that modification of the gold surface with GBP enhanced the limit of detection of the biosensor by a factor of five. The layer by layer assembly of GBP and antibodies are represented in Figure 2.19 (Soh et al., 2003).

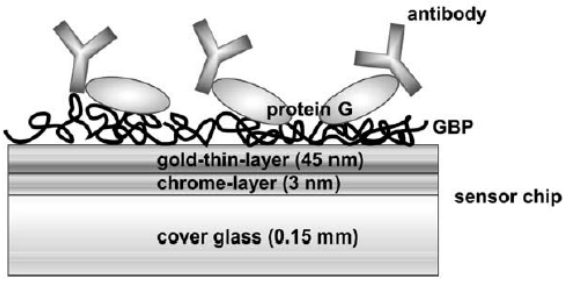

Figure 2.19: Layer by layer assembly of GBP, protein G and antibodies on SPR sensor surface, the chip composed of 45 nms of gold and 3 nms of CrO_2 (Soh et al., 2003).

Biomineralization is the process for the formation of mineral structures by the help of biomolecules. Previously we mentioned about some of the well known samples for the biomineralized structures such as bones and teeth. Molecular recognition is an important concept in the biomineralization activities. Though inorganic binding peptides are also selected for their molecular recognition capabilities; they are also tested for theirs biomineralization activities.

The first studied peptide is GBP as a fusion peptide in chimeric alkaline phosphatase (AP). It was shown that chimeric AP–GBP catalyzes the formation of the large flat gold nanoparticles, in the absence of any other reducing agent. TEM images of the formed gold nanoparticles are given in Figure 2.17 (Brown et al., 2000).

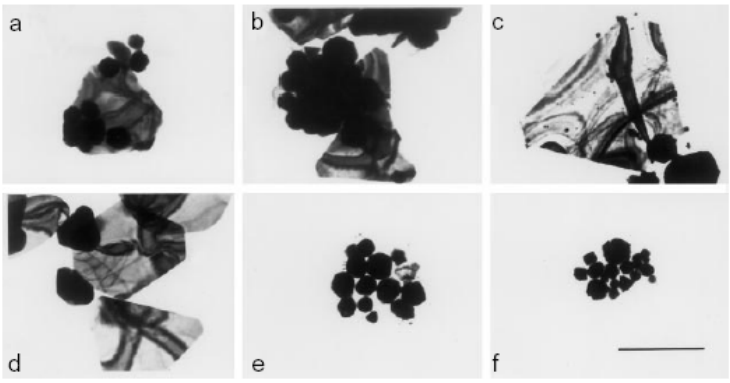

Figure 2.20: Gold nanoparticles formed by using the alkaline phosphates and gold binding peptide fusion (Brown et al., 2000).

A gold and silver binding peptide was utilized in production of gold binding peptide. These nanoparticles were found in a size range of 20 nm and they characterized to have sphere like shape. Due to their unique optical properties silver and gold nanoparticles become very popular, so many silver and gold binding peptides were used to synthesize the gold and silver nanoparticles (Naik, et al., 2000). Silver and cobalt nanoparticles were also synthesized using silver and cobalt binding sequences. As known silver nanoparticles have distinct optical properties and Co is important for its magnetic properties (Naik et al., 2004). Inorganic binding peptides allowed us to synthesize nanoparticles only using the precursors. Germanium precipitating peptides form germania solution found to form germania nanoparticles networks (Dickerson et al., 2004). In another study the formation of the single walled carbon nanotubes was observed by the help of the CNT binding peptides (Wang et al., 2003).

After the demonstration of the binding activity of the Ti binding peptide, Ti binding peptide also recognizes the SiO_2 surface, silification of the TMOS was carried out (Sano et al., 2006). For the formation of another composite material named Co-Pt, Co binding peptide was used (Naik et al., 2004). Synthesis of Cu_2O nanoparticles with GEPIs was demonstrated; peptide controlled the formation of the Cu_2O nanoparticles in a thermodynamically non equilibrium phase (Dai et al., 2005). The detailed characterization of the synthesized nanoparticles was showing a core –shell structure, where the shell is the protein layer and the core is the nanoparticles itself.

Hydroxyapatite is a well known mineral which is found in the structure of many different hard tissues. Hydroxyapatite binding peptide was used to synthesize hydroxyapatite using a $CaCO_3$ as calcium source and beta-glycerophosphate as

phosphate source. The phosphate is released from the beta-glycerophosphate by the enzymatic activity of an alkaline phosphatase enzyme. The peptide was found to control the growth of the hydroxyapetite kinetically. The strong peptide was found to force the crystal to grow as large particles, as the weak binder does the reverse (Gungormus et al., 2008).

3. MATERIALS AND METHODS

3.1 Peptides –Proteins and Buffers:

3.1.1 Solid state peptide synthesis:

GEPIs were chemically synthesized using standard *Fmoc* solid phase peptide synthesis techniques with or without attachment of biotin molecules to their N-terminus. Following the synthesis, they were purified using C-18 reverse phase liquid chromatography (RPLC) to a level > 95% (United Biochemical Research, USA). The peptides and their properties are given in Table 3.1.

Table 3.1. The synthesized peptides and their physicochemical properties

GEPI	Sequence	Theoretical pI	MW (Da)
GBP-1	MHGKTQATSGTIQS	8.5	1446
PtBP1	PTSTGQA	5.9	660
PtBP1C	**C**PTSTGQA**C**	5.5	866
PtBP2	QSVTSTK	8.7	849
PtBP2C	**C**QSVTSTK**C**	8.0	956
QBP1	RLNPPSQMDPPF	5.8	1398
QBP2	QTWPPPLWFSTS	5.5	1446
AuBP1	WAGAKRLVLRRE	11.7	1454
AuBP1C	**CGP**WAGAKRLVLRRE**GPC**	9.6	1967
AuBP2	WALRRSIRRQSY	12.0	1590
AuBP2	**CGP**WALRRSIRRQSY**GPC**	10.7	2104
dnQBP1	PPPWLPYMPPWS	5.9	1467
dnQBP3	SPPRLLPWLRMP	12.0	1462
dnQBP8	RKEDKAEDTKKK	9.4	1475

3.1.2 Buffers and peptide solutions

Purified peptides were stored at 20ºC. GEPI solutions were prepared in various different concentrations mainly in two different buffers. Phosphate buffer is used in gold binding experiments since it was also used in the selection of GBP. Phosphate buffer consists of 1:3 mixtures of 10 mM KH_2PO_4, 10 mM K_2HPO_4 and 100 mM KCl. The other buffer used was the phosphate/carbonate buffer (PC buffer) which was used during phage display selection. PC buffer includes 55 mM KH_2PO_4, 45 mM Na_2CO_3, 200 mM NaCl. The pH of both buffers were adjusted to pH 7.5 using 0.1 M HCl and 0.1 M NaOH. After preparation of the buffers they were filter sterilized using a 0.20 μm filter.

Peptides were dissolved in buffer solution by mixing using a Vortex mixer. In some cases, highly hydrophobic peptides were first suspended in very tiny volume of DMSO (dimethylsulfoxide), then diluted in the buffer solution. A stock solution with a concentration of 1 mg/ml, was prepared and the desired samples were diluted from this stock solution. All of the peptide solutions were kept at +4 ºC. Buffer solutions were always degassed to remove any air bubbles prior to preparation of desired peptide concentrations.

Before dissolving lyophilized peptides, the buffer solution were degassed to remove any air bubbles exist in the buffer solution.

Tetra trifluoroethanol (TFE, Acros Chemicals, 99.8%) was also used in some of the surface plasmon resonance experiments since it was used in circular dichroism experiments as a structure stabilizing buffer.

Enzyme: We used streptavidin fused alkaline phosphatase (SAAP, Invitrogen, PA, USA) to carry out molecular erector experiments. The proteins solutions were prepared in 100 mM phosphate buffer. The enzyme solutions were prepared in a concentration range of 2.5-20 μM.

Nanoparticles: Streptavidin coated quantum dots (QDots) used in the assembly experiments were also purchased from Invitrogen (PA, USA). QDots are in the form of semiconductor nanoparticles. They have CdSe core and ZnS shell. The shells of the QDots were functionalized with poly(ethyleneglycol) (PEG) and streptavidin molecules were attached to the activated PEG. These hybrid assemblies were used to stick QDot nanoparticles on biotinylated peptide decorated surfaces.

3.2 Instruments and Method

The kinetics and thermodynamics of GEP binding were analyzed using Surface Plasmon Resonance Spectroscopy(SPR), and Quartz Crystal Microbalance (QCM).

3.2.1. Surface plasmon resonance spectroscopy

The SPR measurements were made with a dual channel instrument (Kretschmann configuration) developed by Institute of Photonics and Electronics, Prague, Czech Republic. The instrument was equipped with a polychromatic light source (Ocean Optics LS1) connected to the detector via fiber optic cables. The collimator and detector sensors were placed on two mobile arms, allowing adjustment of the incident angle of the light. The flow cell was constructed from PTFE and was placed on a goniometer; and a Mylar gasket was used to prevent leakage between both channels. The instrument has a threshold of detection at a level of 0.0001 refractive index units. The prism and glass slides were both made BK7 glass with a refractive index (RI) of 1.510, and the substrate coupled with immersion oil has a RI = 1.510.The picture of the SPR system used in our studies is given in Figure 3.1.

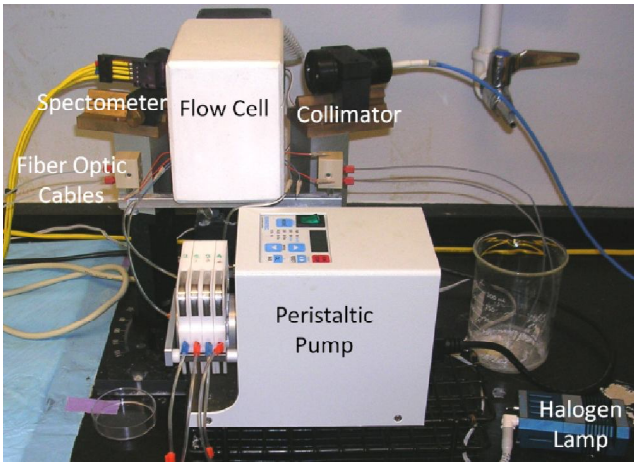

Figure 3.1: The photograph of the surface plasmon resonance system used in our experiments. A home build equipment consists of a Peltier system embedded flow cell coupled with a temperature controller.

3.2.1.1 Preparation of the substrates for SPR based sensing of GEPI adsorption

SPR substrates were prepared using the output from a mathematical model that was developed in our group (Yee, 2005) was used to estimate the thicknesses of the thin film to be coated on the glass substrates. The glass substrates are BK7 glass (Shott Inc.), reflectivity index of 1.517. The size of the glass substrates were 0.5cm x0.5 cm and 0.2 mm thick. The substrates were sonicated first in isopropylalcohol then in ethanol for 5 minutes and lastly rinsed with DI water. The cleaned substrate was further treated in a UV-ozone cleaner system (Novascan Inc., IA, USA).

Coating of the cleaned substrates were carried out in a sputter coater. Gold, Platinum and silica substrates were prepared using an ion beam coater, precision etching coater system (Gatan Inc, PA) operated at 6 keV with an 10mA/cm ^{2} ion current density, 6E-5 Torr vacuum. Platinum, silica, chromium, gold substrates were purchased from Gatan Inc, PA.

Gold, Platinum and Silica substrates were prepared according to the prescription resulted by the reflectivity model. Gold layer was prepared on cleaned BK7 glass which was sputter coated with a layer of 2 nms chromium and 47 nms of gold.

Platinum was prepared by coating the surface of the BK7 glass with a layer of 2 nm of chromium, 33 nm of gold, followed by 2 nm of platinum. The platinum on the surface was visible to the naked eye. Silica substrates were prepared using commercial gold-coated glass substrates. The pre-coated gold substrates, which have 47 nm of gold on top of a 2 nm chromium adhesion layer, were washed and dried in the desicator, then coated with 4 nm of silica. However this architecture was later found to be unstable in aqueous environment, so the thickness of the silica layer was increased to 10 nm.

To realize the experiment for GEPI binding analysis; first the buffer solution was flown on the SPR chip surface, after the base is established the GEPI solution was pumped into the flow cell. The increase in the sensogram was followed until a curvature is formed on sensogram or the signal reached to an equilibrium point. Then the buffer solution was pumped to remove the non specifically and weakly bound peptides from the surface.

3.2.2 Quartz crystal microbalance

In QCM-D systems the peptides or protein were flown through the flow cell onto the quartz crystal system. The mass loaded onto the quartz crystal was followed in real time. During the analysis of adsorbed layer of GEPI, dissipation change during the adsorption of the peptides was also monitored. The mechanic properties were followed as the change in the dissipation of the adsorbed layer and layers. The operating principle of the QCM-D system is represented in Figure 3.2.

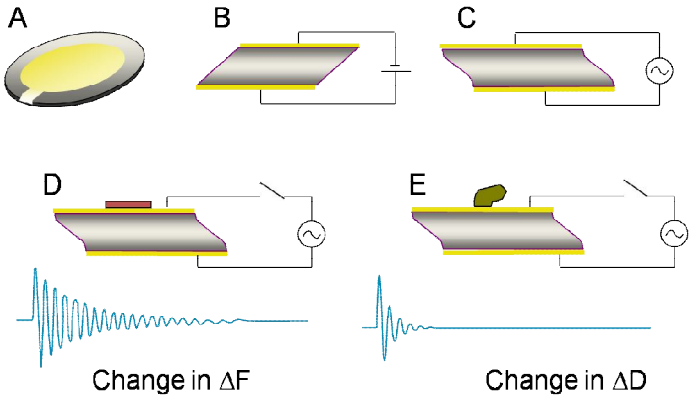

Figure 3.2: (A) The quartz crystal used in the QCM-D. (B) Applying of the direct current to the crystal (C) Applying alternative current to the quartz crystal (D) The change in the frequency upon adsorption of a layer onto the quartz crystal. (E) The change in the dissipation upon adsorption of a viscoelastic layer on to the quartz crystal (reproduced form the user guide of QCM-D apparatus, Q-Sense AB, Sweden)

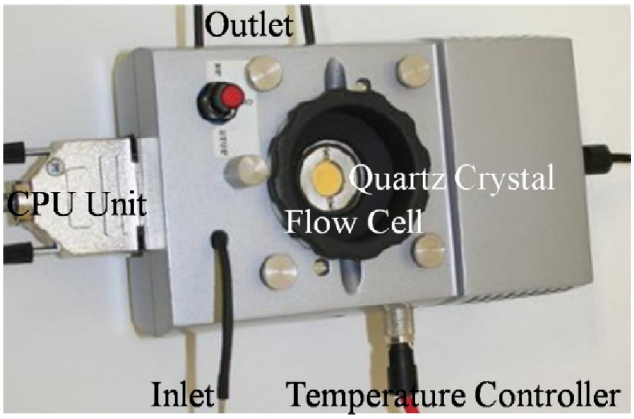

Figure 3.3: The picture of the Quartz Crystal System. The temperature of the QCM-D system is controlled with a Peltier embedded systems coupled with a temperature controller system.

In addition to the SPR experiments we also used QCM-D as an alternative approach to determine the interaction of the peptides with inorganic surfaces. Using the

platinum, gold and silica coated quartz crystals (Q-Sense, Sweden), we monitor the interaction of GEPIs with inorganic surfaces. The photograph of the QCM-D system in our lab is shown in Figure 3.3. PtBP2, QBP1 and GBP were used to monitor their binding activity.

The binding kinetics of GBP was also realized using QCM-D. The peptide solution is flown through the flow cell. After the baseline was established, the peptide solution was flown into the flow cell, and the decrease in the frequency was followed until the signal reached at steady state, or a curvature is formed in the signal. At this stage, buffer was flown to remove the non specifically and weakly bound peptides from the surface of the quartz crystal. We carried QCM-D experiments using a QCM-D system purchased from KSV Instruments, Finland. QCM-D system can measure the frequency change at four five different overtones. It is also possible to monitor the change in dissipation of the adsorbed film onto the surface of QCM-D. The QCM-D crystals used here were purchased from Q-Sense Instruments (Sweden), the crystals oscillates at 5 MHz.

3.2.3 Atomic force microscopy

In order to characterize the platinum, silica and gold surface for SPR analysis, we used atomic force microscopy. Topography data were collected using a Digital Instruments Multi-mode AFM housed in an acoustic isolation box with an external Nanoscope III controller. Nanosensors PPP-NCH tapping mode probes were used for this characterization due to their non-destructive style of probing the surface of soft biological samples. $1um^2$ images were scanned at 1 Hz at a resolution of 512x512 data points and kept constant for each scan. All data was gathered by utilizing the image analysis software provided by Veeco Instruments, Nanoscope v5.3r1. Each substrate is first scanned at 3 x 3 µm to ensure surface homogeneity. A 1 x 1 um scan is then performed for extensive coverage and cross-section analysis by the software.

3.2.4 Circular dichroism spectroscopy

The secondary structures of the peptide were determined using circular dichroism spectroscopy. Lyophilized synthetic peptides were individually dissolved in distilled deionized water to prepare stock solutions. Each stock solution was then diluted to an appropriate concentration for CD spectrometry measurements in 100 µM TrisHCl (pH 7.5). Based on the concentration variation studies, the optimal concentration was

chosen as 30 μM, and this concentration was utilized for further 2,2,2-trifluoroethanol (TFE, Acros Chemicals, 99.8%) titration studies (10, 30, 50, 70, and 90 vol%). All CD spectra were obtained at 25ºC with an AVIV 60 CD Spectrometer, running 60DS software version 4.1t. The CD spectrometer was previously calibrated with d-10-camphorsulfonic acid. Wavelength scans were conducted from 185 to 260 nm with appropriate buffer and solvent background subtraction. For each spectrum, 3 scans were averaged using 1-nm bandwidth and a scanning rate of 0.5 nm/sec. Mean residue ellipticity [θ_M] is expressed in degxcm^2/dmol^{-1}.

3.2.5 Fluorescence microscope

In order to determine and verify the assembly of the Q-Dots on silica surface for during the peptide enabled nano-photonic experiments fluorescence microscopy was used to image the QDot decorated surface of silica substrate. The surfaces was examined using a fluorescence microscope (Olympus B201), equipped with a Xe lamp which illuminates at 400 nm at UV region. The samples were scanned and a representative part of the samples were recorded using a CCD camera.

3.2.6 Photoluminescence intensity counter

Photolimunescence measurements were carried out at NANOTAM, using a Jobin Yvon Traix 550 CCD Photoluminescense System. First the alignmet of the substrate on the holder of the instrument was carried out to get the maximum intensity, then the optimum excitation time was adjusted using different exposure times and then the measuremnt of the sample was carried out. The sample scans were carried out for three times for each of the samples. The samples were excited uisng a He Laser at 350 nm.

3.2.7 Silica sythesis and characterization

The lyophilized peptide was dissolved in a TBS solution consisting of 200 mM NaCl, 45 mM Na_2CO_3, and 55 mM KH_2PO_4, the pH of the solution was adjusted with HCl at 7.4. Silica synthesis was performed using TMOS solution as the precursor material at room temperature. TMOS was hydrolyzed in 0.1 M HCl solution to obtain 1 M TMOS as the final concentration and then the biomineralization was initiated by adding 1 mg/ml QBP1. Formed silica samples were dried by evaporation of the residual TMOS and water molecules and then

Scanning electron microscobe (FEI) and Transmission Eelctron Microscobe (FEI Tecnai G2 F30 with 300 kV) images were taken to characterize the synthesized silica surface. To see the effect of the peptide on silica formation, a control group was also prepared without adding any peptide solution in TMOS to compare silica formation with and without peptide. In negative control groups, same volume of TBS solution was used instead of peptide solution. Furthermore, to observe the effect of different silica binding peptide concentrations on synthesized silica, a series of peptide concentration were tested.

4. RESULTS AND DISCUSSION

4.1 Molecular Binding Characterization of GEPIs

4.1.1 Peptide binding to a given inorganic substrate

The binding characterization of GEPIs with the solid surfaces is crucial for their technological implementation. There are different methods for surface characterization and monitoring the biomolecular interactions. Surface plasmon resonance spectroscopy (SPR) and quartz crystal microbalance (QCM) systems provide real time monitoring of the interactions, and allow kinetic and thermodynamic characterization for the interactions. In GEPI binding characterization, SPR and QCM systems were utilized. However, surface plasmon resonance measurements were suitable only for gold, silver surfaces. Hence the silver was highly unstable (Jung et al, 1998); generally gold was chosen and utilized in the analysis of the interactions. This was a challenge to monitor real time binding kinetics of the GEPIs, considering the fact that GEPIs were selected for different materials such as platinum, palladium, mica etc (Sarikaya et al., 2003). We therefore explored to expand the sensing abilities of SPR by using materials other than gold. In our group, we developed a mathematical model to design SPR chips for materials other than gold (Ng, L. Y., 2005).

4.1.1.1 Mathematical modeling of surface plasmon resonance signal

The model uses the Fresnel equation (given in Appendix D) to simulate the SPR reflection spectrum. The SPR dip spectrum curve should be sharp and close to zero for a reasonable real time monitoring. There are three parameters that dictate SPR signal for our system: 1) dielectric constant of the metal; 2) thickness of the metal and 3) incident angle. The shape of the reflective spectra of SPR is closely related to the dielectric constants of the metal layer. Thickness of the metal is one of the factors that affect the shape of the reflection spectrum. In the process of optical excitation of surface plasmon wave (SPW), a portion of the energy is reflected at the prism-metal interface, and a portion of it becomes the SPW at the metal-sample interface. During

the SPW excitation, part of the energy of the SPW is lost due to the coupling of the SPW to optical radiation back into the prism, and this loss of the energy is called the radiation damping. Figure 4.1 shows the reflection spectrum in different gold thickness for Prism-gold-water configuration.

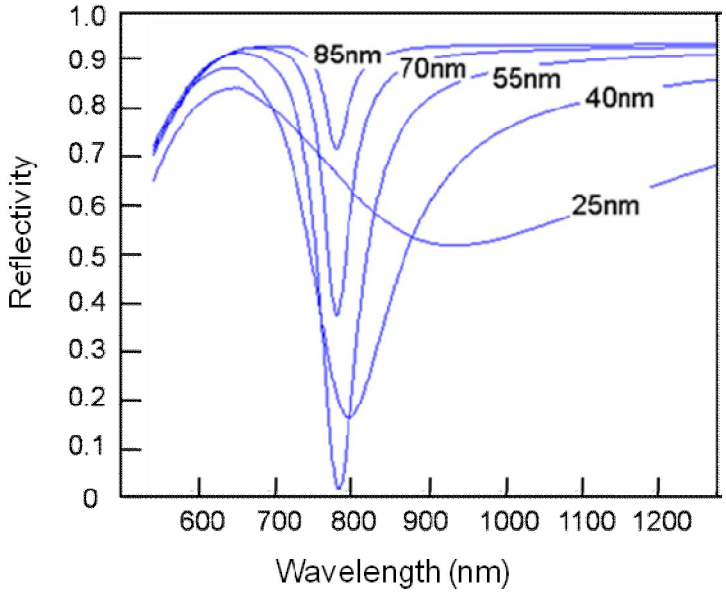

Figure 4.1: The reflection spectrum in different gold thickness for Prism-gold-water configuration (Plotted using the mathematical reflectivity model).

As the thickness of the metal layer increases, the radiation damping is close to zero (due to the reduced influence from the prism which leads to less change in the wave vector) and thus the reflectivity approaches to unity as shown in Figure 4.1.

As the metal thickness decreases, the amount of the back-scattered field radiates back into the prism increases. Since this radiation field is antiphase with the incoming wave, the reflectivity reduces due to the destructive interference between the back-scattered and the incoming field. At a particular condition, when the parameters of the sensor are chosen properly, the reflectivity would become zero. If the thickness of the metal film further decreases, the back-scattered field increases, which bring the reflectivity back to unity.

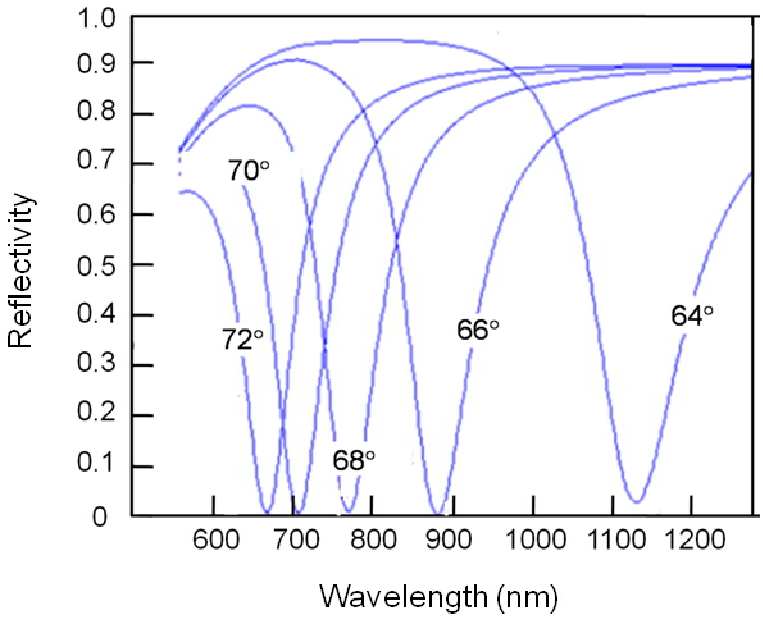

Figure 4.2: The reflection spectrum at different incidence angles at a gold surface thickness of 50 nm, the reflection spectrum is calculated for prism-gold-water system (Plotted using the mathematical reflectivity model).

The angle of incidence greatly affects the wavelength position of the dip (dip wavelength) (Figure 4.2). Therefore, in the real experiment for the wavelength-modulated setup, angle of incidence has to be adjusted very precisely so that the dip wavelength position is accurate. In the laboratory; the incidence angle of the incoming light in the wavelength-modulated SPR setup, is adjusted to 66 degree.

Using the model developed by Ng (2004) and tested as given above; scans for the optimum thicknesses of the platinum surface and silica surface was carried out. At the calculated thickness, one can coat platinum or silica on gold surface by keeping the surface plasmon wave at reasonable degree.

Using the reflectivity model discussed previously, it was found that sufficient plasmon resonance can be achieved using a 5-layer architecture in the case of designing a Pt coated SPR chip. The model indicated that an ideal film would have the following thicknesses: 2nm of chromium, coated by 33 nm of gold, coated by 1 nm of platinum. However, due to the impracticality of creating a continuous film of platinum one nanometer thick, two nanometers of platinum was used. Other adjustments that had to be made included changing the angle of incidence of the white light from 66 to 70 in order to make the dip positing fall in the visible range. The substrates were then coated with the film thicknesses outlined above.

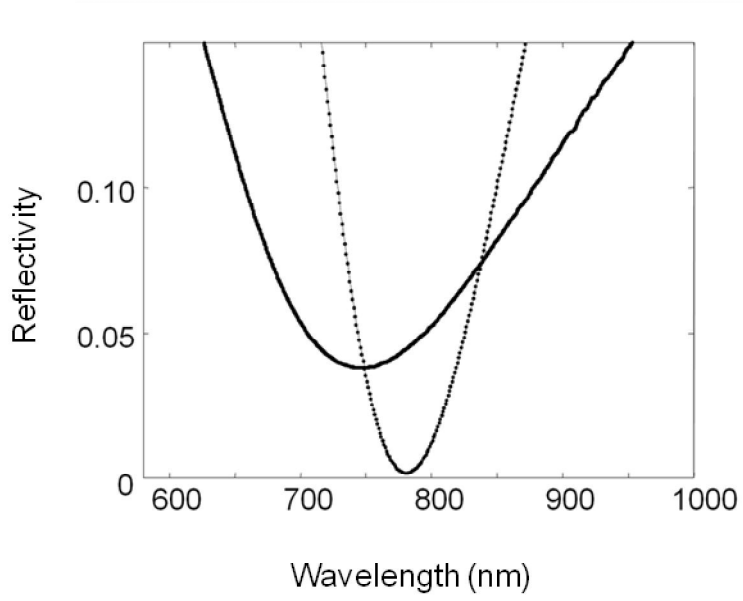

Figure 4.3: (A) Theoretical (dotted) versus experimental (solid) SPR signal from 2 nm of platinum on 33 nm of gold.

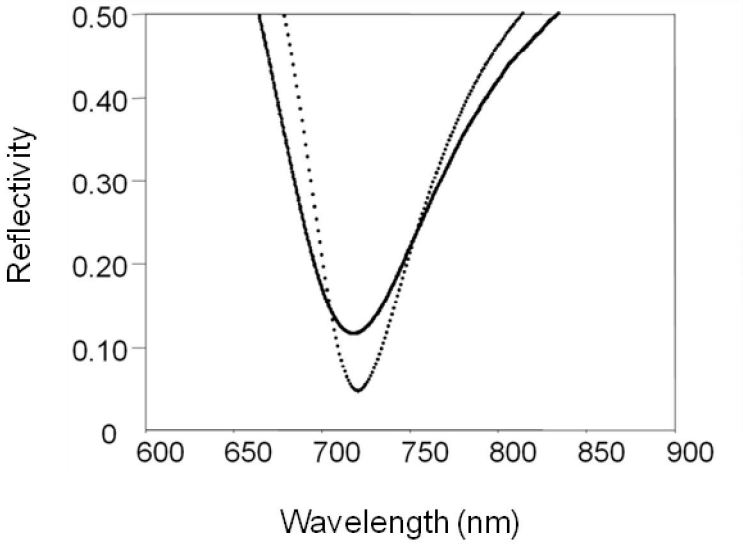

Figure 4.4: Theoretical (dotted) versus experimental (solid) SPR signal for 10 nm of silica on 47 nm of gold.

There was a certain amount of difficulty involved in characterizing the platinum surface, over gold surface as the layer directly underneath it was gold, a very similar material. A wide range of methods were used to determine if the platinum layer was continuous and intact. These included optical microscopy AFM, TEM. All of these methods seemed to indicate a continuous film of platinum on the gold surface; these results are included in Appendix A.

One of the most convincing evidence that the film is continuous comes from TEM, where a free-standing 2 nm platinum film coated by the PECS system was imaged (see Appendix A). Free standing films were made using a technique developed by Allred et al (2007). TEM images showed nanoscale crystals without major gaps in the film. Using the setup prescribed by the model and this method for synthesis, a usable SPR signal was obtained off of a platinum surface for the first time. Several studies were done using these surfaces that will be discussed later. In general the platinum surfaces had worse signal to noise ratio than gold.

Silica and silica-like surfaces are perhaps the most commonly used in biology. However, silica like other dielectrics cannot create surface plasmon waves. In order to achieve a surface plasmon signal, multiple thin films must be used. Modeling showed that coating a gold surface with an oxide does little to disrupt surface plasmon resonance. This is due to the lack of an imaginary component of the dielectric constant. This allows relatively thick layers to be coated on top of a standard gold substrate without losing SPR signal quality.

Studies using a variety of methods have shown the ability to use silica layers up to 100 nm thick. While such thick layers are usable, they are not necessarily advantageous, as the SPW formed at the gold-oxide interface has a limited penetration depth. For our studies a silica film thickness of 10 nm was coated onto standard gold substrates. This thickness was used because the model predicted no signal deterioration and a continuous film could be easily made.

As predicted, the added silica layer resulted in a minor difference in the SPR signal when compared to a bare gold substrate. The major problem with the substrate in this configuration was the poor stability. Substrates when exposed to buffer solutions would often not reach a stable baseline. Even a simple washing step to clean the non-peptide from surface would lead to the detachment of the silica film

Two primary methods have been put forth to deal with this problems. One is to use chromium adhesion layer, and the other uses an elaborate sol-gel process (Kambhampati et al., 2001). In general, the simpler approach of using an adhesion layer does not preferred because it might disrupt the surface plasmon wave. However, in our case, we found that the chromium layer simply shifts the resonance wavelength to the infrared, which can still be detected by our system. With the use of

this method, signal stability greatly improved and reproducible results became obtainable even after more than one use. The SPR reflectivity spectrum obtained for gold, platinum and silica surfaces are presented in the Figure 4.5, with the corresponding AFM images in the insets.

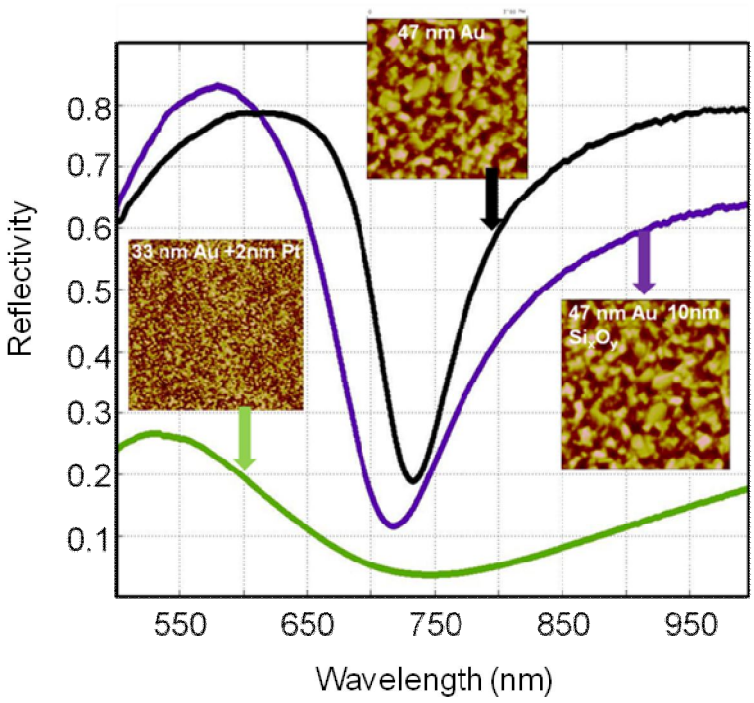

Figure 4.5: The experimental reflectivity of gold, silica and platinum surfaces, the surfaces are also probed with AFM.

The reflectivity model was a base for structuring the surfaces for SPR sensing, which is the heart to monitor the interactions of GEPIs with the corresponding inorganic surfaces.

4.1.1.2 Adsorption models adapted for the quantitative binding analysis of GEPIs

The binding constants of the peptides were calculated using modified Langmuir adsorption models. Langmuir adsorption model assumes a monolayer surface coverage for the adsorbed species on the available sites on a given surface. Additionally the adsorbed molecules on to the available adjacent sites are not interacting (Schessler et al., 1996). Monolayer surface coverage can be considered as a site filling procedure. During the adsorption of the adsorbate on available sites also the desorption takes place. At the equilibrium state the amount of the adsorbed and desorbed molecules is equalized. The adsorption rate depends on the concentration of

the adsorbed molecules.(Chen and Frank, 1989). The adsorption model is given in equation 2.1. if the integral of the Equation 3.1 is taken:

$$\theta(\mathrm{t}) = \frac{C}{C + (\mathrm{k_d} / k_a)}[1 - \exp(-(k_a C + k_d)t)] \quad \textbf{(4.1)}$$

For a given time period and temperature, monolayer formation as a function of time can be described by a single rate constant, called k_{obs}., with . The rate constant k_{obs} represents both the adsorption and desorption coefficients as a function of peptide concentration. Substituting this expression in Equation 4.1 along with the expression for surface coverage $\theta(\infty) = C/[C + (k_d + k_a)]$ yields:

$$\theta(t - t_0) = \theta(\infty)[1 - \exp(-k_{obs}(t - t_0))] \quad \textbf{(4.2)}$$

The time increment $(t - t_0)$ can be considered as any given time at t. Then $\theta(t - t_0)$ is the surface coverage at any given time. And we can take it as the signal of the system in use to follow the adsorption as a function of time. $\theta(\infty)$can be defined as a constant to explain the surface coverage at infinity for a given concentration of the peptide. So, we can rewrite the equation 4.2 as following:

$$S(t) = K[1 - \exp(-k_{obs}(t - t_0))] \quad \textbf{(4.3)}$$

Equation 4.3 describes the single Langmuir isotherm model. However, we realize that not all protein adsorption processes can be described by this model; in fact, there are biomolecular reactions at interfaces which are more complex. For example, in the bi-exponential process, protein adsorption onto a surface involves two events or stages that are governed by different rate constants. We modified Equation 4.3 to reflect the overall observed adsorption process with two different rates; here, the total fractional surface coverage can be represented as:

$$S(t) = K_1[1 - \exp(-k^1{}_{obs}(t - t_0))] + K_2[1 - \exp(-k^2{}_{obs}(t - t_0))] \quad \textbf{(4.4)}$$

Therefore two different adsorption ($k_a{}^1$ and $k_a{}^1$) and desorption constants ($k_d{}^1$ and $k_d{}^2$) were calculated, with two different equilibrium binding constants ($K_{eq}{}^1$ and $K_{eq}{}^2$).

To compare the binding affinity of the peptide on a different surface we used another approach, we calculated the amount of the mass adsorbed on a given surface. We carried this using the SPR data. SPR data gives the amount of the dry mass adsorbed

on the surface. Using SPR one can track the change in the adsorbed mass as a function of refractive index change. In our SPR system however we can only track the change in the surface plasmon wave dip position at the interface. But we calibrated our system to measure the change in the refractive index. Using the SPR response we were able to determine the thickness of the adsorbed layer on SPR chip surfaces using the following equation (Schuck, 1996, Jung et al., 1998):

$$d = (l_d / 2)[R/(m(\eta_a - \eta_s)] \quad \textbf{(4.5)}$$

Where d is the thickness of the adlayer, l_d is the penetration depth of the light in to the substrate, m is the calibration coefficient of the SPR instrument, R is the measured response (in our case change in the dip position shift), η_a and η_b is the refractive index of the adsorbate and buffer. Using the adlayer thickness one can easily calculate the adsorbate coverage in molecule per area, using the following equation (Jung et al., 1998):

$$\theta(molecules/cm^2) = d(cm) * N(molecules/cm^3) \quad \textbf{(4.6)}$$

Here N is the bulk number density; calculated from the density of the adsorbate. The calculation details including the derivation of equations, calibration factors and the calibration graphs are given in Appendix B.

4.2 Demonstration of Binding Affinity of GEPIs

In this section, the affinity of metal, metal oxide and mineral binding peptides were given. The binding affinities of the peptides were calculated from the experimental data obtained from QCM and SPR experiments. The overall binding constants for all of the GEPIs were given in Appendix C.

4.2.1 Affinity of GEPIs specific to metals

In this section, the binding affinities of the gold binding peptides and platinum binding peptides were studied. For gold binding peptides, two different groups were used. First one is l-GBP which is a previously screened and selected peptide by Stanley Brown using a cell surface display library (Brown et al., 2000, Brown, 1997). Gold binding peptide (l-GBP) was selected using the cell surface display. In this approach, the *Eschericia coli* was used as host organism to display the peptide library. The randomized peptides were displayed on the membrane protein of *E. coli*, multiporin, a fusion protein, which does not have any affinity for gold in its native

form. Multiporin was then cloned to make a large number of copies (millions). The gold binding affinity of l-GBP was demonstrated by our group, we further examined the binding kinetics of this peptide and its multiple repeats in this study. The second group of gold binding peptides (AuBPs) were screened and selected by Marketa Hnilova from Sarikaya research groups (Hnilova et al., 2008). The gold-binding peptides (AuBPs) were selected from a FliTrx cell surface random peptide display library. Third group peptides studied were platinum binders that were selected by Sevil Dincer from Sarikaya research group using a phage display peptide library housing $2x10^9$ different randomized peptide sequences (New England Biolab M13PhDC7C).

4.2.1.1 Gold binding peptides

Gold binding peptide (MHGKTQATSGTIQS) is the first isolated inorganic binding peptide, it is a 14mer peptide. Gold binding peptide (GBP) is firstly used as an insert in the alkaline phosphate (AP). The effect of the increasing repeats of GBP on binding activity of AP-GBP constructs was shown (Brown et al., 1996). As a further study of the GBP, AP-GBP constructs were shown to be designer proteins for the biomineralization of the gold nanoparticles (Brown et al., 2000). Later mechanism of the assembly of the gold binding peptide was investigated using a molecule dynamic simulation approach. The effect of the surface topography on binding of l-GBP and the residues interacting with the gold surface was analyzed (Braun et al., 2002). The chemical characterization of 3l-GBP was also carried out using CD and NMR studies; it was shown that 3l-GBP has a random coil secondary structure in solution (Kulp et al., 2004). The binding affinity and specificity of 3l-GBP was investigated by SPR and QCM previously. An equilibrium binding constant of 10^7 was estimated for the formation of the Au/3l-GBPcomplex (Tamerler et al., 2006). The binding specificity of 3l-GBP was also studied by a qualitative approach using florescence microscopy, a patterned surface composed of silica, platinum and gold surfaces was used to test the specificity of 3l-GBP. And the targeted assembly of 3l-GBP was achieved successfully. However, there was a still lack in understanding of the adsorption energetic of the GBP on the gold surface; here we investigated the effect of the multimerization on the binding affinity and specificity of gold binding peptide.

In nature some of the biomineral related peptides found to have repeating units their primary structure. These repeating units found to have a positive effect for the inorganic binding capabilities of these polypeptides (Shiba and Minamisawa, 2007, Miyamoto et al., 1996). To probe the same effect, whether the repeating units of the GEPIs enhance the binding affinity of the peptide, GBP was synthesized in two different forms. Here we synthesized one repeat l-GBP and three repeat 3l-GBP.

The adsorption data for the gold binding peptides is given in Figure 4.6. The data was collected for four different concentrations of l-GBP and 3l-GBP. The time depended adsorption data for l-GBP and 3l-GBP were further analyzed. The data analysis is carried out to extract the adsorption, desorption rates as well as the equilibrium adsorption rate for both of the peptides. The experimental data was fitted to a Langmuir adsorption model and the fitted data was given in Figure 4.7...

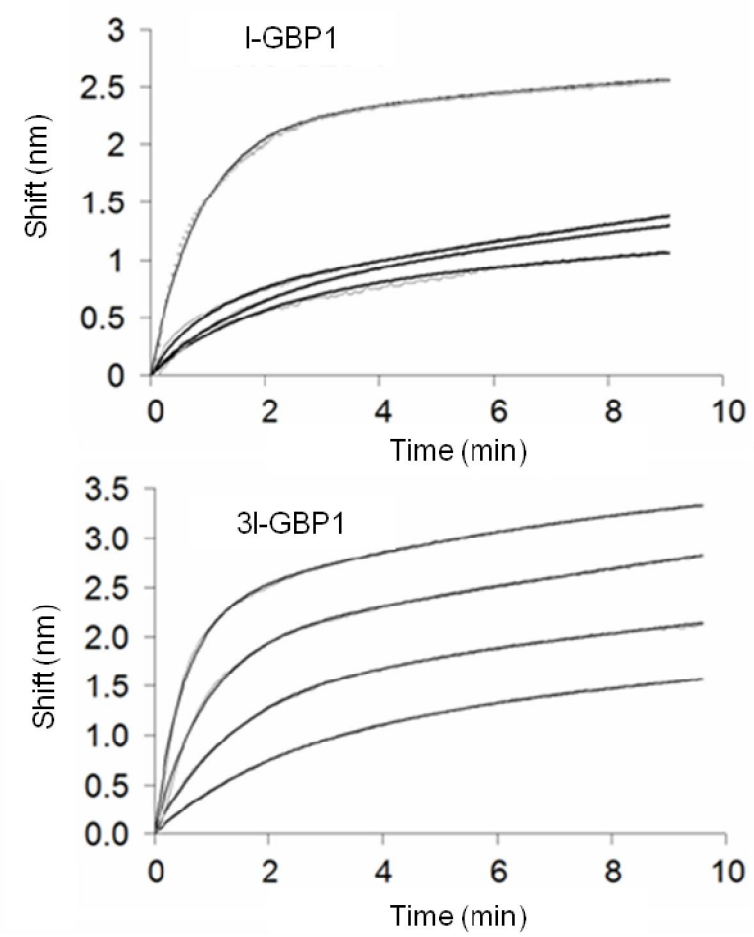

Figure 4.6: Binding sensogram for the l-GBP and 3l-GBPon gold surface. The concentrations used are 0.116 µM, 0.232 µM, 0.464 µM and 0.928 µM.

Here we employed a Langmuir type adsorption model; a simple adsorption model in equation 4.1 is applied. However, this model lack of fitting to the experimental data. So, we suspected that the peptide may behave in a different way that we expected. The peptide does not seem to be adsorbed on a surface following the Langmuir assumptions. We thought the surface heterogeneity may play a role to control the binding behavior of the peptide. This issue can be explained the effect of the surface topography and surface properties on the affinity of the gold binding peptide. This issue was also taken into account in previous studies (Braun et al., 2002 and Tamerler et al., 2006).

Because we applied a bimodal adsorption model, we made the assumption GBPs is adsorbed faster at some sites on the gold surface and slower at some other parts of the surface. We end up with two different binding constants which are given in Appendix C.

We calculated the K_{eq} 1,5x10^6 $M^{-1}$and 6 x10^4 M^{-1} for l-GBP, for 3l-GBP4x10^6 $M^{-1}$and 3 x10^4 M^{-1}. It seems that there is a increase in the binding affinity when increasing the number of the repeats of the peptide.

The binding energies are -8.2 kcal/mol, -8.9 kcal/mol, respectively, for l-GBP and 3l-GBP. The difference in the binding energy is dictated by the faster adsorption of the 3l- peptide on gold surface.

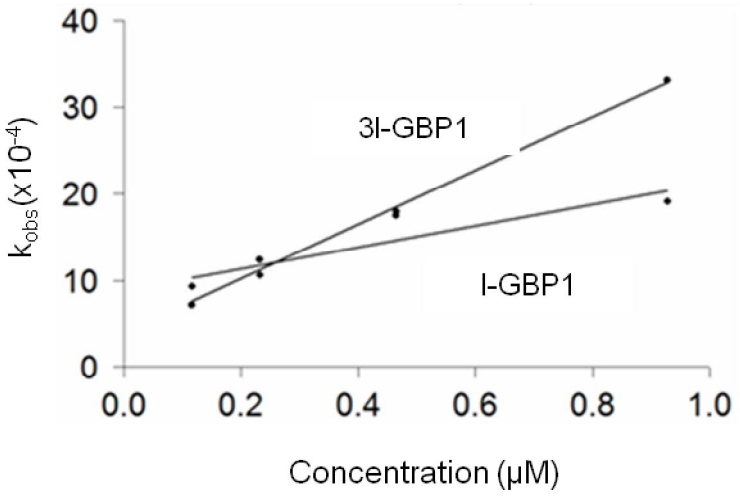

Figure 4.7: Apparent adsorption rates for l-GBP and 3l-GBPas a function of concentration.

In 3l-GBP, the number of amine and hydroxyl groups in the chemical structure has increased. The binding affinity of l-GBP to 3l-GBP is not increased proportionally.

This may show that the importance of the availability of the amine and hydroxyl groups for the binding of the l-GBP. The availability of the binding of the l-GBP on gold surface is directly controlled by by the conformation of the l-GBP.

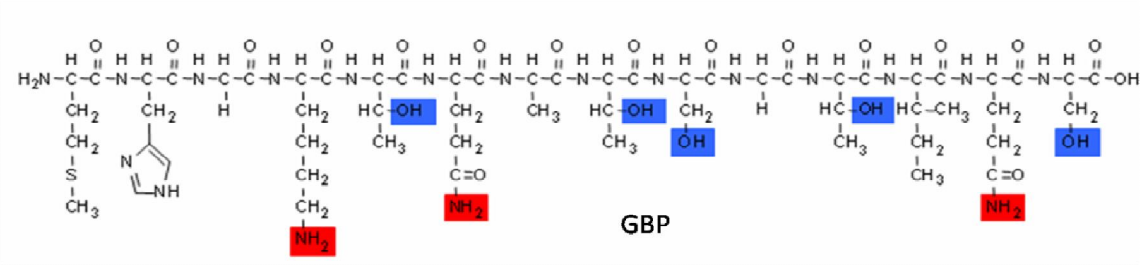

Figure 4.8: The primary structure of l-GBP, the hydroxyl groups and amine groups were highlighted in blue and red respectively.

The increasing number of repeats controls the conformation of the GBP, both l-GBP and 3l-GBP has labile, random coil structure (Kulp et al., 2004). The binding energies and the initial adsorption rates provided an idea that the increasing repeats of GBP has a better affinity to the gold surface. The details of the binding mechanism with respect to the binding thermodynamics are investigated in section 4.4.

FliTrx library selected gold binding peptides were synthesized in two conformational states, in circular (constrained) form and linear form. The constrained form was formed through the oxidation of the cysteine residues attached at the end of the original sequences. The binding activities of the AuBPs were investigated for two different conformations of the AuBPs mentioned above. Binding characteristics of all tested AuBPs found to have similar behavior, except for the constrained form of c-AuBP2. The most remarkable difference in binding kinetics of c-AuBP2 is that it has the lowest desorption among AuBPs. The difference in the desorption rate of the c-AuBP2 is also included in the calculation of the K_{eq} as well as ΔG. The lower desorption rate leads to higher K_{eq} and ΔG values for c-AuBP2 versus other AuBPs. The SPR results also show that the FliTrx-selected l-AuBP1, c-AuBP1 and l-AuBP2 have almost the same binding properties with previously selected gold-binding peptide l-GBP. c-AuBP2 has significantly lower binding energy (-9.7 ± 0.1 kcal/mole) comparing to l-GBP (-8.4 ± 0.1 kcal/mole). A 1.3 kcal/mol difference in the binding energy represents almost an order of magnitude higher equilibrium constant for c-AuBP2 compared to l-GBP. The main difference between two peptides is their desorption rate, k_d.

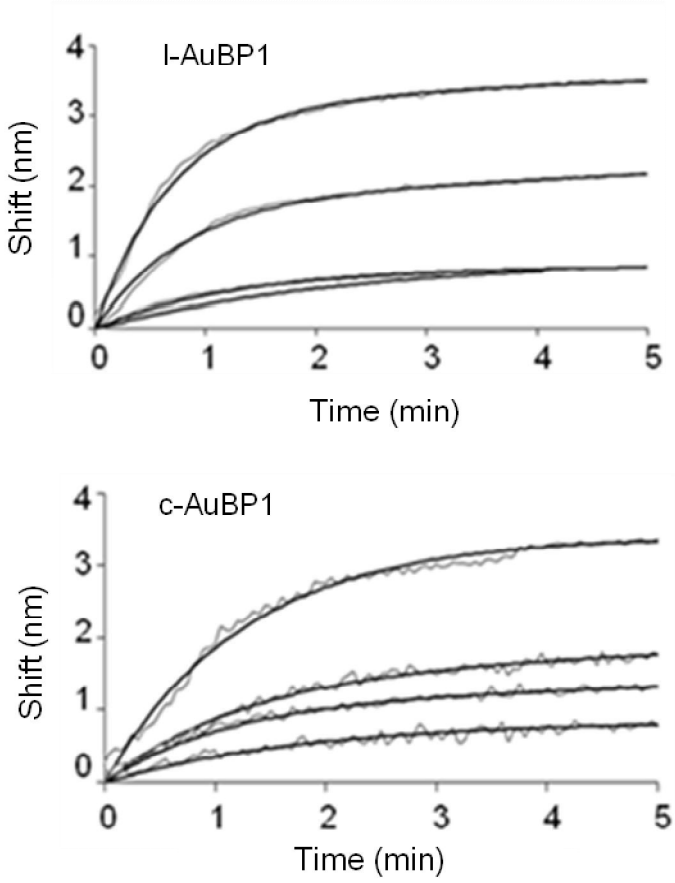

Figure 4.9: Apparent adsorption rates for l-AuBP1 and c-AuBP1 as a function of time.

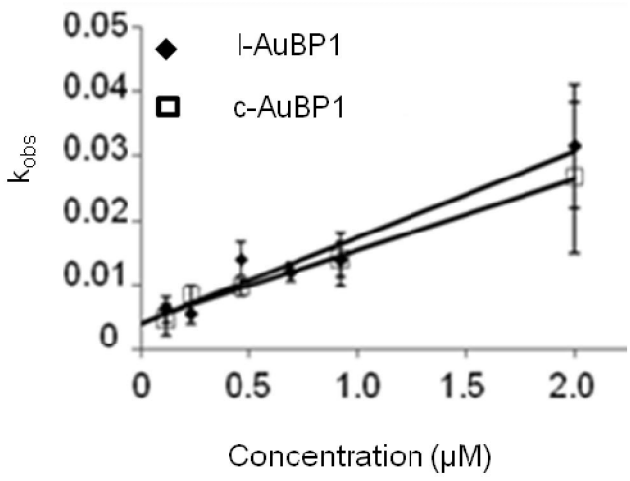

Figure 4.10: The binding sensograms for the c-AuBP1.

Table 4.1: MW, pI, and net charge of F-moc synthesized gold-binding peptides

Name	Sequence	MW (Da)	pI	Charge
l–AuBP1	WAGAKRLVLRRE	1454.7	11.7	+3
c–AuBP1	CGPWAGAKRLVLRREGPC	1967.3	9.7	+3
l–AuBP2	WALRRSIRRQSY	1591.8	12	+4
c–AuBP2	CGPWALRRSIRRQSYGPC	2106.4	10.7	+4
l-GBP	MHGKQATSGTIQS	1446.6	8.5	+1

The binding sensogram and the fitted Langmuir adsorption sensograms for AuBP2s are given in Figure 4.11 and 4.12 below.

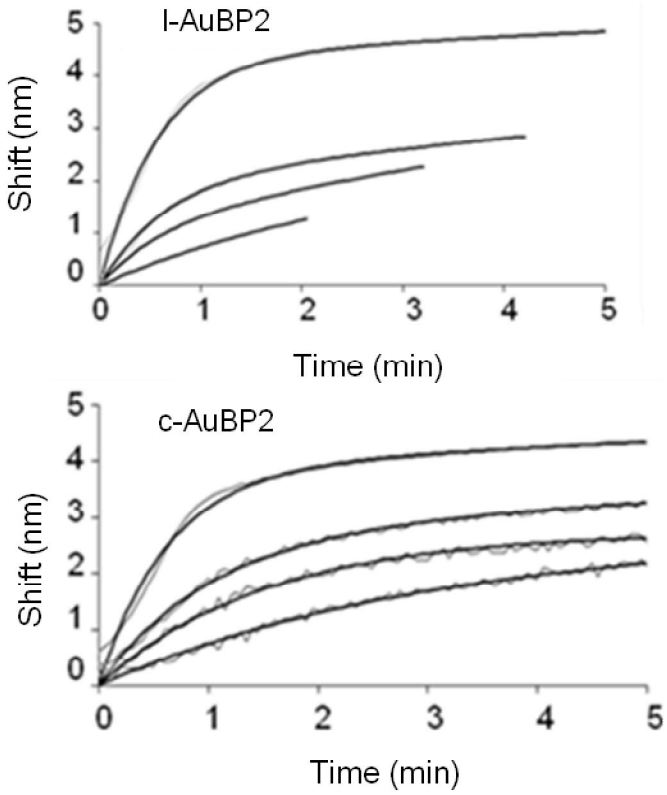

Figure 4.11: The binding sensograms for the c-AuBP2

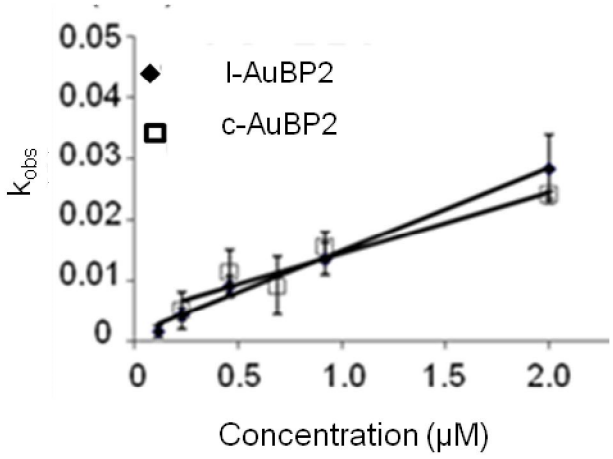

Figure 4.12: Apparent adsorption rates as a function of concentration for c-AuBP2

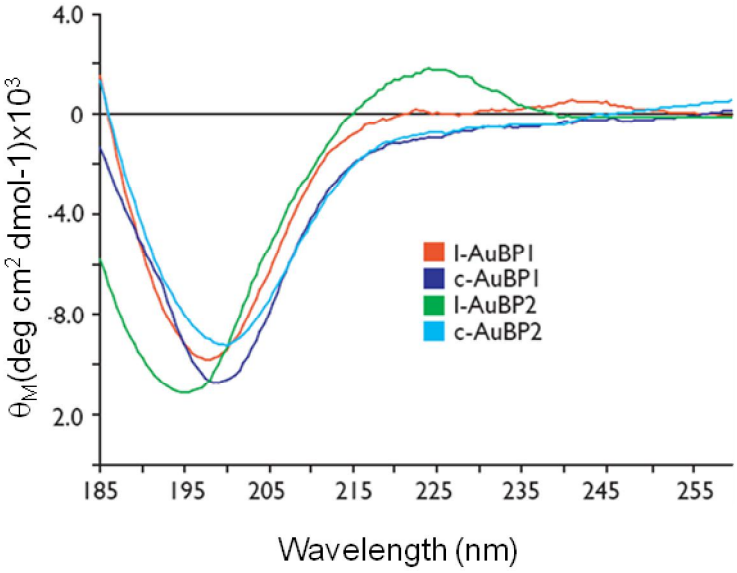

Figure 4.13: CD spectra of AuBPs.

The secondary structures of the AuBPs were investigated and the data is presented in Figure 4.13. All of the AuBPs found to have a secondary structural feature a π- π* transition band centered between 195-201 nm, which is consistent with the presence of the random coil (RC) conformation in equilibrium with other secondary structures. Additionally, l-AuBP1 and l-AuBP2 have second elipticity band (n – π* transition) centered near 220 nm which corresponds to a extended helical structure, polyproline Type II (PPII) secondary structures. The percentage of the PPII structure in the l-AuBP2 is higher than l-AuBP1. This conformational feature can also be related to the polyelectrolytic residues (i.e. –KR-, -RR-). The loop structures acting like a constraint in c-AuBP1 and c-AuBP2 and it was validated by CD experiments that c-AUBP1 and c-AUBP2 do not form extended helical secondary structures.

4.2.1.2 Platinum binding peptides

The highest affinity platinum binding peptides (PtBP) based on semi-quantitative FM analysis was synthesized for detailed molecular binding characterization. Since SPR signal can only be obtained from gold or silver surfaces, we had to modify the surface of the SPR slide for platinum measurements according to the previously developed computational model (Ng, 2004). By employing the mathematical reflectivity model the reflectivity of the light through the platinum surface was estimated.

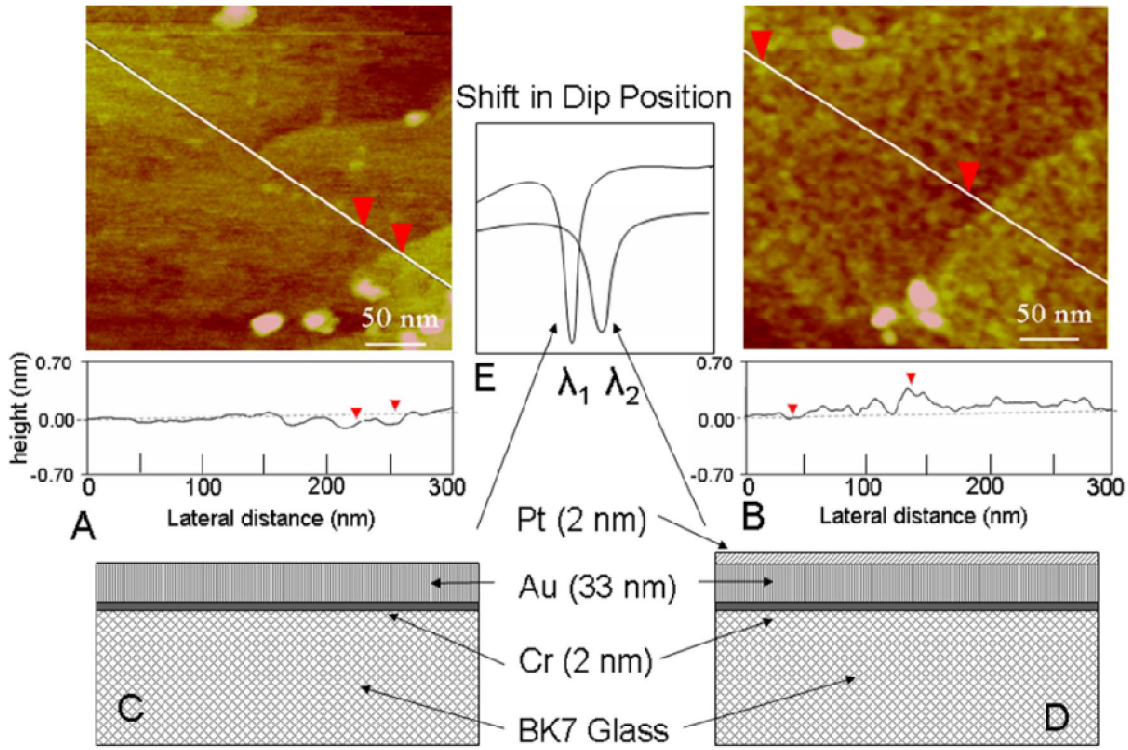

Figure 4.14: Atomic force microscopy images (A and B) from the Au and Pt surfaces and the schematics (C and D) of the layered substrates used for SPR analyses. The change in the reflectivity of the chip due to the 2-nm thick platinum coating is shown in E compared to that from bare gold surface. The insets are surface line profiles showing an RMS roughness of less than 1 nm for each surface.

Empirically, we found that, in order to achieve a reasonable signal using a specific target thin film, one must first create a layer of gold, or silver, beneath the platinum film. For preparation of Pt substrates, previously developed SPR model was calculated the lowest reflectivity at the optimum thicknesses of 2 nm Cr, 33 nm Au, and 2 nm Pt **(**Figure 4.14).

We next tested the binding affinity of two strong platinum binders (PtBP1 and PtBP2) for platinum surfaces. SPR data for platinum binding peptides were fitted to two different adsorption models based on their adsorption curves. Adsorption data from c- PtBP1, 3l--PtBP1 and l-PtBP2, c-PtBP2 were fitted simple Langmuir adsorption model, and l- PtBP1 and 3l--PtBP2 were fitted to a biexponential Langmuir model. These peptides have different secondary structures in solution according to CD data, and therefore each peptide has a different conformation resulting in different adsorption behavior. Similar to the constrained AuBPs, also the PtBPs were synthesized in constrained, linear and three repeats of the peptide. Again the effect of the conformation of the peptide on the binding affinity was investigated.

c-PtBP1 has a binding free energy of -8.9 kcal/mol; this peptide is in a constrained form which was created by disulphide bond between the cysteines residues at the end of the sequence. This structure supposed to be more stable on solid surface because of the limited conformational disturbance, and this may cause for its higher affinity towards the platinum surface. Without the cysteines, the new structure was found to have different affinity compared to constrained one; the binding free energy of this peptide becomes 7.1 kcal/ mol. To test any possible change in the affinity of the l-PtBP1 peptide, original sequence of the peptide was repeated three times (3l--PtBP1). The free energy of 3l--PtBP1 found to be ~7 kcal/mol which is almost similar to the linear peptide, hence the adsorption rate (k_a) of the 3l--PtBP1 is two times higher than l-PtBP1 form, desorption rate of the linear form is slower. Despite the fast adsorption of 3l- PtBP1, molecule cannot interact strongly with surface resulting in the high desorption profile comparing to the l-PtBP1. In general, c-PtBP1 shows a better binding activity comparing l-PtBP1 and 3l-PtBP1.

In the case of the second platinum binder PtBP2, the native form c-PtBP2 has a binding free energy of ~7 kcal/ mol. Leaving the cysteines out of the structure, the affinity did not change at all, but the adsorption and desorption rates are affected. The adsorption rate of constrained peptide c-PtBP2 was found to be slower than l-PtBP2. Three repeat PtBP2 (3l--PtBP2) has an increased affinity compared to both of the l-PtBP2 and c-PtBP2 Adsorption behaviors of both of the platinum binders were found to be different. Therefore, the effect of the constrained conformation on the binding affinity of the platinum binding peptides can not be concluded as a universal

fact. In fact, this shows that each inorganic binding peptide needs to be tested in detail for their adsorption and desorption behaviors.

Table 4.2: Amino acid sequences of inorganic-binding peptides and their physicochemical properties.

Peptide	Sequence	MW (*Da*)	Charge	pI (pH unit)
c-PtBP1	CPTSTGQAC	886.9	0	5.51
c-PtBP2	CQSVTSTKC	956.1	+1	8.06

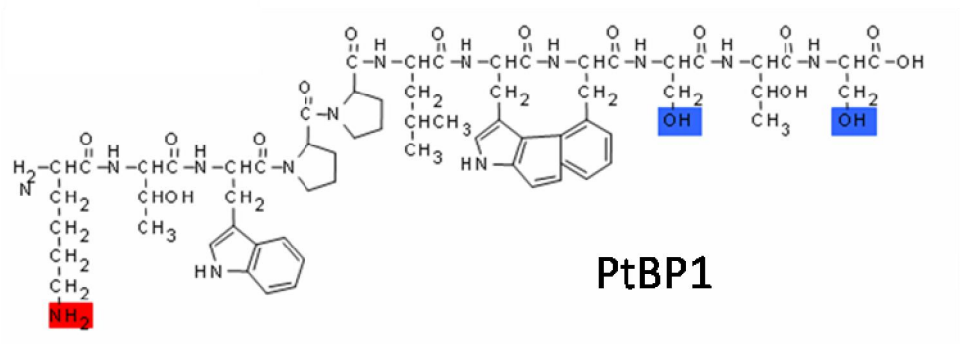

Figure 4.15: The chemical formula for the platinum binding peptides, PtBP1 and PtBP2 in the one repeat linear form.

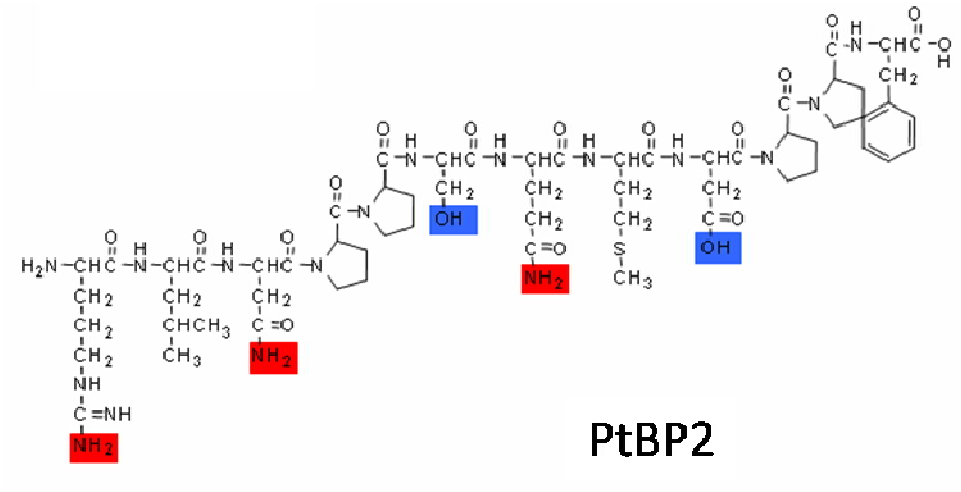

Figure 4.16: The chemical formula for the platinum binding peptides, PtBP1 and PtBP2 in one repeat linear form.

Binding affinity of PtBP1 is increased by creating a constrained structure; however there was not a significant change in the case of the three repeat concatamers of PtBP1. The case was vice versa for PtBP2, this show that the binding is not only controlled by the amino acid sequence, it is also dictated by the secondary structure

of the platinum binding peptides, which is consistent with the results from the study to probe the effect of constrained structure on binding affinity of PtBPs.

The basic difference in the chemical structure of this peptide is the number of the amine and hydroxyl groups on the side, as well as the number of the aromatic ring displayed on the side chain of these peptides. The PtBP2 has three amine groups on the side chain however the PtBP1 has only one, and the PtBP1 is richer in the number of the aromatic rings. So the affinity results showed that l-PtBP1 and l-PtBP2 bids almost at the same K_{eq} ~7.0 x 10^{6} , however in the three repeats of these peptides, the binding energy of the 3l--PtBP2 is higher than 3l-PtBP1, there is a 2 kcal/mol difference between these two peptides. This corresponds to a two orders of magnitude difference in adsorption rate. Investigating the chemical structure of the 3l-PtBP2 may be the increased number of the amine and hydroxyl groups increases the binding affinity of these peptides. However the important issue is not only the presence of the amine and hydroxyl groups. Because one can design another molecule with hydroxyls and amine groups, this does not mean such kind of designed molecules can be able to recognize the target surface. Besides the presence of the hydroxyl and amine groups, the positions of these groups are also important. The correct positioning of the amino acids with the correct functional side groups will mediate the molecular recognition capability of a given inorganic binding peptide to solid surfaces.

Not only the molecular recognition capabilities but also the specificity of the inorganic binding peptides can be tuned by the correct positioning of the amino acids in any given inorganic binding peptide. It is a fact that conformation of a peptide is controlled by the primary structure of the peptide. This fact can be considered as the design principle for the molecular recognition and specificity principles of the inorganic binding peptides.. Because surface plasmon resonance spectroscopy only detects the adsorbed dry mass at the inter phase, as an alternative method quartz crystal microbalance can be utilized. QCM-D not only gives the information of the dry mass but also informs one about the viscoelasticity of the adsorbed peptide layer. So one can easily monitor the changes of any denaturation process of a protein film, which will trigger change in the viscoelasticity of the film.

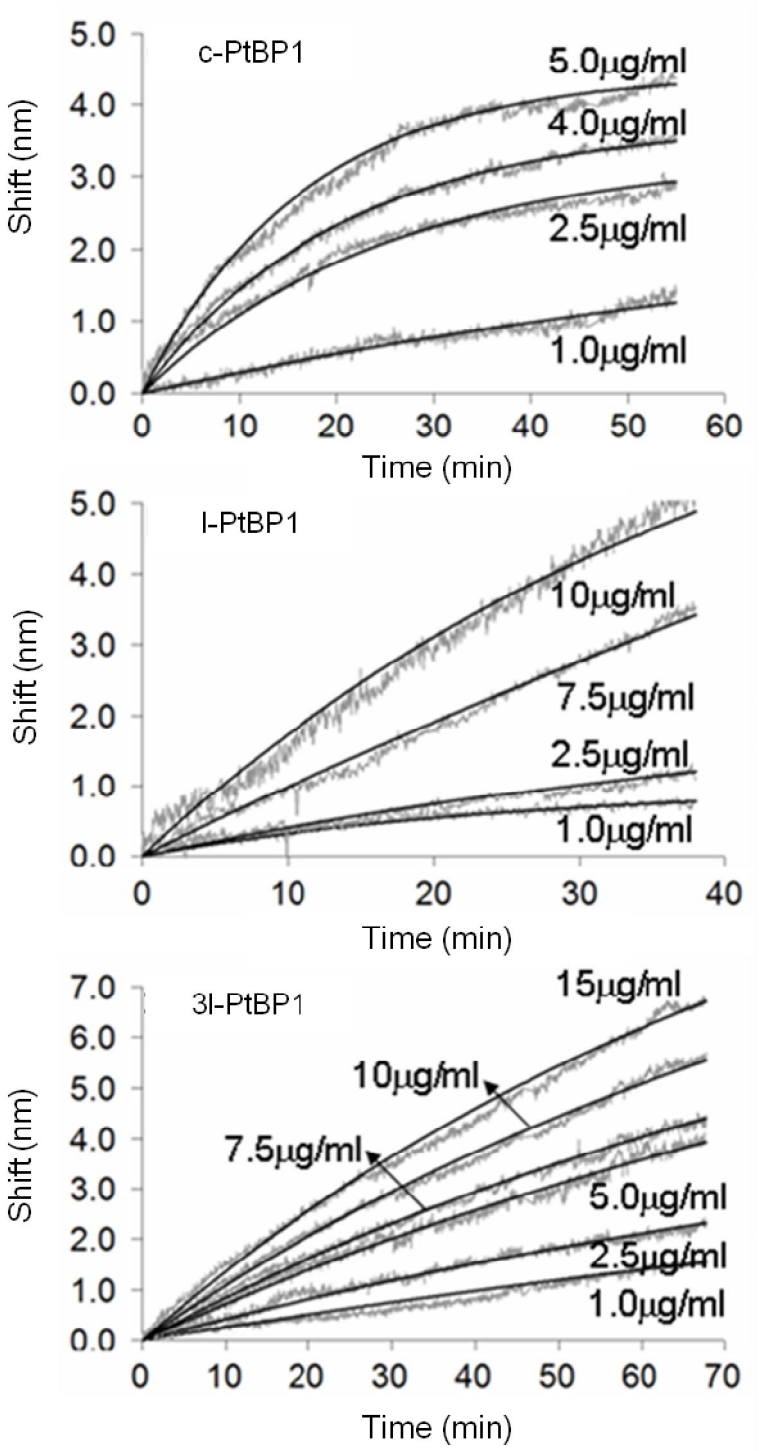

Figure 4.17: Adsorption curves for the three different forms of the platinum binding peptides, c-PtBP1, l-PtBP1 and 3l- continuous black lines represent the fitted model to the data points.

In PtBP1, the number of amine and hydroxyl groups are smaller, the other possibility for the looser binding of 3l-PtBP1 can be the restricted movement of the 3l-PtBP1 molecule in solution due to the high number of the aromatic rings in its structure.

Both of the PtBP1 and PtBP2 were also further analyzed using QCM-D. As expected the K_{eq}, k_a and k_d values are almost similar to the values from the SPR experiments. First the total shift and change in the dissipation for the PtBP2 was carried out. Both from the SPR and QCM-D experiments, we noted that 3l-PtBP2 is the strongest binder among the PtBP2s, however in the dissipation data we realized that at the end of the adsorption of the peptides, both l- and 3l- peptides had almost the same viscoelasticity. By means of the binding affinities l- and 3l- peptides have different affinities as the 3l-PtBP2 has seven times higher affinity compared to that of l-PtBP2. The total shift of the peptides seems to be almost the same respect to the QCM-D data. Compared to the SPR experimental results, it was figured out that the peptides have the same binding behavior monitored by different instruments.

The SPR data for 3l-PtBP2 showed a two stage binding, which is different than that of QCM-D data and fitted model. This difference in adsorption models is a cause of the surface topographical differences between SPR chip and QCM-D crystal surface. The dissipation changes of the 3l-PtBP1 and 3l-PtBP12 have similar characteristics.

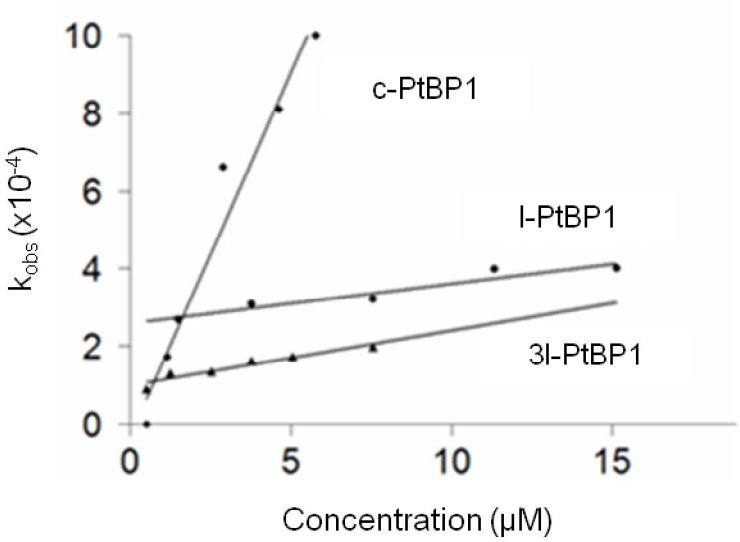

Figure 4.18: The concentration dependency (k_{obs}) of apparent adsorption rates were shown at the bottom.

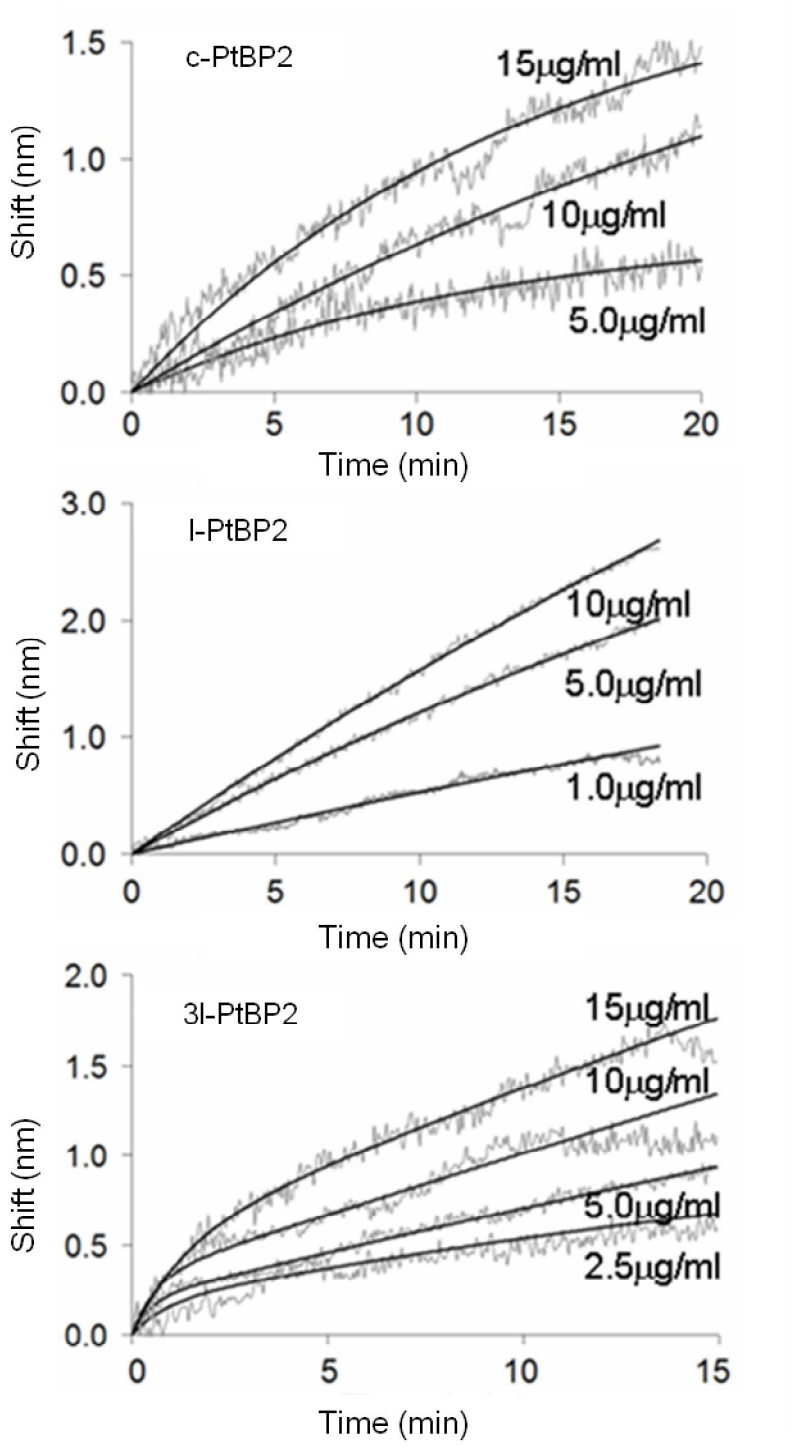

Figure 4.19: Adsorption curves for the three different forms of the platinum binding peptides, c-PtBP1, l-PtBP1 and 3l- continuous black lines represent the fitted model to the data points.

These two peptides were found to be different by means of theirs binding affinity, 3l-PtBP2 has a binding affinity of which is two order of magnitude higher than that of 3l-PtBP1. Also the total shift of 3l-PtBP2 is higher than 3l-PtBP1.

In Figure 4.20**,** the red sets shows the 3l-PtBP2 as the blue set represents 3l-PtBP1, the 3l-PtBP2 binds faster and deposit more mass on Pt coated crystal surface. This data is also in agreement with what we saw in our SPR analysis. In Figure 4.20, the change in the dissipation is of the adsorbed mass of peptides on Pt surface is given. On Figure 4.20, the change in dissipation of the adsorbed peptides is changing as a function of time. The change in dissipation represents the presence of the water molecules adsorbed by the peptides on the surface, namely structured water molecules. In the Figure 4.20 when comparing the dissipation change of the peptides there is a limited deviation between the peptide's water holding capacity. This can support the idea that all of the peptides are adsorbed at different binding rates; however the films formed area having the same water holding capacity in the case of these PtBPs.

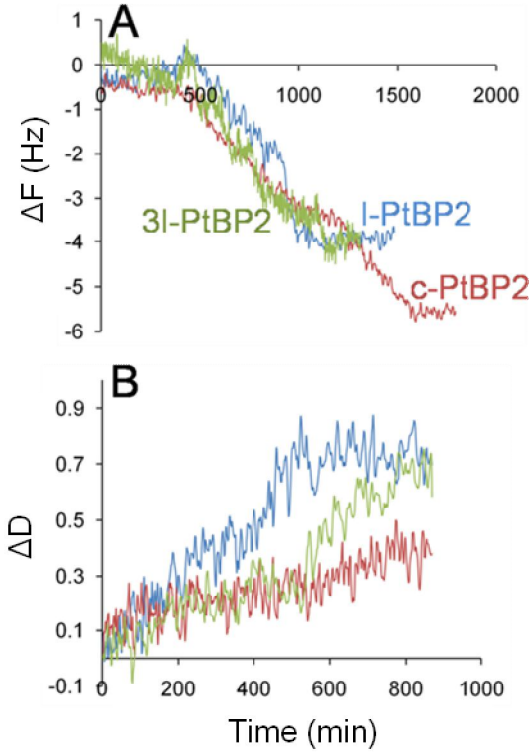

Figure 4.20: (A) Total shift in QCM-D experiments realized by the deposition of the mass on Pt coated QCM-D crystals. (B) Total change in dissipation of the PtBP2s, each color represents the peptide colored in (A).

The difference in adsorption is reflected in the rate and equilibrium constants obtained for both peptides. As sho wn in Appendix C, we note that the k_a and K_{eq} values for cyclic peptide are nearly 20 times greater than those obtained for the linear form. Therefore, there is approximately a 2 kcal/mol difference in the Gibbs free

energy of binding of cyclic versus the linear peptides. Here, we calculated the standard Gibbs free energy of adsorption as an approximation in describing the binding energy, since the calculations are performed based on the equilibrium constant rather than carrying out the binding experiments at different temperatures.

However, it is directly related to the free energy of the peptide and, therefore, we refer to it as binding energy in the lieu of the free energy (Appendix C). Collectively, these findings indicate that cyclic-PtBP1 and linear-PtBP1 both bind to Pt thin films, but are kinetically different with regard to adsorption behavior on a Pt substrate, and the cyclic-PtBP1 is the higher affinity binder of the two sequences.

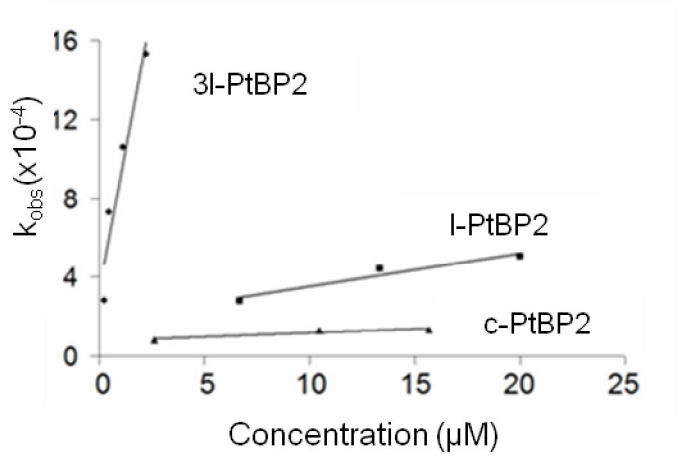

Figure 4.21: The concentration dependency (k_{obs}) of apparent adsorption rates were shown

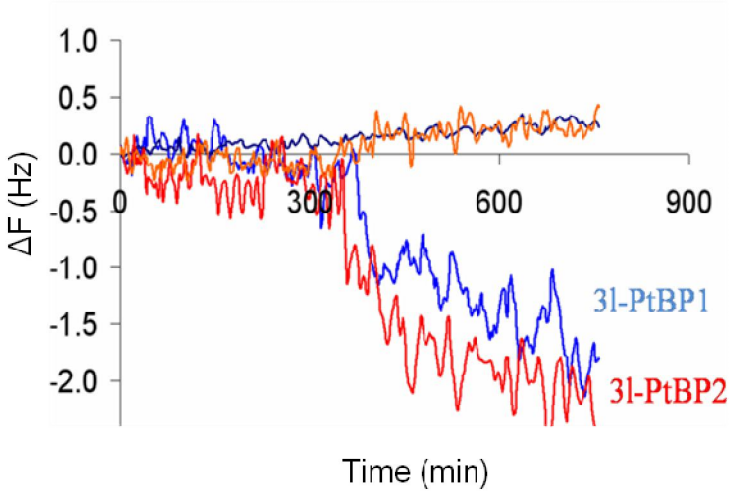

Figure 4.22: The red line represents the frequency change upon adsorption of 3l-PtBP2 as the blue does 3l-PtBP1. The orange and dark blue stands for the dissipation change during the adsorption of 3l-PtBP2 and 3l-PtBP2 respectively.

Given the observed differences in adsorption rates and dissipation change in Figure 4.22, we were interested in learning if linear-PtBP1 and cyclic-PtBP1 differed with regard to internal structure as well. Specifically, we wanted to discover the effect that the cys-cys loop constraint might have on the secondary structure of the integral PtBP1 sequence.

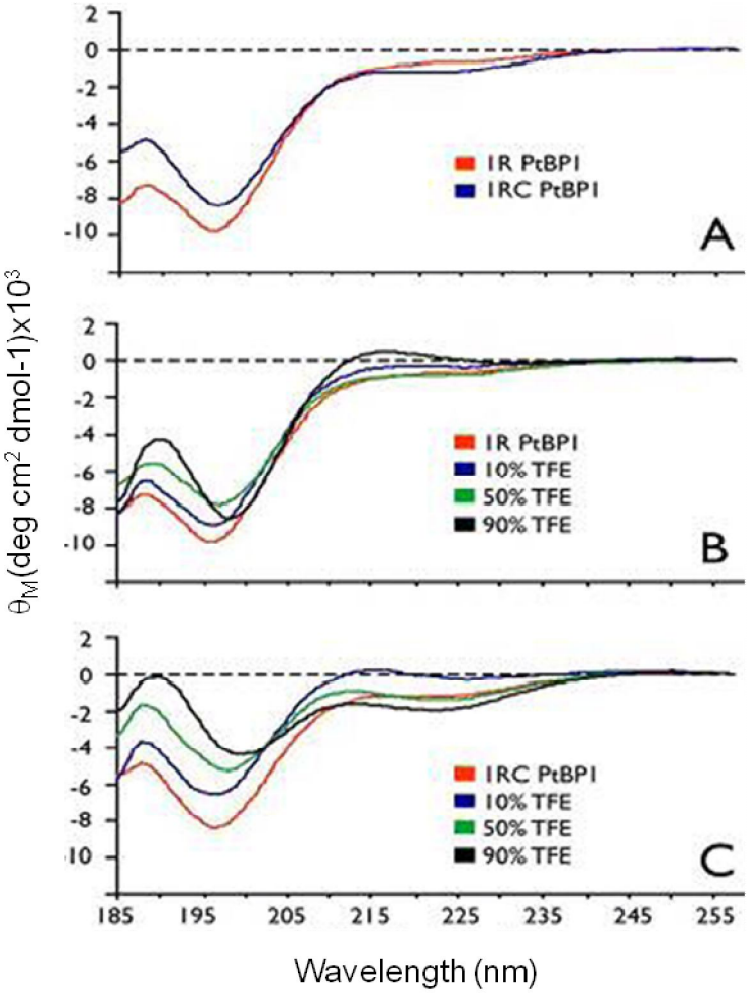

Figure 4.23: CD spectra of 30 μM linear-PtBP1 and cyclic-PtBP1 peptides in (A) 100 μM Tris-HCl, pH 7.5, (B), (C) in the presence of varying volume percentages of TFE in 100 μM Tris-HCl, pH 7.5.

As shown in Figure 4.23-A, the CD spectra for both peptides exhibit (-) π–π* transition bands centered at 197 nm, which is consistent with the presence of random coil (RC) conformation in equilibrium with other secondary structures. Hence, both the linear and cyclic forms exist as unfolded, structurally unstable species under aqueous conditions, a molecular feature that is common to other inorganic-binding peptide sequences. However, upon closer examination, we note that a subtle structural difference exists between the two peptides. Specifically, the ν–π* elipticity

band centered at 220 - 225 nm is weak and linear l-PtBP1 displays a more positive elipticity in comparison to the constrained c-PtBP1.

The presence of a (+) ellipticity band in the 220 – 228 nm wavelength region is consistent with the presence of extended helical polyproline Type II (PPII) secondary structure, which has been noted in short peptides that contain proline, alanine, and glutamine. Thus, although both peptides feature the same integral sequence and possess some degree of random coil, our findings indicate that the linear form of PtBP1 also adopts some degree of PPII structure in solution, but the cyclic version does not. Since PPII forming amino acids comprise the integral Pt binding sequence, it is suspected that the cyclic-PtBP1 peptide does not readily adopt a PPII structure in solution due to the presence of the Cys-Cys loop constraint. To investigate this possibility, CD experiments were performed on both peptides in the presence of varying volume percentages of the structure-stabilizing solvent, 2,2,2-trifluoroethanol (TFE, Figure 4.23-B, C). Here, we qualitatively evaluated conformational stability as the response of each peptide to an external perturbation reagent. For the linear-PtBP1, two phenomena were observed: first, as a function of TFE content, the ν–π* transition ellipticity band (218 nm) increases in (+) intensity and, second, the π–π* ellipticity band experiences a slight red shift to higher wavelength (200 nm).

These spectral features are consistent with an increase in the percentage of PPII structure and the simultaneous loss of random coil structure, which indicates that TFE has an impact on the conformation of the linear-PtBP1 sequence. This is not surprising, since the linear form has unconstrained termini and should be responsive to alterations in solvent conditions. However, slightly different conformational behavior for cyclic-PtBP1 was observed. At low TFE percentages (10% v/v), we initially observe a (+) increase in the ν-π* ellipticity band (218 nm), corresponding to an increase in PPII structure content. However, as TFE content increases beyond 10% v/v, we note that a different structural fate is in store for the cyclic peptide. First, the π–π* ellipticity band shifts to higher wavelength (200 nm), indicating a shift in conformational equilibrium away from random coil secondary structure. Second, the ν-π* band becomes (-) in intensity and shifts to 222 nm, which is consistent with the presence of some degree of alpha-helical structure. Thus, the cyclic-PtBP1 peptide cannot replicate the same TFE-induced conformational

transition exhibited by linear-PtBP1. We interpret these results as follows: (a) Since each peptide possesses the same integral sequence (PTSTGQA) that consists of two PPII forming amino acids, it is likely that the inherent secondary structure of the 7-AA sequence is a combination of RC and PPII. (b) However, with the presence of the covalent cys-cys loop, the cyclic version attempts to adopt a PPII structure (Figure 4.23). Instead, the cyclic sequence adopts an alternant structure in the presence of TFE in equilibrium with RC to satisfy the existing molecular constraint of a covalent loop. This result experimentally verifies earlier findings obtained through molecular modeling studies of the platinum-binding septapeptides conforming that certain molecular architecture containing multiple polypods lattice match to the platinum crystal surface (Oren et al., 2005). The degree of binding might differ with the molecular architecture possessed by the peptide due to the availability of the reactive side groups for the surface interactions.

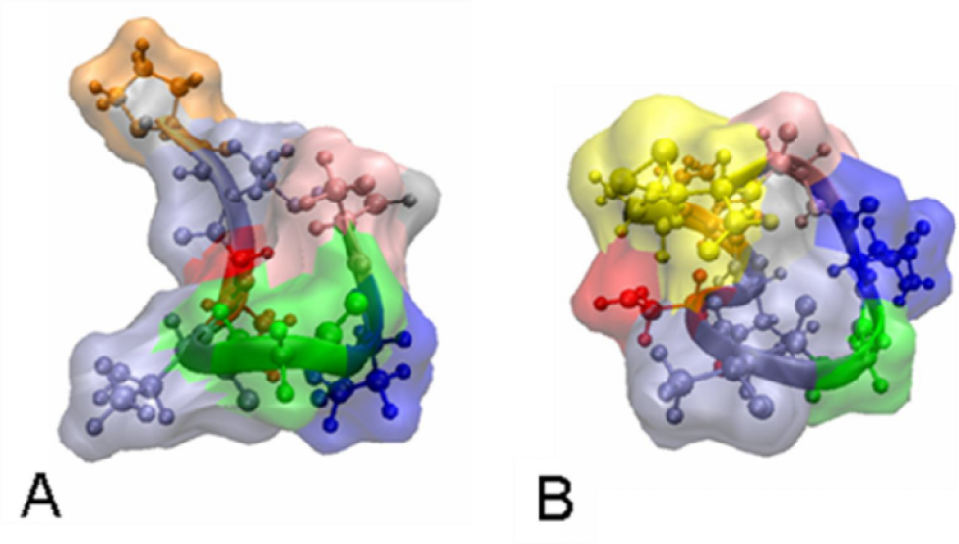

Figure 4.24: Pseudo 3-dimensional view of molecular architectures of (A) linear-PtBP1 and (B) cyclic-PtBP1. The amino acids are colored as CPTSTGQAC.

The conformational features discussed above may be further investigated by modeling studies presented in figure 4.24. Here the molecular models provide more detailed analyses of the cyclic and linear peptides that have either a compact or an open form, respectively. The rigid form is a consequence of constraint exerted on the septapeptide by the presence of the covalent C-C loop resulting in a molecular architecture that is more rigid. Because of the absence of such structural constraints, the linear form of the peptide is more flexible with a high degree of freedom in its

conformation. We postulate, therefore, that the compact structure imposed upon by the Cys-Cys loop affects the motion, the binding dynamics and the adsorption kinetics of the Pt-binding sequence. The linear form, because of its high degree of flexibility, is more floppy and, therefore, has a slower adsorption behavior. The present study provides compelling evidence that molecular features, such as loop constraint, can exert a significant influence on peptide adsorption onto inorganic materials such as Pt. The fact that, linear-PtBP1 exhibits bi-exponential Langmuir adsorption behavior clearly suggests that the adsorption process for the linear form may involve an additional event or step that does not occur in the single Langmuir cyclic-PtBP1 adsorption process.

This additional step may involve peptide conformational rearrangement or repositioning of the short 7-AA sequence on the Pt surface that occurs after the initial peptide binding event on Pt. If we assume that the short linear sequence has some degree of freedom or motion that permits this extra step in the adsorption process, then we conclude that this extra step or event may be prohibitive in the case of the cyclic-PtBP1 sequence due to the presence of the loop restraint and the corresponding loss of degrees of freedom.

4.2.2 Affinity of GEPIs specific to metal oxides

In this section the binding affinity of silica binding peptides were demonstrated using the SPR and QCM data as well as their secondary structure information. The silica binding peptides were selected by Deniz Şahin from Sarikaya-Tamerler research group. These peptides were screened from a phage display library housing $2x10^9$ phage. The phage pIII coat protein contains 12mer random peptides. The silica binding peptides were categorized in two different groups. The first generation peptides were called the phage display selected silica binding peptides. The second generation peptides were designed using the structure – sequence relationship of the first generation silica binding peptides through knowledge based approach developed in our group. These second generation, designed peptides were (*in silico)* designed using bioinformatics tools by Dr. E. Emre Oren from Sarikaya group (Oren et al., 2007).

4.2.2.1 Silica binding peptides

Silica binding peptides were tested on a silica coated SPR substrate for theirs binding affinity.

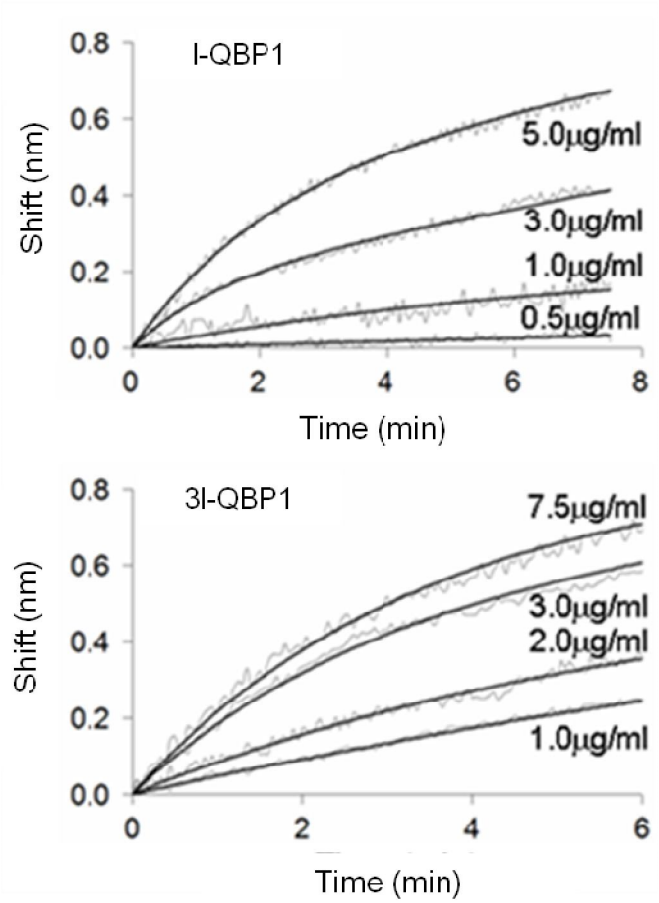

Figure 4.25: Adsorption curves for the three different forms of the silica binding peptides l-QBP1, 3l-QBP1. Continuous black lines represent the model the data points.

The original sequences are linear 12 aa long peptides selected from phage display libraries. Also 36 aa long three repeat of these peptides were synthesized to see any possible effect on binding affinity. Silica binders l-QBP1 and 3l--QBP1 both have binding free energies -6.9 and -8.5 kcal/mol respectively. The desorption rates for both peptides are closer however the adsorption rate for 3l--QBP1 is six times faster than l-QBP1. This causes a 1.6 kcal/mol difference in the binding energies.

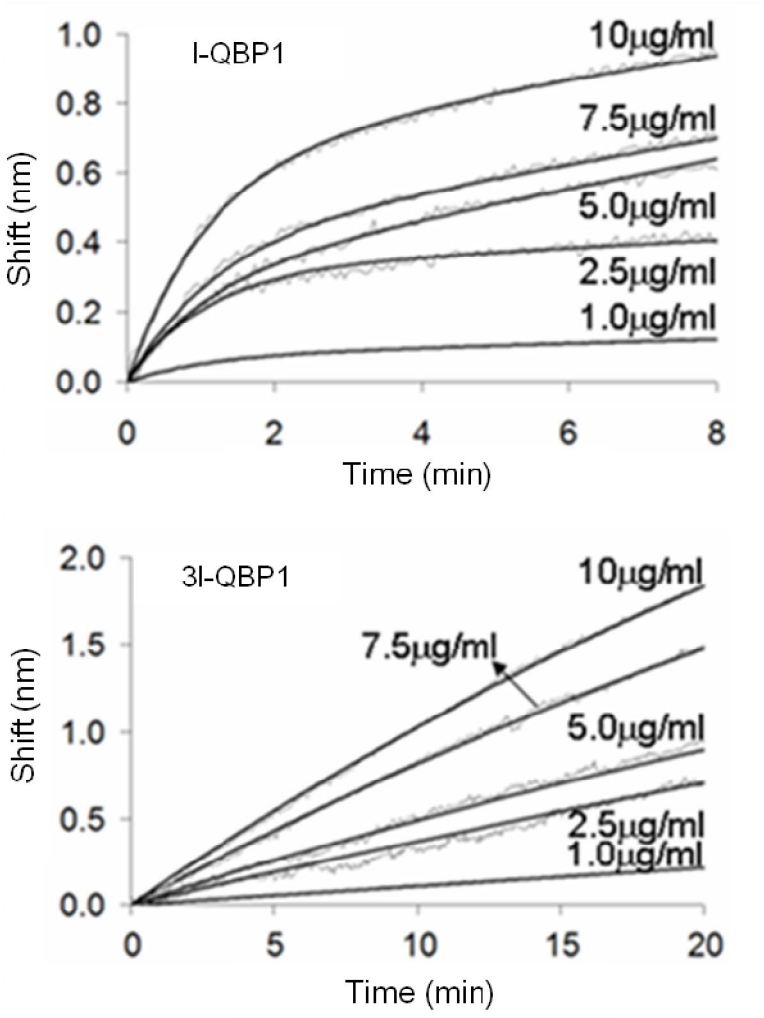

Figure 4.26: Adsorption curves for the three different forms of the silica binding peptides l-QBP2 and 3l-QBP2. Continuous black lines represent the model the data points.

Binding energy of QBP2 did not change as a function of increased number of repeats, the energies were found to be 8.4 kcal/mol and 8.3 kcal/mol respectively for l- QBP2 and 3l-QBP2. Making trimer of the QBP2 increased the adsorption rate of the original sequence four times and also the desorption rate of 3l-QBP2 increased three times.

The 3l-QBP2 was fitted to a two stage Langmuir adsorption model; however all of the other silica binding peptides were fitted to a single Langmuir adsorption model. The adsorption behavior of these silica binding peptides is different when displayed as concatamers. QBP2 is not affected by increasing the number of repeating units by means of binding energy. However, QBP1 peptide is affected by increasing number of the peptide, this effect is mainly reflected by means of the increased adsorption rate. Comparing K_{eq} *s* of the QBP2 almost hundred times lower compared to that of

QBP1. Looking into the chemical structure of the peptide, one can realize the basic difference between these two binders is the number of the aromatic groups. In QBP2, there was a remarkable number of the aromatic rings, the aromatic rings may decrease the degree of freedom of the peptide and thus stabilizes the conformation of the peptide on the surface.

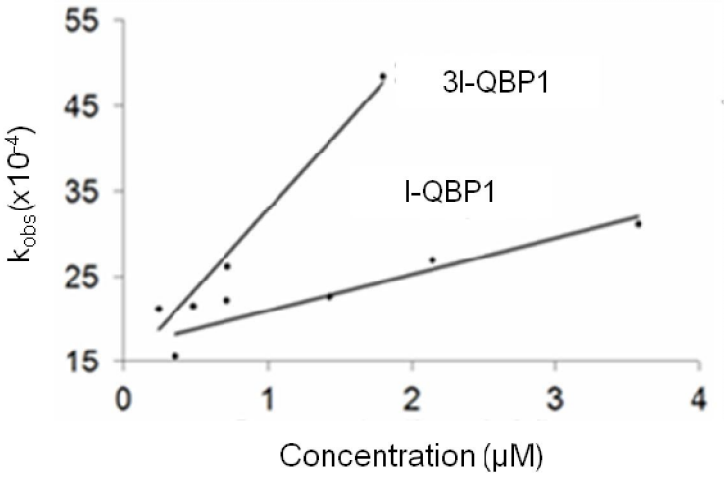

Figure 4.27: The concentration dependency (k_{obs}) of apparent adsorption rates were shown at the bottom.

QCM-D analysis of these peptides provided a detailed information how these peptide were oriented on the surface of the silica. QBP1 and QBP2 are compared in their original conformations (l-QBP1 and l-QBP2). The representative Figures of these QCM runs are given in Figure 4.30. Figure 4.30 reveals that the QBP1 has a slower adsorption compared to that of QBP2, which is also validated with the SPR data. From the QCM-D signals it seems that the films formed by QBPs are densely packed, which is proved with a low degree of change in the dissipation.

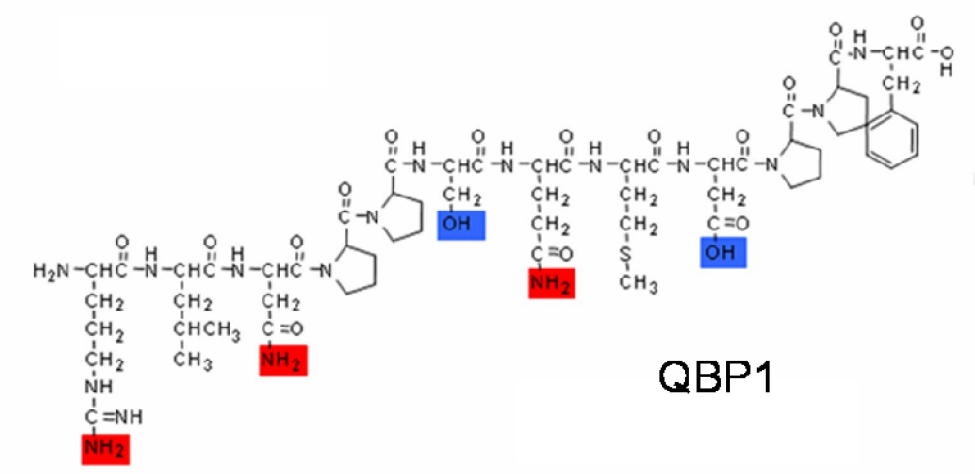

Figure 4.28: Chemical formulas of the QBP1 and QBP2, the amine and hydroxyl groups were highlighted in red and blue respectively.

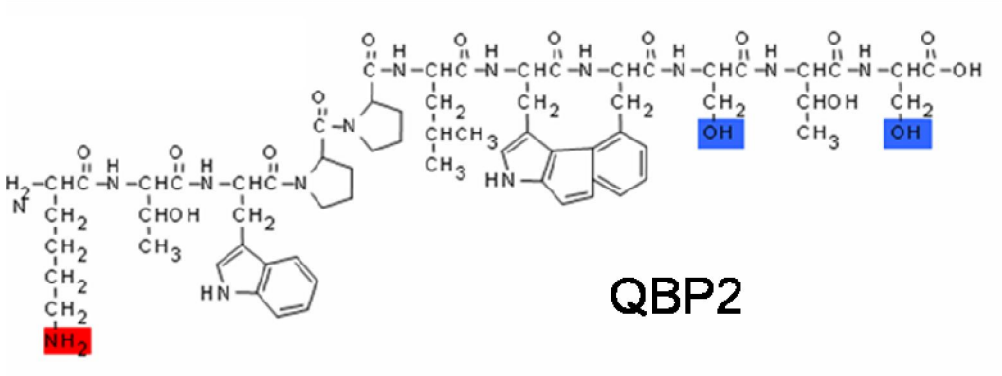

Figure 4.29: Chemical formulas of the QBP1 and QBP2, the amine and hydroxyl groups were highlighted in red and blue respectively.

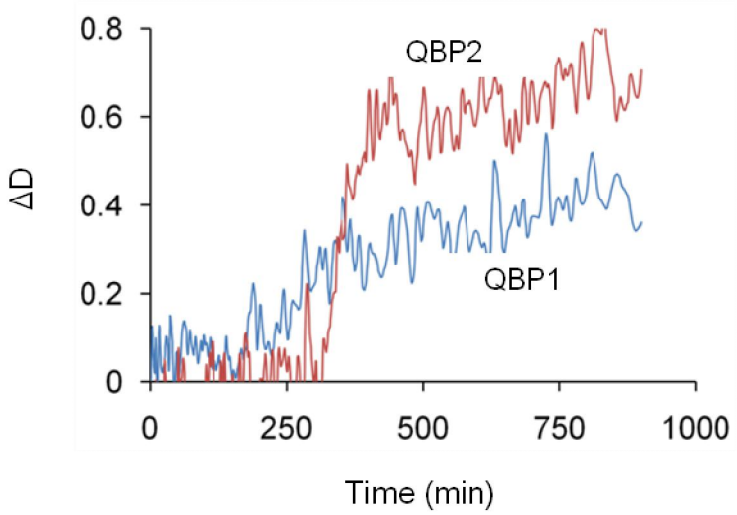

Figure 4.32 Dissipation changes of the QBPs

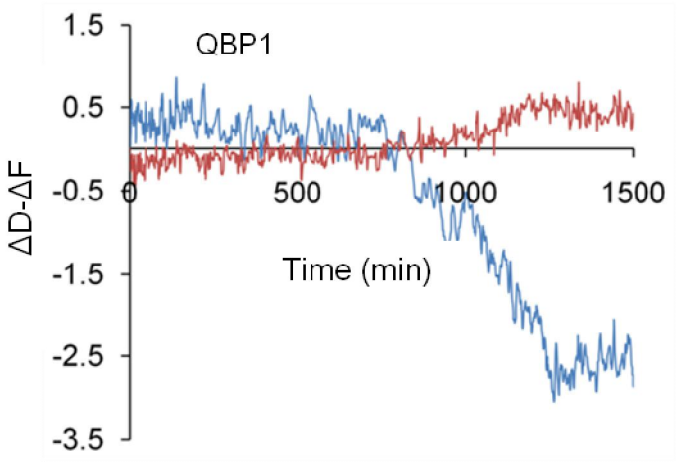

Figure 4.30: QCM-D frequency shifts and dissipation change as function of time for QBP1. Red lines represent the change in dissipation as the blue lines represent the change in the frequency.

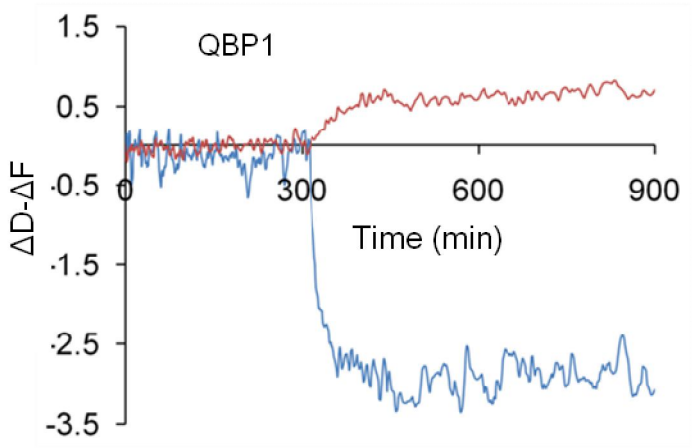

Figure 4.31: QCM-D frequency shifts and dissipation change as function of time for QBP2. Red lines represent the change in dissipation as the blue lines represent the change in the frequency.

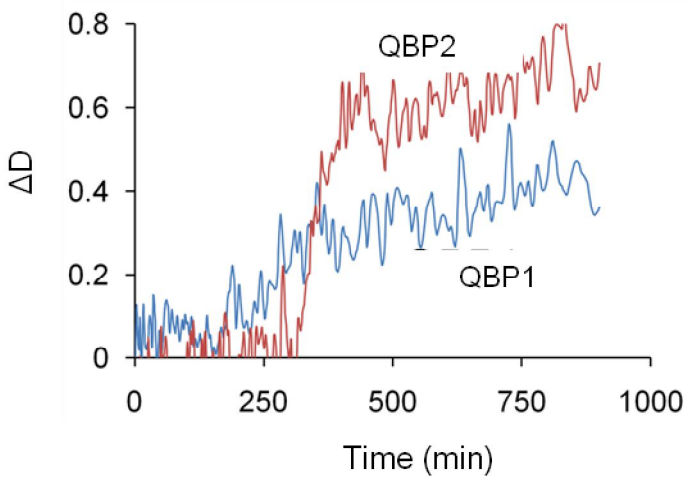

Figure 4.32: Dissipation changes of QBPs

Comparing the change in dissipations, there is a difference between these two QBPs, and they are given in the Figure 4.32.

In figure 4.32, the packing densities of the QBPs can be compared. The dissipation of these peptides actually represents the amount of the water, which these peptides can hold in their structures. GEPIs do not have a tertiary structure, so they are not suspect to a denaturation process when they stack onto a solid surface. So the change in dissipation can be a measure of their packing densities. The change in the dissipation of the QBP1 film, is less then QBP2, so we can conclude that QBP1 is packed densely compared to that of QBP2. The Langmuir adsorption constants of these peptides were also computed from QCM-D data, using a 1:1 Langmuir adsorption interaction. It is obvious that (in Appendix C) the k_a, k_d and K_{eq} value from QCM-D and SPR seem to be very close to each other, which is a cross internal control of two different adsorption monitoring methodologies. QBP1 has a binding energy of -6.3 kcal/mol and QBP2 has a binding energy of -8.7 kcal/mol from QCM-D experiments. Combining the results from the dissipation and the binding affinities of these peptides we can conclude that: The stronger binding peptide and the weaker binding peptide does not have the same orientation on the surface of the silica, as the dissipation of these peptides is different we can conclude the densely packed layer may direct a looser binding.

4.2.2.2 Affinity of the *de novo* designed quartz binding peptides

Silica binding peptides QBP1 and QBP2 were selected using phage display. Using the combinatorially selected and characterized silica binding peptides, the activity (binding to silica surface) sequence relation was exploited to design new solid binding peptides with superior binding affinities. Following the classification of the peptide in three distinct groups as strong, moderate and weak binders, statistical and bioinformatics tools were employed to define the total similarity scores of the selected peptides. Later, through perturbating the existing pam and blossom matrices, Quartz I matrix was developed. Using this matrix, binding affinities of the new generation computationally derived peptides were predicted. To test, we selected two different category of binders, strong binders and weak binders. These peptides were called *de novo* designed silica binding peptides (Oren et al., 2007). To test the prediction power of the knowledge based approach in designing second generation

computationally derived peptides, peptides were first synthesized and investigated for theirs binding affinities. As a first step of the binding analyses, we only compared the total shift in SPR signal. In SPR the shift in the signal corresponds to the amount of deposited mass of peptide on SPR chip surface. So if the peptide is adsorbed tightly on to the silica surface the shift in SPR signal must be higher compared to the weakly bound peptide. Here, the peptides were compared with the first generation phage display selected peptides, and *de novo* binders were found to have higher affinity compared to strongest phage display selected one. Further characterization of the de novo designed peptides was carried out both structural points of view as well as binding affinity. The strongest binders from the whole set of the second generation peptides and the weakest binder were selected for further characterization with SPR and the structural properties of these peptides were related to their binding affinity. As reflected in the Figure 4.33 the strong binding dnQBPs showed higher shift compared to the weak binder which is also the case for most the concentration of the peptides.

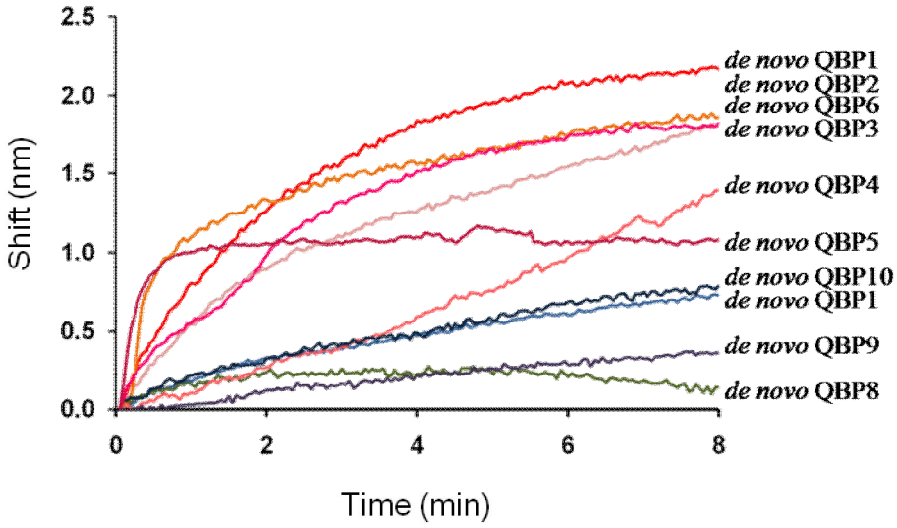

Figure 4.33: Surface plasmon resonance spectral analysis that measures the amount of bound peptide versus time was performed at 4 μM concentrations. The higher the shifts in the dip position at a particular time, the stronger the binding and also the sharper the shift reveals a faster binding.

The adsorption behavior of de novo QBP1, 3 and 8 were analyzed in details: The adsorption isotherms were given in Figure 4.34. The data gathered as a function of time for the adsorption was fitted to a simple Langmuir adsorption model.

This shows that our peptide concentrations are at the range of the monolayer formation. We calculated binding constants from fitted data, the Keq values were calculated as $1.6x10^6$ M^{-1}, $5.0x10^6$ M^{-1}, $1x10^5$ M^{-1} for dnQBP1, dnQBP3 and dnQBP8 respectively.

The binding energies for strong binding de novo QBPs (1-3) are found to be ~8 kcal/mol. Comparing the the two strong binding peptides it was found that the QBP1 and QBP3 has almost the same energies however the binding mechanisms for these peptides may differ, the adsorption rate for the dnQBP3 is seven times higher than the adsorption rate for the dnQBP1. However, desorption rate of the dnQBP3 is almost twenty times lower compared to the dnQBP3. We can note that in the case of dnQBP3 adsorption dominates whereas in the case of dnQBP1 desorption dominates while the equilibrium state is taking place. This may caused by the number of the proline residues included by dnQBPs which are six pralines in the dnQBP1 and four proline residues in dnQBP3 respectively. Proline has a rigid structure and it is found to stabilize the structure of the peptides, which may increase the binding affinity of these peptides (Krane, 2008, Berisio et al., 2006). The proline residues restrict the free movement of the peptides on silica surface, which results in enhanced adherence of the peptide mass on silica surface.

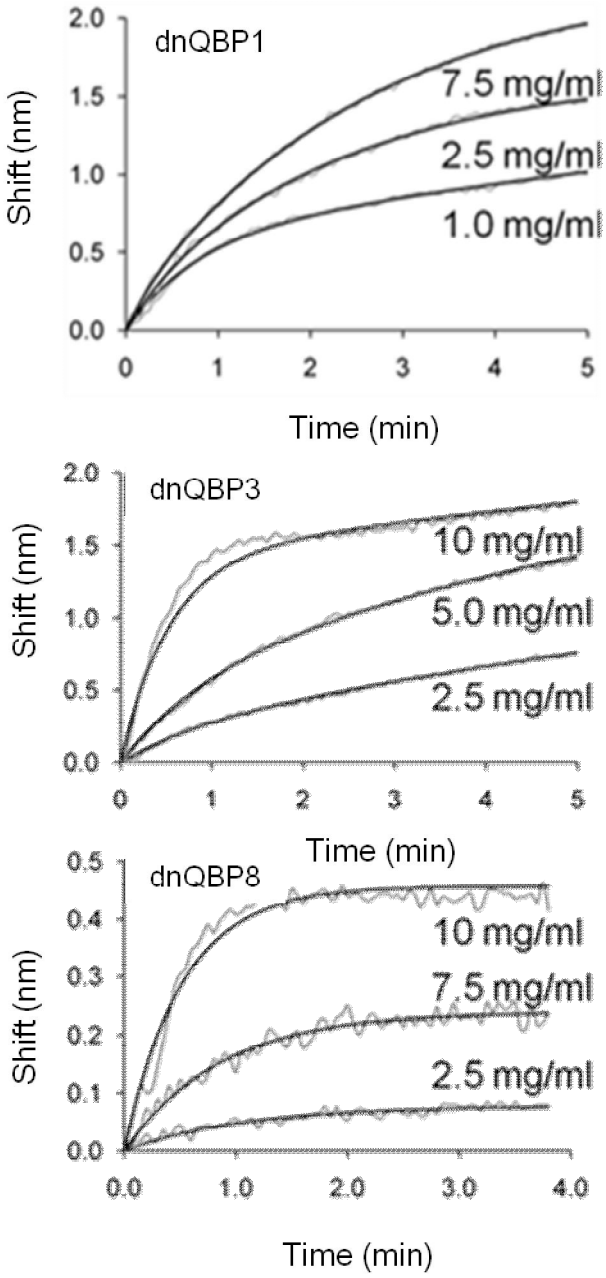

Figure 4.34: Adsorption curves for the three different forms of the silica binding peptides l-QBP1, 3l--QBP1, l-QBP2 and 3l--QBP2. Continuous black lines represent the model the data points.

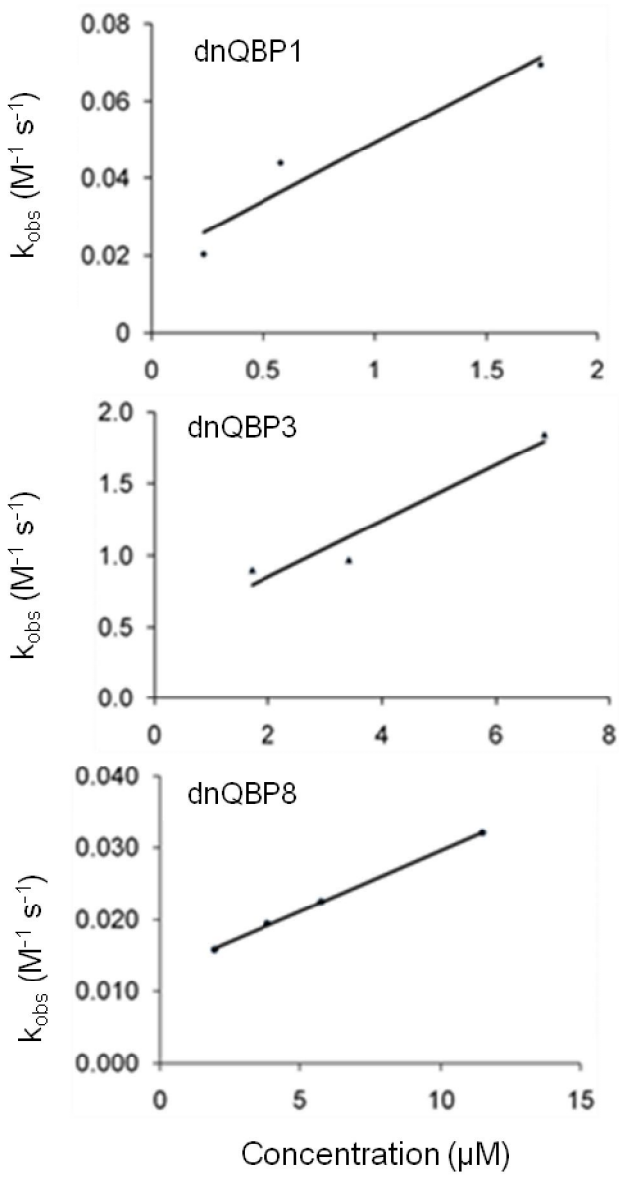

Figure 4.35: The concentration dependency (k_{obs}) of apparent adsorption rates were shown at the bottom.

We observed a fundamental difference between the weak and strong binders for their binding energies which is controlled by the adsorption rate. The dnQBP8 has almost the same desorption rate with the dnQBP3. However the adsorption rate of the peptide dnQBP8 is ~100 lower compared to both of the strong binders. To make a stronger conclusion we also investigated the secondary structural motifs for these three different dnQBPs. The observed differences in SiO_2 adsorption behavior and binding affinities suggest that there may also be structural features which distinguish these peptides. To explore this issue, we performed CD experiments on the QBP1, 03, and 08 *de novo* polypeptides in identical solution conditions (neutral pH). It was found that each of the SiO_2 binding polypeptides possesses structural characteristics

that correlate with affinity (Figure 4.36). QBP1 and QBP3 sequences exhibit a (-) ellipticity band centered near 200 nm (π–π* transition), and a (+) ellipticity band centered near 230 nm (n – π* transition). These ellipticity bands are consistent with the presence of polyproline Type II secondary structure (PPII), which has been noted in short peptides and most likely forms as a result of the presence of Pro in both sequences. Interestingly, the n – π* transition band for QBP3 is less intense than the one obtained for QBP1, and we attribute this to the differences in Pro content in each sequence (QBP1 possesses six proline residues, QBP3 possesses four). In comparison, the weak binding QBP8 sequence primarily features a (-) ellipticity band at 198 nm, which is consistent with the presence of random coil conformation in equilibrium with other secondary structures.

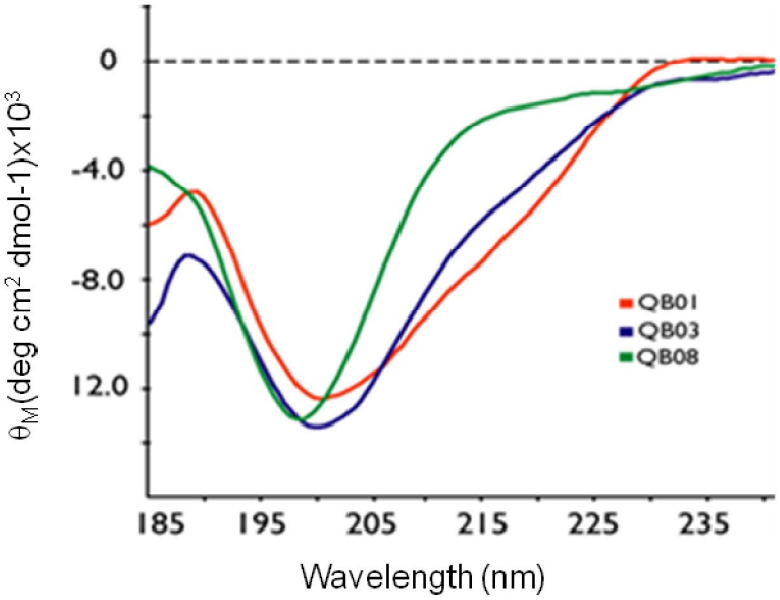

Figure 4.36: Secondary structure of the dnQBP1, dnQBP3, dnQBP8.

One can note that this peptide sequence is Pro deficient and possesses two Lys residues which are separated from one another by two intervening residues. This close positioning of repulsive (+) charge within the QBP8 sequence may destabilize the conformation of this peptide, which would explain why the random coil conformation is formed in solution. Thus, our CD experiments reveal that both the high and moderate affinity SiO_2 sequences feature PPII conformations, with the highest affinity sequence possessing a greater degree of this secondary structure. Conversely, the weak affinity sequence adopts a random coil or unstructured conformation under the same conditions. Presumably, the random coil conformation somehow compromises the binding affinity of QBP8. Given the involvement of PPII

conformation in a number of protein interaction scenarios this secondary structure may facilitate moderate (QBP3) and high (QBP1) affinity binding of *de novo* sequences to SiO_2.

4.3 Material Selectivity of GEPIs

The first step in the characterization of the inorganic binding peptides was to determine the binding affinity of the peptides in a quantitative manner. However, for the full molecular characterization of these peptides, the affinity test was not enough. Affinity does not necessarily mean the material selectivity. To check if GEPIs may have a selective affinity towards a material, for example gold binding peptide supposed to recognize the gold surface but it is not expected to bind to platinum surface or silica surface. The overarching goal of this study is to show that GEPIs can differentiate only one material in multi-material systems, which will lead to open new avenues in the applications toward bio- and nanotechnological applications.

In the previous section the binding affinities of the inorganic binding peptides were calculated. Beyond testing of each peptide on its selected surface, each peptide was tested on several other surfaces to test their specificity. Many of the proposed applications of such peptides require a high degree of specificity to a specific substrate. Specificity also represents a key advantage that peptides have over other chemical approaches for use as SAMs and linkers.

A comprehensive kinetic analysis was done on with all 16 peptides on three surfaces (gold, platinum, and silica). However, due to the amount of data produced (16 peptides x 3 surfaces x 5 concentrations x several repeats of each test), and the low binding of some of the peptide-surface combinations, the data was presented in bar graphics. Figure 4.38 shows raw data from tests with GBPs, PtBPs, and QBPs. From inspection of the raw data, the binding behavior of the peptides falls into three primary categories: high adsorption, low desorption; high adsorption, high desorption; and low adsorption. Figure 4.37 represents these three behaviors.

However, quantitatively the Langmuir model showed quite a poor fit when applied to the data, consistently calculating desorption rate values did not correspond well with the desorption phase of the test. In the end only one peptide material combination showed a good fit to Langmuir's model (3l-GBPon silica).

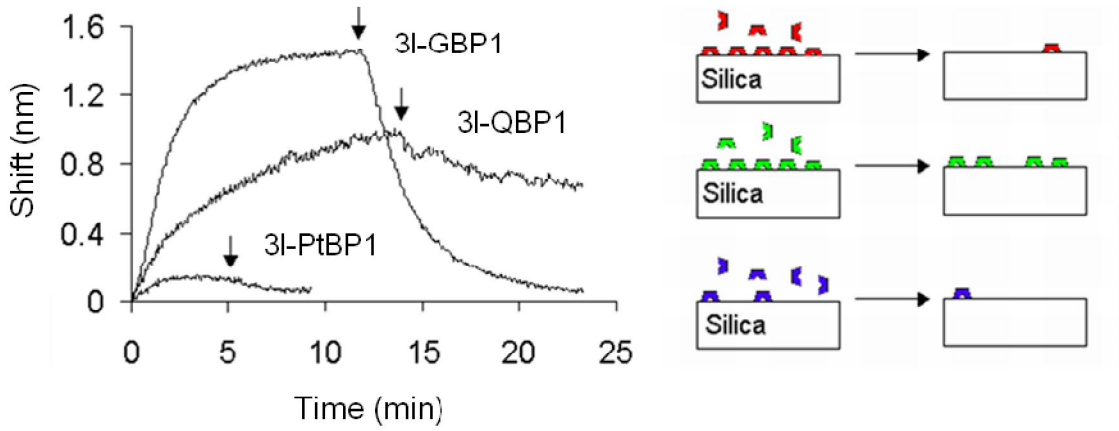

Figure 4.37: Schematic of different binding behaviors seen in specificity studies. Data from adsorption studies of each peptide on a silica surface. These behaviors include weak binders (blue), strong binders (green) and low specificity binders (red).

The other combinations showed isotherms with either heterogeneous binding and/or with extremely low desorption rates that were beyond our instruments ability to effectively measure. Instead of comparing the binding by constants from Langmuir's equation, we compared peptides based on the amount of the peptide left on the surface following the desorption phase. This allows the relative stability and density of the SAM to be compared for each peptide-material combination. The comparison of this data is shown in Figures 4.40-41. In general, peptides showed high affinity to their specific substrate, resulting in material selectivity. The three repeat peptides generally bound stronger than their one repeat counterpart.

The one notable exception was l-PtBP1, which bound much stronger than 3l--PtBP1 to platinum. 3l-GBPhad the highest surface coverage on gold, and 3l--QBP2 had the highest surface coverage on silica. In most cases, very little desorption was observed, indicating that the monolayers formed were quite stable.

When tested on other substrates, the peptides showed a wide range of affinities. In general, there was poor binding on substrates other than the target surface. For example, l-QBP1 showed more than an order of magnitude higher surface coverage on silica than on gold or platinum. The most obvious exception was l-QBP2, which actually showed higher surface coverage on platinum than it did on silica. 3l-GBP also showed high surface coverage on silica, however a high desorption rate meant all the peptide quickly desorbed from the surface, indicating weak binding. These results show the based on combinatorial biology selection, affinity of the peptides

can be predicted but, there is an unpredictability associated with the selectivity of binders.

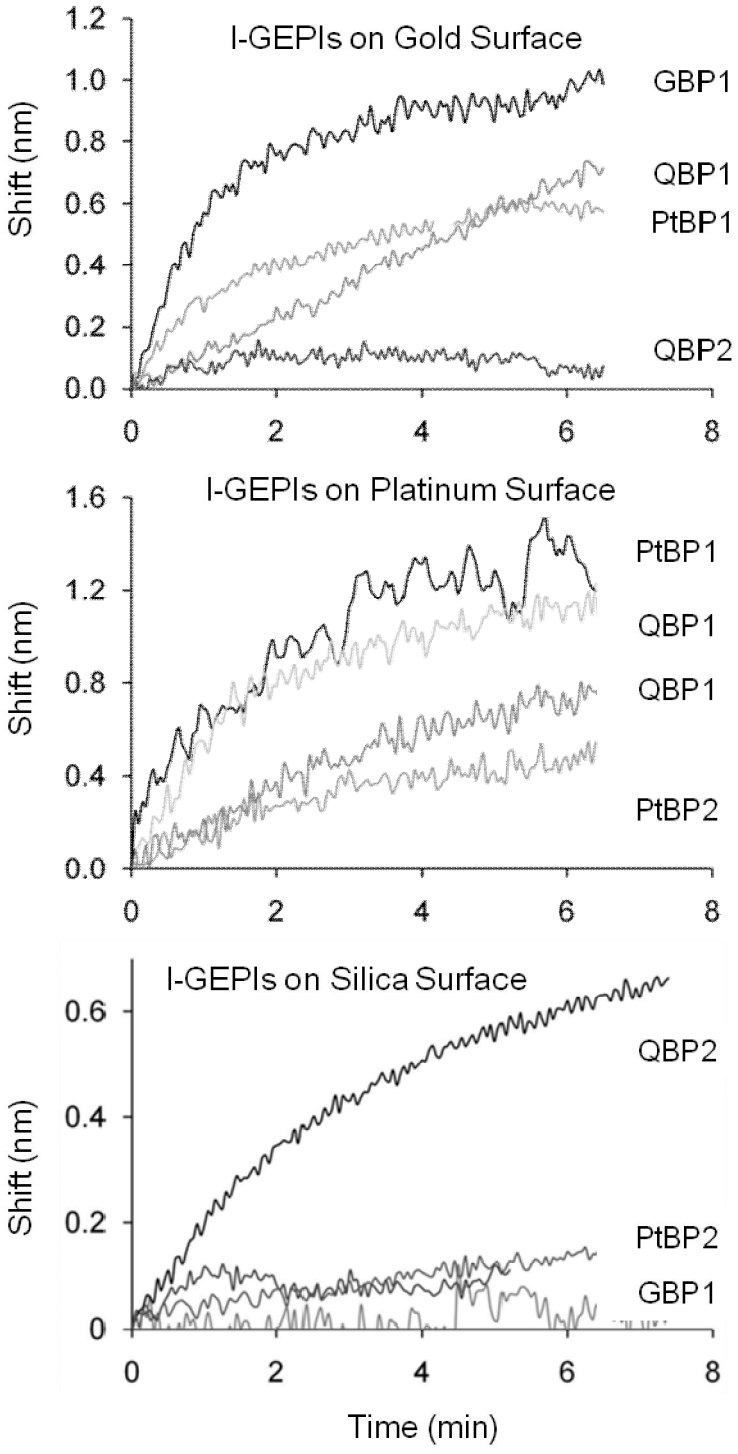

Figure 4.38: Adsorption isotherms of ten inorganic binding peptides to gold, platinum and silica surfaces.

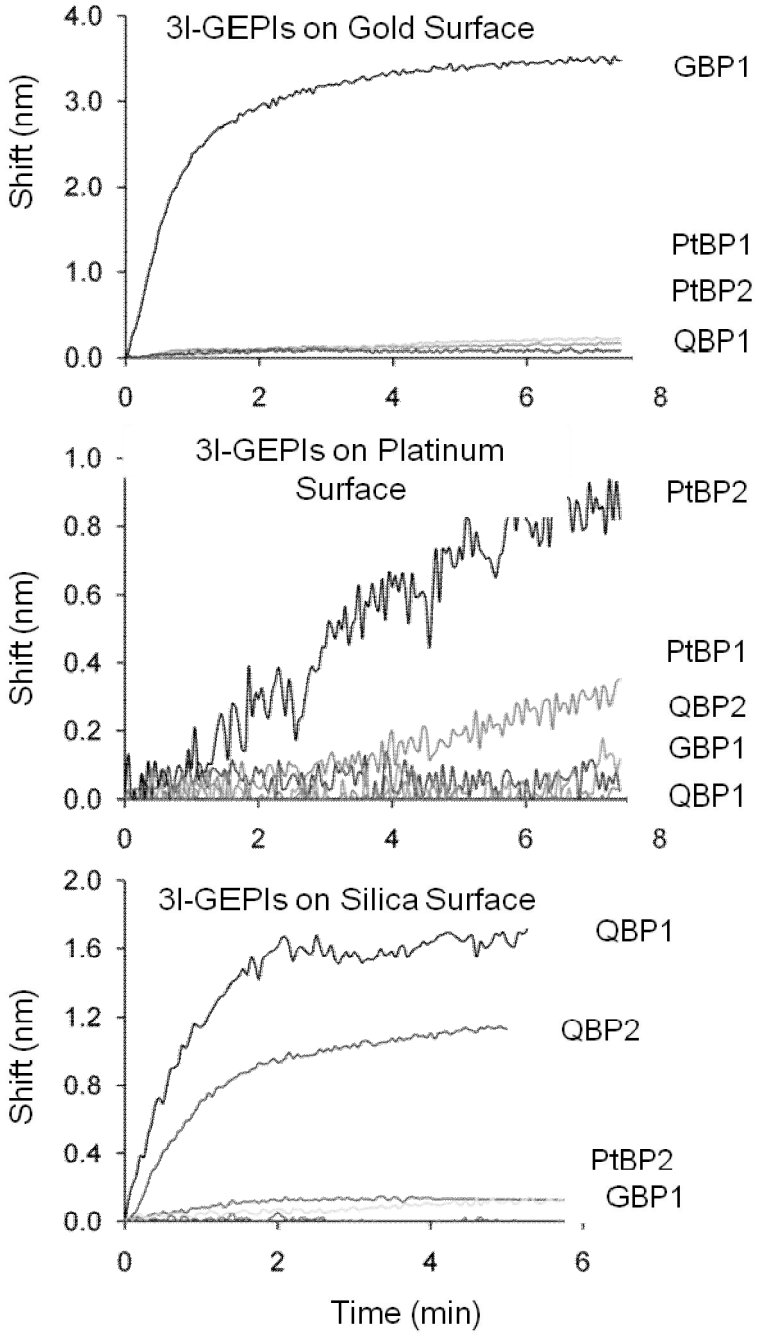

Figure 4.39: Adsorption isotherms of ten inorganic binding peptides to gold, platinum and silica surfaces.

The peptides did bind to the surfaces they were indented to bind to and had a wide range of results on other material surfaces. This also indicates the importance of affinity versus selectivity when one employs peptides for material selective applications. In our results we also observed that in general three-repeat form resulted in better binding properties. Clearly, adding extra repeats to peptides will neither always increase the binding affinity nor necessarily increase the material

selectivity, the effect of structure based on sequence is dominant on the control of the binding property

Despite the unpredictability of peptide behavior, our results show that peptides that are truly specific to a material can be identified. For example, except for the one case of l-PtBP2, the peptides showed very different affinity to gold than to platinum. This is significant because both gold and platinum are noble metals, with applications in nanotechnology. Also, at least one peptide was found that bound only to gold and only to silica. This shows the potential for a high level of material selectivity in peptides that is not observed in purely chemical methods such as thiols. This is promising for future applications that require highly specific binding to an individual material. Several more interesting observations can be made from this data. For example, another observation from our the analysis is that the quartz binding peptides were selected to bind to single crystal quartz substrates, yet still showed good affinity to the amorphous silica substrate used in this study.

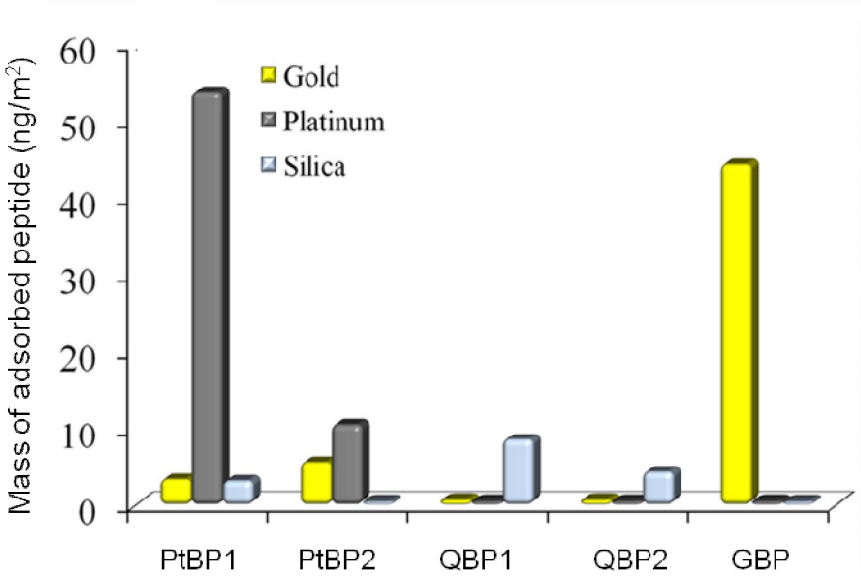

Figure 4.40: Comparison of peptide binding on gold, platinum, silica surfaces, in one repeat. The value compared is the mass of the adsorbed peptide remaining on the surface after the rinsing phase, and thus the strongly bound peptides.

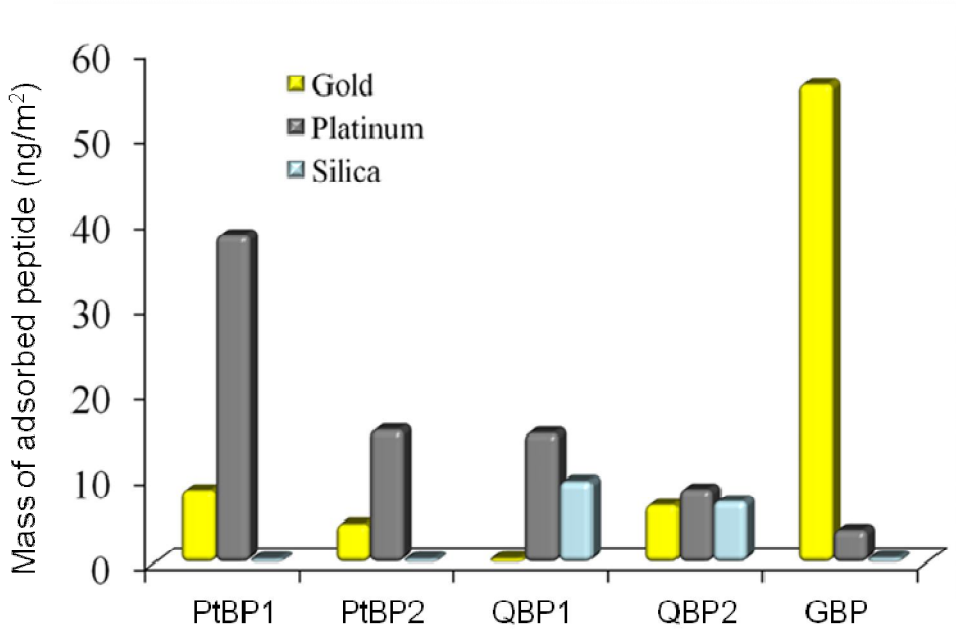

Figure 4.41: Comparison of peptide binding on gold, platinum, silica surfaces, in three repeat forms. The value compared is the mass of the adsorbed peptide.

This would indicate that, at least in the case of quartz binders, although the surface structure may play an important role in binding, the specific binding could be obtained at a high level for different surface, such as amorphous versus crystalline. This may be likely due to the peptide bonding to the charged surface of silica. Another observation, while changing the number of repeats of a peptide did not always lead to an increased affinity to the target material, it can still be an important factor in tuning the binding behavior of the peptide.

4.4 Thermodynamics of Binding and Structure-Activity Relation in GEPIs: Case Study Gold Binding Peptide

The binding kinetics of the gold binding peptide was given previously in section 4.2. Both the adsorption and desorption rates of this peptide was analyzed in details, which also lead us to calculate the binding energy of the peptide both in one repeat and three repeat forms. However we like to deduce more information on the mechanism which makes the 3l-GBP binds better.

To extend our observations beyond simple adsorption studies for kinetics parameter determination, which certainly provide essential tool for practical applications of these peptides, we now turn to characterization methods that can quantify these

thermodynamic terms and provide fundamental insights into the two-stage adsorption process. Our overarching goal is to understand their role and significance in the understanding of the solid-binding phenomena. Thermodynamic studies have been conducted to study the adsorption of the proteins onto polymeric biomaterials and colloidal surfaces, chromatographic solid supports (Lee et al., 2005) and on hydroxyapatite (HAP) (Goobes et al., 2006). Typically, the general strategy involves the use of calorimetric methods (e.g., DSC, ITC) to determine the free energy change of adsorption from equilibrium state analysis at several temperature points. A more robust, surface-sensitive method, surface plasmon resonance spectroscopy (SPR), was employed to determine the equilibrium and corresponding thermodynamic parameters of protein adsorption (Day et al., 2002 and Cannon et al., 2002). Thus, the SPR approach can not only provide thermodynamics energy terms (ΔS, ΔG, ΔH), with kinetic parameters, as adsorption, desorption and equilibrium constants.

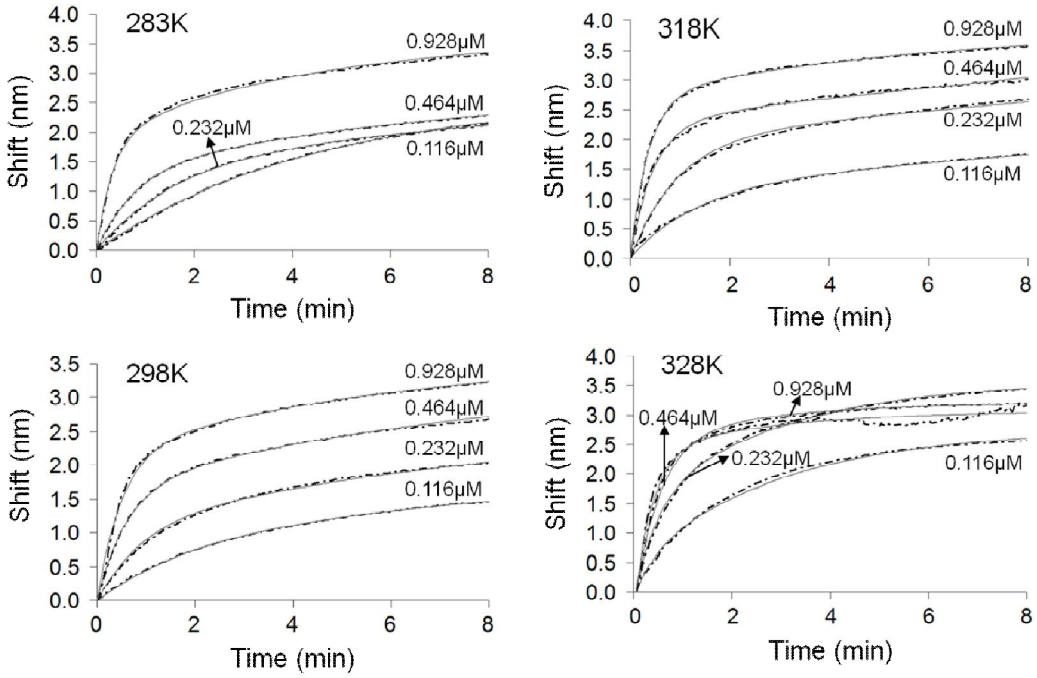

Figure 4.42: SPR sensogram for the adsorption of l-GBP on gold surface

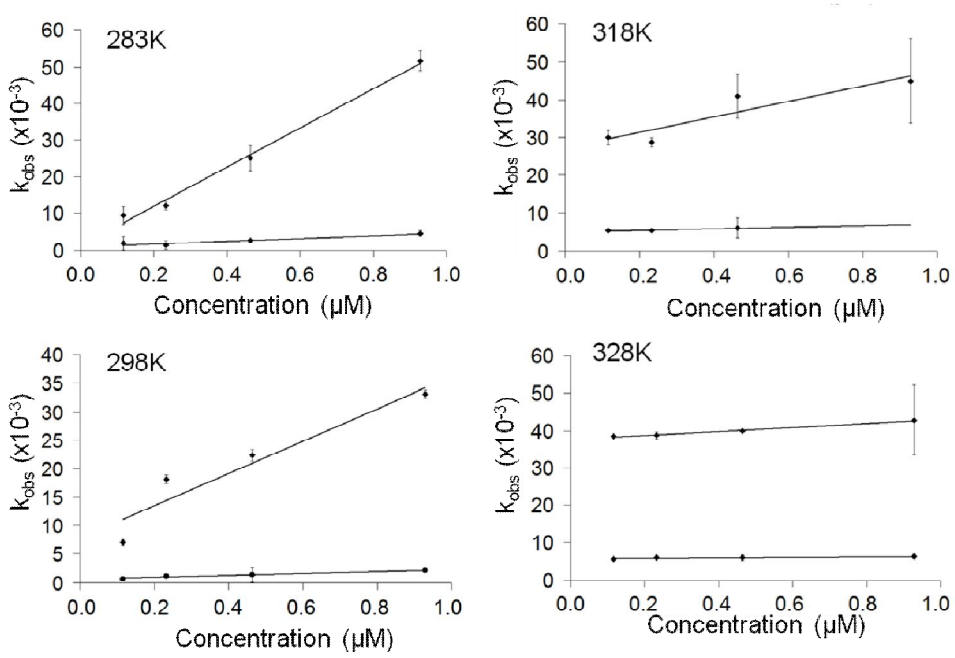

Figure 4.43: The change of the observed adsorption rate (k_{obs}) as a function of peptide concentration for l-GBP.

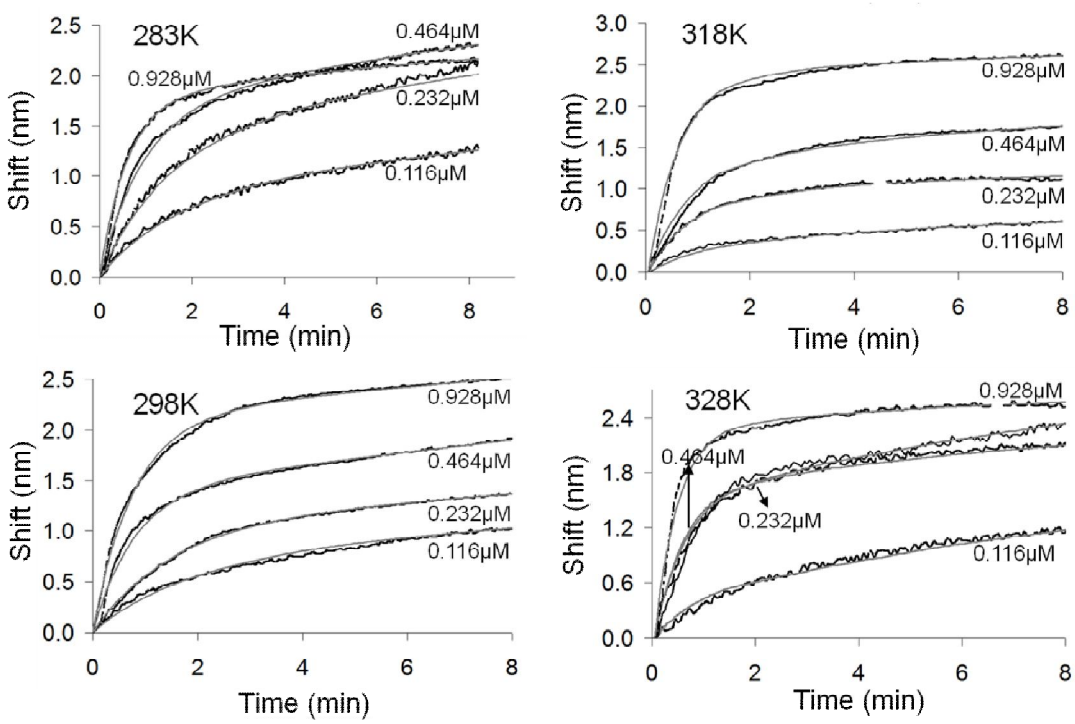

Figure 4.44: SPR sensogram for the adsorption of 3l-GBP on gold surface

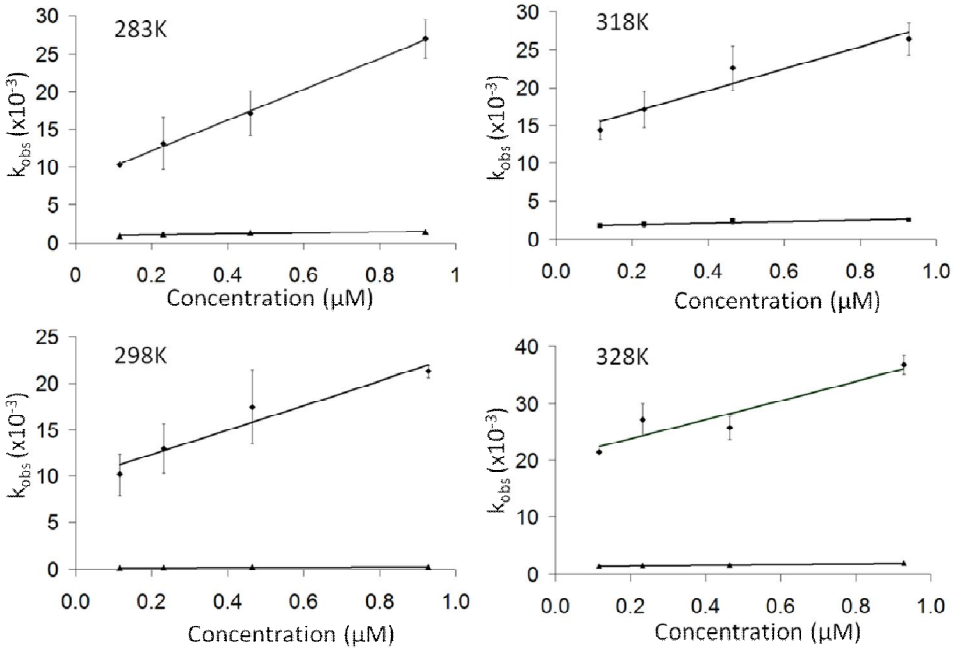

Figure 4.45: The change of the observed adsorption rate (k_{obs}) as a function of peptide concentration for 3l-GBP.

Table 4.3: Adsorption, desorption and equilibrium constants for one repeat GBP. The constants were calculated using the bimodal curve fitting, for two different adsorption processes resulting in two different constants.

T (K)	Peptides	k_a^1 x 10^4 ($M^{-1}s^{-1}$)	k_a^2 x 10^3 ($M^{-1}s^{-1}$)	k_d^1 x 10^{-3} (s^{-1})	k_d^2 x 10^{-4} (s^{-1})	K_{eq}^1 x 10^6 (M^{-1})	K_{eq}^2 x 10^6 (M^{-1})
283	l-GBP	**2.16±0.30**	**6.40±0.64**	**7.18±1.05**	**9.5±0.60**	**3.07±0.70**	**6.79±1.10**
	3l--GBP	5.37±0.80	3.64±0.43	1.20±1.54	10.7±6.10	44.7±11.0	3.42±0.57
298	l-GBP	**1.36±0.80**	**1.12±0.20**	**8.88±1.45**	**2.0±0.00**	**1.56±0.30**	**5.61±1.05**
	3l--GBP	2.86±0.16	1.66±0.20	7.70±1.83	6.50±3.70	3.71±1.22	3.27±1.89
318	l-GBP	**1.43±3.53**	**9.41±4.69**	**14.0±2.05**	**18.0±2.20**	**1.07±0.46**	**5.51±3.55**
	3l--GBP	2.07±0.44	2.47±1.48	27.2±1.10	47.3±1.51	0.76±0.30	0.52±0.05
328	l-GBP	**1.65±0.32**	**5.81±0.80**	**21.0±1.93**	**14.0±0.00**	**0.80±0.23**	**4.15±0.57**
	3l--GBP	0.77±0.14	0.75±0.16	37.8±0.64	56.7±0.60	0.15±0.04	0.13±0.03

We studied the adsorption of l- and 3l-GBP on solid gold using SPR technique at different temperatures to determine the effect of the repeat number on adsorption isotherms and binding equilibrium. In tandem with these studies, we investigated the secondary structure and the conformational stability of each form of GBP in the presence of the structure-stabilizing solvent, 2,2,2-trifluoroethanol. These TFE

studies provide an indirect means of ascertaining the potential of each GBP molecule to undergo conformational reorganization in response to external perturbation. We first determined the kinetics parameters of l and 3l-GBPusing SPR data (Figure 4.42-43-44-45).

We calculated the equilibrium constants at different temperatures both for low and fast adsorption rates (Table 4.3), and then used the Van't Hoff equation to calculate thermodynamic constants (Table 4.4). Similar to l-GBP, the equilibrium constant for 3l-GBP decreases as a function of temperature. However, compared to l-GBP, 3l-GBP has a larger change in equilibrium adsorption rate. Interestingly, the adsorption rate is decreasing by a half for l-GBP, whereas the corresponding rate for 3l-GBP increases more than thirty times as a function of temperature. The total change in K_{eq} is calculated as 4x and 300x for l-GBP and 3l-GBP, respectively. We also note a large entropy change for 3l-GBP upon binding, which indicates that other processes taken place besides simple adsorption process at the Au interface (Table 4.4). We propose that these changes are related to the differences in the chain lengths of the GBP molecules.

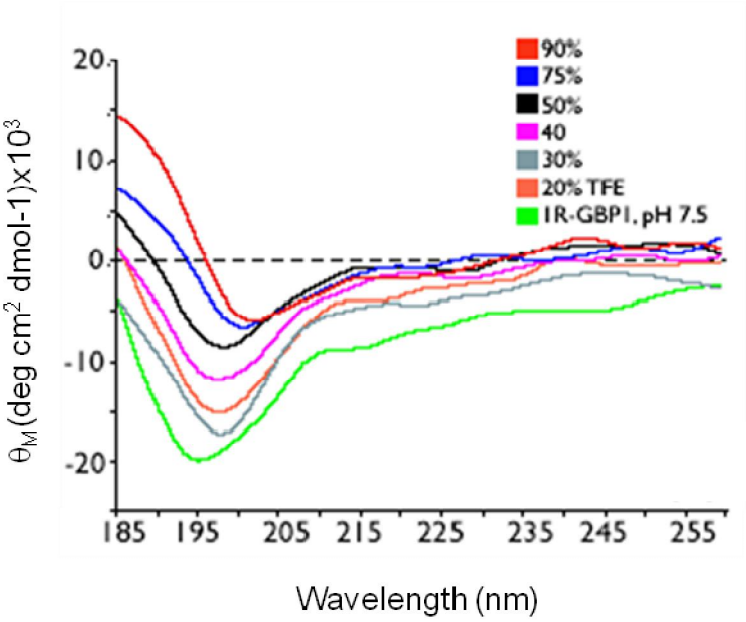

Figure 4.46: Circular dichroism spectroscopy of l-GBP in 100 μM Tris-HCl buffer, pH 7.5 in the presence and absence of 2,2,2-trifluoroethanol (TFE). Note that in (B), there is overlap between the 30%, 50% and 40%, 75% TFE ellipticity curves. To represent this, we have portrayed each of these curves as dashed lines.

Given the large, negative change in entropy associated with the binding of 3l-GBP onto Au surface, it is plausible to suggest that one of the events that occur during the two-stage polypeptide adsorption on to solid Au process is conformational rearrangement of the 42 AA sequences.

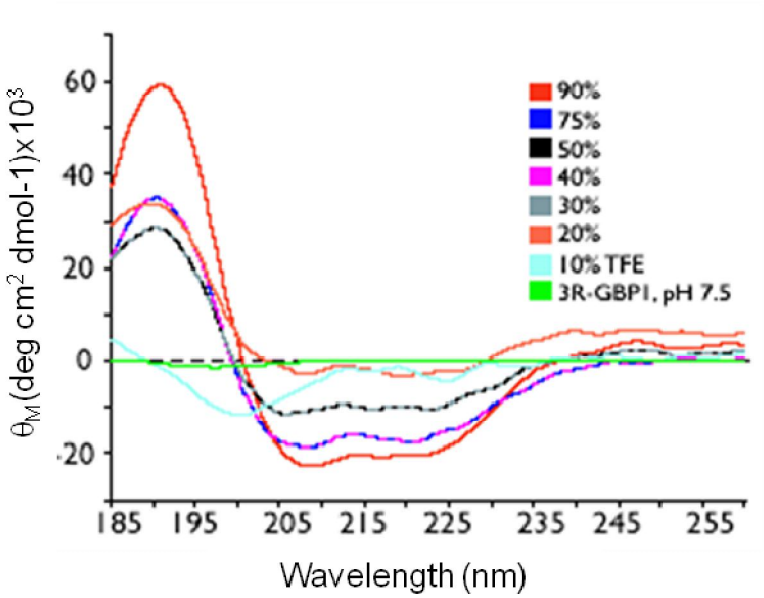

Figure 4.47: Circular dichroism spectroscopy of 3l-GBP in 100 μM Tris-HCl buffer, pH 7.5 in the presence and absence of 2,2,2-trifluoroethanol (TFE).

Table 4.4: Thermodynamic parameters of adsorption of GBP were determined by equilibrium analysis.

Parameters	l-GBP	3l-GBP
ΔH_1 (kcal/mol)	-5.09 ± 0.25	-22.1 ± 3.0
ΔH_2 (kcal/mol)	-1.84 ± 0.53	-13.4 ± 1.5
ΔS_1 (kcal/mol*K)	+10.90 ± 1.30	43.4 ± 8.5
ΔS_2 (kcal/mol*K)	+19.60 ± 2.20	-16.6 ± 4.6
Surface Area (Å^2)	1738	4536
Volume (Å^3)	3493	10010
Mass (Da)	1430.6	4291.8

Given that the solution structures of l- and 3l-GBP are both conformational labile, we were curious to learn if either polypeptide exhibited tendencies to adopt specific conformations in response to changes in environment. Earlier, we established that M13 phage display selected sequences specific for Pt metal exhibited different structural responses (Seker et al., 2007) to the structure-stabilizing solvent, 2,2,2-

trifluoroethanol (TFE), and that these structural response correlated with observed Pt –peptide affinities. Thus, we utilized CD spectrometry and TFE solvent titrations to evaluate the response of the l- and 3l-GBP polypeptides to environmental perturbation (Figure 4.46-47).

As stated earlier, in the absence of TFE both the l- and 3l-GBPmolecules at pH 7.5 exist as an equilibrium mixture of random-coil and non-random coil conformations (Kulp et al., 2004), as evidenced by the predominant π - π * transition-associated (-) ellipticity band centered at 195 – 198 nm (Figures 4.46-4.47). When TFE is introduced to l-GBP, we note that the negative π - π * ellipticity band experiences a gradual red shift to 205 nm, a wavelength associated with beta turn conformation in equilibrium with random coil. Note that we do not observe the appearance of any other definitively ellipticity bands as a function of TFE content. However, when TFE is introduced to the 3l-GBPpolypeptide, a different result is obtained (Figure 4.46 and 4.47). Here, at 10% v/v TFE content, we note the presence of three negative ellipticity bands centered at 200, 215 and 222 nm. The simultaneous presence of the 215 nm and 222 nm negative bands, which are characteristics of beta-strand and alpha-helix, respectively, suggest that the 3l-GBP molecule exists in a non-random coil conformational equilibrium that possesses some degree of these two secondary structures. At 20% v/v TFE, a strong (+) ellipticity band appears at 192 nm, and, (-) ellipticity bands at 208 and 222 nm, which increase in intensity as TFE content increases up to 90% v/v. Thus, at TFE content of 20% v/v and higher, the conformational equilibrium of 3l-GBP polypeptide appears to shift again and the 42 AA sequences now adopts a predominantly alpha helical structure in this solvent mixture.

From these results, the followings can be concluded: (a) both the 1l- and 3l-GBPpeptides can be further stabilized by the addition of TFE and can be induced to adopt non-random coil structures; (b) at TFE content > 50% v/v, each version of GBP adopts different secondary structures, indicating that, as a result of chain length differences, each GBP polypeptide responds differently to organic solvent perturbation; (c) at low TFE content (10 – 20% v/v), the longer 42 AA polypeptide exhibits two different, detectable secondary structures. This feature may be an indication of different folding capabilities that are inherent within 3l-GBP.

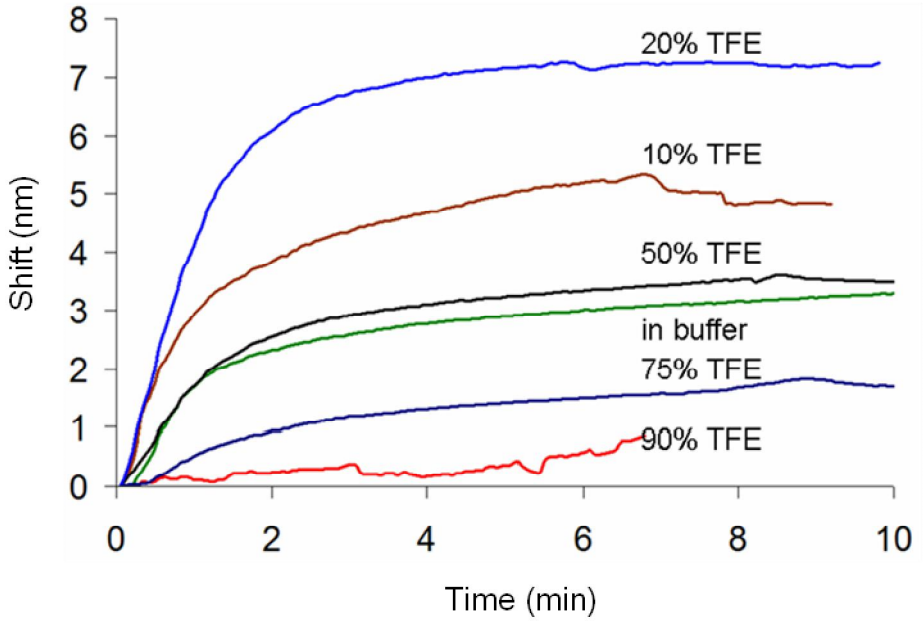

Figure 4.48: SPR sensogram for the 3l-GBP in varying TFE concentration, the shift represents the total change in the dip position of the SPR dip position. The shift represents a higher amount of peptide adsorbed on the surface of the gold. Binding affinity of 3l-GBPas a function of TFE (v/v, %) concentration.

Given the conformational effects that occur in the presence of TFE, we were curious to learn if this structure-stabilizing solvent also had an impact on GBP adsorption onto Au surfaces. To probe this, we chose the higher affinity 3l-GBP peptide and repeated our SPR binding experiments in the presence of TFE (Figure 4.48). Here, it was noted that the binding isotherm in the presence of TFE is non-linear, in contrast to what we observe under aqueous buffer conditions. Moreover, as shown in Figure 4.48, the binding affinity of 3l-GBP on Au surfaces changes in response to TFE content. At TFE content of 20% v/v or less, we note that the binding affinity of 3l-GBP increases compared to aqueous buffer conditions. At TFE content > 20% v/v, we observe decreasing binding affinity, and at 90% v/v TFE, the binding affinity is abolished. Interestingly, the range of TFE content which induces higher affinity (10 – 20% v/v) correlates with the presence of different secondary structures (i.e., beta-strand, alpha-helix) within the 3l-GBP polypeptide. These results indicate that TFE not only affects the conformation and stabilization of 3l-GBP in solution, but can modulate the affinity of this polypeptide for Au surfaces, which further supports our conclusion that structural rearrangements are occurring in 3l-GBP during the adsorption process. Consequently, one can suggest that there is correlation of conformational instability (or adaptability) and binding ability.

4.4.1 Effect of constraints on binding of GBP

The binding of both 3l-GBP and 1lGBP was found to be controlled by the conformation –secondary structure- of the peptides. By using a secondary structure stabilizing agent TFE, we explored the binding affinity of 3l-GBP at different conformations. As mentioned above by changing the degree of the helical secondary structure of the peptide, we were able to increase and decrease the binding affinity of the 3l-GBP. In addition to these finding we observed the effect of proline content in the primary structure of the de novo QBPs at a high degree, especially in those which have a strong binding affinity of towards the silica surface. This may be similar to the PtBP1 case as well. Proline is known to have rigid structure which will not allow a peptide to move freely in the solution; therefore proline can be used as a design parameter to introduce certain level of constraint conformation in the structure of the peptide. Here, we assumed that this structural constraint may increase the binding of the peptide. We tested the fact by making a point mutation in the amino acid sequence of the 3l-GBP as given in the Figure 4.49. To replace flexibility with rigidity, each glycine position was exchanged with a proline sequence. This mutation supposed to lead a conformational constrained structure and though a stronger binding of the peptide.

The mutant GBP was further tested for its binding affinity by means of the increased torsion at the Proline positions, and SPR analysis was followed. The glycine-proline replacement cause ~25 times increase in the binding affinity of the peptide, which corresponds to a binding energy increase around 2 kcal/mol. Our results indicate that the constrained structure of the peptide enhances the binding affinity, at least in the case of the binding of the GBP to gold surface. The comparison of the mutant 3l-GBPand native 3l-GBP is given in the Table 4.5 below.

The mutant peptide and the native sequence of gold binding peptide can be written as below:

MHGKTQATSGTIQSMHGKTQATSGTIQSMHGKTQATSGTIQS
MHPKTQATSPTIQSMHPKTQATSPTIQSMHPKTQATSPTIQS

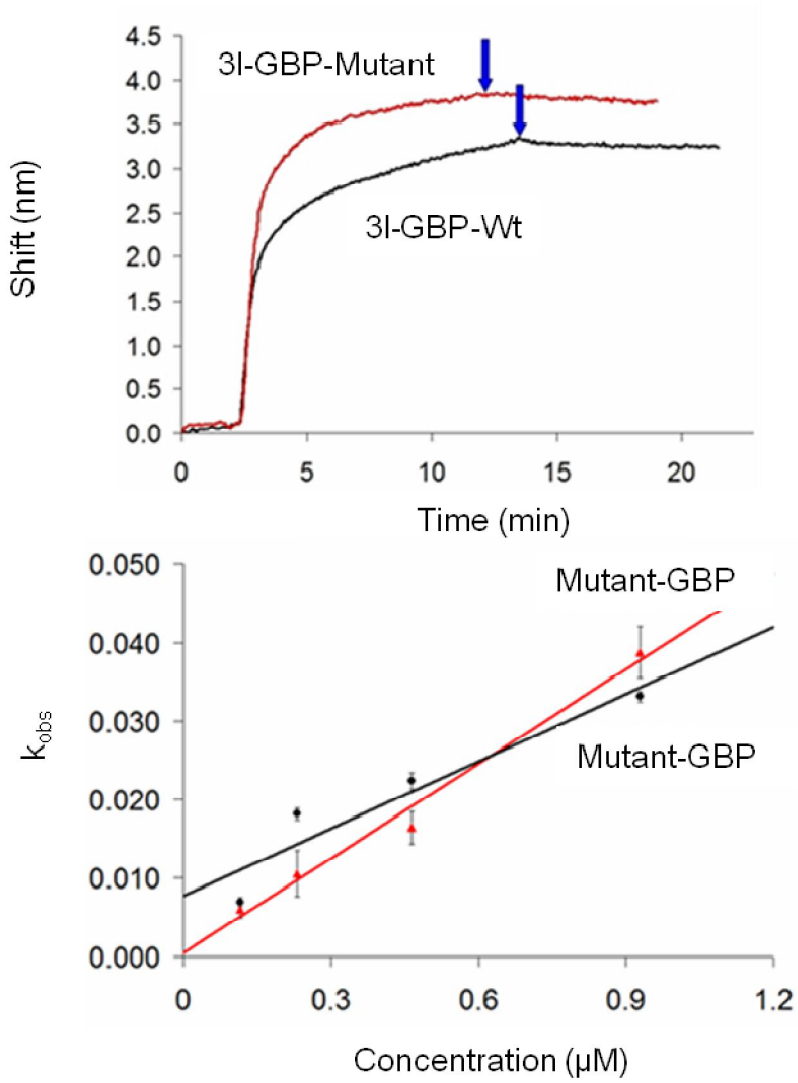

Figure 4.49: Comparison of the mutant and Wt-GBP for their binding affinity by means of total shift and initial adsorption rate.

Table 4.5: The affinity constants for the mutant and native GBP.

Peptide	G-P 3l-GBP	3l-GBP
k_a	4.03×10^{4}	2.86×10^{4}
k_d	4.30×10^{-4}	7.73×10^{-3}
K_{eq}	9.37×10^{7}	3.70×10^{6}
ΔG	10.70	8.82

4.5 Application of GEPIs as Molecular Linkers for Nano- and Biotechnology

In previous section, the molecular binding characterization of the GEPIs was investigated. Here using the classification, specificity, selectivity and conformational analysis of GEPIs, we will demonstrate their utilization in nano and biotechnological

applications. Our examples will include the usage of GEPIs as molecular erector for enzyme immobilization, as molecular tools for biomineralization and immobilization of nanoparticles.

4.5.1 GEPI based enzyme immobilization

Enzyme immobilization has been used for biosensor applications, immunoassays, protein arrays and bioseparation purposes (Stenlund et al., 2006; Schmidinger et al., 2006). The motivation for immobilization of the proteins on to a plain surface is to make them re-usable for several times with reasonable retained activity. It is a known fact that immobilization increases the stability of the enzymes; beside this there is an obvious decrease of the enzymatic activity.

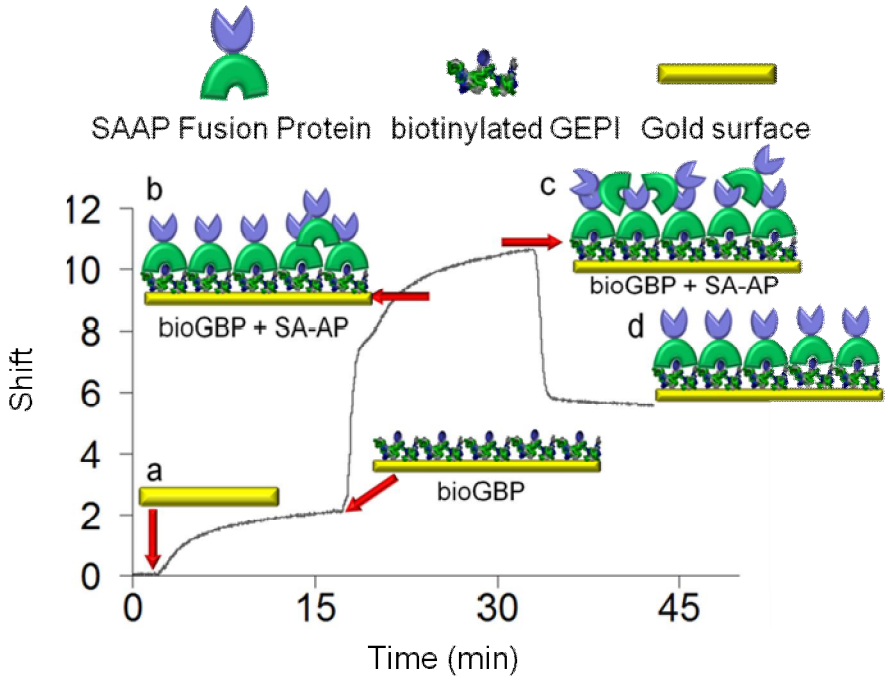

Figure 4.50: (A) The overall adsorption process of the bioGEPI and SAAP on bioGEPI activated surface. (a) bare gold surface, (b) adsorption of the biotinylated GEPI on surface.(c) initial adsorption of SAAP on bioGEPI activated surface. (d) adsorption of the SAAP on bioGEPI activated surface and a washing step follow this process. (d) Strongly and oriented bound SAAP on bioGEPI activated surface.

The main reason of a decrease in enzyme activity is either an unexpected conformational change happen near active site or direct blockage of the active site upon immobilization. There are different methods to immobilize proteins, by means of, chemical entrapment in a matrix, physical adsorption and covalent bonding of the enzyme to the surface via a chemical linker molecule. In this study, we utilized three

inorganic binding biotin tagged peptides, silica (bioQBP202, gold (bioGBP) and platinum (bioPtBP1) binding peptides to immobilize streptavidin fused alkaline phosphatase (SAAP). The kinetic of protein ligand interaction was monitored using surface plasmon resonance spectroscopy. Biotin was used as ligand to streptavidin (SA). Using this ligand-protein interaction AP was immobilized on gold, platinum and silica surfaces via inorganic peptides.

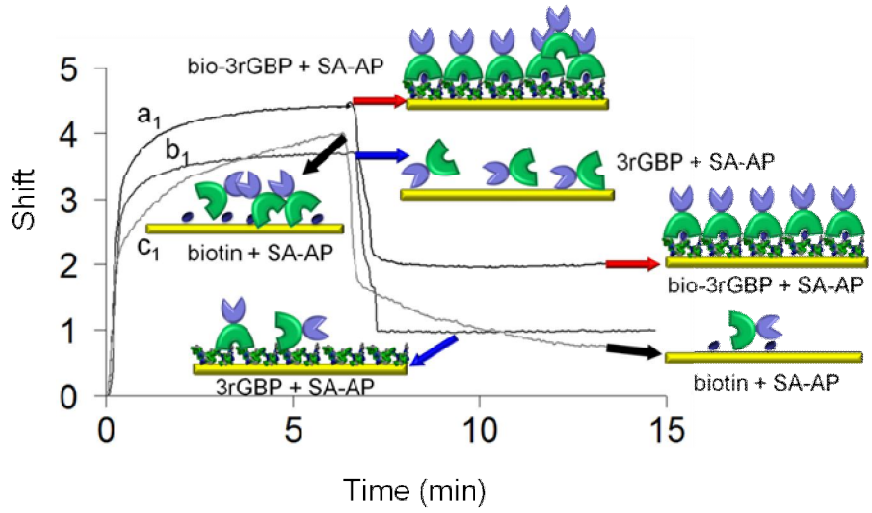

Figure 4.51: The control experiments to check the non specific interaction of SAAP with gold and non specifically biotin bound gold surface. (a_1) adsorption of the SAAP on bioGEPI activated surface of gold (b_1) adsorption of the GEPI functionalized gold surface (c_1) non specific adsorption of SAAP on gold surface.

The first step in using GEPIs as molecular erectors sets was to see if the GEPIs have the ability to enhance the amount of the protein SAAP on inorganic surfaces. For this purpose we carried out a set of control experiments, where we tested the amount of the SAAP retained on the surface following the adsorption of these proteins. We employed SPR to monitor the binding of the SAAP on gold, on biotin decorated gold (non-specifically biotins were adsorbed on gold) and on biotinylated GEPI decorated gold surface, these studies were taken as a basis for the other studies carried out on platinum and silica surfaces.

Given that the GEPIs are increasing the immobilization efficiency of the SAAP, we carried out a series of adsorption experiment of the SAAP on gold, silica and platinum surfaces, to determine the binding affinities of SAAP on different inorganic surfaces decorated with GEPIs. Here we first assembled the GEPIs, GBP on gold surface and QBP1 on silica surface and PtBP1 on platinum surface. Later we

assembled SAAP at different concentrations. Next, using the bimodal Langmuir adsorption model, we calculated the binding affinities of the SAAP. This was a crucial step for creating the supramolecular assemblies using the SAAP on inorganic surfaces. The overall adsorption sensograms are given in Figure 4.52.

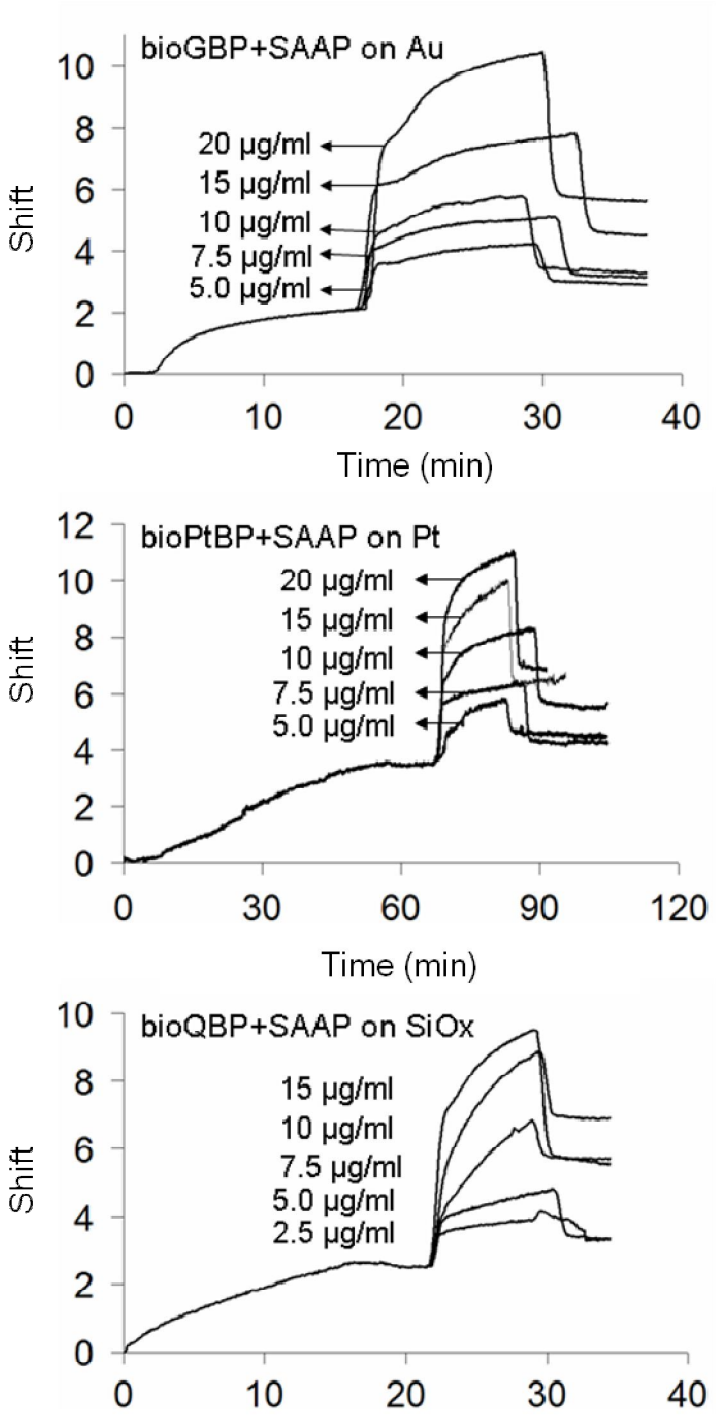

Figure 4.52: Adsorption, desorption and overall interactions of SAAP with GEPI decorated surface are given.

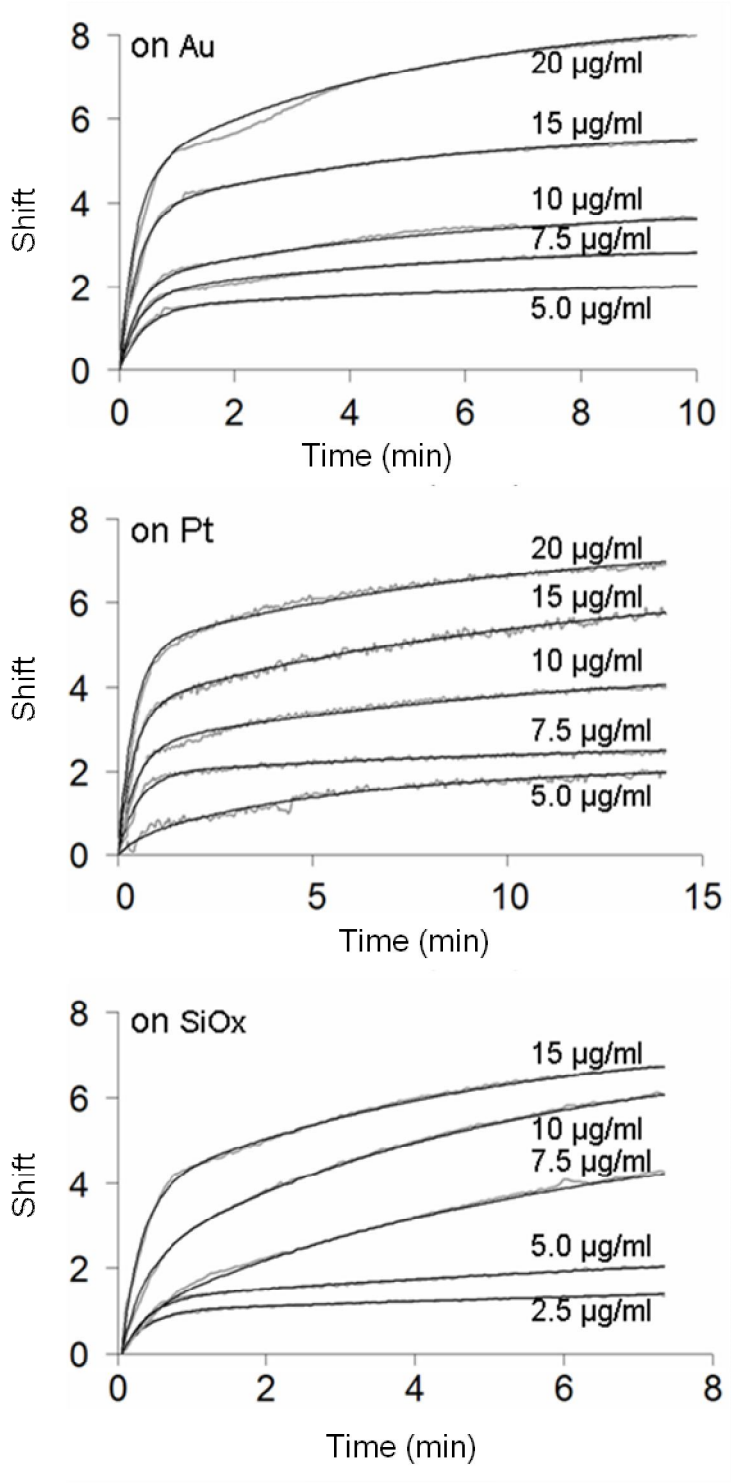

Figure 4.53: Adsorption of SAAP onto GEPI decorated surfaces are given.

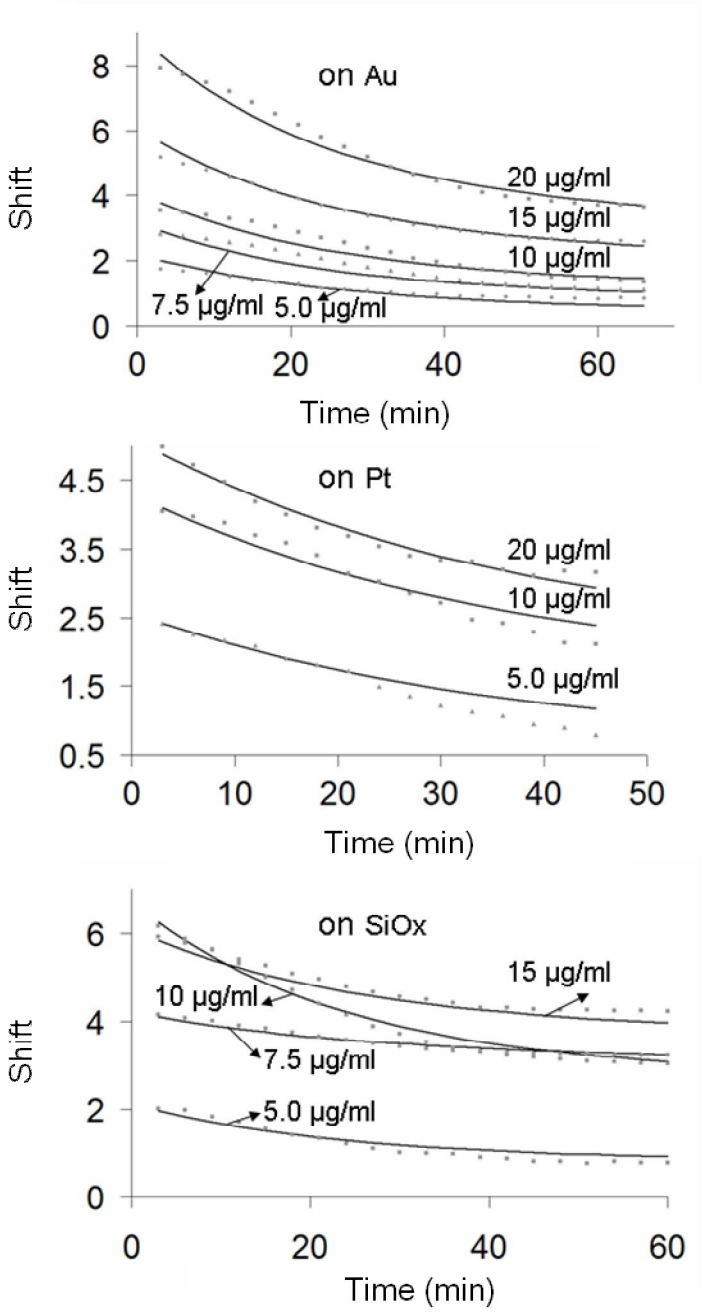

Figure 4.54: Desorption of SAAP from GEPI decorated surfaces are given.

The desorption of the SAAP from the bioGEPI surface was monitored and the calculated k_a and k_d values were fit to the desorption curves of the SAAP.

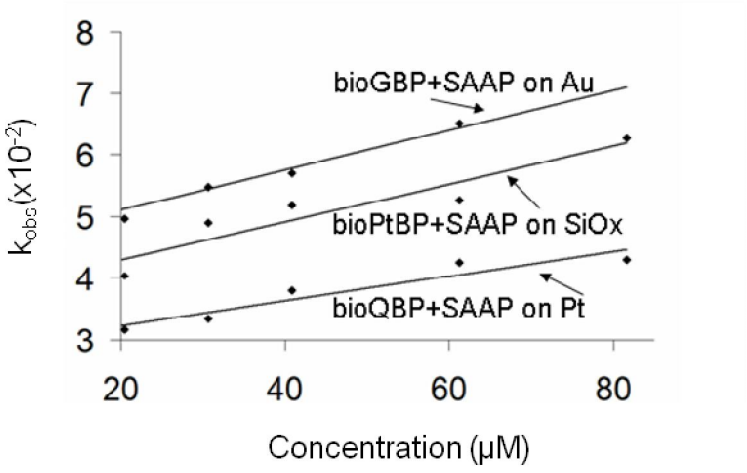

Figure 4.55: Concentration dependency of the apparent adsorption rates of the SAAP adsorbed on bioGEPI functionalized surfaces.

Table 4.6: Affinity Constant of the SAAP toward different surfaces decorated with GBP, QBP1 and PtBP1 peptides. The curve fitting of data was given in **Figure 4.55**, given above.

SA-AP on	k_a	k_d	K_{eq} *(1/M)*	*ΔG(kcal/mol)*
bioGBP	1.0×10^{8}	2.04×10^{-2}	4.90×10^{9}	13.30
bioPtBP1	2.0×10^{8}	2.13×10^{-2}	9.39×10^{9}	13.69
bioQBP1	1.4×10^{5}	4.41×10^{-2}	3.17×10^{6}	8.92

The affinity constant and adsorption desorption constants reflects a good binding of SAAP on inorganic surfaces decorated with GEPIs. The binding of SAAP on gold and platinum surface through the biotinylated GBP and PtBP1 has nearly the same binding energies, and affinity constants. The adsorption rate of SAAP on Pt surface is two times higher to that of on GBP decorated gold surface, however this does not count a high difference between their bindings. The main difference is noted when metals are compared with silica (a metal oxide). Interestingly, the desorption rates of SAAP in all three case seems to be the same, however the adsorption rates of SAAP on metals is three orders of magnitude higher compared to that of silica surface. This difference may be due to the difference in the orientation of the GEPIs on the surfaces, which determines the available biotin sites to get in touch with SAAP. Also, the assembly of the GEPIs may be more densely packed compared to that of silica, which increases the number of the variables sites open for conjugation available.

After the assembly of SAAP on inorganic surfaces, we used to find out the activities of the proteins. Because not only the assembly of SAAP is the important issue, also the SAAP molecules must be active after they are immobilized on solid surface. To realize the activity test of SAAP we monitored the activity of the enzymes in situ using SPR This novel approach allowed us to follow the enzyme-substrate relationship in real time. SPR signal depends on the change of the refractive index which is caused either by polymerization or change in the color, or the change in the electrochemical properties of the sample on the SPR chip surface. In our case we used PNPP (para-nitrophenyl phosphate) as an enzyme substrate.

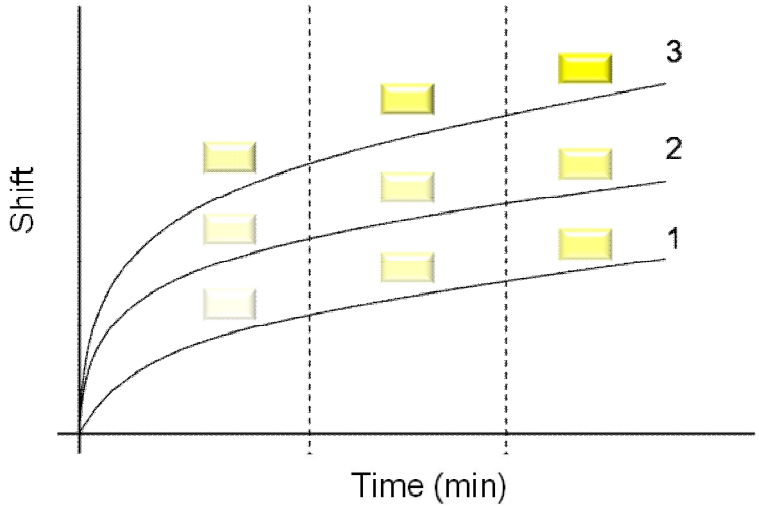

Figure 4.56: Monitoring of conversion of PNPP to inorganic phosphate and *p*-nitrophenyl (*p*-NNP). As (*p*-NNP) is degraded by SAAP on surface the color of the side products become more intense which gives a change in the shift of the SPR signal. Different PNPP concentrations yield in more intense yellow color.

The change in the color of the *p*-NNP during its breakdown to products (to p-nitro phenyl and inorganic phosphate) and intermediates can be detected by SPR the change in color will result in the change of the refractive index of the reaction medium. The schematic representation can be shown as in Figure 4. 56.

After the assembly of the bioGEPIs and SAAP on SPR chip surface either on gold or platinum or silica the substrate of AP, (*p*-NNP) was pumped in the SPR flow cell. The concentration of the substrate was as 10 mM, 20 mM, 30 mM, 40 mM, 50 mM, 60mM, and 80mM. After the substrate was introduced and it was clear from the sensogram that the substrate is totally pumped in, then the pump was turned off to allow the enzyme to induce its activity. In each experiment, one of the channels was

used as blank used only for pumping the buffers and substrates. All the experiments were carried out 37° C, and at a flow rate of 100µl/ min. As it can be seen from the Figure 4.57 each experiment was repeated with a control experiment to ensure that the breakdown of PNPP is achieved by the SAAP immobilized on the SPR chip surface.

The enzymes activities was monitored using SPR and each SAAP that were immobilized on different surfaces, was tested for theirs enzyme activity. The enzyme activities was monitored as mentioned above the change in the refractive index was recorded and the change in the refractive index in starting from the beginning was saved to calculate the initial reaction rates of the enzymes.

Here we used the Michelis-Menten type first order kinetic equation given in equation 4.7.

$$v = \frac{v_{\max}[S]}{K_m + [S]} \qquad \textbf{(4.7)}$$

The enzymatic reaction rate is changing as a function of the substrate concentration. The amount of substrate is decreasing in the reaction medium as a function of time. So to avoid a complex situation only the initial reaction rate is considered to determine kinetic constants. The enzymes are characterized by two parameters, the half amount of the substrate concentration to reach the maximum reaction rate (K_m) and the maximum enzymatic reaction rate (V_{max}).

The enzyme activity test was recorded as given in Figure 4.58. In order to calculate the enzymatic reaction rates of SAAP immobilized using three different approaches, different concentrations of PNNP was used. For each concentration a negative control experiments was carried out. In this experiment, the substrate solution PNPP was pumped on the channels where no SAAP was immobilized on the surface. It can be seen on Figure 4.57, there is not any change in the refractive index on the control channels. The control experiment showed that *p*-NNP solution was not degraded and caused a change in the signal due to light or any other effect.

$$\frac{1}{V} = \frac{[S] + K_M}{V \max[S]} = \frac{[S]}{V \max[S]} + \frac{K_M}{V_{\max}[S]} = \frac{1}{V_{\max}} + \frac{K_M}{V_{\max}} \frac{1}{[S]} \qquad \textbf{(4.8)}$$

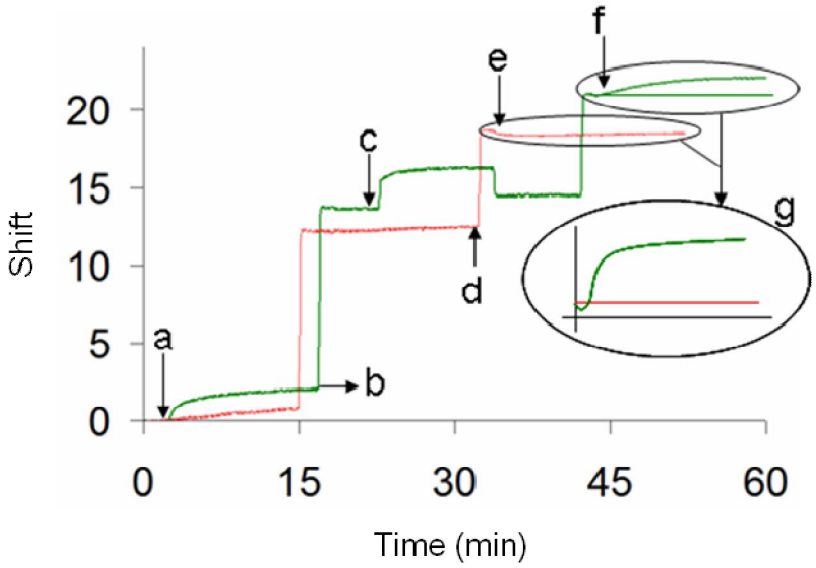

Figure 4.57: The overall adsorption process and activity of SAAP on inorganic surface. The red line is experiment for activity monitoring and green line is for control experiment. (a) Injection of bioGEPI on inorganic surface, in control experiment this only the injection of buffer. (b) the buffer is changed from phosphate buffer to Tris-HCl, until new baseline is established (c) Injection of SAAP on bioGEPI activated surface, for control experiments, this was only Tris-HCl. (d) Injection of PNPP into control channel (e) there is no increase in the dip position shift in control channel. (f) Injection of PNPP on bioGEPI functionalized and SAAP immobilized surface, and the breakdown of PNPP results in a shift change in SPR signal. (g) The reaction of PNPP with SAAP on the activated channel.

V denotes the initial reaction rate of the enzymatic reaction; *S* is the concentration of the substrate. From the experimental data we can calculate the initial reaction rate from the slope of activity curve. The reaction rate will be given in refractive index units in our case, therefore it will be in nm/min, K_m will be calculated in concentration units. The calculated initial rates from the slope of the curves are given. Using the equation 4.8, 1/*V* vs 1/*S* was plotted which is displayed in Figure 4.59. The intercept of 1/*V* gives the 1/*Vmax*, as the intercept of 1/*S* yields in $-1/K_{max}$. Using these two equations, we were able to calculate the enzymatic reaction rates for SAAP on all of the surfaces.

Not only the activity of SAAP immobilized on bioGEPI modified surface was measured, but also as a control group the activity of SAAP immobilized on bare gold, platinum and silica surfaces was measured. The increase of SAAP activity

upon binding on bioGEPI modified surface was compared to the control surface. The maximum activity increase was noted in the case of bioGBP decorated gold surface.

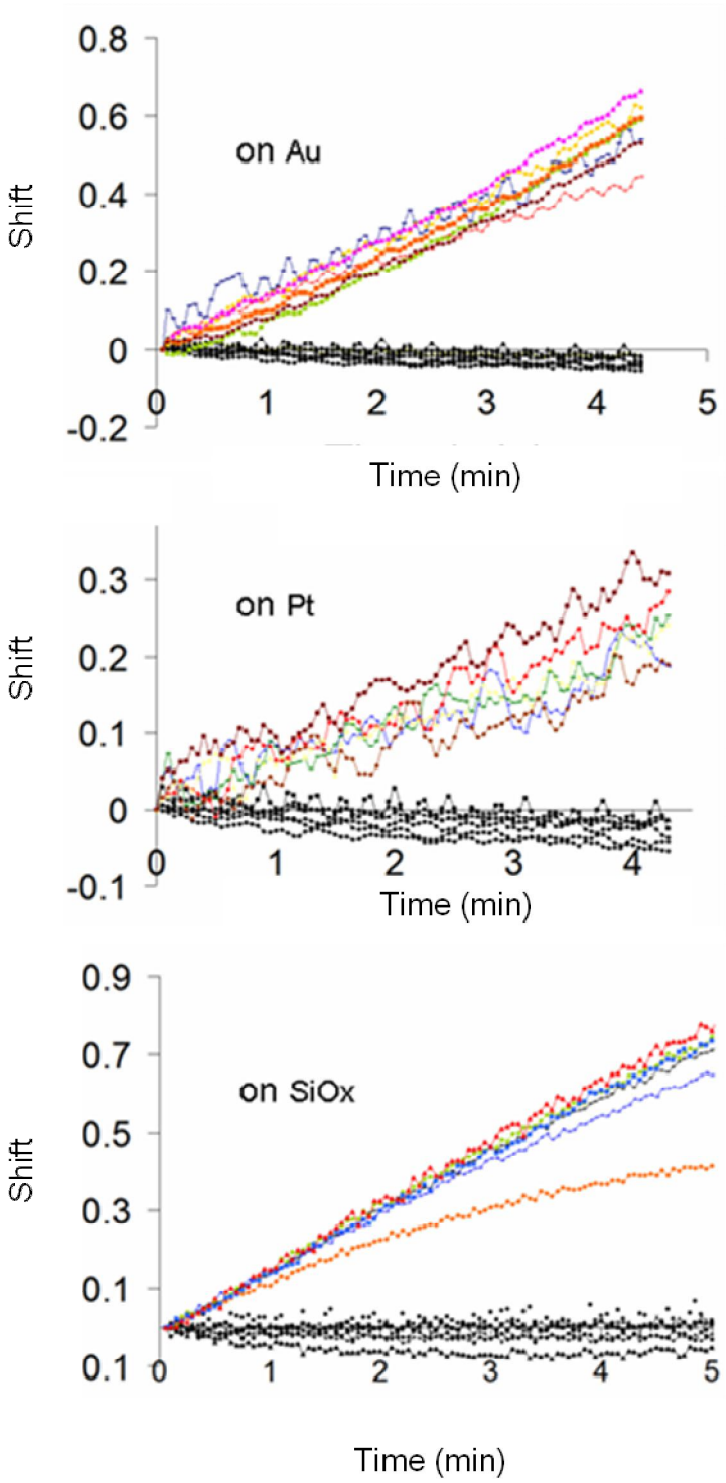

Figure 4.58: The black lines represent the change in the shift and the others show the SAAP activity on functionalized channels, the different lines represent different concentrations of SAAP.

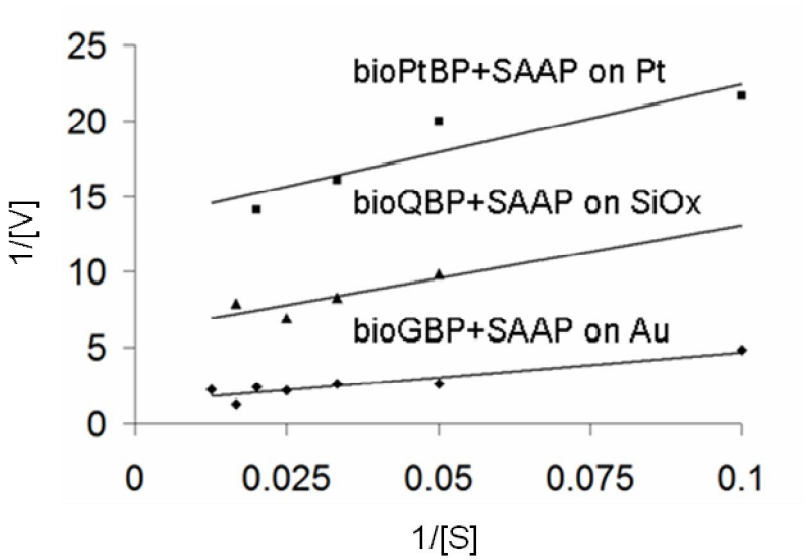

Figure4.59: Lineweaver-Burk plots for SAAP activity (adsorbed on bioGEPI activated gold, platinum and silica surfaces).

The results were found to be promising for using the GEPIs as linker molecules for immobilization. GEPIs can be exploited in two distinct ways to enhance enzyme immobilization, one approach is making GEPIs bifunctional using biotin tag on GEPIs, here what we employed and the kinetic calculations showed a high affinity between the SAAP fusion and the biotin. However, the other one is using GEPIs genetic insertion in protein and creating molecular constructs, which will be discussed in the next section. Immobilization is achieved in a very specific manner here; the protein is immobilized in an oriented manner. The peptide linkers used were also specific to the different surfaces. Here, both oriented protein immobilization and surface specific immobilization was achieved. In the control group we found out that biotin-streptavidin interaction is not enough to keep the immobilized molecule on the surface of the gold without any linker molecule on the gold.

4.5.2 Real time monitoring of gepi enhanced biomineralization

In section 3.2.1 GEPIs were used as linker molecule, in this approach the peptide is assembled on surface to create modified surfaces and later by using another interaction between the immobilized peptide and the protein of interest, one can further develop different systems. We utilized streptavidin-biotin interaction to link the peptide to the protein in previous section. Another approach can be genetic fusion of the peptide into the protein. Previously in our group, we studied gold binding

peptide fused alkaline phosphatase enzyme, this system was utilized in the formation of the gold nanoparticles, as well as for targeted immobilization of the alkaline phosphatase on gold surfaces (Brown et al. 2000).

Alkaline phosphatase (AP) is known to cleave inorganic phosphate from phosphate sources. Previously, in our group we used an enzyme mediated reaction to monitor the biomineralization. AP is used to release the inorganic phosphate form a phosphate source (beta-glycerophosphate) and later by the addition of a Ca^{++} source to the environment, the formation of the HAP is initiated. The kinetics of HAP formation is only measured by using additional assays which relies on the determination of leftover amount of calcium and phosphate. Here the effect of peptide on the formed mineral was demonstrated (Gungormus et al., 2008) Here, we studied SPR for real time monitoring of the biomineralization. We used a five repeat GBP inserted AP, which is genetically fused and the new chimera is called AP-5l-GBP.

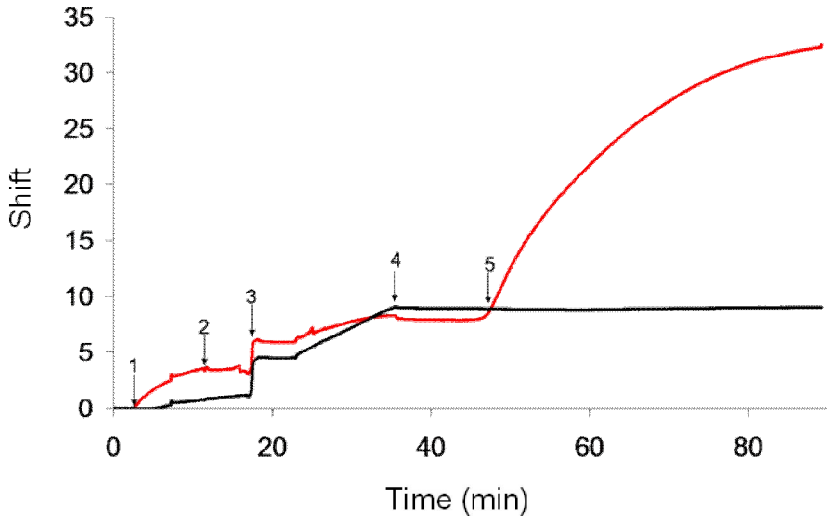

Figure 4.60: The curve is representing the overall biomineralization process of hydroxyapatite. Black line represents the control groups to non AP-5l-GBP that was immobilized in the channel, red line represents the AP5l-GBP mediated HAP biomineralization (1) Injection of AP-5l-GBP solution (2) injection of Tris buffer to remove loosely bound and non-specifically interacting AP-5GBP molecules. (3) injection of the biomineralization mixture, composing of 14.4 mM $CaCO_3$ and β-glycerophosphate (4) Stop flow of mineralization mixture and initiation of the lag phase of the biomineralization. (5) Initiation of the biomineralization process.

The immobilization of AP-5l-GBP is favored by the interaction of 5l-GBP with gold surface. The binding affinity of the AP-5GBP was calculated as $2x10^8$ M^{-1}in a

previous work. This affinity number is 10 times higher compared to that of native AP (Kacar et al., 2009). After the assembly of the protein, the addition of the biomineralization mixture was carried out. Here, the mixture both contains the $CaCO_3$ and β-glycerophosphate as phosphate source. We followed the release of the phosphate by the enzymatic action of the AP-5l-GBP on gold surface.Following the release of the phosphate the reaction between the Ca^{++} and phosphate takes place, this is a spontaneous reaction. To achieve this there is a need that the free phosphate amount reaches a critical value. As soon as the crystals started to form, we recorded this change on gold surface as a change in the refractive index change by surface plasmon resonance spectroscopy. We have successfully recorded the increase in the refractive index change as a function of formation of crystal particles. To note that we have shown the formation of the crystals using a solution assay and the TEM analysis of the formed crystals are given in a previous study of our groups (Gungormus et al., 2007).

As we mentioned earlier there is a lag phase before the biomineralization takes place, (between the points 4-5), here AP-5GBP reacts with β-glycerophosphate and releases the inorganic phosphate (P_i) from its structure. The concentration of P_i needs to reach a critical value to for biomineralization to start.

We need to note that in SPR, the SPW can only penetrate into a depth of 200 nm, in a thicker layer than this size, the SPR signal will be destroyed. Not only the SPW but also the penetration of the light will be impossible in this case. In such a case additionally, dip position not only changes its position on horizontal scale, but also its position is changing in vertical scale as well. After a certain size of the minerals formed in the SPR flow cell, it is impossible to observe any signal change in the sensograms (Figure 4.61).

Here we are utilizing two important features of a designer protein, AP-5GBP. First we are not using any additional chemical/physical method for the immobilization of the AP; we are using the molecular linker property of gold binding peptide. In addition to this, we are still capable of using the activity of AP. Hence insertion of 5GBP did not affect the enzymatic activity of AP adversely (Kacar et al. 2009).

Following initial experiments, we interested in changing some of the parameters, enzyme concentration to be immobilized was the first parameter to investigate to see

its effect on the biomineralization activity. So we carry out the immobilization of 5 μg/ml and 15 μg/ml of AP-5GBP on gold surface (Figure 4.62). We next carried out the biomineralization on these enzyme concentrations. We observed that the biomineralization activity was affected by increasing the amount of enzyme (AP-5GBP) immobilized on the surface (Figure 4.62). However, the increase in the biomineralization rate was not very high at initial steps of the biomineralization. The difference between the biomineralization profiles is profound during the late biomineralization phase. This is verified by the decrease in the rate of biomineralization.

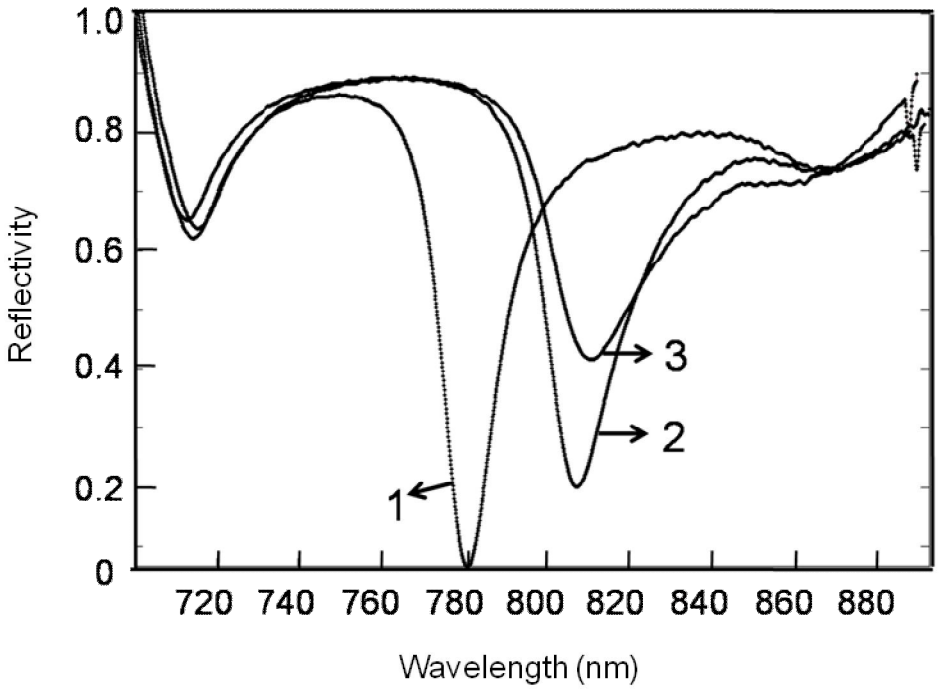

Figure 4.61: SPR dip position change during the biomineralization process. (1) Dip position at the initiation of biomineralization process (2) dip position shift during the mid phase of biomineralization and (3) is at the plateau value.

We demonstrated here that SPR techniques can be used to monitor the biomineralization in the presence of different kinds of chemicals and biological agents to observe their effects as a first screening test. To sum up, using a designer protein AP-5GBP we were able to monitor the biomineralization of HAP in real time. Here we also achieved to test the bi-functionality of AP-5GBP, which can be immobilized on gold surface effectively (almost no desorption from the surface), and still keeps its activity to release inorganic phosphate from the phosphate sources.

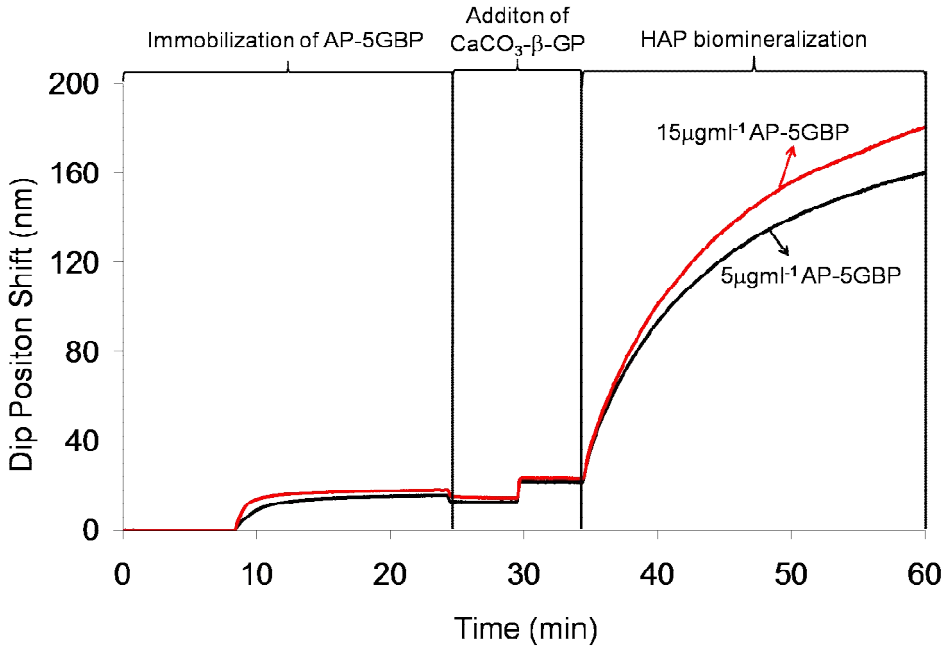

Figure 4.62: Monitoring the biomineralization of HAP usign immobilized AP-5GBP on gold surface.

4.5.3. GEPI as molecular erector to monitor the fibril elongation in Huntington's disease

Our next demonstration for the utilization of GEPIs is to monitor diseases. Huntington's disease (HD) is a neurodegenerative disorder characterized by the formation and deposition of protein aggregates in neurons. These aggregates are consists of fibrils containing misfolded protein Huntingtin (Htt), with an expanded polyglutamine repeat. Htt is known to form fibrils when the number of glutamine repeats in the structure of the Htt reaches over 35, as previously reported (Scherzinger et al., 1997, Dobson et al., 2004). There is a correlation between cell degeneration and abnormal protein deposition but not a certain observation showing that inclusion bodies are the reason of toxicity. The most possible explanation is that inclusion bodies are the last step of a cascade and the previous steps in the cascade are more related with pathogenesis than inclusions themselves. Therefore, understanding the steps involved in fibrillogenesis is very important. Here we apply surface plasmon resonance technology to study the interactions of Huntingtin monomers with Huntingtin fibrils to resolve the kinetics of fibril elongation.

Traditionally, the methods used for fibrilogenesis have been fluorescent microscopy, circular dichroism, quasielastic light scattering, electron microscopy, mass spectroscopy, HPLC and AFM (Larson et al., 2000, Colby et al., 2006, Chen et al.,

2002). These approaches provide information about fibrillogenesis over relatively long periods of time (hours). To track the fibrilogenesis relatively in shorter times (from 3 sec to 30 min), surface based detection methods such as SPR and QCM-D were successfully applied in different diseases (Cannon et al., 2004, Knowles et al., 2007). Not only is the shorter time required for analysis of fibrilogenesis but also this method allows one to directly measure the kinetic rate constants at each step of the fibrilogenesis as a function of time. In addition to these effects of additional compounds on the fibrilogenesis such as ions and chaperons were studied successfully. We, therefore, selected SPR system to investigate HD fibrilogenesis kinetics, using a GEPI based functionalization, as a first time application of such a technique in monitoring Htt fibrillation kinetics.

First two Htt proteins were constructed, one is a 53 glutamine repeat containing Huntington protein Htt53 which is known to form fibrils and the control protein is Htt20 a Huntington protein with 20 repeats.

Surface based detection of fibrilogenesis become popular in recent years, which is easier and with high repeatability compared to that of in solution methods (Berthelier et al., 2001, O'Nuallain et al., 2005). However, the main disadvantage here is to find out a suitable immobilization method to stick the fibrils of interest on to the desired surface. In conventional methods people have been using thiols chemistry to stick the fibrils on a surface to monitor fibril elongation. To be able to introduce a more accurate and controlled assembly of the fibrils for the analysis of the fibril elongation, we genetically fused gold binding peptide (GBP) in to the structure of the HD-53Q and the control one Htt-20. After this we incubated Htt53-GBP and Htt20-GBP to form fibrils. However we did not see any fibrils formed in the case of Htt20-GBP and Htt20 as well. So we investigated the interaction of Htt20-GBP and Htt20 monomers. On the other hand Htt53-GBP formed fibrils were immobilized on SPR chip surface. Later the Htt53 was found to interact with the seed fibril on this surface and an elongation profile was recorded.

The extensive kinetic analysis of the GBP showed that GBP is a good candidate to be utilized as a linker molecule to coat biomolecules on gold surface for analytical purposes. In our approach we utilized three repeat of the GBP as a fusion partner with the huntingtin, Huntington’s disease protein. After the construction of the Htt-GBP we immobilized the construct through the interaction of the GBP with gold

surface without using any chemical coupling methodology. The interaction of the monomers towards formation of the fibrils was studied using SPR. Collected data was further analyzed using a two step kinetic model and the kinetic constants as well as the free energies of the monomer interaction with the fibril surfaces was investigated.

In the literature in most of the cases for the monitoring of the fibril formation, the fibrils were sonicated to increase efficiency of immobilization with maximum sites for fibrils elongation available. In our approach we also tested the effect of the sonication on the assembly of the fibrils. As it can be seen on Figure 4.64, sonication can change the adsorption kinetics of the fibrils depending the time of sonication. However, the final amount of immobilized fibril did not deviate too much, which is around 2000 μRIU. Further experiments showed that sonication may increase the availability of the fibrillation sites.

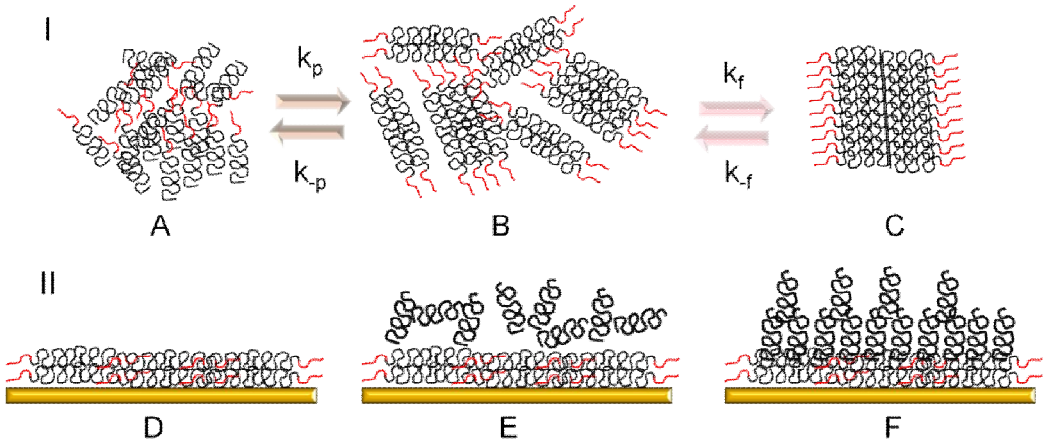

Figure 4.63: (I) Fibrilogenesis using the 3-GBP inserted Huntington's protein. (A) Monomeric 3-GBP Huntington protein. (B) the formation of the protofibrils in Huntingtin. (C) Fibrils of 3-GBP Huntingtin formed. (II) Monitoring the fibril elongation in Huntingtin using the HD-3GBP protein as seed protein on the surface of SPR slide. (D) Immobilization of the Huntingtin protein on gold surface via the GBP-gold surface interaction. (E) Addition of the Huntingtin protein (HD) monomers on to the seed fibrils. (F) Fibril elongation of the HD protein, the monomeric proteins which did not take place during the fibril elongation was removed by means of buffer wash.

We assume that Htt monomers specifically bind to the available sites on the surface of the bound fibrils, and after binding to the fibrils, we expect Htt monomers not to come off, as they become a part of the bound fibril and cause a further elongation via this specific interaction. Before testing this we carried out a series of experiments to

detect whether formed fibrils of Htt cause any elongation on the bound fibril. As seen on Figure 4.65, we noticed an increase in the refractive index upon the interaction of the Htt fibrils with bound fibril however, this cause no significant elongation, as it was removed from the bound fibril surface by buffer injection. Similar to this trial we also tested a negative control and positive control experiment.

As a negative control we send the BSA on the immobilized fibrils on sensor surface, we first noticed an increase in refractive index however we easily removed this non specific binding of BSA on fibril surface by washing with buffer. Following this control experiments, we next sent HD monomer on the surface of the immobilized fibril, which saw an increase in the amount of fibril on the sensor surface, through fibril elongation. These can be apparently seen on Figure 4.67. As expected two different concentrations of HD-20Q were removed without interacting of the surface bound HD-20Q-3GBP, as given in Figure 4.64.

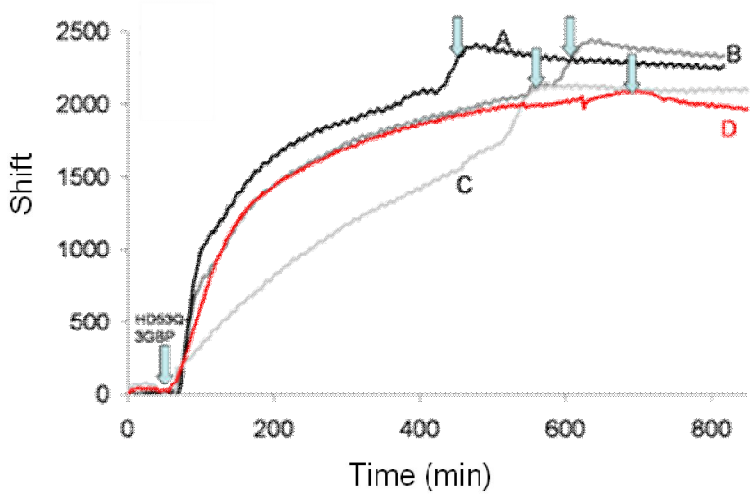

Figure 4.64: (I) Comparison of the sonicated and non sonicated fibrils for ther adsorption rates. The arrows indicates where the buffers were sent to remove non specifically and weakly bound fibrils from gold surface. A. 2 mins sonicated fibril B. 5 mins sonicated fibril C. 10 mins sonicated fibril and D. Unsonicated fibril.

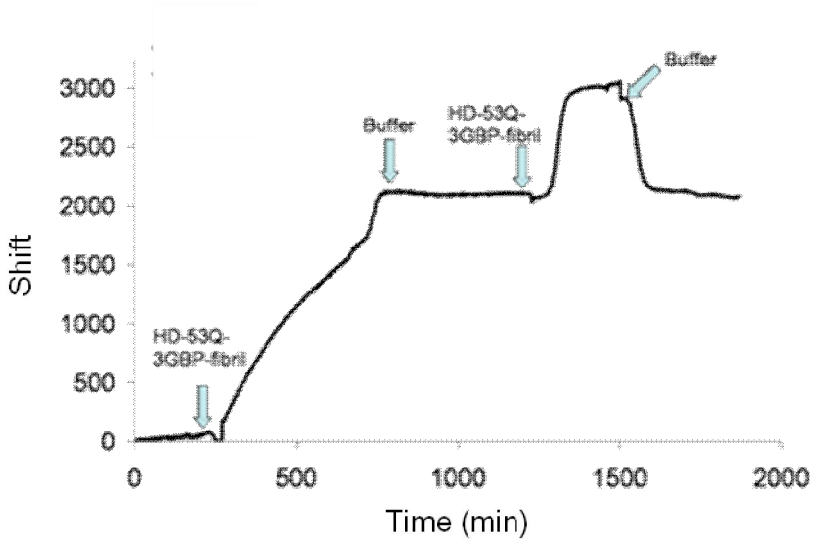

Figure 4. 65: The control experimnets to show that the fibrils of Htt53Q does not interact with the surface bound fibrils.

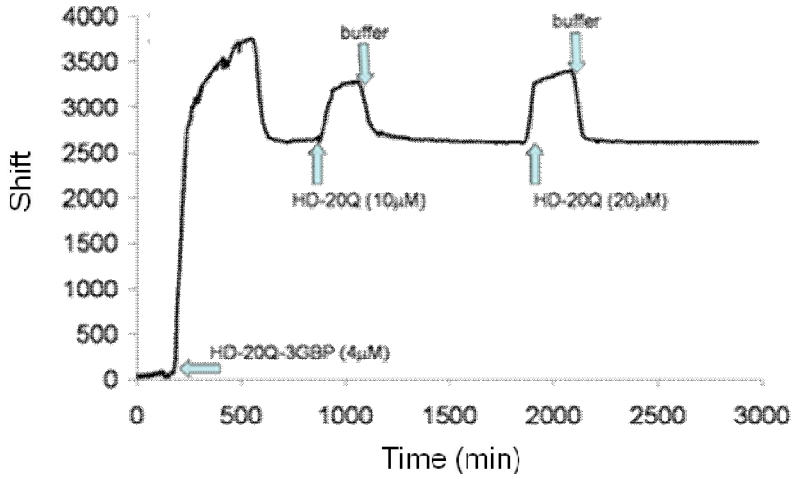

Figure 4. 66: The fibril elongation test for the Htt20Q. These prtoein is known not to form fibrils. Here as the fibrils are not formed and the monomers does not have any tendency to form fibrils so they do not stick surface bound Htt20Q.

Following all these control experiments, we carried out experiments for the real time monitoring of the fibrilogenesis of the Htt-53Q. We first immobilized HD53Q-3GBP fibrils on SPR sensor, after carrying out the routine immobilization procedure. Htt53Q monomers, at a concentration of 4 μM, 10 μM and 20 μM, were sent on the surface of immobilized fibrils. Later the sensograms were further analyzed using a two stage binding model which includes the interaction of the monomers with the fibrils. This is also followed by a conformational change of the monomer upon

sticking on the surface of the bound fibril, which may be caused by a conformational destabilization of the monomeric Htt-53Q.

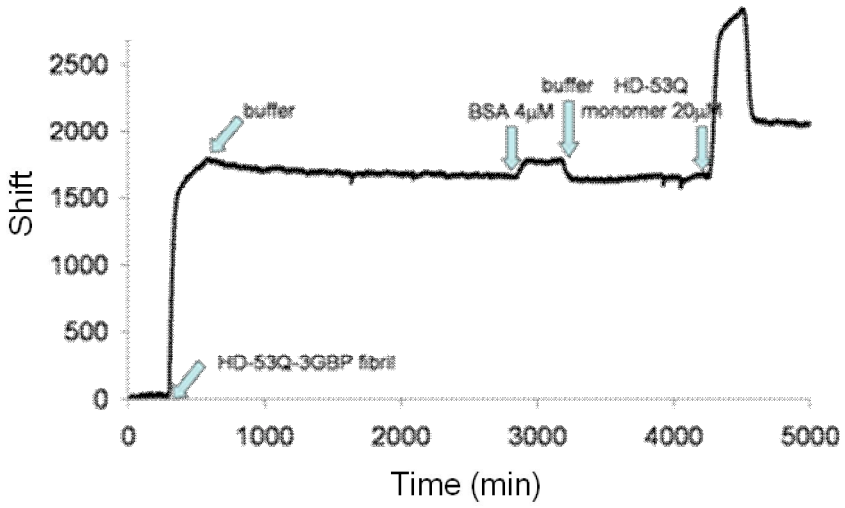

Figure 4. 67: A positive and negative control to test the Htt53Q monomers are interacrting with the surface bound fibrils. BSA was sent as a negative control, show that only the monomers are interacting with the surface bound seed fibrils.

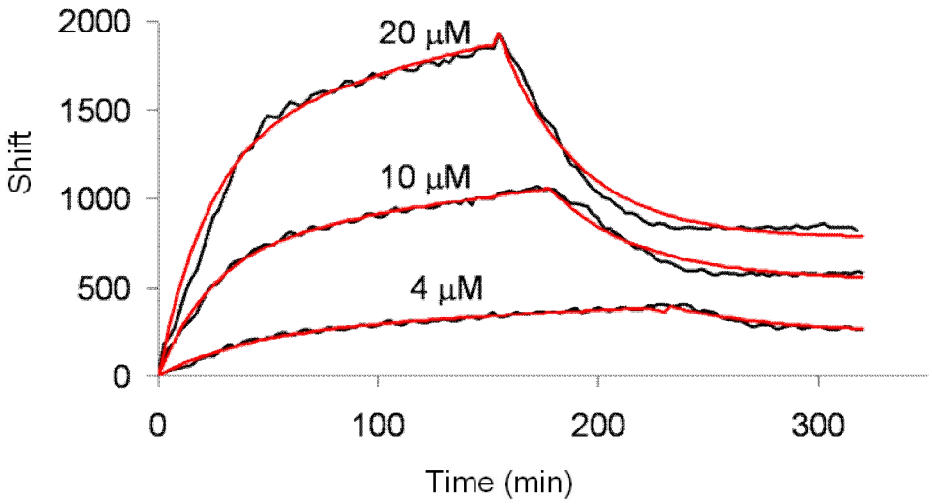

Figure 4.68: Sensogram for the fibril elongation of the Htt53Q by interacting surface bound seed Htt53-3GBP fibrils.Thebred line represents the fitted lines as the black ones represents the experimenbtal data, a two stage model was applied for the global fitting.

The calculated kinetics constants are given in Table 4.7. In Figure 4.68, the sensograms for the HD monomers were given at above given concentrations, using the kinetic model we first calculated the response for the fibril elongation and later the calculated signal was compared with the measured response, and the values of

the rate constants were found by minimizing the sum of square errors. To achieve this, we used the Solver function of Microsoft Excel, which performs a constrained nonlinear fitting based on the generalized reduced gradient algorithm. The curve fitting of the data was given in Figure 4.68.

In our case we proposed a two stage model as the on stage and three stage models did not fit to our data very well. However beside this it is also important to check the mechanism of the fibril elongation with other methods such as using AFM, one can be be guided what kind of a model to choose and use during SPR analysis.

Table 4.7: Kinetic rate constants calculated using a two stage model for the fibril elongation of Htt53Q.

	k_1 ($M^{-1}s^{-1}$)	k_{-1} (s^{-1})	k_2 ($M^{-1}s^{-1}$)	k_{-2} (s^{-1})
Htt53Q	9.17×10^{2}	2.80×10^{-2}	1.25×10^{2}	2.01×10^{-4}

To monitor the fibrilogenesis in the Htt-53Q, a genetic conjugation based immobilization was achieved. Bound fibrils was successfully utilized as seed to monitor fibril elongation and a two state kinetic model was used to determine the kinetic constants for the fibril formation in Htt53Q. Different than the previously reported fibril elongation mechanisms Htt53Q fibril follows a two stage fibrillation model. This may caused by the structural differences between the monomers for Htt53Q compared to the amyloidal fibril formations in other neurodegenerative diseases.

4.5.4 Targeted self assembly of quantum dot nano emitters using GEPIs.

We demonstrate targeted self-assembly of quantum dot light emitters bound only onto the top of our light emitting diodes but not on the metal contacts or anywhere else on the chip. For that, we introduce an innovative approach of self-assembling quantum dots on the targeted specific surfaces using genetically engineered peptides (GEPI) as smart linkers.

Q-Dots made of II-VI Group semiconductors (e.g., hetero-nanocrystals of CdSe/ZnS in core-shell structure) have been used in many different nano and biotechnological applications. With their unique optical and electronic properties, they have been studied for photonic, electronic and biomedical applications. Especially in recent studies in photonic applications their capabilities for white light generation and tunability of white light have been explored (Nizamoglu et al., 2007 and Demir et al.,

2007). In the previous studies, Q-Dots were commonly assembled in host polymers such as PMMA or by using films of poly-electrolytes, or sometimes Q-dots are closely packed by themselves without using host or additional film (Li et al., 2007 and Gupta et al., 2008). However, the non-specific assembly is the main drawback of these approaches. To assemble Q-Dots only within targeted regions on a multi-material patterned chip, as is usually the case, these non-specific approaches may lack applicability or the assembly process may take several steps.

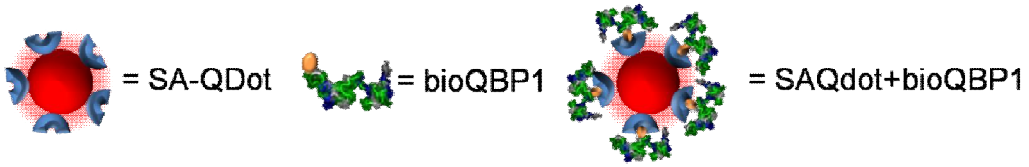

Figure 4.69: The schematic representation of the bare and surface modified nanoparticles.

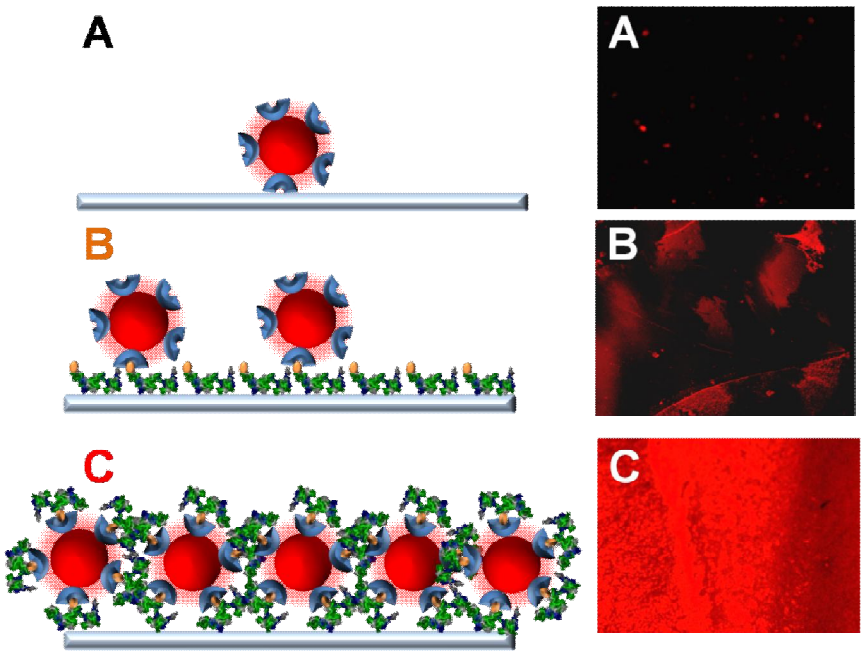

Figure 4.70: The targeted self-assembly of quantum dots (emitting in red at 610 nm) on silica surfaces. (a) streptavidin conjugated quantum dots (SA-Qdots) on silica surface (b) silica surface decorated with bioQBP1 and SA-QDots assembled on modified silica surface. (c) assembly of bioQBP1 modified SA-QDots on silica surface.

GEPIs provide the ability to recognize targeted surfaces for specific binding through molecular level interactions. In molecular biology and genetics, typically a monolayer of GEPI is first incubated on a desired surface and quantum dots are subsequently immobilized on the top of this GEPI thin film. Although this approach works fine for labeling and imaging purposes, it lacks the required level of

reproducibility and uniformity for device applications, for example, in photonics. This conventional approach suffers mainly from the problem of diffusion-limited mass transfer of quantum dots on GEPI film.

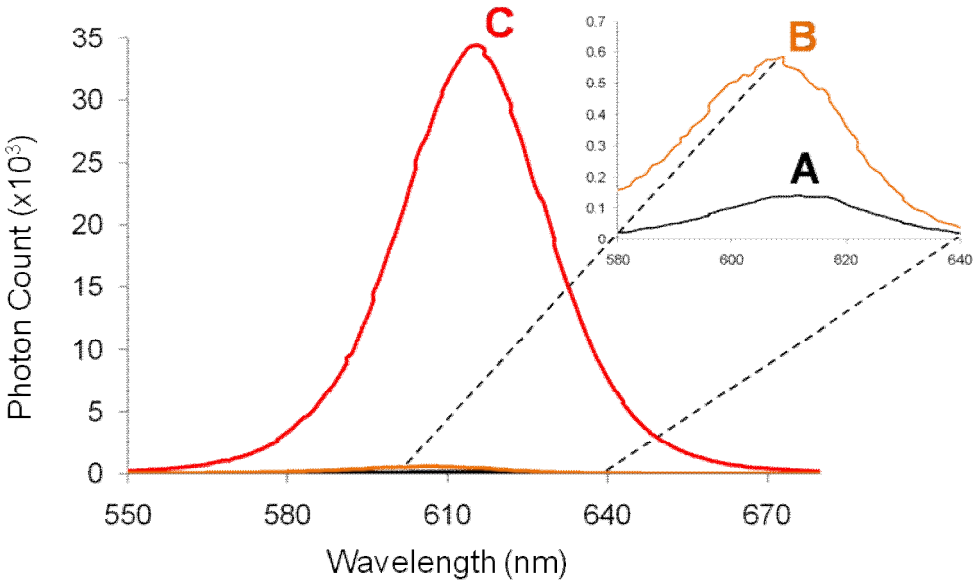

Figure 4.71: The PL spectra for all cases (A), (B), and (C) are represented on the graph, with the inset showing a zoom-in at low intensity levels for (B) and (c). Compared to the negative control group (A), the conventional approach (B) LED to 60 fold improvement and the innovative approach (C) resulted in 250 fold.

To address this problem, we developed an alternative approach of first forming GEPI-quantum dot hybrid nanoassembly in solution and then immobilizing them altogether on the desired surface. In Figure 4.71, the variation in the PL intensity of the SA-Q-Dots from different parts of the same silica surface shows a nonhomogenous spreading of the SA-Q-Dots, this results in some the regions on the chip to exhibit as low PL as the control group. This observation points out that mass transfer diffusion can be a problem for these Q-dots dropped on the peptide film during their self-assembly process. In our case, bioQBP1 functionalized silica surface contains a large number of biotin stuck on the surface, due to the bioQBP1 film; and the streptavidin must be able to get in contact with the biotin on the surface by diffusion to assemble the SA-Q-Dots on the surface . Thus, assemble of the SA-Q-Dots with the surface biotin is a mass transfer limited interaction, as there is no further mixing during the drop casting.

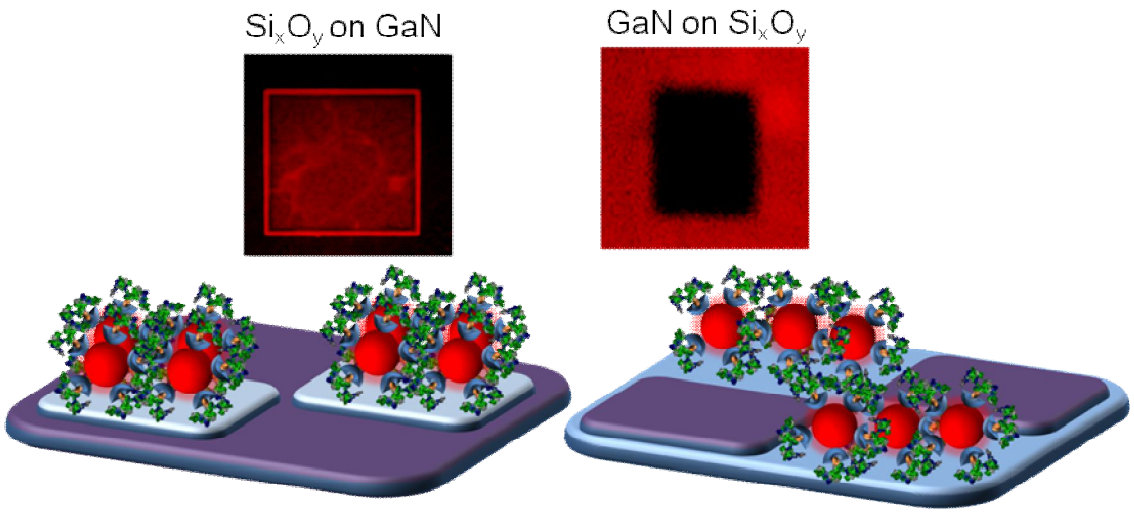

Figure 4.72: Cross specificity of the bioQBP1 decorated Sa-QDots. The assembly of hybrid nanoassemblies on gold patterned silica surface and silica patterned gold surface.

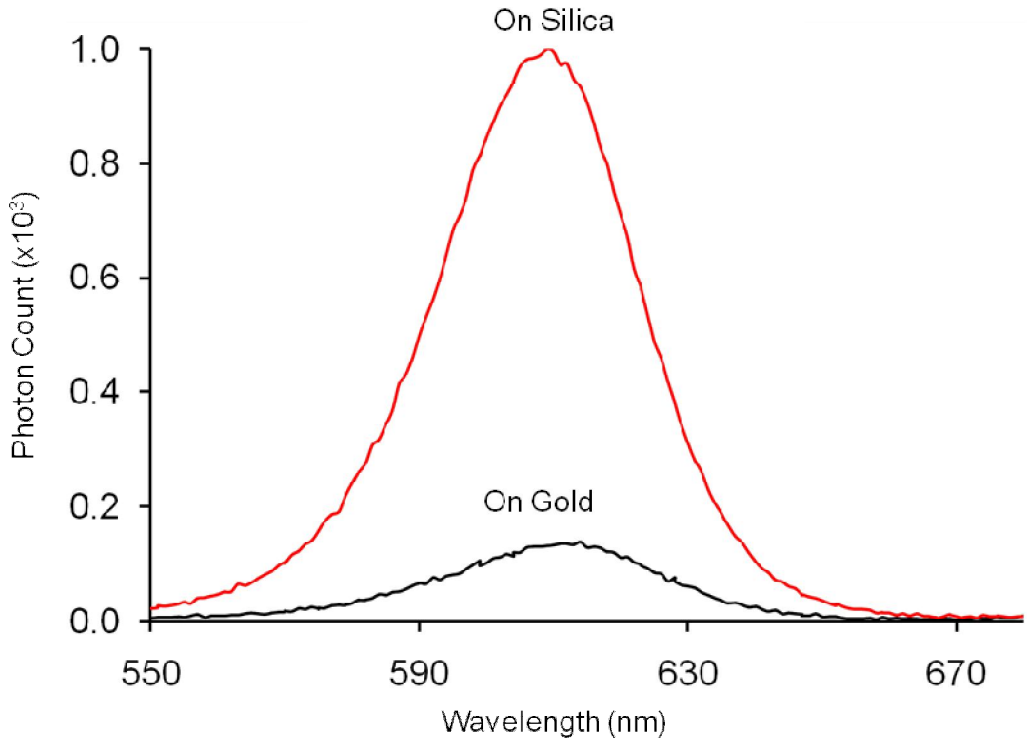

Figure 4.73: The peak photoluminescence intensity of QBP1-QDots assembled on the silica surface is 9 times stronger than that of QBP1-QDots assembled on the gold surface

Figure 4.74: Cross specificity of the bioQBP1 decorated Sa-QDots. The assembly of hybrid nanoassemblies on gold patterned GaN surface and silica patterned GaN surface.

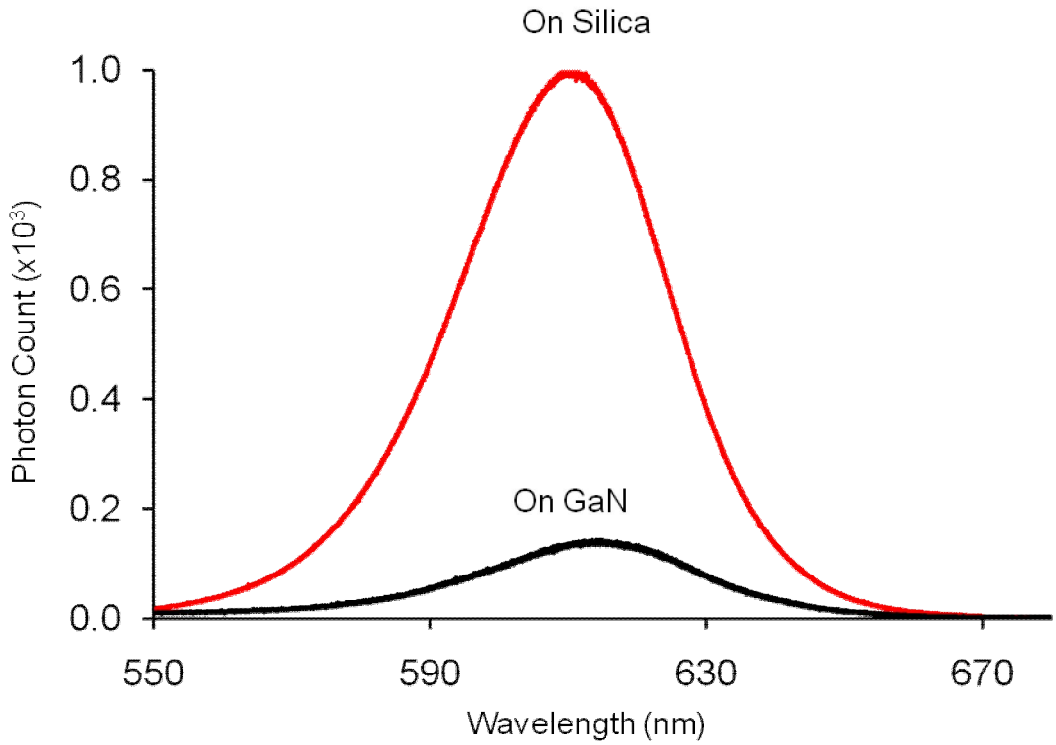

Figure 4.75: The peak photoluminescence intensity of QBP1-QDots assembled on silica surface (in red) is 9 times stronger than that of QBP1-QDots assembled on GaN surface (in black).

To overcome this problem, the SA-Q-Dots were blended with bioQBP1 in the buffer solution. Blending SA-Q-Dots and bioQBP1 before drop casting and the high degree of affinity between SA and biotin which has an equilibrium desorption constant (K_D) of 10^{-16} helped decoration of SA-Q-Dots with the bioQBP1.

In our approach, we observed a significant enhancement in the PL intensity of the GEPI assisted assembly of the Q-Dots on silica surface; here not only the enhancement in PL measurements was achieved, but also a comparable homogeneity was accomplished on the same sample surface in this method. In Figure 4.70, fluorescence microscopy (FM) images show a homogenous distribution of bioQBP1-SA-Q-Dots on the surface.

Furthermore, the samples with hybrid bioQBP1-SA-Q-Dots show almost ~70 times higher peak PL intensity compared to the control groups. As studied previously, since the interaction between the biomolecules is affected by the salt concentration, we also further tested and optimized the optimum salt concentration.

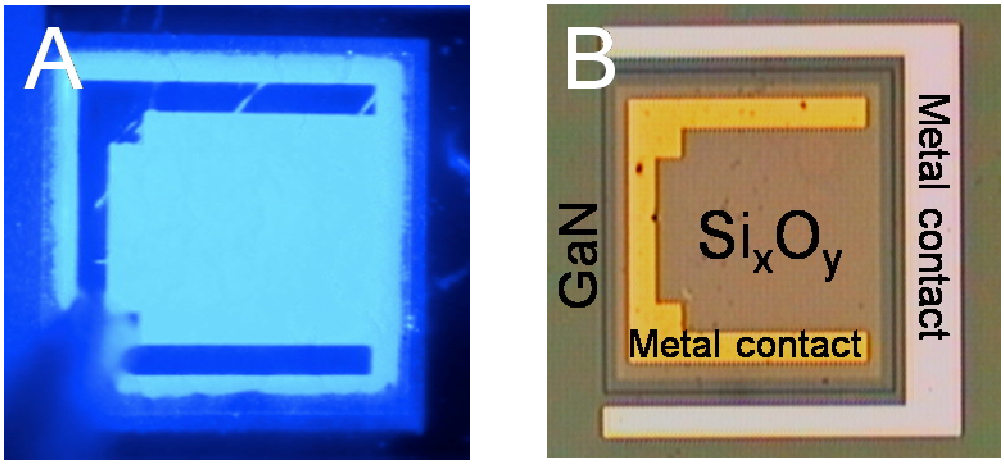

Figure 4.76: (A) Electroluminescence of the microfabricated LED alone at 380 nm in near-UV, with a tail in the violet making LED appear violet. (B) Plan view of microfabricated LED with the corresponding metal, semiconductor, and dielectric surfaces.

As the next step, the binding specificity of bioQBP1 was demonstrated on a real optoelectronic microchip surface which was fabricated for solid-state based lighting applications. For such an optoelectronic chip, there is a need for binding specificity between at least three different types of materials patterned on the chip, the dielectric film, the metal film and the semiconductor film. For this purpose, we first analyzed the binding specificity of bioQBP1 on gold patterned silica surface and silica patterned gold surfaces in which silica were used as the dielectric film and the gold as the metal film.

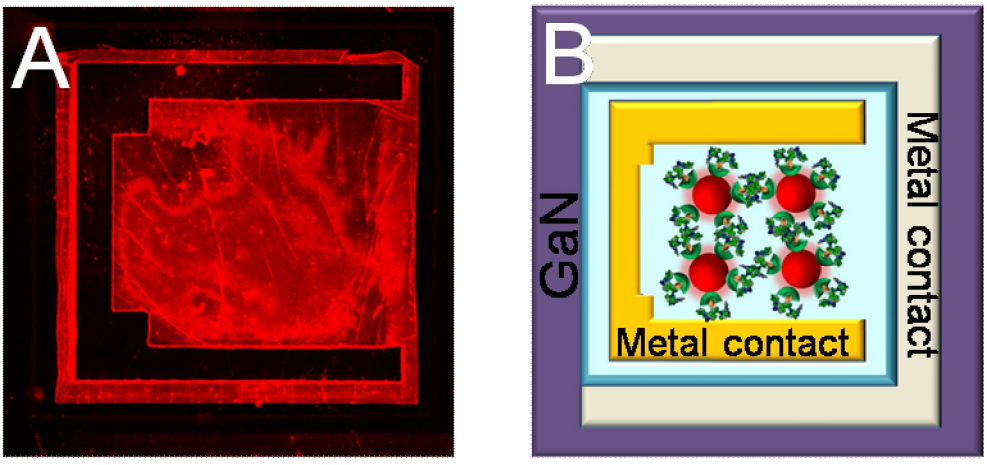

Figure 4.77: (A) Conformation of the targeted self-assembly of the QBP1-QDots on the silica surface of the LED using florescence microcopy. (B) Schematic representation of the LED shown in (A) along with QBP1-QDots (emitting in red at 620 nm) targeted to be assembled specifically on silica on the LED.

Working on such two different configurations, we investigated the feasibility of decorating the smaller features of patterned device mesas in complementary geometries in a typical optoelectronic chip. Both surfaces were incubated with hybrid bioQBP1-SA-Q-Dots and then washed as previously described. In Figure 4.73, the PL intensity of bioQBP1 assisted assembly of Q-Dots was shown both on gold and silica. Since the bioQBP1 is only specific to silica but not gold, the PL intensity peak of the silica part of the chip is 10 times higher than the PL intensity peak of the gold part. None bioQBP1 decorated SA-Q-Dots were also incubated on the patterned chip surfaces; however, in this case, both on gold and silica part of the chips, the SA-Q-Dots showed significantly lower amount of binding and PL intensity because of the absence of bioQBP1. Besides, as silica surface is rich in terms of –OH groups in solution, the amount of non-specifically bounded SA-Q-Dots is almost same as the bioQBP1 decorated SA-Q-Dots adsorbed on gold surface. In addition to the gold versus silica binding specificity, another set of binding specificity experiments was carried out with silica (as the dielectric film) versus GaN (the semiconductor film), which is an important component of a real light emitting diode (LED) chips. As shown in Figure 4.75, like the silica versus gold experiment we obtained the same result from the binding specificity studies for GaN versus silica experiments, bio-QBP1 exhibited a very low affinity towards Au and GaN compared to the silica surface. The affinity of the bioQBP1 was almost at the same ratio compared to the control group experiments where we had only SA-Q-Dots, which were not decorated with bioQBP1.

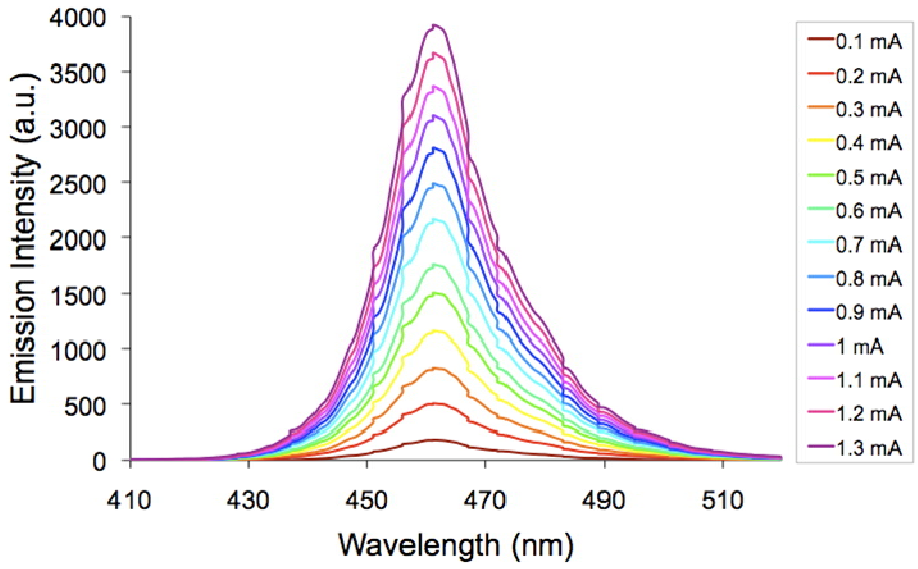

Figure 4.78: Profiles, respectively, of electroluminescence of the microfabricated LED device stand-alone at 460 nm and at various levels of driving current at room temperature.

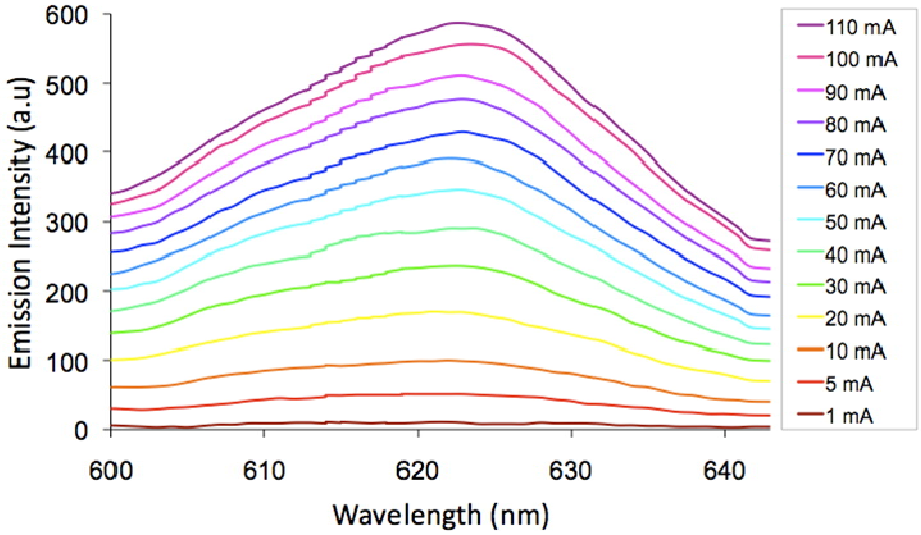

Figure 4.79: Photoluminescence of the hybrid construct targeted assembled on the silica that is optically pumped by the electrical driven LED at room temperature.

In our study, we produced and demonstrated hybrid organic-inorganic nano building blocks for photonic applications composed of two main parts, the binding part (the bioQBPs) and the optically active part (the Q-Dot). Unlike the conventionally created chemical based nano structures, our hybrid structures exhibit multi-binding specificity. They are specific to silica surface, and their affinity towards silica does not only consider specificity to silica. The binding specificity towards GaN and Au are also included. Although GEPIs have been used in the previous studies of our

groups and others, this is the first time that multi-specificity of a GEPI on a real microchip (on an LED chip) was investigated. Further for the layer-by-layer assembly of Q-dots, it is important to provide free peptide ends in each layer. These free peptides on Q-dots, which are not bound on silica surface, will allow for creating a platform for biominerilization of inner layers for the layer-by-layer assembly. This will lead us to open new avenues in the research for nanophotonics, which will result in a more specific and controlled assembly and building of novel biomolecular organic-inorganic hybrid devices.

4.5.4.1 Kinetics of self assembly of quantum dot nano emitters using GEPIs

The previous studies showed that the bound bioQBP1 has a fractional surface coverage of 80% on silica surface. We obtained the maximum adsorbed QD mass on the silica surface using bioQBP1. In Figure 4.80-A , control group shows the case where the peptide linkers were not used neither on the silica surface nor on SA-QD surface, SA-QDs are adsorbed on silica surface at some degree due to some non-specific interactions between SA and the silica surface, in particular hydrophobicity and physical adsorption of the charged residues. In Figure 4.80-B, with the use of bioQBP1 in decoration of the silica surface, more SA-QDs are adsorbed on the silica surface via the supramolecular interaction between biotin and SA. However, there are some limitations in the sequential assembly of QDs on peptide modified silica surface; for example the steric hindrances between the SA-QD molecules. Furthermore, the mass transfer of SA-QDs is diffusion limited, since their interaction with immobile biotin part of the peptides, for effective adsorption. In fact, for stronger adsorption, SA-QDs have to interact with bioQBP1 on surface, which is less possible compared to the interaction of the SA and biotin in solution. Therefore, formation of the bioQBP1-SA-QD hybrid nanoassemblies before immobilization significantly improves the SA-QD adsorption.

Moreover, the Langmuir model fit to actual data points were much better, given in Figure 4.80-D, where the apparent adsorption rate is recorded as function of SA-QD concentration. The adsorption equilibrium constants, and the change in the Gibbs free energy for binding process, were found from the SPR data for each cases. As given in Table 4. 8, the adsorption equilibrium constant increases when we used silica binding peptide bioQBP1 as smart molecular linker. Using sequential

assemblies exhibit 3.4 folds enhancement in the adsorption equilibrium constant compared to control group, in which SA-QDs were only immobilized on non-modified silica surface.

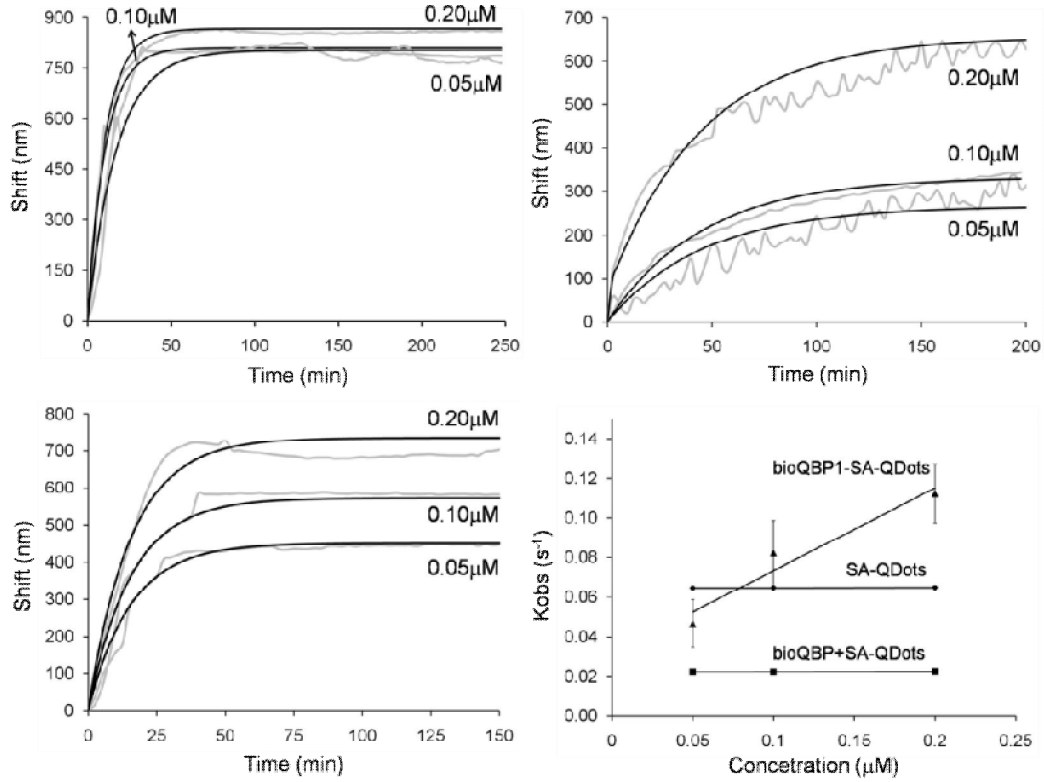

Figure 4.80: The SPR wavelength shift as a function of time for QD adsortion onto silica surface in the case where (a) SA-QDs are immobilized on non-modified silica surface (control group), (b) SA-QDs are immobilized on silica binding peptide (bioQBP1) modified silica surface (sequential assembly approach), (c) Hybrid nanoassemblies SA-QDs are hybridized with silica binding peptides before interacting with the surface) are immobilized on non-modified silica surface. The adsorption rate is given as function of SA-QD concentration in (d).

This increase in the adsorption constant points out an improvement in the binding affinity of the SA-QDs on silica surface and it is favored by the specific interaction of the SA molecules with the surface bound biotin molecules, which are bound to the silica surface through the specific interaction of the silica binding peptide with silica. In this approach, there are two possible dominating effects determining the amount of SA-QD adsorption on peptide modified silica surface. The first dominating effect comes from the amount of bioQBP1 adsorption on silica surface since for the SA-QD adsorption first silica surface must have been sufficient covered with peptide. The previous studies showed that the bound bioQBP1 has a fractional surface coverage of 80% on silica surface. Secondly, noting the interaction between SA and biotin is one

of the strongest known interactions in nature, it definitely influences the SA-QD adsorption on silica surface.

Table 4.8: The binding constants and binding free energies of SA-QDots on silica surface, in three different cases. Adsorption of SA-QDot on silica surface, functionalization of SA-QDot with silica binding peptide (QBP1) and the binding of SA-QDot on silica binding peptide decorated silica surface.

	SA-QDot	bioQBP1 + SA-QDot	bioQBP1-SA-QDot
$K_D(\mu M)$	2.46×10^4	8.4×10^4	2.03×10^6
ΔG (kcal/mol)	-6.0	-6.7	-8.1

However, these two effects are not the only influences on SA-QD adsorption, since the interaction of the biotin molecule with the active site of SA is restricted with the mass transfer problem of SA-QDs on the stationary biotin ends of the bound peptides. To improve the binding of the SA-QD on silica surface, the hybrid nanoassemblies were formed by filling the available sites on SA on the outer shell of SA-QD with biotins in solution so that SA-QD surface was fully hybridized with silica binding peptide. These new hybrid nanostructures have an enhanced capability to assemble on silica surface in a more controlled and robust manner. Comparing to the control group where the SA-QDs were immobilized on the non-modified surface, with hybrid nanoassemblies 82.5 times enhancement in the binding affinity was achieved.

In Table 4.8, calculated Gibbs free energies, for three different QD binding approaches are given. For hybrid nanoassemblies, the Gibbs free energy is minimum, which means that this system is thermodynamically more stable than sequential assembly technique and control group since this process can take place without intervention of external forces and it give rise to a lower Gibbs free energy for QD adsorption.

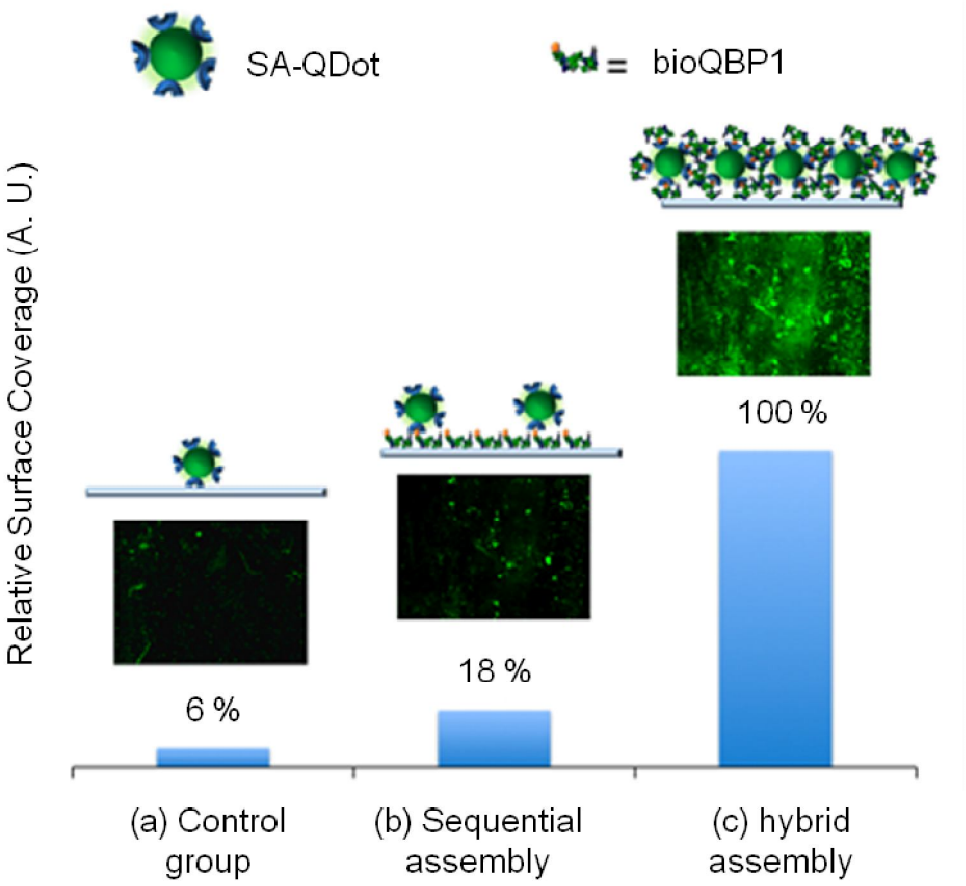

Figure 4.81: Relative surface coverage of (a) control group, where SA-QDs are immobilized on non-modified silica surface (b) sequential assemblies where SA-QDs are immobilized on silica binding peptide mediated silica surface, and (c) hybrid nanoassemblies where SA-QDs are hybridized with silica binding peptide before immobilization onto the silica surface. Surface coverage values are normalized with surface coverage of hybrid nanoassemblies. Additionally, for each experimental set, a schematic showing relative amount of adsorbed SA-QDs and fluorescence microscopy images are given. While there is an improvement in the number of SA-QD adsorbed onto silica surface in sequential assembly technique, maximum SA-QD adsorbance was achieved with hybrid nanoassemblies.

The surface coverage of SA-QDs was calculated from eq 4 and normalized with the surface coverage of hybrid nanoassemblies (BioQBP-SA-QDs) since the highest adsorption and surface coverage of SA-QDs was obtained with hybrid nanoassemblies. The normalized surface coverage for the each case was given in Figure 4.81, coupled with schematics representing adsorbed SA-QDs and fluorescence microscopy images of the SPR slides with 0.25 μM SA-QD concentration. The fluorescence microscopy images also supports SPR data and adsorption results as well as the surface coverage percentages.

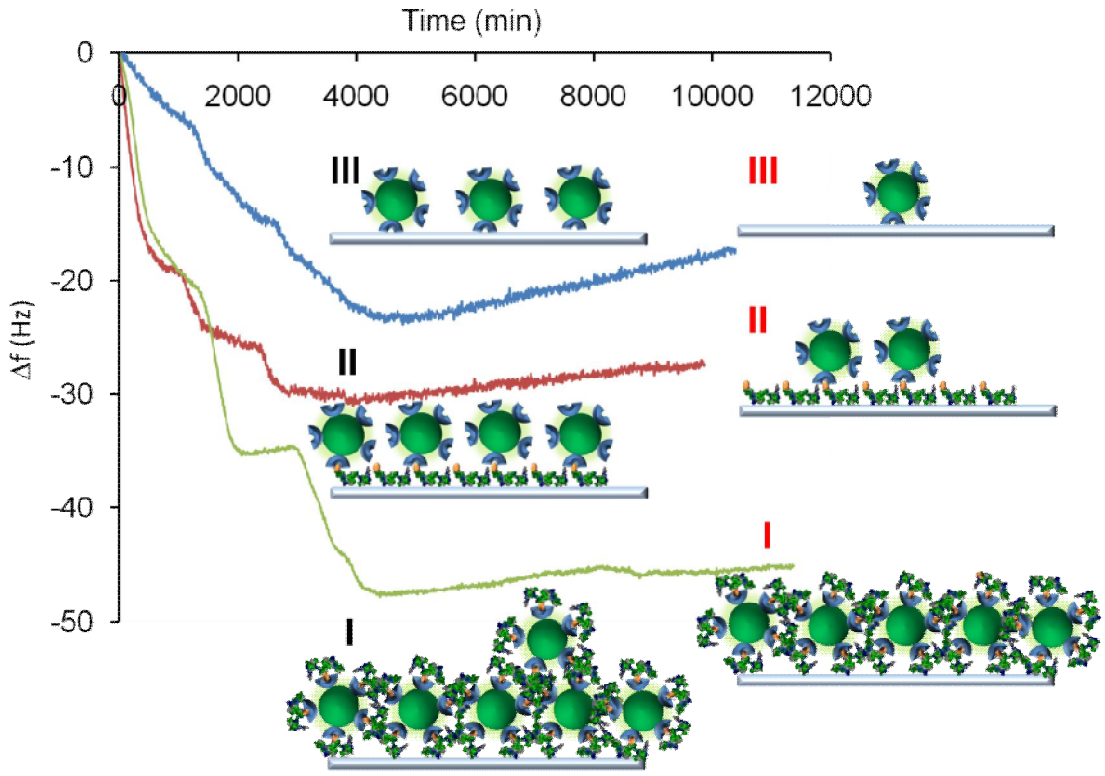

Figure 4.82: QCM-D real time monitoring of the binding of SA-QDs (a) in control group, (b) with sequential assembly technique, and (c) with hybrid nanoassembly method on silica surface. Total change in the resonance frequency was the highest in hybrid nanoassemblies and therefore SA-QD adsorption was maximum in this case. On the other hand, while we expect to see highest dissipation of adsorbed SA-QDs from silica surface since it has the highest surface coverage, the change in the resonance frequency does give this result. Actually, it implies that closely adsorbed hybrid nanoassemblies do not entrap water molecules as expected.

The gradual increase in the brightness of fluorescence microscopy images from control group to hybrid nanoassemblies implies a direct correlation between the surface coverage of the SA-QDs and total luminescence of adsorbed SA-QDs.

We further verified adsorption behaviour of the SA-QDs on silica surface in three experimental sets with quartz crystal microbalance (QCM) system, which is another powerful technique for real time monitoring of molecular interactions. Even though SPR and QCM-D can be interchangeably used to study adsorption kinetics of molecules, in fact they give different information about molecular interactions. For instance, while SPR gives an idea about the film thickness and deposited dry mass by measuring the change in the refractive index, QCM-D can also monitor the dissipation of the film deposited on the sensor crystal by recording data at different

overtones . This change in the dissipation of the film gives direct information about the amount of water held by the molecules in the system, which is not possible to detect in SPR measurements. It is also reported that the entrapment of the water molecules is related with the surface coverage. At higher surface coverage levels, molecules become more dissipative due to the entrapment of the high amount of water on the sensor surface. QCM results revealed that the change in the dissipation is maximum in hybrid nanoassemblies and it is minimum in the control group. However, compared to the shifts in resonance frequency in each case, the change in the resonance frequency is smaller than expected in Figure 4.82. In SPR results and fluorescence microscopy images, the surface coverage is higher in the case of hybrid nanoassemblies adsorption; therefore, it would be expected that the change in the dissipation to be larger, as a higher surface coverage leads to more water entrapment. But this not the case, so this situation indicates the film of the hybrid nanoassemblies is condensed and in contrast to high surface coverage, the densely packed hybrid nanoassemblies do not hold large amount of water. The frequency shifts and dissipation changes given in Figure 4.82 are good indications of the quality of the film formed and the enhancement of the adsorbed QD on the surface by the help of the peptide hybridization of SA-QDs.

Self-assembly process is a well established tool to create ordered nanostructures for application in physical and life sciences. One of the challenges is to build and control these systems by means of molecular recognition. The biological molecules and systems are including many of the samples of the self assembled systems. Herein, we exploit a combinatorial biology selected peptide, which is capable of specifically binding to silica surface. We utilized this peptide as a smart molecular linker for the controlled assembly of the SA-QDs on silica surface. The binding kinetic of SA-QDs on silica surface using different approaches was investigated. Hybridization of SA-QDs with bioQBP1 enhanced the binding of SA-QDs on silica surface. These hybrid nanoassemblies have been found to have a higher surface coverage compared to the assembly of SA-QDs on silica surface or assembly of SA-QDs on bioQBP1 decorated surface. We observed that hybrid nanoassemblies are attached to the silica surface at a higher affinity and the formed film on the silica surface is more densely assembled compared to other cases. This quantitative study showed that fundamental

work toward understanding the adsorption behavior of the nanostructures is crucial to control building new nanostructures.

4.5.5 Silica synthesis using the quartz binding peptide

The synthesis of silica was carried out by using the peptides as agents to control the formation of the silica from TMOS. In previous studies, it was shown that hydrolysis of TMOS under mild acidic conditions results in the formation of silica; however with the use of the peptide, this leads to controlled formation. The comparison of the QBP1 added case and its negative control group is given in Figure 4.83. As one can note that in the non-peptide case, the resulting structure seems to be formed in islands with very deep cracks between them, which illustrates that this approach is not good enough to create homogenous silica surfaces. Being able to synthesize homogenous and uniform silica surface as a separating layer is essential for building layer by layer assemblies of QDots with high PL intensity, otherwise random and non-uniform distribution of QDots may result in comparatively low PL intensity. Adversely, in the case of peptide-controlled synthesis of silica, a more controlled surface structure and topography is observed to be formed in Figure 4.85.

QBP1 has a high affinity towards silica surface such that the binding energy of QBP1 on silica surface is around -7 kcal mol^{-1}. This high affinity between the peptide and the silica surface may occur though the interaction of the side chains of the peptide. In previous studies in which polypeptides with positive charge were used to form silica platelets and silica surfaces, it was stated that the formation of silica was considerably affected by the charge of peptides (Kroger et al., 1999). Additionally, in nature it was also found that some organisms use heavily positively charged polypeptides for the formation of the silica structures (Miyamoto et al., 1996; Shiba and Minamisawa, 2007). However, in our case the QBP1 peptide does not include any charged group in its structure and it is neutral in terms of the total charge (calculated using ProtParam tool, http://expasy.org/tools/protparam.html) and it is not in zwitterionic form (pI; 5.95) in the pH range of the buffer we used in this study.

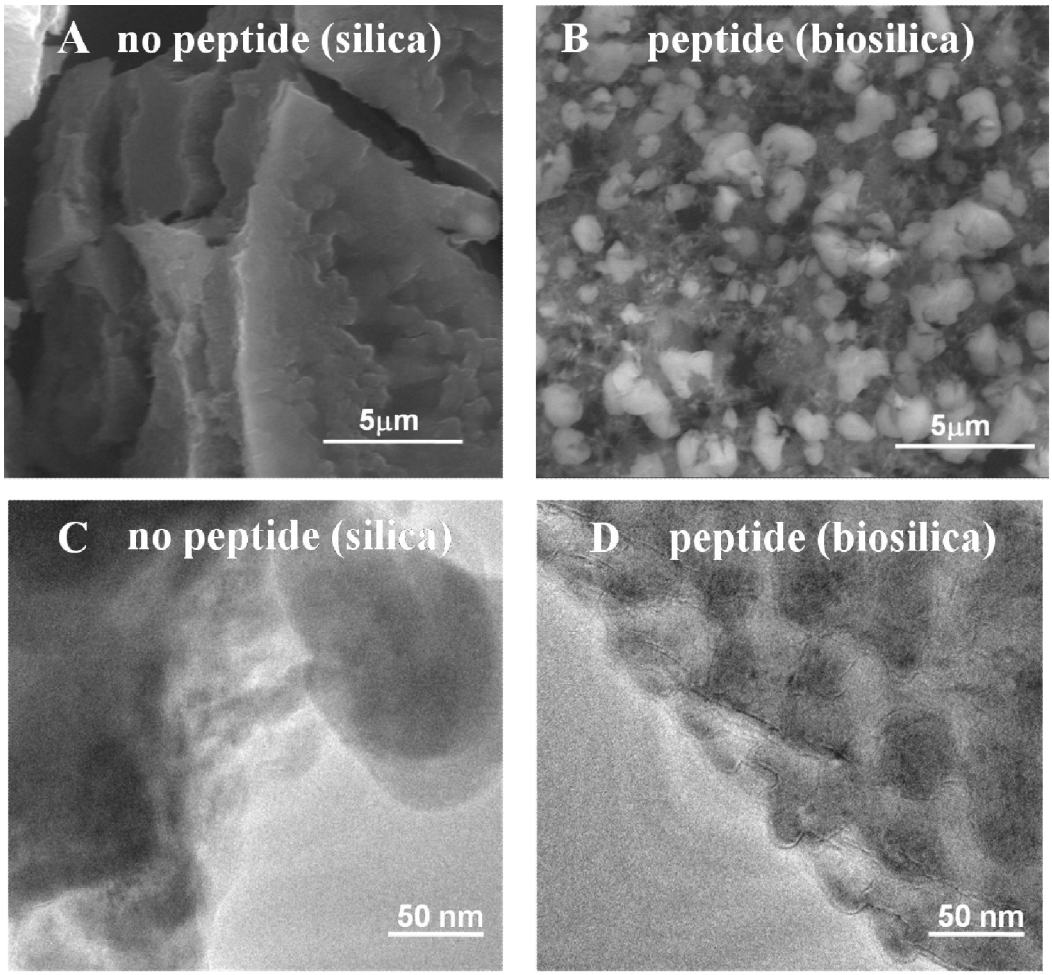

Figure 4.83: (A) SEM image of the silica surface formed in the absence of the silica binding peptide (QBP1). (B) SEM image of the silica surface formed in the presence of the QBP1. (C) TEM image of the silica surface formed in the absence of the silica binding peptide (QBP1). (D) TEM image of the silica surface formed in the presence of the QBP1.

Therefore, we can conclude that the formation of the silica by using QBP1 was triggered by the deposition of the silica on the peptide surface which formed a template for the formation of silica. As seen in Figure 4.83-A, the silica formed in the absence of the peptide is different than that of peptide controlled synthesis shown in Figure 4.83-B. In peptide controlled synthesis, the peptide restricted the growth of silica layer in every direction, so the silica surface was grown in continuum with homogeneously size distributed spherical structures. The TEM images also support the idea that the silica binding peptide controls the formation of the silica film. In Figure 4.83 (C), the formation of silica in the absence of peptide was shown, compared to the peptide-controlled synthesis of the silica on Figure 4.83 (D), silica is more randomly grown. The peptide-controlled synthesis of the silica seems more oriented and ordered in Figure 4.83 (D). At this point, we can state that if the peptide

constitutes the template for the deposition of the silica, then the peptide concentration should be effective in the formation of silica. To test the effect of the peptide concentration on the silica formation, we probed the silica formation as a function of peptide concentration varied from 50 µg/ml up to 800 µg/ml. In Figure 4.84, the images were sorted from left to right in an increasing order of peptide concentration. In Figure 4.84 (A), the peptide was observed to form branched structures, and in Figure 4.84 (B) and Figure 4.84 (C) as the peptide concentration rises, the density of branched like structures increases as well because of improved surface coverage, which may also be the reason for the peptide restricted the growth in the formation of silica structures. If this is the case, then the peptide concentration should be carefully adjusted to obtain a homogenous and continuous surface structure so that we set the peptide concentration to 500 µg/ml to be used in our silica growth. After the formation of the silica surface, we worked on creating a self-assembled layer of QDots on biomimetically synthesized silica surface. Here, we intended to explore the possibility of utilizing these biosilica structures as a platform for a layer-by-layer assembly of QDots. First, we formed bifunctional QDots, where the outmost layers of these QDots were decorated with bioQBP through the interaction of the streptavidin (SA, chemically conjugated around QDots) and biotin (bio, chemically inserted at the N-terminus of peptides) conjugation.

The optical emission at wavelengths longer than 515 nm were collected by the detector and in each image an area of 450 µm by 450 µm was scanned. The Figure shows that the silica formed in the absence of the bioQBP1 and in the presence of the bioQBP1 has different surface structures, on both of which the bioQBP1-SA-QDot can be attached with high affinity. The only difference is the homogeneity of the distribution of the nanostructures, while the PL intensity of both samples was locally almost the same. Additionally, to quantify the emission of the self-assembled bioQBP1-SA-QDot, the PL measurements were performed. To study the specificity of bioQBP1-SA-QDot on silica surface and to ensure that the hybrid nanostructures do not have any cross affinity towards silicon, which is the base material for silica, a control experiment was performed by assembling and washing bioQBP1-SA-QDot on silicon surface, which is also another way of probing the presence of silica in positive control. The PL measurements indicated that there is no attachment of bioQBP1-SA-QDot on bare Si surface. The control experiment for the non-binding

of the bioQBP1-SA-QDot is important, as the silicon is the main material, which is used in the formation of the silica by using different kind precursor materials.

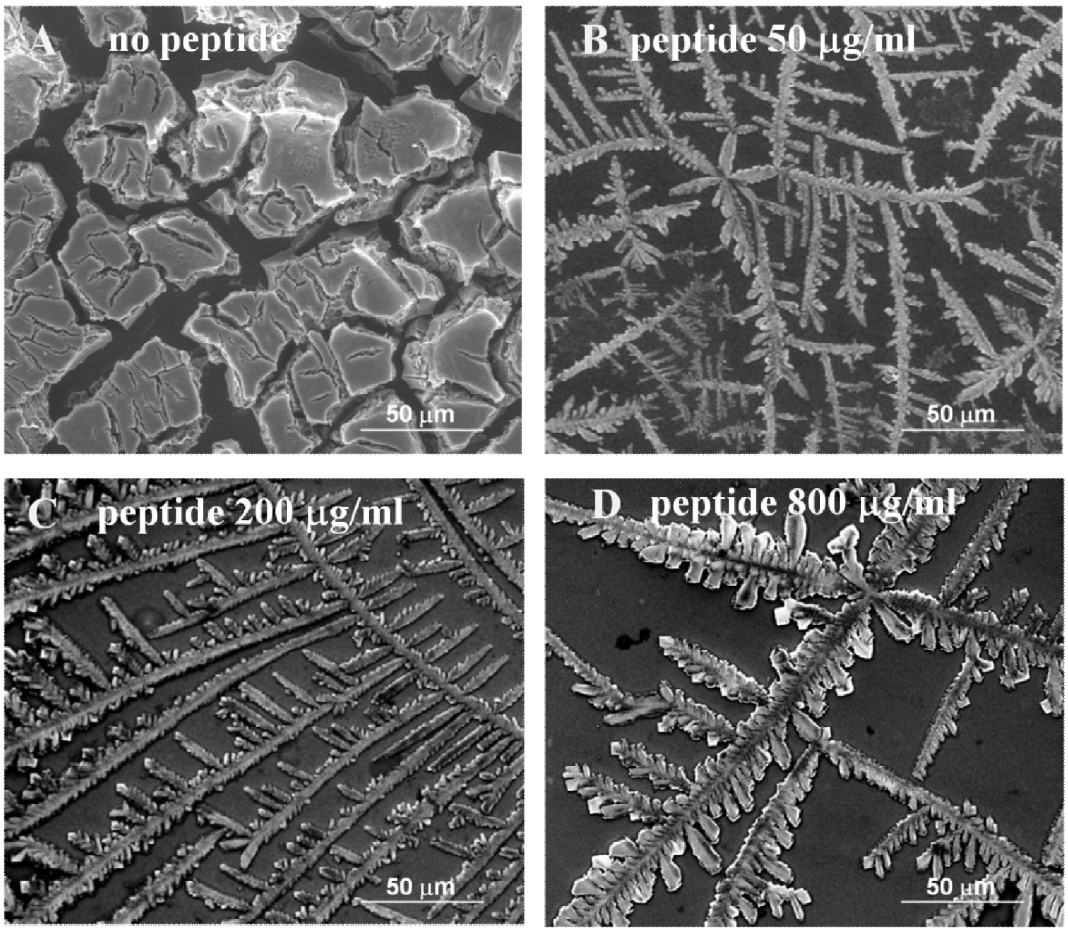

Figure 4.84: Silica formation carried out in the absence (A) and presence (B, C, D) of silica binding peptide (QBP1). Silica formation was carried out as a function of concentration of silica binding peptide. (50 μg/ml (B), 200 μg/ml (C) and 800 μg/ml (D)).

Material synthesis towards creating supramolecular assemblies for nanotechnological applications needs a controlled route of processing. Inorganic binding peptides are good candidates to synthesize materials in a controlled manner, which was previously proved in the synthesis of materials and is also applied and explored in this study. With their molecular recognition ability and through supramolecular interaction, QBP1 was successful in controlling the formation of silica surface. Furthermore, self-assembly of nanostructures on target surfaces by using chemical approaches is an arduous work due to the requirements of vast surface modifications. On the other hand, by exploiting inorganic binding peptides and hybridizing these peptides around the QDots, we easily achieved the assembly of the bioQBP1-SA-QDot on biosilica surface.

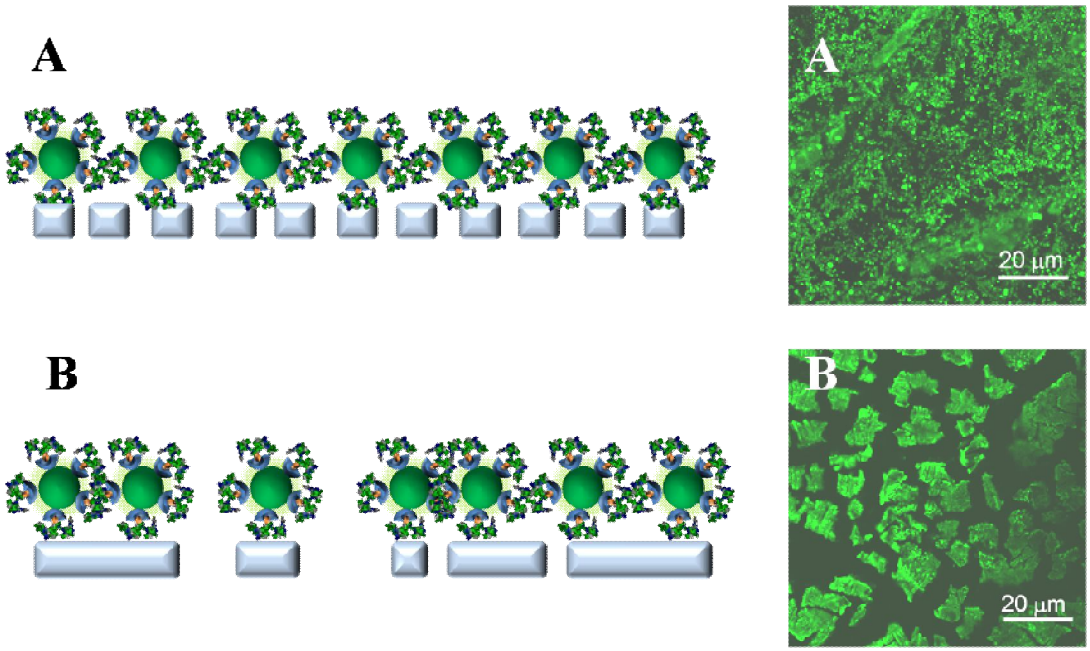

Figure 4.85: The schematics and photoluminescence intensity of the assembly of the bioQBP1 -SA-QDot hybrid nanostructures on silica synthesized in the presence (A) and absence of the silica binding peptide (QBP1) (B).

To point out the bi-functionality of bioQBP1-SA-QDot, while the hybrid nanostructures can specifically bind to silica surface, they can also control synthesis of silica surface. As the QDots were decorated with these peptides, the binding of QDots on silica surface was achieved by the interaction of the peptides with silica surface. The binding of the QDots on silica surface was carried out in the absence of the bioQBP1, which is reported previously. Also, we showed the specific binding interaction of the bioQBP1 by its non-binding on silicon surface. The silica binding peptide was shown to have a restriction effect on the growth of the silica film. This helps the silica films to grow in a manner that one can control the homogeneity of the film. However, in the absence of the peptide the silica surface is grown in large islands, which are not useful towards creation of layer-by-layer assembled films. The silica binding peptide acts an element to control the morphology of the silica. Also the formed silica structure was probed by using the bioQBP1-SA-QDot. Silica binding peptide acts as a tool for the self-assembly of the nanotechnological entities, in addition silica binding peptide can be used as a tool to control the morphology of the synthesized silica.

5. CONCLUSIONS

In this study, we investigated the molecular binding characterization of GEPIs on solid surfaces and applications of GEPIs as molecular linkers.

The first part of the study is molecular characterization of GEPIs as potential molecular linkers. Molecular characterization tools to explore solid-peptide (protein) interface is limited. Here, we utilized surface plasmon resonance spectroscopy and quartz crystal microbalance (QCM-D) as the basic tool towards characterization of the solid-peptide interface. The majority of the studies towards characterization of the solid-protein interface were carried out using gold surface. However, GEPIs were screened and selected to many different materials; we therefore explored the possibilities to extend the sensing capabilities of SPR on different material surfaces. In our group, a mathematical model estimating the optimum thickness to get a signal from a SPR sensor chip was developed. This model allowed use to determine the optimum thickness of adlayers to be coated on top of the gold or silver surface to be able to track the interaction between any given GEPI specific to a surface of interest. Using this approach, we were able to monitor avidity of the platinum, silica and gold binding peptides. We calculated the thicknesses of layers of silica or platinum to be coated on gold surface for a reasonable signal usable in SPR. For a platinum chip, we coated 2 nm of Pt, and 33 nm of gold with a 2 nm of chromium adhesive layer on a glass slide. For the silica surface, 4 nm of silica was sputtered on 45 nm of gold. After preparing the SPR slides, the adsorption experiments were carried out. The data collected from SPR experiments was used to determine the binding equilibrium constant, adsorption and desorption constants. The SPR data was analyzed using Langmuir and modified Langmuir adsorption model equations. The model equations were fit to the data point using least square curve fitting algorithm. To explain the mechanism and extract the adsorption constants either a one to one or bi-exponential models were used. In some cases, the simple Langmuir interaction was modified to explain two stage binding of the peptides. In a two stage binding model, we assumed two different binding rates of GEPI on solid surface. This might be because of the

surface heterogeneity. We found that the solid surface has sites with different energetic for binding of GEPIs.

The surface coverage of the peptide can also be determined by the thickness of the film on a given surface area. We first collected the data for SPR experiments. Then we determined the refractive index change upon adsorption of the GEPI on a solid surface. The difference between the adsorbate and the surface was also used to determine the thickness of adsorbed material on a given surface. We used this approach to be able to compare SPR data for binding of different GEPIs, on different surfaces. In section 4.3 the adsorbed mass on Pt, SiO_2 and Au surface were calculated using this method. Both, reflectivity and adsorption models for GEPIs were exploited for the molecular characterization of GEPIs.

Here the binding kinetics of five different gold binding peptides were investigated. First, we investigated the binding kinetics of a cell surface display selected gold binding peptide, GBP both in its original one repeat and three repeat forms. We found that increasing the number of repeats in GBP, increases the K_{eq} almost three times. Previous studies showed that, changing the number of repeats in gold binding peptide effects the conformation. In a different study, a core group of residues were assigned as the potential binding domain of GBP. We can therefore suggest that the increase in the binding of GBP resulted in an increase of the functional groups on the side chain of the GBP. Interestingly this is not the case for other group of the gold binding peptides. Flagella display selected AuBPs were found to behave differently, they were synthesized in cyclic (c-) and open linear (l-) conformations. One can expect a major difference between the binding affinity of linear and constraint forms of the peptides due to their differences in conformational behavior. The avidities of l-AuBP1 and c-AuBP1 were comparable (K_{eq}, ~$3x10^6$ M-1) to each other, whereas in AuBP2 there was a six fold increase when the peptide displayed in a constrained form (K_{eq}, ~$2x10^6$ M^{-1} and ~$12x10^6$ M^{-1}). Secondary structure analysis of gold binding GEPIs revealed a high content of random coil structure, additionally presence of extended polyproline type II helical structure was noted for the open linear form of the AuBP1-2. It is obvious that in the case of the gold binding peptides not only the conformation but also the chemistry of the residues plays a crucial role.

Platinum binding peptides PtBP1 and PtBP2 were synthesized in three conformations. Open linear form (l) , three tandem repeat (3l) and cyclic (c) of the

one repeat to probe the effect of conformational adaptability as well effect of the increase number of functional groups on the side chains of the residues. c-PtBP1 found to have the highest binding affinity compared to open linear and three repeat tandem repeat of the peptide. And surprisingly l- and 3l- forms tend to have the same affinity towards platinum surface. On the other hand, PtBP2s l, c and 3l forms have totally different behavior. The cyclic one has the lowest affinity compared the other two forms. linear form has twice and 3l-PtBP2 has 50 times higher affinity compared to c-PtBP2 forms. The results showed that the binding mechanism of PtBP2 works totally different than the rest of the peptides. In PtBP1, conformational constraints plays a positive role in the binding of the peptide, however in the PtBP2 instead of conformational constraint a more labile structure play a crucial role binding of the peptide. One can conclude that the binding in PtBP2 is affected by the avidity of the functional side groups. Like in gold binding AuBP2, we saw a remarkable effectiveness in the affinity of the peptide when a conformational restriction is applied to the structure of the peptide. In AuBP2 the difference in secondary structure was the absence of PPII type helical structure in constrained form. In the case for the PtBP1 we noted that linear version of the peptide and cyclic version of the peptide both exhibit a random coil structure, but the linear form also has some degree of PPII type structure while the cyclic form has not. When pertubating the structure of PtBPs (with varying concentrations of TFE), the structural difference become more obvious during the structural transition of peptides. During the structural transition, linear form had a loss in random coil while the percentage of PPII structure becomes more obvious. However, cyclic form follows a different way and the degree of PPII decreases and it folds into a nonrandom coil and random coil structure which satisfies the presence of a covalent loop.

Two phage display selected silica binding peptides were analyzed, QBP1 and QBP2. Silica binding peptides were synthesized in one repeat and three repeat linear forms. Among the silica binding peptides, the more hydrophobic QBP2 or a slower adsorption and desorption rates but higher binding constant compared to that of QBP1. However, in the three repeat forms of these two peptides there is hardly any difference in the adsorption equilibrium constants but much faster binding processes in the more hydrophilic peptide (i.e., 3l-QBP1). We observed a ten times increase in the affinity of silica binding peptide QBP1, when we tested the three repeats of it.

On the other hand silica recognition and affinity didi not change for QBP2, when we increased the number of repeating units.

Adsorption experiments guided us to characterize the solid binding event at the molecular level. Additionally a detailed thermodynamic analysis of solid binding of GBP was probed in conjugation with a structure-activity relationship analysis. From our previous knowledge from adsorption experiments we assumed that the adsorption of 1r- and 3r-GBP1 molecules at Au interfaces involves common key events. The adsorption process for both molecules most likely involves polypeptide interaction with adsorbed water molecules on the Au surfaces, desorption of the adsorbed water molecules in exchange with the corresponding peptide molecule, and a subsequent loss of solvent ordering on the surface. However, for 3r-GBP1, the presence of a large, positive entropy change suggests that another important step must take place as well. The basis of entropy change may originate from the stability of molecules in solution versus on the surface, conformational changes of the molecules on the surface, and the supramolecular assembly of the 3l-GBP1. As shown by CD/TFE studies, conformational rearrangement can occur within the 3l-GBP1 molecule, and this process also takes place at the Au interface as well. We conclude that conformational change controls the binding of 3l-GBP1 on Au interfaces to a greater extent that it does for 1r-GBP1. In the case of l-GBP1, desorption of the adsorbed water molecules from the surface dominates in the overall entropy term, which is a positive entropy and characteristic of hydrophobic interactions. However, in the case of 3l-GBP1, both the water desorption and conformational change phenomena are the dominating factors in the overall process. The main conclusion drawn from this proposed mechanism is that the use of multiple sequence repeats for higher affinity material binding invariably introduces a conformational term that can influence the rate and affinity of that polypeptide for that particular interface. If this turns out to be true for the majority of genetically derived, material-selected sequences, then careful selection of the inherent and inducible conformation(s) of a particular polypeptide sequence could affect the resulting adsorption rate, affinity, and thus allow to “tailor” the resulting composite material for different technological applications.

Five peptides were used to probe the materials specificity of GEPIs: two platinum-, two quartz- and one gold-binding peptides ranging in amino acids from 7 to 12 and

14, respectively. These short GEPIs generally bind well to the surface they were originally selected for when used in their original molecular architectural forms, i.e., cyclic in platinum-binding and linear in silica- and gold-binding cases. These peptides were demonstrated to bind poorly to other materials. For example, even in the case of platinum versus gold, where surfaces are structurally and chemically similar, there is high degree of materials selectivity. There is also a significant difference in the binding of peptides to their own solids when they are used in form of three-repeat sequences. In this case, binding to other solids also changed, resulting in significant decrease in material specificity. A simple tandem repeat of the same peptide sequence, therefore, does not necessarily increase the binding of the peptide to its counterpart solid and, in fact, it might decrease its material selectivity. Short peptides are more likely to retain their conformed structures and longer ones, i.e., simple tandem repeats, may conform into other available conformations reducing their ability of materials selectivity. Materials selectivity quantitatively studied here, on the hand, could provide a platform for future investigations towards fundamental understanding of molecular-scale selectivity of solid materials. On the other hand, the ability of a genetically-selected peptide to recognize and bind to a specific solid (and not to others) due to their conformational stability provides a novel molecular tool for a wide range of materials and medical applications requiring material-specific molecular-linkers, -erectors, and -assemblers for utility, e.g., in targeted assembly of functional nanostructures, biosensors, and biomolecular probing.

Molecular characterization of GEPIs allowed one to utilize them in different applications. Here, we used GEPIs as molecular linkers to immobilize an enzyme (alkaline phosphatase), to immobilize semiconductor nanoparticles (quantum dots) toward building optoelectronic devices and for biomineralization purposes.

A case study for GEPI enhanced protein immobilization was carried out. GEPIs can be exploited in two distinct ways to enhance enzyme immobilization, one is using GEPIs inserted in protein and creating molecular constructs. The other is making GEPIs bifunctional using biotin tag on GEPIs, here we employed the second approach and the kinetic calculations showed a high affinity between the SA-AP fusion and the biotin. Immobilization is achieved in a very specific manner. The protein is also immobilized in an oriented manner via the fused streptavidin. The

peptide linkers used were also specific to the particular surfaces, so oriented protein immobilization and surface specific immobilization was achieved. In the control group we found that biotin-strepavidin interaction is not enough to keep the immobilized molecule on the surface of the gold without any linker molecule on the gold. Using these assemblies, it was also possible to monitor the enzyme activity directly on the surface of the SPR slide in real time. This is the first proof of principle study. There are other possible approaches employing inorganic binding peptides to immobilize the enzymes on solid surfaces. This approach will open new avenues in the construction of the protein arrays and building up new generation MEMS devices.

In previous studies the application of GEPIs as molecular linkers was shown successfully. Here we tested their usability as molecular linkers for the assembly of semi conductor nanoparticles on a light emitting diode chip surface. We explored the best method for the assembly of QDots on silica surface first. We utilized computationally designed QBP1 as a smart molecular linker for the controlled assembly of the SA-QDs on silica surface. We investigated the binding kinetics of SA-QDs on silica surface using different approaches. Hybridization of SA-QDs with bioQBP1 enhanced the binding of SA-QDs on silica surface. These hybrid nanoassemblies were found to have a higher surface coverage compared to the assembly of SA-QDs on silica surface or assembly of SA-QDs on bioQBP1 decorated surface. We observed that hybrid nanoassemblies were attached to the silica surface at a higher affinity and the formed film on the silica surface is more densely assembled compared to other cases. In addition to the assembly studies of GEPI decorated QDots with SPR, fluorescence spectroscopy and photoluminescence measurement showed the assembly of QDots on targeted surfaces on a real light emitting diode chip. Hybridization of SA-QDs with bioQBP1 enhanced the binding of SA-QDs on silica surface. These hybrid nanoassemblies were found to have a higher surface coverage compared to the assembly of SA-QDs on silica surface or assembly of SA-QDs on bioQBP1 decorated surface. We observed that hybrid nanoassemblies were attached to the silica surface at a higher affinity and the formed film on the silica surface was more densely assembled compared to other cases. This quantitative study showed that fundamental studies towards understanding the

adsorption behavior of the nanostructures is crucial to control building new nanostructures.

Biomineralization is another part that we utilized peptides as molecular tool to control mineral formation from the precursor of the silica TMOS (tri-orto-methyl silicate). We achieved a control in the formation of silica in the presence and absence of the silica binding peptide QBP1.We showed that QBP1 control the formation of the small spherical feature which are densely packed and formed a continuous film. This behavior makes QBP1 a good candidate to create interlayer silica layer when creating layer by layer assembled structures.

Lastly utilization of GEPIs as molecular linkers for biosensor applications was realized. This was achieved for construction of a biosensor for real time monitoring of the $CaPO_4$ biomineralization. Finally, the fibril elongation mechanism in Huntington disease was investigated using a biosensor based approach. We successfully exploited the molecular recognition and self assembly capabilities of GBP to enhance the immobilization of preformed fibrils on the surface of SPR sensor chip. Using this setup we tracked the fibril elongation in Huntington's disease in real time.

To sum up, here the GEPIs have been extensively studied for their molecular binding characterization. The outcome for the fundamental knowledge generated on binding of GEPIs was further utilized as a basis for practical applications. GEPIs were used; as molecular linkers for the immobilization of proteins and nanoparticles, as fusion partner for designer proteins for biosensor applications and as inorganic synthesizer.

The research both for fundamental understanding of GEPI self assembly-binding mechanism and for practical applications still continues. In near future, a more comprehensive answer for GEPI binding and assembly will be elicited. GEPIs will be the next generation of molecular tools to open new avenues to achieve the challenges at the nano- bio interface.

REFERENCES

Abdulhalim, I., 2009. Surface plasmon TE and TM waves at the anisotropic film-metal interface, *Journal of Optics A-Pure and Applied Optics*, **11** (1), 015002.

Aizenberg, J., Black, A.J., Whitesides, G. M., 1999. Control of crystal nucleation by patterned self-assembled monolayers, *Nature*, **398,** 495-498.

Allred, D. B., Zin, M., Ma, H., Sarikaya, M., Baneyx, F., Jen, A .K. Y., Schwartz, D. T., 2007, Direct nanofabrication and transmission electron microscopy on a suite of easy-to-prepare ultrathin film substrates, *Thin Solid Films*, **515** (13), 5341-5347.

Averitt, R. D.; Westcott, S. L.; Halas,N. J., 1999. *Journal of the Optical Society of America B-Optical Physics*, **16**, 1814-1832.

Bain, C. D., Whitesides, G. M., 1989. Attenuation Lengths of Photoelectrons in Hydrocarbon Films, *Journal of Physical Chemistry*, **93 (4)**, 1670-1673.

Belcher, A. M., Wu, X. H., Christensen, R. J., Hansma, P. K., Stucky, G. D., Morse, D., 1996. Control of crystal phase switching and orientation by soluble mollusk-shell proteins, *Nature*, **381** (6577), 56-58.

Berisio, R., Loguercio, S., De Simone, A., Zagari, A., Vitagliano, L., 2006. Polyproline helices in protein structures: A statistical survey, *Protein and Peptide Letters*, **13** (8), 847-854.

Berman, A., Addadi, L., Weiner, S., 1988. Interactions of sea-urchin skeleton macromolecules with growing calcite crystals: a study of intracrystalline proteins, *Nature*, **331**, 546–548.

Berthelier, V., Hamilton, J. B., Chen, S. M., Wetzel, R., 2001. A microtiter plate assay for polyglutamine aggregate extension, *Analytical Biochemistry*, **295** (2), 227-236.

Blaaderen, A., Ruel, R., Wiltzius, P., 1997. Template-directed colloidal crystallization, *Nature*, **385,** 321-324.

Bloom, J. D., Labthavikul, S. T., Otey, C. R., and Arnold, F. H., 2006. Protein stability promotes evolvability, *Proceedings of the National Academy of Sciences of the United States Of America*, **103** (15), 5869-5874.

Bourgeat-Lami, E., Tissot, I., Lefebvre, F., 2002. Synthesis and characterization of SiOH-functionalized polymer latexes using methacryloxy propyl trimethoxysilane in emulsion polymerization, *Macromolecules*, **35** (16), 6185-6191.

Braun, R., Sarikaya, M., Schulten, K., 2002. Genetically Engineered Gold-Binding Polypeptides: Structure Prediction and Molecular Dynamics, *Journal of Biomaterial SciencePolyme Edition*, **13** (7), 747–757.

Brown S, 1992. Engineered Iron Oxide-Adhesion Mutants Of The Escherichia-Coli Phage-Lambda Receptor, *Proceedings of The National Academy of Sciences Of The United States Of America*, **89** (18), 8651-8655.

Brown, S., 1997. Metal recognition by repeating polypeptides, *Nature Biotechnology*, **15** (3), 269-272.

Brown, S., Sarikaya, M., Johnson, E., 2000. A genetic analysis of crystal growth, *Journal of Molecular Biology*, **299**, 725-735.

Bryant, M. A., Pemberton, J. E., 1991**.** Surface Raman-Scattering of Self-Assembled Monolayers Formed From 1-Alkanethiols - Behavior of Films at Au and Comparison to Films at Ag, *Journal of the American Chemical Society*, **113** (22), 8284-8293.

Burns, M. M, Fournier, J. M., Golovchenko, J. A., 1991. Optical Crystallization Work – Response**,** *Science*, **252**, 1049.

Cannon, M. J., Myszka, D. G., Bagnato, J. D., Alpers, D. H., West, F. G., Grissom, C. B., 2002. Equilibrium and Kinetic Analyses of the Interactions between Vitamin B12 Binding Proteins and Cobalamins by Surface Plasmon Resonance, *Analytical Biochemistry*, **305** (1)**,** 1-9**.**

Cannon, M. J., Williams, A. D., Wetzel, R., Myszka, D. G., 2004. Kinetic analysis of beta-amyloid fibril elongation, *Analytical Biochemistry*, **328**, 67-75.

Cariolou, M. A., Morse, D. E., 1988. Purification and Characterization of Calcium-Binding Conchiolin Shell Peptides from the Mollusk, Haliotis-Rufescens, As a Function of Development, *Journal of Comparative Physiology B-Biochemical Systemic And Environmental Physiology*, **157** (6), 717-729.

Carvalho, A.; Geissler, M.; Schmid, H.; Micel, B.; Delamarche,E., 2002, Self-assembled monolayers of eicosanethiol on palladium and their use in microcontact printing *Langmuir*, **18**, 2406-2412.

Chen, H.,Su, X., Neoh, K. G., and Choe, W. S., 2006. QCM-D Analysis of Binding Mechanism of Phage Particles Displaying a Constrained Heptapeptide with Specific Affinity to SiO_2 and TiO_2, *Analytical Chemistry*, **78**, 4872-4879

Chen, S. H., Frank, C. W., 1989. Infrared and Fluorescence Spectroscopic Studies of Self-Assembled N-Alkanoic Acid Monolayers, *Langmuir*, **5** (4), 978-987.

Chen, S., Ferrone, F. A., Wetzel, R., 2002., Huntington's disease age-of-onset linked to polyglutamine aggregation nucleation, *Proceedings of the National Academy of Sciences of The United States of America*, **18**, 11884-11889.

Colby, D. W., Cassady, J. P., Lin, G. C., Ingram, V. M., Wittrup, K. D., 2006. Stochastic kinetics of intracellular Huntingtin aggregate formation, *Nature Chemical Biology*, **6**, 319-323.

Collino S. and Evans, J. S., 2007. Structural Features That Distinguish Kinetically Distinct Biomineralization Polypeptides, *Biomacromolecules*, **8** (5), 1686 -1694.

Culha, M., Stokes, D., Allain, L. R., Vo-Dinh, T., 2003. Surface-enhanced Raman scattering substrate based on a self-assembled monolayer for use in gene diagnostics *Anaytical Chemistry*, **75**, 6196-6201.

Dai, H., Choe, W. S., Thai, C. T., Sarikaya, M., Traxler, B., Baneyx F. and Schwartz, D. T., 2005. Nonequilibrium Synthesis and Assembly of Hybrid Inorganic-Protein Nanostructures Using an Engineered DNA Binding Protein, *Journal of the American Chemical Society*, **127**, 15637-15643

Daoud, W. A., Xin, J. H., Zhang, Y. H., 2005. Surface functionalization of cellulose fibers with titanium dioxide nanoparticles and their combined bactericidal activities, *Surface Science*, **599** (1-3), 69-75.

Das, J., Huh, C. H., Kwon, K., Park, S., Jon, S., Kim, K., Yang, H., 2009. Comparison of the Nonspecific Binding of DNA-Conjugated Gold Nanoparticles between Polymeric and Monomeric Self-Assembled Monolayers, *Langmuir*, **25** (1), 235-241.

Day, Y. S. N.; Baird, C. L.; Rich, R. L.; Myszka, D., G., 2002. Direct comparison of binding equilibrium, thermodynamic, and rate constants determined by surface- and solution-based biophysical methods, *Protein Science*, **11** (5), 1017-1025.

Debs, J. E., Ebendorff-Heidepriem, H., Quinton, J. S., Monro, T. M., 2009. A Fundamental Study Into the Surface Functionalization of Soft Glass Microstructured Optical Fibers via Silane Coupling Agents *Journal of Lightwave Technology*, **27** (5-8), 576-582.

Demir, H. V., Nizamoglu, S., Ozel, T., Mutlugun, E., Huyal, I. O., Sari, E., Holder, E., Tian, N., 2007. White light generation tuned by dual hybridization of nanocrystals and conjugated polymers, *New Journal of Physics*, **9**, 1-13.

Dickerson, M. B., Naik, R. R, Stone, M. O., Cai, Y. and Sandhage, K. H., 2004. Identification of peptides that promote the rapid precipitation of germania nanoparticle networks *via* use of a peptide display library, *Chemical Communications*, **15**, 1776-1777.

Dobson, C. M., 2004. Principles of protein folding, misfolding and aggregation, *Seminars in Cell & Developmental Biology*, **15**, 3-16.

Donatan, S., Yazici, H., Bermek, H., Sarikaya, M., Tamerler, C., Urgen, M. 2008, Physical elution in phage display selection of inorganic-binding peptides, *Materials Science & Engineering C-Biomimetic and Supramolecular Systems*, **29** (1), 14-19.

Dostalek, J., Vaisocherova, H., Homola, J., 2005. Multichannel surface plasmon resonance biosensor with wavelength division multiplexing, *Sensors and Actuators B-Chemical*, **108** (1-2), 758-764.

Dowling, D. P.; Donnelly, K.; McConnell, M. L.; Eloy, R.; Arnaud, M. N., 2001. Deposition of anti-bacterial silver coatings on polymeric substrates, *Thin Solid Films*, **602**, 398-399.

Dubois, L. H.; Nuzzo, R. G., 1993. Synthesis, Structure, and Properties of Model Organic-Surfaces, *Annual Reviews of Physical Chemistry*, **43**,437-463.

Dubois, L. H.; Zegarski, B. R.; Nuzzo, R. G., 1993. Molecular Ordering of Organosulfur Compounds on Au(111) and Au(100) - Adsorption From Solution and in Ultrahigh-Vacuum, *Journal of Chemical Physics.*, **98**, 678.

Evans, J. S., Samudrala, R., Walsh, T. R., Oren, E. E., Tamerler, C., 2008. Molecular design of inorganic-binding polypeptides, *MRS Bulletin*, **33** (5), 514-518.

Falini G, Albeck S, Weiner S, Addadi L., 1996. Control of aragonite or calcite polymorphism by mollusk shell macromolecules Source, *Science*, **271** (5245), 67-69.

Flynn, C.E., Mao, C., Hayhurst, A., Williams, J.L., Georgiou, G., Iverson, B., Belcher, **A.M.,** 2003, Synthesis and organization of nanoscale II-VI semiconductor materials using evolved peptide specificity and viral capsid assembly, *Journal of Materials Chemistry*, **13**, 2414-2421.

French, R. W., Milsom, E. V., Moskalenko, A. V., Gordeev, S. N., Marken, F., 2008. Assembly, conductivity, and chemical reactivity of sub-monolayer gold nanoparticle junction arrays, *Sensors and Actuators B-Chemical*, **129** (2), 947-952.

Goddard, J. M., Erickson, D., 2009. Bioconjugation techniques for microfluidic biosensors, *Analytical and Bioanalytical Chemistry*, **394 (2)**, 469-479.

Gokoglu, G., Bachmann,M, Çelik, T. and Janke, W., 2006. Structural properties of small semiconductor-binding synthetic peptides, *Physical Review E*, **74**, 41802.

Goobes, R., Goobes, G., Campbell, C.T., Stayton, P. S., 2006. Thermodynamics of statherin adsorption onto hydroxyapatite, *Biochemistry*, **45**, 5576-5586.

Goren, M., Galley, N., Lennox, R. B., 2006. Adsorption of alkylthiol-capped gold nanoparticles onto alkylthiol self-assembled monolayers: An SPR study, *Langmuir*, **22** (3), 1048-1054.

Grayy, J. J., 2004. The interaction of proteins with solid surfaces, *Current Opinion in Structural Biology*, **14** (1), 110-115

Gungormus, M., Fong, H., Kim, W., Evans, J. S., Tamerler, C., Sarikaya, M., 2008. Regulation of in vitro calcium phosphate mineralization by combinatorially selected hydroxyapatite-binding peptides, *Biomacromolecules*, **9** (3), 966-973.

Gupta, S., Uhlmann, P., Agrawal, M., Lesnyak, V., Gaponik, N., Simon, F., Stamm, M., Eychmuller, A., 2008. Covalent immobilization of quantum dots on macroscopic surfaces using poly(acrylic acid) brushes, *Journal of Materials Chemistry*, **18**, 214-220.

Hartgerink, J. D., Beniash, E., Stupp, S. I., 2001. Self-assembly and mineralization of peptide amphiphile nanofibers, *Science*, **294 (5547)**, 1684-1688.

Hayashi, T., Sano, K., Shiba, K., Kumashiro, Y., Iwahori, K., Yamashita, I., Hara, M., 2006. Mechanism underlying specificity of proteins targeting inorganic materials, *Nano Letters*, **6 (3)**, 515-519.

Haynes, C. L.; Van Duyne, R. P., 2001. Nanosphere lithography: A versatile nanofabrication tool for studies of size-dependent nanoparticle optics. *J*ournal of *Physical Chemistry.* B, **105**,5599-5611.

Hirsch, L. R.; Stafford, R. J.;Bankson, J. A.; Sershen, S. R.; Rivera, B.; Price, R. E.; Hazle, J.D.; Halas, N. J.; West, J. L., 2003. Nanoshell-mediated near-infrared thermal therapy of tumors under magnetic resonance guidance. *Proceedings of the National Academy of Sciences of the United States of America*, **100**, 13549-13554.

Hnilova, M., Oren, E. E., Seker, U. O. S, Wilson, B. R., Collino, S., Evans, J. S., Tamerler, C., Sarikaya, M., 2008. Effect of Molecular Conformations on the Adsorption Behavior of Gold-Binding Peptides, *Langmuir*, **24** (21), 12440-12445.

Homola, J.; Lu, H. B. B.; Nenninger, G. G.; Dostalek, J.; Yee, S. S, 2001. A novel multichannel surface plasmon resonance biosensor, *Sensors and Actuators B-Chemical*, **76**, 403-410.

Hostetler, M. J.; Templeton, A. C.; Murray, R. W., 1999. Dynamics of place-exchange reactions on monolayer-protected gold cluster molecules, *Langmuir*, **15**, 3782.

Jackson, A. M., Myerson, J. W., Stellacci, F., 2004. Spontaneous assembly of subnanometre-ordered domains in the ligand shell of monolayer-protected nanoparticles, *Nature Materials*, **3** (5), 330-336.

Jackson, J. B.; Halas, N. J., 2001. Silver nanoshells: Variations in morphologies and optical properties *Journal of Physical Chemistry* B, **105**, 2743-2746.

Jahangir, A. R., McClung, W. G., Cornelius, R. M, McCloskey, C. B., Brash, J. L., Santerre, J. P., 2002. Fluorinated surface-modifying macromolecules: modulating adhesive protein and platelet interactions on a polyether-urethane, *Journal of Biomedical Materials Research*, **60**, 135-147.

Jennings, G. K., Laibinis, P. E., 1996. Self-assembled monolayers of alkanethiols on copper provide corrosion resistance in aqueous environments, *Colloids and Surfaces A-Physicochemical and Engineering Aspects*, **116** (1-2), 105-114.

Jensen, T. R.; Malinsky, M. D.; Haynes, C. L.; Van Duyne, R. P., 2000. Nanosphere lithography: Tunable localized surface plasmon resonance spectra of silver nanoparticles *Journal of Physical Chemistry* B, **104**, 10549-10556.

Jensen, T. R.; Schatz, G. C.;Van Duyne, R. P., 1999. Nanosphere lithography: Surface plasmon resonance spectrum of a periodic array of silver nanoparticles by ultraviolet-visible extinction spectroscopy and electrodynamic modeling, *Journal of Physical Chemistry* B, **103**, 2394-2401.

Jung, L. S. and Campbell, C. T., 2000. Sticking Probabilities in Adsorption of Alkanethiols from Liquid Ethanol Solution onto Gold, *Journal of Physical Chemistry. B,* **104**, 11168-11178

Jung, L. S. and Campbell, C. T., 2000. Sticking Probabilities in Adsorption from Liquid Solutions: Alkylthiols on Gold, Physical Review Letters, **84** (22), 5164-5167.

Kacar, T., Ray, J., Gungormus, M., Oren, E. E., Tamerler, C, Sarikaya, M, 2009. Quartz Binding Peptides as Molecular Linkers towards Fabricating Multifunctional Micropatterned Substrates, *Advanced Materials*, **21** (3), 295-299.

Kacar, T., Zin, M. T., So, C., Wilson, B., Ma, H., Gul-Karaguler, N., Jen, A. K. Y., Sarikaya, M., Tamerler, C., 2009. Directed Self-Immobilization of Alkaline Phosphatase on Micro-patterned Substrates via Genetically-Fused Metal-Binding Peptide, *Biotechnology and Bioengineering*, **103,** 696-705.

Kambhampati, D. K., Jakob, T. A. M., Robertson, J. W., Cai, M., Pemberton, J. E., Knoll, W., 2001. Novel silicon dioxide sol-gel films for potential sensor applications: A surface plasmon resonance study, *Langmuir*, **17** (4), 1169-1175.

Kantarci, N., Tamerler, C., Sarikaya, M., Haliloglu, T., Doruker, P., 2005. Molecular dynamics simulations on constraint metal binding peptides, *Polymer*, **46** (12), 4307-4313.

Karpovich, D. S. and Blanchard, G. J., 1994. Direct Measurement of the Adsorption Kinetics of Alkanethiolate Self-Assembled Monolayers on a Microcrystalline Gold Surface, *Langmuir*, **10** (9), 3315-3322.

Kausaite, A., Dijk, M., Castrop, J., Ramanaviciene, A., Baltrus, J. P., Acaite, J. and Ramanavicius, A., 2007. Surface Plasmon Resonance Label-free Monitoring of Antibody Antigen Interactions in Real Time, *Biochemistry and Molecular Biology Education*, **35** (1), 57–63.

Kawaguchi, T., Shankaran, D. R., Kim, S.J, Gobi, K. V. , Matsumoto, K., Toko, K., Miura, N., 2007. Fabrication of a novel immunosensor using functionalized self-assembled monolayer for trace level detection of TNT by surface plasmon resonance, *Talanta*, **72** (2), 554-560.

Khan, F., He, M. Y, Taussig, M. J., 2006. Double-Hexahistidine Tag with High-Affinity Binding For Protein Immobilization, Purification, and Detection on Ni-Nitrilotriacetic Acid Surfaces, *Analytical Chemistry*, **78** (9)**,** 3072-3079.

Kilian, K. A., Boecking, T., Gooding, J. J., 2009. The importance of surface chemistry in mesoporous materials: lessons from porous silicon biosensors, *Chemical Communications*, **6**, 630-640.

Kingshott, P., Griesser, H. J., 1999. Surfaces that resist Bioadhesion, *Current Opinion in Solid State & Materials Science***, 4**, 403-412.

Knowles, T. P. J., Shu, W., Devlin, G. L., Meehan, S., Auer, S., Dobson, C. M., 2007. Kinetics and thermodynamics of amyloid formation from direct measurements of fluctuations in fibril mass, *Proceedings of the National Academy of Sciences of The United States of America*, **24**, 10016-10021.

Krane, S. M., 2008. The importance of proline residues in the structure, stability and susceptibility to proteolytic degradation of collagens, *Amino Acids*, **35** (4), 703-710.

Krauland, E. M., Peelle, B. R., Wittrup, D. K., Belcher, A. M., 2007. Peptide Tags for Enhanced Cellular and Protein Adhesion to Single-Crystalline Sapphire, *Biotechnology and Bioengineering*, **97** (5), 1009-1020.

Kroger, N., Deutzmann, R., Sumper, M., 1999. Polycationic peptides from diatom biosilica that direct silica nanosphere formation, *Science*, **286,** 1129-1132.

Kuhlman, B., Dantas, G., Ireton, G. C., Varani, G., Stoddard, B. L., Baker, D., 2003. Design of a novel globular protein fold with atomic-level accuracy, *Science*, **302** (5649), 1364-1368.

Kulp J. L., Shiba, K. and Evans, J. S., 2005. Probing the Conformational Features of a Phage Display Polypeptide Sequence Directed against Single-Walled Carbon Nanohorn Surfaces, *Langmuir*, **21** (25)**,** 11907 -11914.

Kulp, J. L, Sarikaya M. and Evans, J. S., 2004. Molecular characterization of a prokaryotic polypeptide sequence that catalyzes Au crystal formation, *Journal of Materials Chemistry*, **14**, 2325–2332.

Laibinis, P. E.; Whitesides, G. M.; Allara, D. L.; Tao, Y. T.;Parikh, A. N.; Nuzzo, R. G., 1991. Comparison of The Structures and Wetting Properties of Self-Assembled Monolayers of Normal-Alkanethiols on The Coinage Metal-Surfaces, Cu, Ag, Au *Journal of American Chemical Society*, **113**, 7152.

Larson, J. L., Ko, E, Miranker, A.D., 2000. Direct measurement of aβ amyloid polypeptide fibrillogenesis by mass spectrometry, *Protein Science*, **9**, 427–431.

Lee, S. M., Cho, S. N., Cheon, 2003. Anisotropic shape control of colloidal inorganic nanocrystals, *Advanced Materials*, **15**, 441-444.

Lee, S. M., Jun, Y. W., Cho, S. N., Cheon, J., 2002. Single-crystalline star-shaped nanocrystals and their evolution: Programming the geometry of nano-building blocks, *Journal of the American Chemical Society*, **124** (38)**,** 11244-11245.

Lee, S., Puck, A., Graupe, M., Colorado, R., Shon, Y. S., Lee, T. R., Perry, S. S., 2001. Structure, wettability, and frictional properties of phenyl-terminated self-assembled monolayers on gold, *Langmuir*, **17** (23), 7364-7370.

Lee, V. A., Craig, R. G., Filisko, F. E., Zand, R., 2005**.** Microcalorimetry of the adsorption of lysozyme onto polymeric substrates, *Journal of Colloid and Interface Science*, **288** (1), 6-13.

Li, S.; Toprak, M. S; Jo, Y. S; Dobson, J.; Kim, D. K; Muhammed, M., 2007. Bulk synthesis of transparent and homogeneous polymeric hybrid materials with ZnO_2 quantum dots and PMMA, *Advanced Materials*, **19** (24), 4347.

Li, Z.; Chang, S.-C.; Williams, R. S., 2003. Self-assembly of alkanethiol molecules onto platinum and platinum oxide surfaces, *Langmuir*, **19**, 6744-6749.

Lin, F. Y., Chen, W. Y., Hearn, M. T. W., 2001. Microcalorimetric studies on the interaction mechanism between proteins and hydrophobic solid surfaces in hydrophobic interaction chromatography: Effects of salts, hydrophobicity of the sorbent, and structure of the protein, *Analytical Chemistry*, **73** (16), 3875-3883.

Long, J. R., J. L. Dindot, H. Zebroski, S. Kiihne, R. H. Clark, A. A. Campbell, P. S. Stayton, and G. P. Drobny. 1998. A peptide that inhibits hydroxyapatite growth is in an extended conformation on the crystal surface. *Proceedings of the National Academy Of Sciences Of The United States Of America*, **95** (21)**,** 12083-12087.

Love, J. C., Estroff, L. A., Kriebel, J. K., Nuzzo, R. G., Whitesides, G. M., 2005. Self-assembled monolayers of thiolates on metals as a form of nanotechnology, **105** (4), 1103-1169

Love, J. C.; Wolfe, D. B.; Haasch, R.; Chabinyc, M. L.; Paul, K.E.; Whitesides, G. M.; Nuzzo, R. G., 2003. Formation and Structure of Self-Assembled Monolayers of Alkanethiolates on Palladium, *Journal of the American Chemical Society*, **125**, 2597.

Lowenstam, H. A., 1981. Minerals Formed by Organisms, *Science*, **211** (4487), 1126-1131.

Lukosz, W., 1991. Principles and Sensitivities of Integrated Optical And Surface-Plasmon Sensors For Direct Affinity Sensing and Immunosensing, *Biosensors & Bioelectronics*, **6** (3), 215-225.

Malinsky,M. D.; Kelly, K. L.; Schatz, G. C.; Van Duyne, R. P., 2001. Nanosphere lithography: Effect of substrate on the localized surface plasmon resonance spectrum of silver nanoparticles, *Journal of Physical Chemistry* B**, 105**, 2343-2350.

Manna, L.; Scher, E. C.; Alivisatos,A. P., 2000, Synthesis of soluble and processable rod-, arrow-, teardrop-, and tetrapod-shaped CdSe nanocrystals , *Journal of the American Chemical Society*, **122**, 12700-12706.

Mao; C., Flynn; C. E., Hayhurst;A., Sweeney, R., Qi;J., Georgiou; G., Iverson; B., Belcher, A. M., 2003. Viral Assembly of Oriented Quantum Dot Nanowires, *Proceedings of the National Academy of Sciences of the United States of America*, **100** (12), 6946-6951.

Marubayashi, K.; Takizawa, S.; Kawakusu, T.; Arai, T.; Sasai,H., 2003. Monolayer-protected Au cluster (MPC)-supported Ti-BINO Late complex, *Organic Letters*, **5**, 4409-4412.

Marx, K. A., 2003. Quartz crystal microbalance: A useful tool for studying thin polymer films and complex biomolecular systems at the solution-surface interface, *Biomacromolecules*, **4**, 1099-1120.

Matouschek, A., Kellis, J.T., Serrano L., Fersht A. R., 1989. A Mapping the Transition-State and Pathway of Protein Folding by Protein Engineering. *Nature*, **340**, 122-126.

Miyamoto, H., Miyashita, T., Okushima, M., Nakano, S., Morita, T., Matsushiro, A., 1996. A carbonic anhydrase from the nacreous layer in oyster pearls, *Proceedings of the National Academy of Sciences of The United States of America*, **93**, 9657-9660.

Moore, J. C. and Arnold, F. H.,1996. Directed evolution of a para-nitrobenzyl esterase for aqueous-organic solvents, *Nature Biotechnology*, **14** (4), 458-467.

Mrksich, M., 1997. Using self-assembled monolayers to understand the biomaterials interface, *Current Opinion in Colloid & Interface Science*, **2**, 83-88.

Mrksich, M.; Sigal, G. B.; Whitesides, G. M., 1995. Surface-Plasmon Resonance Permits In-Situ Measurement of Protein Adsorption on Self-Assembled Monolayers of Alkanethiolates on Gold, *Langmuir*, **11**, 4383-4385.

Murayama, H.; Narushima, T.; Negishi, Y.; Tsukuda, T., 2004. Structures and stabilities of alkanethiolate monolayers on palladium clusters as studied by gel permeation chromatography, *Journal of Physics Chemistry* B, **108**, 3496.

Muskal, N.; Turyan, I.; Mandler, D., 1996. Self-assembled monolayers on mercury surfaces, *Journal of Electroanalytical. Chemistry*, **409**, 131.

Naik, R. R., Brott, L. L., Clarson, S. J., Stone, M. O., 2002. Silica-precipitating peptides isolated from a combinatorial phage display peptide library. *Journal of Nanoscience and Nanotechnology*, **2** (1), 95-100

Naik, R. R., Jones, S. E., Murray, C. J., McAuliffe, J. C., Vaia, R. A., Stone, M. O., 2004. Peptide templates for nanoparticle synthesis derived from polymerase chain reaction-driven phage display, *Advanced Functional Materials*, **14** (1), 25-30.

Naik, R. R., Stringer, S. J., Agarwal, G., Jones, S. E., Stone, M. O., 2002. Biomimetic synthesis and patterning of silver nanoparticles, *Nature Materials*, **1**, 169-172.

Needleman, S. B., Wunsch, C. D., 1970. A General Method Applicable to Search for Similarities in Amino Acid Sequence of Proteins, *Journal of Molecular Biology*, **48** (3), 443.

Ng, L. Y., 2004. Surface plasmon resonance sensing on new materials, *MSc Thesis*, University of Washington, Seattle, WA.

Nizamoglu, S., Ozel, T., Sari, E., Demir, H. V., 2007. White light generation using CdSe/ZnS core-shell nanocrystals hybridized with InGaN/GaN light emitting diodes, *Nanotechnology*, **18**, 065709.

Nomura, M., 1973. Assembly of Bacterial Ribosomes, *Science*, **179**, 864-873.

Nuzzo, R. G.; Allara, D. L., 1983. Adsorption of Bifunctional Organic Disulfides on Gold Surfaces, *Journal of America Chemical Society*, **105**, 4481-4483.

Nygaard, S., Wendelbo, R., Brown, S., 2002, Surface-specific zeolite-binding proteins *Advanced Materials*, **14**, 1853-1856.

O'Nuallain, B., Shivaprasad, S, Kheterpal, I., Wetzel, R., 2005. Thermodynamics of A beta(1-40) amyloid fibril elongation, *Biochemistry*, **44** (38), 2709-12718.

Oren, E. E., Tamerler, C., Sahin, D., Hnilova, M., Seker, U. O. S., Sarikaya, M., Samudrala, R, 2007. A novel knowledge-based approach to design inorganic-binding peptides, *Bioinformatics*, **23** (21), 2816-2822.

Oren, E. E., Tamerler, C., Sarikaya, M., 2005. Metal recognition of septapeptides via polypod molecular architecture, *Nano Letters*, **5** (3), 415-419.

Park, T. J.; Lee, S. Y.; Lee, S. J.; Park, J. P.; Yang, K. S.; Lee, K. B.; Ko, S.; Park, J. B.; Kim, T.; Kim, S. K.; Shin, Y. B.; Chung, B. H.; Ku, S. J.; Kim, D. H.; Choi, I. S., 2006. Protein nanopatterns and biosensors using gold binding polypeptide as a fusion partner, *Analytical Chemistry*, **78**, 7197-7205.

Pender, M. J., Sowards, L. A., Hartgerink, J. D., Stone, M. O. and Naik, R. R., 2006. Peptide-Mediated Formation of Single-Wall Carbon Nanotube Composites, Nano Letters, 6 (1), **103**, 40-44.

Peng, X. G.; Manna, L.; Yang, W. D.; Wickham, J.; Scher, E.;Kadavanich, A.; Alivisatos, A. P., 2000. Shape control of CdSe nanocrystals, *Nature*, **404** (6773), 59-61.

Pfleging, W., Kohler, R., Schierjott, P., Hoffmann, W., 2009. Laser patterning and packaging of CCD-CE-Chips made of PMMA, *Sensors and Actuators B-Chemical*, **138** (1), 336-343.

Poirier, M. A., Li, H., Macosko, J., Cai, S., Amzel, M., Ross, C. A., 2002. Huntingtin Spheroids and Protofibrils as Precursors in Polyglutamine Fibrilization, *Journal of Biological Chemistry*, **277**, 41032–41037.

Porter, M. D.; Bright, T. B.; Allara, D. L.; Chidsey, C. E. D., 1987. Spontaneously organized molecular assemblies .4. Structural characterization of normal-alkyl thiol monolayers on gold by optical ellipsometry, infrared-spectroscopy, and electrochemistry, *Journal of American Chemical Society*, **109**, 3559-3568.

Poulsen, N., Sumper, M., Kröger, N, 2003. Biosilica Formation in Diatoms: Characterization of Native Silaffin-2 and Its Role in Silica Morphogenesis. *Proceedings of the National Academy of Sciences of the United States of America*, **100** (21), 12075-12080

Rajagopalan, R., Misialck, S., Stevens, S. K,, Myszka, D. G., Brandhuber, B. J., Ballard, J. A., Andrews, S. W., Seiwert, S. D., Kossen, K., 2009. Inhibition and Binding Kinetics of the Hepatitis C Virus NS3 Protease Inhibitor ITMN-191 Reveals Tight Binding and Slow Dissociative Behavior, *Biochemistry*, **48** (11), 2559-2568.

Ratner, B. D., Bryant S. J., 2004. Biomaterials: Where we have been and where we are going, *Annual Review of Biomedical Engineering*, **6**, 41-75.

Reynolds, N. P., Tucker, J. D., Davison, P. A., Timney, J. A., Hunter, C. N., Leggett, G. J., 2009. Site-Specific Immobilization and Micrometer and Nanometer Scale Photopatterning of Yellow Fluorescent Protein on Glass Surfaces, *Journal of The American Chemical Society*, **131** (3), 896-900.

Richardson, J. S., **Richardson**, **D. C**, 1989. The De novo Design of Protein Structures, *Trends in Biochemical Sciences*, **14**, 304-309.

Riepl, M., Enander, K., Liedberg, B., Schaeferling, M.;Kruschina, M., Ortigao, **F.**, 2002, Functionalized surfaces of mixed alkanethiols on gold as a platform for oligonucleotide microarrays, *Langmuir*, **18**, 7016-7023.

Roy D., Fendler, J., 2004. Reflection and absorption techniques for optical characterization of chemically assembled nanomaterials, *Advanced Materials*, **16 (6)**, 479-508.

Sainsbury. T., Ikuno, T., Okawa, D., Pacile, D., Frechet, J. M. J., Zettl, A.,2007. Self-assembly of gold nanoparticles at the surface of amine- and thiol-functionalized boron nitride nanotubes, *Journal of Physical Chemistry C*, **111** (35), 12992-12999.

Sakiyama, T., Ueno, S., Imamura, K., Nakanishi, K., 2004. Use of a novel affinity tag selected with a bacterial random peptide library for improving activity retention of glutathione S-transferase adsorbed on a polystyrene surface, *Journal of Molecular Catalysis B-Enzymatic*, **28 (4-6)**, 207-214.

Salem, A. K.; Chao, J.; Leong, K. W.; Searson, P. C., 2004. Receptor-mediated self-assembly of multi-component magnetic nanowires, *Advanced Materials*, **16**, 268.

Samant, M. G., Brown, C. A., Gordon, J. G., 1991. Structure of an Ordered Self-Assembled Monolayer of Docosyl Mercaptan on Gold (111) By Surface X-Ray-Diffraction, *Langmuir*, **7** (3), 437-439.

Sambles, J. R., Bradbery, G. W., Yang, F. Z., 1991. Optical-Excitation of Surface-Plasmons - an Introduction, *Contemporary Physics*, **32**, 173.

Sano, K. I., Ajima, K., Iwahori, K., Yudasaka, M., Iijima, S., Yamashita, I. and Shiba, K., 2005. Endowing a Ferritin-Like Cage Protein with High Affinity and Selectivity for Certain Inorganic Materials, *Small*, **1** (8-9), 826 –832.

Sano, K. I., Sasaki, H. and Shiba, K., 2006. Utilization of the Pleiotropy of a Peptidic Aptamer To Fabricate Heterogeneous Nanodot-Containing Multilayer Nanostructures, *Journal of the American Chemical Society*, **128**, 1717-1722.

Sano, K. I., Yoshii, S., Yamashita, I. and Shiba, K., 2007. In Aqua Structuralization of a Three-Dimensional Configuration Using Biomolecules, *Nano Letters*, **7** (10), 3200 -3202.

Sano, K. I.; Sasaki, H.; Shiba, K., 2005. Specificity and biomineralization activities of Ti-binding peptide-1 (TBP-1), *Langmuir*, **21**, 3090-3095.

Sano, K.I. and Shiba, K., 2003, A Hexapeptide Motif that Electrostatically Binds to the Surface of Titanium, *Journal of the Chemical Society*, **125**, 14234-14235

Sarikaya M and Aksay I., 1993. *Biomimetics: Design and Processing of Materials*, AIP Series in Polymers and Complex Materials, American Institute of Physics.

Sarikaya, M., 1999. Biomimetics: Materials fabrication through biology, *Proceedings of the National Academy of Sciences of the United States Of America*, **96 (75)**, 14183-14185.

Sarikaya, M., Tamerler, C., Jen, A. K. Y., Schulten, K. , Baneyx, F., 2003. Molecular biomimetics: nanotechnology through biology, *Nature Materials*, **2** (9), 577-585.

Sarikaya, M., Tamerler, C., Schwartz, D. T., Baneyx, F. O., 2004. Materials assembly and formation using engineered polypeptides, *Annual Review of Materials Research*, **34**, 373-408.

Scherzinger, E., Lurz, R., Turmaine, M., Mangiarini, L., Hollenbach, B., Hasenbank, R., Bates, G. P., Davies, S. W., Lehrach, W., Wanker, E. E., 1997. Huntingtin-Encoded Polyglutamine Expansions Form Amyloid-like Protein Aggregates *in vitro* and *in vivo*, *Cell*, **90**, 549–558.

Schessler, H. M., Karpovich, D. S. and Blanchard, G. J. 1996. Quantitating the Balance between Enthalpic and Entropic Forces in Alkanethiol/Gold Monolayer Self Assembly, *Journal of the American Chemical Society*, **118** (40), 9645-9651.

Schmidinger, H., Susani-Etzerodt, H., Birner-Gruenberger, R., Hermetter, A., 2006 Inhibitor and Protein Microarrays for Activity-Based Recognition of Lipolytic Enzymes, *Chembiochem***, 7** (3)**,** 527-534.

Schmidt, T. G. M, Koepke, J., Frank, R., Skerra, A., 1996. Molecular Interaction Between the Strep-Tag Affinity Peptide and Its Cognate Target, Streptavidin, *Journal Of Molecular Biology*, **255,** 753.

Schrevandijk, P., Ghiringhelli, L. M., DelleSite, L., van der Vegt, N. F. A., 2007. Interaction of Hydrated Amino Acids with Metal Surfaces: A Multiscale Modeling Description, *Journal of Physical Chemistry C*, **111**, 2631.

Schuck, P., 1996. Kinetics of ligand binding to receptor immobilized in a polymer matrix, as detected with an evanescent wave biosensor .1. A computer simulation of the influence of mass transport, *Biophysical Journal*, **70** (3), 1230-1249.

Schwartz, D., Baneyx, F., 2007. Selection and analysis of solid-binding peptides, Current Opinion in Biotechnology, **18** (4), 312–317.

Seker, U. O. S, Wilson, B., Dincer, S., Kim, I. W., Oren, E. E., Evans, J. S., Tamerler, C., Sarikaya, M., 2007. Adsorption behavior of linear and cyclic genetically engineered platinum binding peptides, *Langmuir*, **23** (15), 7895-7900.

Seker, U. O. S., Wilson, B. R., SahinTamerler, C., Sarikaya, M., 2009. Quantitative Affinity of Genetically Engineered Inorganic Binding Peptides, *Biomacromolecules*, **10** (2), 250-257.

Shen, M., Martinson, L., Wagner, M. S., Castner, D. G., Ratner, B. D., Horbett, T. A., 2002. PEO-like plasma polymerized tetraglyme surface interactions with leukocytes and proteins: in vitro and in vivo studies, *Journal of Biomaterials Science:Polymer Edition*, **13**, 367-390.

Shiba, K.; Minamisawa. T., 2007. A synthesis approach to understanding repeated peptides conserved in mineralization proteins, *Biomacromolecules*, **8**, 2659-2664.

Shon, Y. S.; Mazzitelli, C.; Murray, R. W., 2001. Unsymmetrical disulfides and thiol mixtures produce different mixed monolayer-protected gold clusters, *Langmuir*, **17**,7735-7741.

Slocik, J. M., Stone, M. O., Naik, R. R., 2005. Synthesis of gold nanoparticles using multifunctional peptides, *Small*, **1** (11), 1048-1052.

Smith, G. P., 1985. Filamentous Fusion Phage - Novel Expression Vectors That Display Cloned Antigens On The Virion Surface, *Science*, **228**, 1315-1317

Smith, T. F., Waterman, M. S., 1981. Identification of common molecular subsequences, *Journal of the Molecular Biology*, **147,** 195–197.

Soh, N., Tokuda, T., Watanabe, T., Mishima, K., Imato, T., Masadome, T., Asano, Y., Okutani, S., Niwa, O., Brown, S. 2003. A surface plasmon resonance immunosensor for detecting a dioxin precursor using a gold binding polypeptide, *Talanta*, **60** (4), 733-745.

Solanki, P. R., Arya, S. K., Nishimura, Y., Iwamoto, M., Malhotra, B. D., 2007. Cholesterol biosensor based on amino-undecanethiol self-assembled monolayer using surface plasmon resonance technique, *Langmuir*, **23** (13), 7398-7403.

Stenlund, P., Frostell-Karlsson, A., Karlsson, O. P., 2006. Studies Of Small Molecule Interactions With Protein Phosphatases Using Biosensor Technology**,** *Analytical Biochemistry***, 353** (2)**,** 217-225**.**

Subramanian, A.R., 1985. The Ribosome and Its Evolutionary Diversity and the Functional-Role of One of Its Components, *Essays in Biochemistry*, **21**, 45-85.

Tamerler, C., Duman, M., Oren, E. E., Gungormus, M., Xiong, X., Kacar, T., Parviz, B. A. and Sarikaya, M., 2006a. Materials Specificity and Directed Assembly of a Gold-Binding Peptide, *Small*, **2** (11), 1372 – 1378**.**

Tamerler, C., Oren, E. E., Duman, M., Venkatasubramanian, E., Sarikaya, M, 2006b. Adsorption kinetics of an engineered gold binding peptide by surface plasmon resonance spectroscopy and a quartz crystal microbalance, *Langmuir*, **22**, 7712-7718.

Tamerler, C., Sarikaya, M., 2007. Molecular biomimetics: Utilizing nature's molecular ways in practical engineering, *Acta Biomateriala*, **3** (3), 289-299.

Templeton, A. C.; Wuelfing, W. P.; Murray, R. W., 2000. Monolayer protected cluster molecules. *Accounts in Chemical. Research*, **33**, 27-36.

Texter, J., Tirrell, M., 2001. Chemical processing by self-assembly, *AIChE Journal*, **47**, 1706-1710.

Thai, C. K., Dai, H., Sastry, M. S. R., Sarikaya, M., Schwartz, D. T., Baneyx, F., 2004. Identification and Characterization of Cu2O- and ZnO-Binding Polypeptides by Escherichia coli Cell Surface Display: Toward an Understanding of Metal Oxide Binding, **87** (2), 129-137

Thornton, J. M., Gardner S. P., 1989. Protein Motifs And Data-Base Searching, *Trends in Biochemical Sciences*, **14** (7), 300-304.

Tomasio, S. M., and Walsh, T. R., 2007. Atomistic Modeling of The Interaction Between Peptides and Carbon Nanotubes, Molecular Physics, **105**, (2–3), 221–229.

Umetsu, M., Mizuta, M., Tsumoto, K., Ohara, S.; Takami, S., Watanabe, H., Kumagai, I., Adschiri, T., 2005. Bioassisted room-temperature immobilization and mineralization of zinc oxide-The structural ordering of ZnO nanoparticles into flower-type morphology, *Advanced Materials*, **17**, 2571-2575.

Url-1. <*http://www.q-sense.com/*>, accessed on 26.09.2009.

Voet, D., Voet, J. G., 1995. *Biochemistry*, John Wiley & Sons, New York. NY, USA.

Walczak, M. M.; Chung, C.; Stole, S. M.; Widrig, C. A.; Porter,M. D., 1991. Structure and Interfacial Properties of Spontaneously Adsorbed Normal-Alkanethiolate Monolayers On Evaporated Silver Surfaces, *Journal of the American Chemical Society*, **113**, 2370-2378.

Walters, D. A., Smith, B. L., Belcher, A. M., Paloczi, G. T., Stucky, G. T., Morse, D. E., Hansma, P. K., 1997. Modification of Calcite Crystal Growth by Abalone Shell Proteins: An Atomic Force Microscope Study, *Biophysical Journal*, **72**, 1425-1433.

Wang, S., Humphreys, E.S., Chung, S.Y., Delduco, D.F., Lustig, S.R., Wang, H., Parker, K.N., Rizzo, N.W., Subramoney, S., Chiang, Y.M., Jagota, A., 2003, Peptides with selective affinity for carbon nanotubes, *Nature Materials*, **2**, 196-200.

Westcott, S. L.; Oldenburg, S. J.; Lee, T. R.; Halas, N. J., 1998. Formation and adsorption of clusters of gold nanoparticles onto functionalized silica nanoparticle surfaces, *Langmuir*, **14**, 5396-5401.

Whaley, S. R.; English, D. S.; Hu, E. L.; Barbara, P. F.; Belcher, A. M., 2000. Selection of peptides with semiconductor binding specificity for directed nanocrystal assembly, *Nature*, **405**, 665-668.

Whitesides, G. M. and Grzybowski, B., 2002. Self-Assembly a t All Scales, *Science*, **295** (5564), 2418-2421

Whitesides, G. M., Mathias, J.P., Seto, C. T., 1991. Molecular Self-Assembly and Nanochemistry-A Chemical Strategy for the Synthesis of Nanostructures, *Science*, **254** (5036), 1312-1319

Wittrup, K. D., 2001. Protein engineering by cell-surface display, *Current Opinion in Biotechnology*, **12**, 395-399.

Wrighton, M. S., 1986. Surface Functionalization of Electrodes With Molecular Reagents, *Science*, **231** (4733), 32-37.

Xiong, J.-P.; Stehle, T.; Diefenbach, B.; Zhang, R.;Dunker, R.; Scott, D. L.; Joachimiak, A.; Goodman, S. L.;Arnaout, M. A. 2001. Crystal structure of the extracellular segment of integrin alpha V beta 3, *Science*, **294**, 339-345.

Xiong, J.-P.; Stehle, T.; Zhang, R.; Joachimiak, A.; Frech, M.;Goodman, S. L.; Arnaout, M. A., 2002. Crystal structure of the extracellular segment of integrin alpha V beta 3 in complex with an Arg-Gly-Asp ligand, *Science*, **296**, 151-155.

Zin, M. T., Ma, H., Munro, A. M., Ginger, D. S., Gungormus, M., Leong, K., Tamerler, C., Sarikaya M. and Jen, A. K.-Y., 2006. Well-Controlled Arrays of Core-Shell Quantum Dots with Tunable Photoluminescence Properties, *Poly. Mater. Sci. Eng.*, **95,** 1002-1003.

Zin, M. T., Ma, H., Sarikaya, M. and Jen, A. K.-Y., 2005. Assembly of Gold Nanoparticles using Genetically Engineered Poypeptides, *Small*, **1** (7), 698-702.

APPENDICES

APPENDIX A. Characterization of Surface Plasmon Resonance chip surfaces

APPENDIX B. Calibration of surface plasmon resonance signal

APPENDIX C. Kinetic constants for the adsorption of GEPIs on solid surfaces

APPENDIX A

The substrates were synthesized using a GATAN PECS sputtering system. BK-7 glass was cleaned and dried. The substrates were then coated with the film thicknesses outlined in section 4.2.1.2. There was a certain amount of difficulty involved in characterizing the platinum surface, as the layer directly underneath it was gold, a very similar material. A wide range of methods were used to determine if the platinum layer was continuous and intact. These included optical microscopy, SEM, AFM, TEM, and circular voltametry. All of these methods seemed to indicate a continuous film of platinum on the gold surface. Perhaps the most convincing evidence that the film is continuous comes from TEM, where a free-standing 2 nm platinum film coated by the PECS system was imaged (see Figure A1). Free standing films were made using a technique developed by Allred et al TEM images showed nanoscale crystals without major gaps in the film.

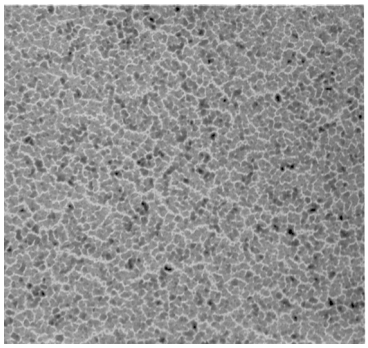

Figure A1. Free-standing 2nm thick platinum film, imaged using TEM. The film shown was produced on the same system used to create platinum coated SPR chips. Micrograph shows the platinum film to be continuous.

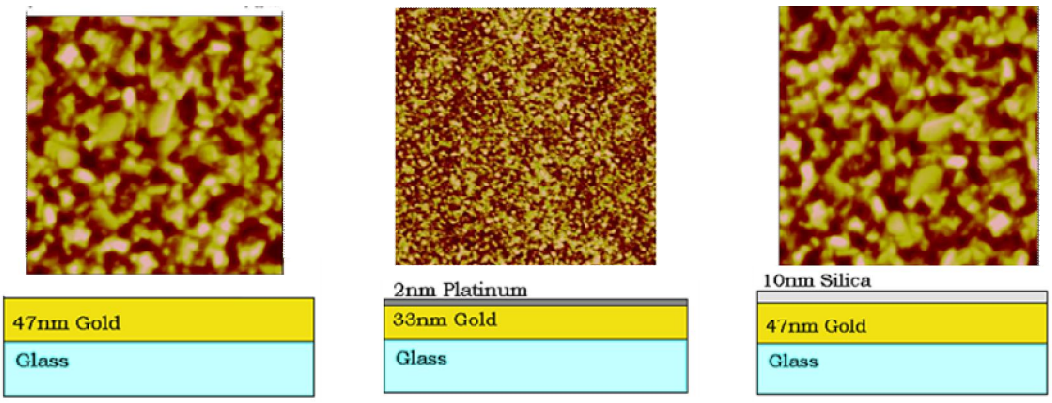

Figure A2. Shows AFM images of the three surfaces used for SPR analysis and the corresponding structure

APPENDIX B

In order to determine the adsorbed mass, the surface plasmon resonance signal of our SPR system was calibrated. The calibration of these system was carried out, for the gold, platinum and silica surfaces. Calibration coefficients for gold, silica and platinum surfaces were calculated. The change of the shift in SPR shift was probed. The refractive index on the surface was changed, by changing the concetration of the ethanol concetration. Ethanol was delivered at the volumetric ratios (5%, 20% , 30 and 40%) on to the SPR sensor chip coated with either gold platinum or silica.

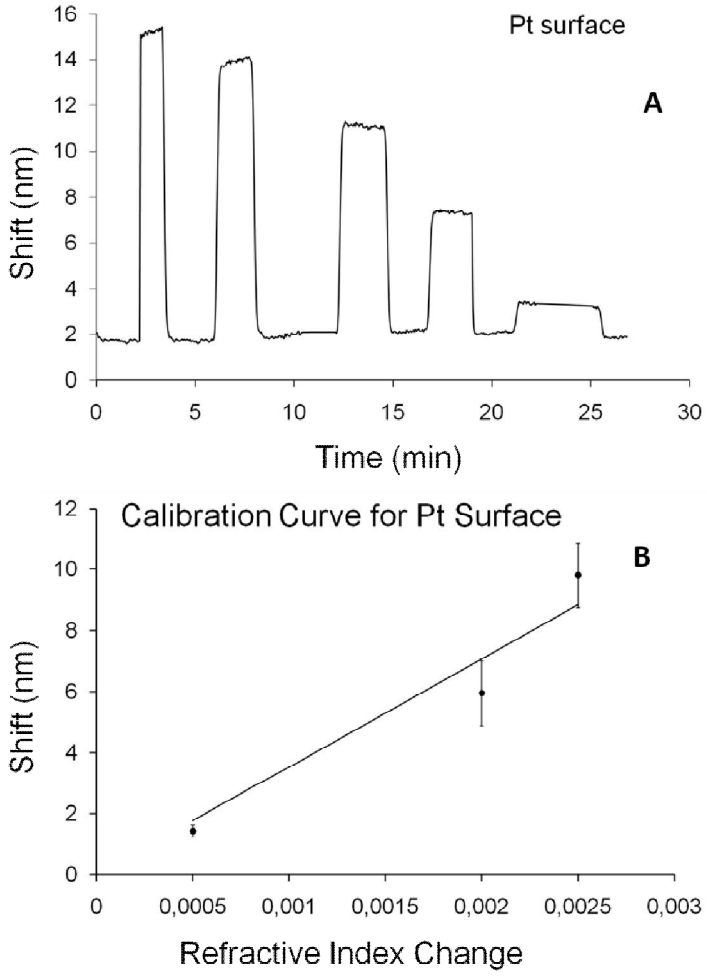

Figure B1. The calibration signal change upon the change in the refractive index on the gold surface, the response of the system was recorded for platinum surface.

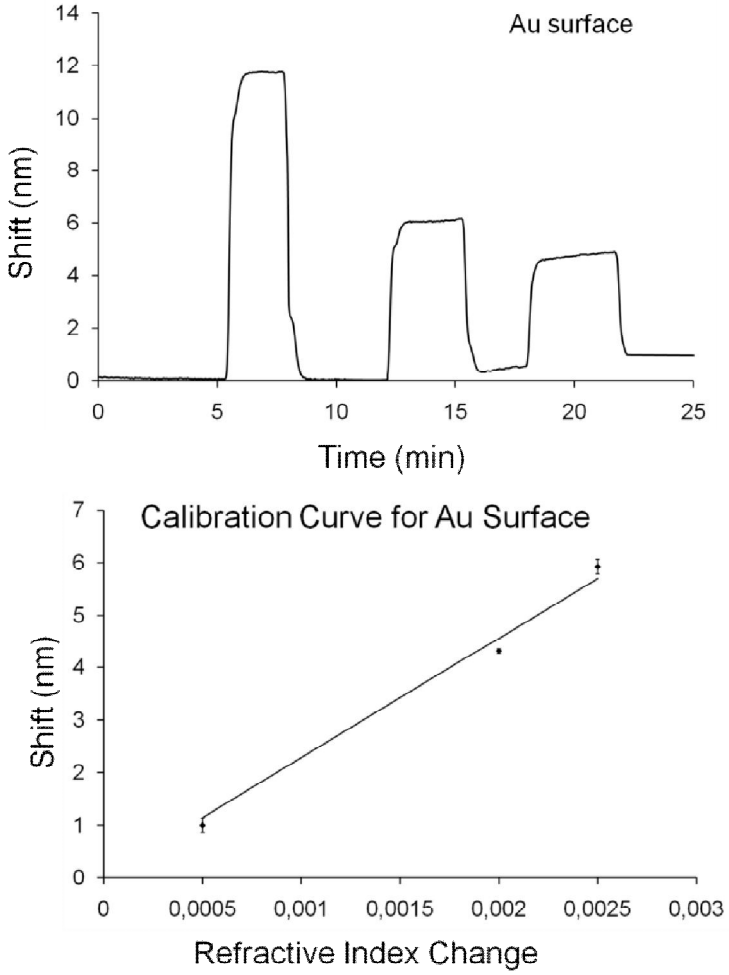

Figure B2. The calibration signal change upon the change in the refractive index on the gold surface, the response of the system was recorded for platinum surface.

The calibration curve and the SPR signal shift for Pt was given in Figure B1. The calibration curve for gold surface is given in Figure B2. As mentioned earlier in section 4.1.1.2 we carry out the calculation of the adsorbed mass onto the surface of interest using the following approximation.

$$d = (l_d / 2)[R/(m(\eta_a - \eta_s)] \quad \textbf{(A.1)}$$

Where d is the thickness of the adlayer, l_d is the penetration depth of the light in to the substrate, m is the calibration coefficient of the SPR instrument, R is the measured response (in our case change in the dip position shift), η_a and η_b is the refractive index of the adsorbate and buffer.

η_a is the refractive index of the peptide 1.334 and η_b is the refractive index of the buffer, 1.52. l_d is the penetration depth of the light in to the substrate, m is the calibration coefficient of the SPR instrument are given for corresponding surfaces.

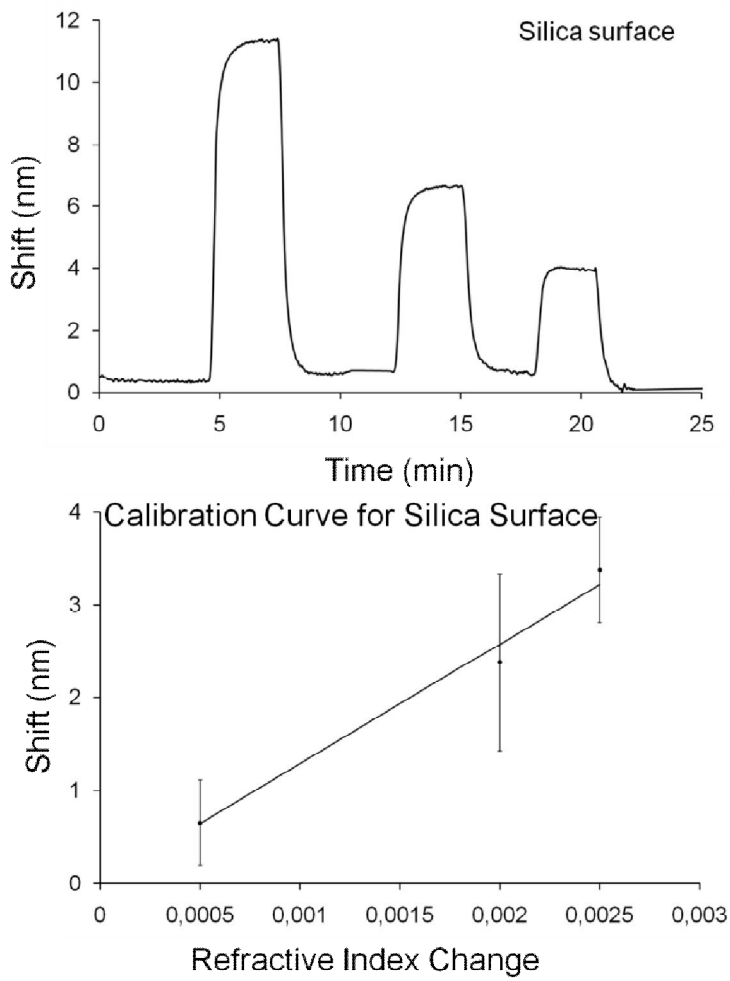

Figure B3. The calibration signal change upon the change in the refractive index on the gold surface, the response of the system was recorded for silica surface.

Table B.1 l_d is the penetration depth of the light in to the substrate, m is the calibration coefficient.

Surface	m	l_d
Platinum (Pt)	3206	117,5
Gold (Au)	2745	135.7
Silica (SiO_2)	2573	119

Using the equation 4.6 we were able to calculate the thickness of teh adsorbed mass on inorganic surface, given the equation 4.6 here:

$$\theta(molecules/cm^2) = d(cm) * N(molecules/cm^3) \quad \textbf{(A.2)}$$

N is the bulk density of the adsorbed mass which is 1.2 here.

APPENDIX C

Table C.1 Adsorption rates k_a, desorption rates k_d, equilibrium adsorption coefficients K_{eq}, the and free energies of adsorption ΔG_{ads}, of peptides on a given surface. The values calculated using a bi-exponential adsorption model, are labeled (1) and (2) represents the first and second part of the adsorption model.

peptides	k_a^1 (M^{-1} s^{-1})	k_a^2 (M^{-1} s^{-1})	$k_d^1 \times 10^{-5}$ (s^{-1})	$k_d^2 \times 10^{-4}$ (s^{-1})	$K_{eq}^1 \times 10^6$ (M^{-1})	$K_{eq}^2 \times 10^4$ (M^{-1})	ΔG_{ads}^1 (kcal/mol)	ΔG_{ads}^2 (kcal/mol)
c-PtBP1	170 ± 3.44		5.00 ± 0.88		3.40 ± 0.89		−8.9 ± 0.1	
l-PtBP1	8.27 ± 0.92	10.2 ± 1.3	5.00 ± 0.57	3.00 ± 0.33	0.16 ± 0.04	3.39 ± 1.24	−7.1 ± 0.1	−6.2 ± 0.2
3l-PtBP1	16.88 ± 4.07		9.00 ± 1.00		0.19 ± 0.07		−7.2 ± 0.2	
c-PtBP2	5.32 ± 1.15		6.28 ± 1.55		0.09 ± 0.04		−6.7 ± 0.3	
l-PtBP2	21.8 ± 2.2		15.22 ± 5.0		0.16 ± 0.07		−7.1 ± 0.3	
3l-PtBP2	1603 ± 52	15.5 ± 4.9	26.11 ± 12	3.6 ± 0.5	6.73 ± 2.49	3.87 ± 1.24	−9.3 ± 0.3	−6.3 ± 0.2
l-QBP1	238 ± 1.0		200 ± 4.0		0.122 ± 0.03		−6.9 ± 0.1	
3l-QBP1	1912 ± 88		130 ± 1.0		1.48 ± 0.23		−8.5 ± 0.1	
l-QBP2	37.1 ± 2.7	484 ± 94	3.0 ± 0.2	200 ± 2	1.24 ± 0.1	3.2 ± 0.7	−8.4 ± 0.04	−6.2 ± 0.12
3l-QBP2	112.9 ± 11.49		10 ± 0.1		1.13 ± 0.12		−8.3 ± 0.1	
l-GBP1	1.4 ± 0.1 × 10^4	112 ± 21	890 ± 150	2 ± 0.01	1.56 ± 0.28	56 ± 10	−8.2 ± 0.1	−7.8 ± 0.1
3l-GBP1	2.9 ± 0.2 × 10^4	1.6 ± 0.2 × 10^3	773 ± 183	6.5 ± 3.7	3.91 ± 1.22	330 ± 190	−9.0 ± 0.2	−8.9 ± 0.3

a The values calculated using the biexponential adsorption model are labeled with the superscripts “1” and “2”, representing the first and second part of the exponential, respectively.

CURRICULUM VITA

Candidate's full name: Urartu Özgür Şafak Şeker

Place and date of birth: Ankara, 1978

Permanent Address: Ankara

Universities and Colleges attended:

Hacettepe University, Food Engineering (B. Sc, 2001)

Istanbul Technical University,

Molecular Biology-Genetics and Biotechnology (MSc, 2003)

Istanbul Technical University,

Molecular Biology-Genetics and Biotechnology (PhD, 2009)

Publications:

- Gulis Zengin, Urartu Ö. Ş. Şeker, Hilmi Volkan Demir, Evren Mutlugun, Emre Sari, Candan Tamerler, Mehmet Sarikaya. Targeted Assembly of Quantum Dot Light Emitters in an LED using Engineered Peptides, *Nano Letters*, 2008 (in review).
- Urartu Ö. Ş. Şeker, Brandon Wilson, Deniz Sahin, Candan Tamerler, Mehmet Sarikaya. Quantitative Affinity of Genetically Engineered Repeating Polypeptides to Inorganic Solids, *Biomacromolecules*, 10 (2), 2009, **250-257**.
- Marketa Hnilova, Ersin Emre Oren, Urartu Ö. Ş. Şeker, John Evans, Candan Tamerler, Mehmet Sarikaya, Effect of Conformation on Adsorption Behavior of Gold Binding Peptides, *Langmuir*, 24 (21), 2008.
- Urartu.Ö. Ş. Şeker, Brandon Wilson, Sevil Dincer, Ill Won Kim, Ersin Emre Oren, John S. Evans, Candan Tamerler, Mehmet Sarikaya. Adsorption Behavior of Genetically Engineered Platinum Binding Peptides, *Langmuir*, 23 (15), 7895-7900, (2007).
- E. Emre Oren, Candan Tamerler, Deniz Sahin, Marketa Hnillova, Urartu Ö. Ş. Şeker, Mehmet Sarikaya, Ram Samudrala. A Novel Informatics-Based Approach to Design Inorganic Binding Peptides, *Bioinformatics*, 24 (21), 2816-2822, (2007).
- Boyaci Ismail.H. , Urartu.Ö. Ş. Şeker , Bas D., Topcu A, Tamerler C., Saldamli I., Statistical Modeling of Product Inhibition Effect on β-Galactosidase Enzyme During Lactose Hydrolysis, *Food Biotechnology*, 20 (1), 79-91, (2006)
- Zeynep P. Çakar, Urartu .Ö. Ş Şeker, Candan Tamerler, Marco Sonderegger, Uwe Sauer, Evolutionary Engineering of Multiple Stress

Resistant Saccharomyces cerevisiae, *FEMS Yeast Research*, (6-7), 569-578 (2005)

- Urartu Ö. Ş. Şeker, Tunc Catal, Yilmaz Taptık, Candan Tamerler, Hakan Bermek, Enhanced production of manganese peroxidase by the white rot fungus Bjerkandera adusta using media engineering. *Biotechnology and Biotechnological Equipment*, 22 (3), 844-848 (2008).
- Bahadir Kepenek, Urartu Ö. Ş. Şeker, Ali Fuat Çakır, Mustafa Ürgen, Photocatalytic Bactericidal Effect of TiO2 Thin Films Produced by Cathodic Arc Deposition Method, *Key Engineering Materials*, (254-2), 463-467 (2004)
- Boyacı İ. H., Urartu Ö. Ş. Şeker and Mutlu M., Determination of β-glucan content of cereals with amperometric glucose electrode, *European Food Research and Technology* (15), 538-541 (2002).